VIBRATION CONTROL AND DESIGN OF COMPOSITE CANTILEVERS TAKING INTO ACCOUNT STRUCTURAL UNCERTAINTIES AND DAMAGE

by

Donghoon Oh

Dissertation submitted to the Faculty of the
Virginia Polytechnic Institute and State University
in partial fulfillment of the requirements for the degree of

DOCTOR OF PHILOSOPHY

in

Engineering Mechanics

APPROVED:

L. Librescu, Chairman

M.S. Cramer

L. Meirovitch

R.H. Plaut

S. Thangjitham

April, 1993

Blacksburg, Virginia

VIBRATION CONTROL AND DESIGN OF COMPOSITE CANTILEVERS TAKING INTO ACCOUNT STRUCTURAL UNCERTAINTIES AND DAMAGE

by

Donghoon Oh

Committee Chairman: Dr. L. Librescu

Professor of Engineering Science and Mechanics

(ABSTRACT)

Within this work a study of the vibrations of laminated composite cantilevers exhibiting structural uncertainties and damage is accomplished. The study is performed within both the Classical Lamination (CLT) and the First-order Transverse Shear Deformation Theories (FSDT). Upon comparing the natural frequencies and mode shapes obtained by both theories, the effects of transverse shear deformation will be emphasized. Other nonclassical effects as e.g. the bending-twist coupling and the warping restraint on the cantilevered structure are also considered. As passive techniques of vibration control, structural tailoring and optimization are implemented. To deal with structural uncertainties, a probabilistic discretization technique for the governing system is developed. Statistical properties of natural frequencies are obtained by means of a second-moment method and a first-order perturbation technique. Structural tailoring is reconsidered to reduce the sensitivity of the dynamic behavior to parameter uncertainties. Next, the damage effect on the structure is considered in the design process. As a result, the problem of the robustness of structures in the presence of damage is addressed. This work also

deals with the active feedback control of cantilevered structural systems. An efficient control technique for continuous structures, namely modal control, is adopted and the control gain is obtained by an optimal control law. The comparison of controlled and uncontrolled dynamic responses is made between two models based on CLT and FSDT with emphasis on the influence played by transverse shear deformation and warping restraint.

ACKNOWLEDGEMENTS

I wish to express my sincere appreciation to the chairman of my advisory committee, Dr. L. Librescu, for his devoted guidance, insightful suggestions, continuous encouragement and moral support during the course of this study.

I would like to thank Dr. L. Meirovitch and Dr. R.H. Plaut for providing invaluable advice during my research. Furthermore, I extend my thanks to Dr. M.S. Cramer and Dr. S. Thangjitham for being on my committee and guiding me.

Fruitful technical discussions with Dr. O. Song are also appreciated.

Mostly, a special word of heartfelt appreciation goes to my wife for her patience, love and encouragement, to my brother for understanding my study, and to my lovely daughter Grace for providing me so much joy and comfort.

I dedicate this work to my parents who have made sacrifices throughout their lives for their children.

TABLE OF CONTENTS

LIST OF FIGURES

LIST OF TABLES

1. INTRODUCTION

1.1 Motivation

Based on their outstanding properties, fiber-reinforced composite materials have been increasingly used in aircraft and spacecraft structures, and it is sure that this trend will continue and intensify in the future. In addition to the well-known superior features of composite material systems, the ability to tailor their anisotropic properties according to given requirements provides new advantages, enabling one to improve the dynamic characteristics of laminated composite structures.

However, besides their superior properties, composite material structures exhibit high flexibilities in transverse shear. Moreover, unavoidable uncertainties exist in composite structures. As a result, probabilistic analysis must be incorporated to evaluate their structural response. Monte Carlo simulation has been used for statistical analysis. Large samples, however, may be needed in order to find correct statistical parameters of the structures, thus; this method becomes very expensive. Another disadvantage of the Monte Carlo simulation is that due to independent sampling, correlated random variables are excluded in this analysis. To circumvent this ineffectiveness, the *probabilistic finite element method* has been used for the analysis of composite structures with parameter uncertainties. In this study, the *Stochastic Rayleigh-Ritz method* is developed to predict the effects of the uncertainties on free vibration characteristics.

It should be pointed out that flying vehicles are exposed during their life operation to various types of damage which may result in dramatic reductions of their

structural integrity. The damage can produce a change of vibration characteristics and even the failure of the structure. Due to the increasing use of composite materials in lifting surfaces of flying vehicles, structural safety must be taken into account during their service life. Although there are a number of studies dealing with the effect of damage on free vibration of cantilevered beams, to the best knowledge of the author, studies are not available dealing with the alleviation of the deteriorating effect of the damage on the dynamic behavior of composite beams. The increase of the level of safety of cantilevered composite structures by increasing their resistance capability to damage is studied herein. Being designed to withstand damage and uncertainties, the catastrophic failure of the structure can be avoided.

The classical beam theory based on the Bernoulli-Euler assumption that the lines normal to the midline before deformation remain straight and normal after deformation is widely applied in the design of metallic beam structures, where this theory provides reliable results. However, with the advent of advanced composite material systems, this theory fails to provide reliable results. For composite material structures, it is found that the bending-twist coupling has a significant effect on natural frequencies and mode shapes. In addition, for cantilevered beams, the warping inhibition effect should be accounted for in modeling of the structure.

In contrast to the metallic structures, in the case of the composite ones their elastic stiffnesses depend on the stacking sequence of laminae and ply orientation. Therefore dynamic performance can be enhanced by structural tailoring and optimization techniques. The freedom of tailoring the elastic characteristics of fiber-reinforced composite structures has a great importance on the design of robust structures. Using the unique directionality characteristics of anisotropic materials, dramatic improvements of the dynamic performance can be achieved.

A number of studies have revealed that the warping restraint effect can be beneficial in the case of the undamped vibration problem of cantilevered composite structures.

In connection with structural vibration control, a large number of works have been devoted to conventional metallic structures. For composite material structures, however, a very limited number of studies are available. The idea of implementing linear feedback control is to make the system asymptotically stable by locating all open-loop poles to the left-hand side of the complex domain. The continuous structures possess an infinite number of modes; consequently, controlling all modes is impractical even if possible. Vibration response of mechanical structures is governed by lower modes, thus effective control of these critical modes is desired.

1.2 Outline of Present Study

This study is concerned with vibration control of cantilevered composite structures in the presence of parameter uncertainties and damage. A shear deformable cantilevered beam accounting for the effects of warping restraint and bending-twist coupling is considered. For the sake of comparison, the classical lamination counterpart is also considered.

Variational methods are used to find approximate solutions for the coupled bending and torsional vibration problem. To deal with structural uncertainties, probabilistic methods are incorporated in the discretization process. A second moment method and a perturbation technique are used to solve the stochastic eigenvalue problem. In the modeling of damaged structures, the damage is characterized in terms of damage parameters. For the safe operation of cantilevered structures, the ones are constructed to be robust to uncertainties and damage.

To minimize the control effort in vibration, structural tailoring and optimization are proposed. Specific dynamic performance goals, such as the increase of natural frequencies and a lower sensitivity to structural uncertainties and damage, can be achieved by using structural tailoring and optimization techniques.

In addition to this, active control is applied to reduce vibration response in an effective manner. An optimal control design method is presented on the basis of linear quadratic control where the minimizing of the performance index leads to a Riccati equation.

This work consists of eleven chapters.

Chapter 2 gives a brief review of the literature.

In Chapter 3, the equations of motion of laminated composite shear deformable beam structures, along with its classical lamination counterpart, are derived via Hamilton's principle for the study of the following structural problems:

· Free vibration

· Structural tailoring and optimization

· Analysis of structures with unavoidable uncertainties

· Analysis of structures with possible damage

· Design of robust structures to uncertainties and damage

· Active vibration control

In Chapter 4, the deterministic eigenvalue problem is presented using variational methods, while in the subsequent Chapters 5 and 6, passive vibration control for cantilevered composite structures is accomplished by applying structural tailoring and optimization techniques, respectively.

In Chapter 7, a stochastic discretization technique is presented for uncertain distributed-parameter structures. Material properties, elastic moduli, mass density and design parameters such as stacking sequence, fiber orientation and layer thickness are considered as random variables.

In Chapters 8 and 9, to ensure proper operating conditions for the structures, possible damage effects are predicted and robust structures are constructed to increase the resistance capability to damage and uncertainties.

In Chapter 10, a stable closed-loop system can be achieved without modifying the structural modes by applying a convenient modal control theory to continuous structures. For the purpose of implementing active control into cantilevered composite structures, the governing equations of motion are expressed in terms of state variables, then transformed into natural coordinates by a coordinate transformation.

Finally, in Chapter 11, a summary of the results from previous chapters and some concluding remarks emerging from this study are outlined. Recommendations for possible future work related to this study are also presented in this chapter.

2. LITERATURE REVIEW

In this section, the previous literature on modeling of composite cantilevers with structural uncertainties and damage, and on passive and active vibration control, is reviewed, along with a brief presentation of the current approaches to these topics.

2.1 Modeling of Cantilevered Structures

The understanding of the vibration behavior of the cantilevered type of structures is of high technological importance in the design of lifting surfaces because the aircraft wings and fuselage as well as helicopter blades are modeled as cantilevered beams.

It is known that in beam theory, Timoshenko [1] was the first one to refer to the classical Euler-Bernoulli beam theory by accounting for the effect of transverse shear deformation. Kruszewski [2] considered both transverse shear and rotary inertia terms in his vibration analysis of a uniform beam. Traill-Nash and Collar [3] found that the effect of shear flexibility was considerably more significant than that of rotary inertia. Cowper [4] introduced shear correction factors to account for the effective transverse shear strains. Huang [5] studied the effect of shear deformation and rotary inertia on the natural frequency and natural modes for beams with simple end conditions.

In the above investigations, most of the papers included both the effects of transverse shear and rotary inertia, However, in spite of its importance, the warping constraint effect was disregarded. Reissner and Stein [6] have emphasized the

importance of the axial warping inhibition on the torsion of thin cantilevered structures. Later, Librescu et al. [7] have accounted for this restraint to aeroelastic divergence of multi-cell metallic wings.

In a number of monographs (Ambartsumian [8], Librescu [9]) fundamental theories of anisotropic elastic plates and shells have been developed. During that time, Whitney and Leissa [10] have also carried out analytical studies devoted to heterogeneous anisotropic plates.

In connection with the dynamic characteristics of composite wing structures, Crawley and Dugundji [11] have performed a study of the vibration of cantilevered graphite/epoxy beams. The estimation of natural frequencies was accomplished by incorporating the effect of warping restraint and use of the Rayleigh-Ritz and Finite Element methods. Their study was continued with the investigation of the effect of bending-torsion stiffness coupling on natural frequencies and modes of unbalanced laminated cantilevered beams [12]. Jensen et al. [13] have revealed that inclusion of chordwise bending is significantly important for anisotropic beams, even for high aspect ratio beams.

Recently, Kaza and Kielb [14] presented the effect of warping on the torsional vibration of rotating pretwisted beams as their aspect ratio was varied. They suggested that the structural warping term must be accounted for in the modeling of blades, even if isotropic materials are used. Song [15] has incorporated the warping restraint effect in the study of composite thin-walled beam structures. Hodges et al. [16] have studied the coupling effects on the free vibration characteristics of composite box beams by incorporating the cross-sectional warping.

Meanwhile, for a better understanding and evaluation of static and dynamic behavior, refined models have been developed. Higher-order theories for laminated composite structures have been developed without the necessity of shear

correction coefficients by Reddy [17] and Librescu [18]. Quite recently, Librescu and Simovich [19] have presented a refined wing structural model by incorporating the warping restraint effect. The governing equations are described by two independent variables, namely plunging and twist deflections w and θ, respectively. Thangjitham and Librescu [20] used this model for the study of vibration characteristics of anisotropic composite wing structures. At the same time, Karpouzian and Librescu [21] proposed an explicit model based on first-order transverse shear deformation theory (FSDT), also incorporating the warping restraint effect.

To analyze the free vibration response of laminated panels with complex boundary conditions, there is no choice but to use approximate methods such as Rayleigh-Ritz, Galerkin or Finite Element. In Refs. [22-24], these techniques were discussed, and discretization procedures for continuous structures were accomplished. Meirovitch [33] restricts the validity of approximate solutions by Rayleigh-Ritz to only lower modes, indicating that higher frequencies are of little significance in the vibration response of flexible structures. The convergence of Extended-Galerkin techniques was examined for both conservative [25] and non-conservative systems [26].

On the other hand, exact solution approaches were carried out by Song [15], Librescu and Thangjitham [27,20], and Oyibo [28]. Oyibo [28] used the conventional linear operator method to obtain the fundamental natural frequency where mode shapes are required to satisfy the associated boundary conditions. Song [15], Librescu and Thangjitham [27], and Thangjitham and Librescu [20] employed the Laplace Transformation technique to determine natural frequencies and natural modes. The suggested technique offers a unified manner of solution procedure, thus accurate solutions to general problems in vibration can be obtained in the same manner without consuming lots of operational effort.

2.2 Structural Optimization and Tailoring Techniques

A first study on the design synthesis of laminated composites was presented by Bert [33]. He obtained closed-form solutions for the eigenvalues of simply supported plates composed of cross-ply symmetric laminates, and then the eigenfrequencies were maximized. Starnes and Haftka [34], and Shin et al. [35] have presented design methodologies for laminated plates with constraints on buckling to increase the maximum load capacity. Rao and Singh [36] used linear programming when performing optimal weight design of symmetric laminated structures. On the other hand, Hirano [37] used nonlinear programming based on Powell's method [38] in the optimum design of laminated plates under uniaxial and biaxial compression. Mesquita and Kamat [39] showed that improvement in dynamic performance could be achieved through maximization of structural frequencies. Recently, Haftka and Walsh [40] presented *integer-programming formulations* for the design of symmetric and balanced laminated plates under biaxial compression.

A comprehensive survey on structural optimization and aeroelastic tailoring of aircraft design was made in Ref. [41]. Weisshaar and Foist [42] discussed vibration tailoring of laminated composite beam-like structures with moderate-to-high aspect ratio. Their study has revealed the capability of controlling mode shape and nodal lines as well as natural frequencies by changing ply angles and considering the degree of elastic coupling in terms of the bending-twist coupling parameter. In the paper by Jensen et al. [12] the aeroelastic performance of unbalanced laminated wings featuring bending-torsion stiffness coupling and warping stiffness was studied.

Librescu and Simovich [19] have investigated the aeroelastic divergence instability of composite swept-forward wing structures. In a subsequent work, Librescu and Khdeir [43] have analyzed the same problems and obtained additional results

which concern the effect of warping inhibition on the static aeroelastic instability. Later, Thangjitham and Librescu [20] applied a structural tailoring technique to dynamic problems to improve vibration characteristics. The variations of the first three natural frequencies of coupled dynamic structures with or without warping constraint were presented as function of wing aspect ratio and ply angles. Recently, Seitz [44] demonstrated the benefits of using the anisotropicity of a composite layup to tailor the response of a low-aspect wing. The tailoring technique was applied in both spanwise and chordwise directions, and showed that the vibration and flutter responses are significantly affected.

2.3 Structures with Parameter Uncertainties

Structures with parameter uncertainties are modeled by stochastic differential equations with random coefficients. The parameter variations in the structural system results in corresponding variations in natural frequencies and dynamic responses. To estimate the effects of the uncertainties, variations in structural properties are often interpreted in a probabilistic sense.

Boyce [45] gave a statistical description of the eigenvalues and eigenvectors by calculating their probability density functions. Collins and Thomson [46] have considered the eigenvalue problem for dynamic systems with uncertain structural parameters. The analysis has revealed a good representation of the statistics of the eigenvalues and eigenvectors. Soong [47] has referred to elastic beams as disordered systems, where the uncertain spring constants of the lumped-parameters model represent the variation of the stiffness matrix. Lin and Yang [48] considered the eigenvalue problem of disordered periodic beams to determine the variance of natural frequencies and normal modes under fluctuation of bending stiffness in a random field. Ang and Tang [49] used a second-order Taylor series expansion when

reanalyzing a system after a small change in design parameters. Romstad et al [50] applied a general power series method with a perturbation technique to discrete systems to obtain the variations of eigenvalues. Their work provided the basis of later studies of random eigenvalue problems. Chen and Soroka [51] have studied the dynamic response of multi-degree of freedom dynamic systems with statistical properties. The statistics of the response was calculated once random eigenvalue and eigenvectors were determined. Their results revealed that the response of stochastic systems was higher than that of deterministic ones.

Vanmarcke [52] and Nakagiri and Hisada [53] treated continuous systems with parameter uncertainties by applying the finite element method with distributed structures. This procedure is referred to as the *Stochastic* or *Probabilistic Finite Element method* in the sense of discretizing the structure in a stochastic sense by a second-moment method and a perturbation technique. Vanmarcke et al. [54] gave a survey of developments in the field of stochastic finite element analysis. They pointed out that the *Stochastic Finite Element method* based on a probabilistic approach requires much less computational time than statistical analysis based on Monte Carlo simulation. Later, Ibrahim [55] reviewed a number of topics related to the dynamics of structures exhibiting parameter uncertainties. A number of problems as, e.g., design optimization, reliability, as well as random eigenvalue problem, were addressed.

The *Stochastic Finite Element method* was applied to composite material structures by Nakagiri et al. [56]. In isotropic material structures, the parameters are influenced by material properties such as elastic constants and mass density. For anisotropic structures composed of composite materials, the uncertainties associated with the ply orientation, stacking sequence, and layer thickness are taken

into account. These design parameters are treated as random variables, resulting in complicated eigenvalue problems.

In the previous approach [53,56], the finite elements were assumed to be fully correlated. To obtain satisfactory results, the element size must be much smaller than half of the correlation distance of the random field. Consequently, the computational cost could be high since a large number of elements is required. Weiqiu and Weiqiang [57] considered local averages of the random field in the *Stochastic Finite Element method* to improve convergence of second-order statistics. In addition, they performed a second-order perturbation to improve stochastic solutions. Based on their results, it was concluded that introduction of local averages to the *Stochastic Finite Element method* provided better convergence. The second-order perturbation offered only a little improvement, however, and a large amount of computational time and huge memory storage were consumed.

Liaw and Yang [58] used the *Stochastic Finite Element method* for the reliability analysis of laminated composite shells. They applied a mean-centered second-moment method and a perturbation technique based on the assumption that the eigenvalues and eigenvectors exhibit sufficiently small variations from their mean. Engelstad and Reddy [59] have calculated the variations of static deflections and interlaminar stresses by introducing a probabilistic approach with the layerwise theory. Thangjitham and Rantis [60] have investigated the probabilistic static stability of a laminated composite plate by determining the distribution function of the critical bucking loads.

2.4 Analysis of Damaged Structures

Sato [63] has studied the effect of change of the cross-section of a beam on its free vibration response. The discontinuity of bending stiffness was shown to result in a drop of natural frequency significantly due to abrupt changes of the cross-section. He stated that localized stress deformation played a dominant role in global deformation. Cawley and Adams [64] have offered an analytical method to locate damage sites and their magnitudes in plates. They also checked directional damage by introducing the sensitivity of natural frequencies to the changes of structural stiffness in modal analysis.

Hamming and Venkayya [65] have studied the dynamic aeroelastic instability (flutter) of damaged, optimized flight vehicles. This study was extended by Eastep et al. [66] to the static aeroelastic problem (divergence) of swept-forward composite wings with damaged layers. They concluded that damage tolerance should be considered in the design of aircraft structures through failure analysis. Castel and Kapania [67] introduced bending-extension coupling induced by asymmetry resulting from damage.

Joshi and Madhusudhan [68] studied the influence of the localized damage on free vibration and flutter characteristics of rectangular panels. For an isotropic structure, a material defect induced by damage was modeled as a reduction in local Young's modulus. Kim and Stragnac [69] examined aeroelastic stability of composite structures. From the micromechanical point of view, it has been known that matrix cracking induces reduction of stiffness. They argue that the damages in composite structures are unavoidable, therefore they can occur internally as well as externally by combat damage or impact. They included damage growth, providing mathematical model of progressive damage, resulting in changes in aeroelastic stability corresponding to changes in stiffness.

2.5 Active Vibration Control

Porter and Crossley [70] studied modal control for lumped-parameter linear systems and later Gould [71] extended its application to linear distributed-parameter systems. Wykes and Mori [72] made a feasibility study on control of elastic modes of a supersonic aircraft using modal control theory. Simmon and Mitter [73] also contributed to the modal control theory by providing a similar concept. Brogan [74] studied modal decomposition to describe the system behavior in a reduced set of coordinates. The procedure was simple, but it had computational difficulties in determining the modal matrix.

Meirovitch [75] presented a new modal approach, namely the modal space control. Within this approach, the system of equations of motion was decoupled by means of a modal coordinate transformation; then global optimality could be achieved by an optimal control law. In Ref. [76] two types of modal synthesis, independent modal-space control and coupled control, were presented and the basic differences between the two approaches were compared. This approach was used in self-adjoint systems [77] and non-self-adjoint systems [78] as well.

Practical implementations of the active control theory to wing type structures have been done by a number of authors. Krabs [79] has studied the boundary controllability of one dimensional vibrating systems such as string or beam. Timoshenko beams were shown to be stabilized by optimal control [80] and by boundary control [81], respectively. Meirovitch [82] presented a method for the active vibration suppression of a wing using the modal control theory. Horikawa et al. [83] also used a modal approach to build a system model for beams subjected to a nonconservative force. Related to the location of controllers, Schulz [84] has proposed a determination technique of actuator/sensor positions for control of flexible structures considering the dissipation of energy due to control action. Williams

[85] simulated digital control on a flexible beam where the effect of parameter uncertainties and the conversion of modal forces were investigated. Weinmann [86] considered the influence of uncertainties on the closed-loop system. He provided the concepts of robust control design with respect to perturbed or uncertain system parameters.

Recently, Soong [87] introduced instantaneous optimal control incorporating external excitation into the control algorithm. He examined the control efficiencies associated with instantaneous optimal control algorithms and compared them to classical optimal control. He indicated that instantaneous optimal control algorithms gave slightly better results.

Motivated by the new modal control theory, in parallel, experiments were conducted by Schäfer [88] to study the active vibration control of cantilevered beams. A systematic study of a control observer related to the vibration problems was presented. Inman and Garcia [89] conducted experimental and analytical studies on vibration control of a flexible cantilevered beam by incorporating smart materials. In their experiments, piezo-ceramic panels were bonded where displacements were converted to electric signals for the vibration response to be measured.

It should be remarked that, in contrast to metallic structures, the active control of composite structures has rarely been studied. An implementation of an active control methodology in composite beams and plates by employing the modal approach to suppress structural vibration response was achieved by Chang [90]. Anisotropy, transverse shear deformation and the geometric parameters were revealed to have a great influence on the controlled as well as uncontrolled responses of the composite structures. Adali et al. [91] considered distributed control of composite plates with damping; later they conducted a study on optimal vibration control of laminated cross-ply cylindrical panels [92].

3. DERIVATION OF GOVERNING EQUATIONS

3.1 Overview

Modeling of cantilevered structures was mostly done using the classical lamination theory (CLT). Within this theory the influence of transverse shear deformation is discarded, which is equivalent to postulating an infinite rigidity in transverse shear. This theory has been amply used in the study of the vibration characteristics of aircraft structures and of helicopter blades.

However, the classical lamination theory of structures made of advanced composite materials has been known to be inadequate for the vibration analysis. Discrepancies between the predictions based on CLT and the more realistic models have been revealed. Moreover, in the majority of cases a free warping twist model was used to approach various problems of cantilevered beams.

As a result, a clear understanding of the effects played by transverse shear, warping inhibition and elastic coupling on dynamic characteristics of cantilevered structures is needed. With these facts in mind, the present work is intended to incorporate essential effects which are of considerable importance in the accurate prediction of the dynamic behavior of anisotropic cantilevered structures. The implications of the effects will be explicitly investigated.

3.2 Modeling of Composite Cantilevered Structures

The cantilevered structure is referred to a Cartesian system of rectangular coordinates x, y, z, where the mid-plane coincides with the x-y plane. The x-, y-coordinates are referred to as the chordwise and spanwise coordinates, respectively.

The basic geometry of rectangular cantilevers and the associated coordinates are depicted in Figure 3.1. The uniform plate thickness and in-plane dimensions, span and chord lengths, are denoted by h, l, and c, respectively. The origin of the coordinate system is located at the intersection of the root chord with the leading edge of the cantilever, at $z = 0$.

3.2.1 First-order Transverse Shear Deformable Beam Theory:

Kinematics and Constitutive Relations:

The displacement field $u_1(x, y, z; t)$, $u_2(x, y, z; t)$, $u_3(x, y, z; t)$ is represented as

$$\begin{aligned} u_1(x, y, z; t) &= u(x, y; t) + z\psi_x(x, y; t), \\ u_2(x, y, z; t) &= v(x, y; t) + z\psi_y(x, y; t), \\ u_3(x, y, z; t) &= w(x, y; t), \end{aligned} \tag{3.1}$$

where u, v, and w denote displacements in the x-, y-, and z-coordinate directions, and ψ_x and ψ_y are the rotations of the normal about the y and x axis, respectively.

Upon postulating the chordwise non-deformability of the cantilevered structure, it results that the deformation is a function of the spanwise coordinate y only. As a result, and in order to reduce the 3-D problem to an equivalent 1-D one, the displacement field becomes

$$\begin{aligned} u_1 &= z\theta(y; t), \\ u_2 &= v(y; t) + z(\psi + x\varphi), \\ u_3 &= w(y; t) - (x - x_o)\theta(y; t), \end{aligned} \tag{3.2}$$

where θ denotes the twist angle, and ψ and φ are quantities related to the rotation of the normal about the x-axis and to the warping of the cross section, respectively. The displacement function u_3 represents the total vertical displacement due to plunging w measured at the elastic axis and twist θ about the elastic axis x_o. Using

the equations of the 3-D elasticity theory, the strain-displacement relationships become

$$\begin{aligned} e_{22} &= v_{,y} + z(\psi_{,y} + x\varphi_{,y}), \\ \gamma_{12} &= z(\theta_{,y} + \varphi), \\ \gamma_{23} &= \psi + x\varphi + w_{,y} - x\theta_{,y} + (x_o\theta)_{,y}, \end{aligned} \tag{3.3}$$

where $(\ )_{,y} \equiv \partial(\ )/\partial y$. For further use we introduce the notation: $(\dot{\ }) \equiv \partial(\ )/\partial t$ where t denotes the time. The other strain components, e_{11}, e_{33}, and γ_{13}, are zero, and the term $zx\varphi_{,y}$ is associated with the warping restraint.

Within this theory the constitutive equations are given by

$$\begin{Bmatrix} \sigma_{11} \\ \sigma_{22} \\ \sigma_{12} \end{Bmatrix} = \begin{bmatrix} \bar{Q}_{11} & \bar{Q}_{12} & \bar{Q}_{16} \\ \bar{Q}_{12} & \bar{Q}_{22} & \bar{Q}_{26} \\ \bar{Q}_{16} & \bar{Q}_{26} & \bar{Q}_{66} \end{bmatrix} \begin{Bmatrix} e_{11} \\ e_{22} \\ \gamma_{12} \end{Bmatrix}, \tag{3.4}$$

and

$$\begin{Bmatrix} \sigma_{13} \\ \sigma_{23} \end{Bmatrix} = K^2 \begin{bmatrix} \bar{Q}_{44} & \bar{Q}_{45} \\ \bar{Q}_{45} & \bar{Q}_{55} \end{bmatrix} \begin{Bmatrix} \gamma_{13} \\ \gamma_{23} \end{Bmatrix}, \tag{3.5}$$

where $\bar{Q}_{ij}$'s are the transformed reduced-stiffness coefficients, K^2 is a shear correction factor, $\sigma_{11}, \sigma_{22}, \sigma_{12}$ denote the in-plane stresses, and $\sigma_{\alpha 3}$ $(\alpha = 1, 2)$ are the transverse shear stresses.

Governing Equations of Motion:

The equations of motion can be derived via Hamilton's principle

$$\delta \int_{t_o}^{t_f} (T - U - V)dt = 0 \tag{3.6}$$

where T denotes the kinetic energy, U the strain energy and V the potential energy of the body and surface forces. In a more detailed form, Eq. (3.6) is written as

$$\int_{t_o}^{t_f} \left[\int_V \sigma_{ij}\delta e_{ij} dV - \int_V \rho(f_i - \ddot{u}_i)\delta u_i dV - \int_S \sigma_i \delta u_i dS \right] dt = 0 \tag{3.7}$$

where S denotes the bounding surface, V the volume of the beam, and f_i are the components of the body force vector, while δ denotes the variation sign.

Substituting the kinematic equations (3.2), (3.3), and constitutive equations (3.4-5) into Eq. (3.7) leads to the following equations of motion in terms of the displacements, $v, \psi, \varphi, w, \theta$, and composite stiffness coefficients, A', B', and D's. The laminate stiffness coefficients of the A, B, and D matrices are expressed as

$$(A_{ij}, B_{ij}, D_{ij}) = \int_{-h/2}^{h/2} \bar{Q}_{ij}(1, z, z^2)dz, \quad i,j = 1,2,6,$$

$$A_{ij} = \int_{-h/2}^{h/2} \bar{Q}_{ij}dz, \quad i,j = 4,5 \tag{3.8}$$

and for the k^{th} layer as

$$\begin{Bmatrix} A_{ij}^k \\ B_{ij}^k \\ D_{ij}^k \end{Bmatrix} = \begin{Bmatrix} (z_{k+1} - z_k) \\ \frac{1}{2}(z_{k+1}^2 - z_k^2) \\ \frac{1}{3}(z_{k+1}^3 - z_k^3) \end{Bmatrix} \bar{Q}_{ij}^k, \tag{3.9}$$

In addition, the mass terms, m_1, m_2, and m_3, are defined as

$$(m_1, m_2, m_3) = \int_{-h/2}^{h/2} \rho\ (1, z, z^2)dz. \tag{3.10}$$

The mass terms depend upon the density ρ which, in general, depends on the material of each layer.

Finally, integrating by parts and collecting the terms leads to the following five coupled governing equations of motion:

$$\left[A_{22}v_{,y} + B_{22}\psi_{,y} + \frac{c}{2}\delta_w B_{22}\varphi_{,y} + B_{26}\theta_{,y} + B_{26}\varphi\right]_{,y}$$
$$= m_1\ddot{v} + m_2\ddot{\psi} + \frac{c}{2}m_2\ddot{\varphi}$$

$$\left[B_{22}v_{,y} + D_{22}\psi_{,y} + \frac{c}{2}\delta_w D_{22}\varphi_{,y} + D_{26}\theta_{,y} + D_{26}\varphi\right]_{,y}$$

$$
\begin{aligned}
&- \left[A_{55}\psi + \frac{c}{2}A_{55}\varphi + A_{55}w_{,y} + A_{55}(x_o\theta)_{,y} - \frac{c}{2}A_{55}\theta_{,y} \right] \\
&= m_3\ddot{\psi} + m_2\ddot{v} + \frac{c}{2}m_3\ddot{\varphi}
\end{aligned}
$$

$$
\begin{aligned}
&\left[\frac{c}{2}\delta_w B_{22}v_{,y} + \frac{c}{2}\delta_w D_{22}\psi_{,y} + \frac{c^2}{3}\delta_w D_{22}\varphi_{,y} + \frac{c}{2}\delta_w D_{26}\theta_{,y} + \frac{c}{2}D_{26}\varphi \right]_{,y} \\
&- \left[B_{26}v_{,y} + D_{26}\psi_{,y} + \frac{c}{2}D_{26}\varphi_{,y} + D_{66}\theta_{,y} + D_{66}\varphi \right] \\
&- \left[\frac{c}{2}A_{55}\psi + \frac{c^2}{3}A_{55}\varphi + \frac{c}{2}A_{55}w_{,y} + \frac{c}{2}A_{55}(x_o\theta)_{,y} - \frac{c^2}{3}A_{55}\theta_{,y} \right] \\
&= \frac{c^2}{3}m_3\ddot{\varphi} + \frac{c}{2}m_2\ddot{v} + \frac{c}{2}m_3\ddot{\psi}
\end{aligned}
\tag{3.11}
$$

$$
\begin{aligned}
&\left[A_{55}\psi + \frac{c}{2}A_{55}\varphi + A_{55}w_{,y} + A_{55}(x_o\theta)_{,y} - \frac{c}{2}A_{55}\theta_{,y} \right]_{,y} + \mathcal{P} \\
&= m_1\ddot{w} - (\frac{c}{2} - x_o)m_1\ddot{\theta}
\end{aligned}
$$

$$
\begin{aligned}
&\left[B_{26}v_{,y} + D_{26}\psi_{,y} + \frac{c}{2}\delta_w D_{26}\varphi_{,y} + D_{66}\theta_{,y} + D_{66}\varphi \right]_{,y} \\
&- \left[\frac{c}{2}A_{55}\psi + \frac{c^2}{3}A_{55}\varphi + \frac{c}{2}A_{55}w_{,y} + \frac{c}{2}A_{55}(x_o\theta)_{,y} - \frac{c^2}{3}A_{55}\theta_{,y} \right]_{,y} \\
&+ x_o \left[A_{55}\psi + \frac{c}{2}A_{55}\varphi + A_{55}w_{,y} + A_{55}(x_o\theta)_{,y} - \frac{c}{2}A_{55}\theta_{,y} \right]_{,y} + \mathcal{T} \\
&= \left[m_3 + \left(\frac{c^2}{3} - x_o c + x_o^2 \right) m_1 \right] \ddot{\theta} - (\frac{c}{2} - x_o)m_1\ddot{w}
\end{aligned}
$$

and the associated boundary conditions. At the root ($y = 0$) of the cantilevered beam, these conditions are:

$$
v = 0, \qquad \psi = 0, \qquad \varphi = 0, \qquad w = 0, \qquad \theta = 0, \tag{3.12}
$$

and at the tip ($y = l$), these are:

$$A_{22}v_{,y} + B_{22}\psi_{,y} + \frac{c}{2}\delta_w B_{22}\varphi_{,y} + B_{26}\theta_{,y} + B_{26}\varphi = 0$$

$$B_{22}v_{,y} + D_{22}\psi_{,y} + \frac{c}{2}\delta_w D_{22}\varphi_{,y} + D_{26}\theta_{,y} + D_{26}\varphi = 0$$

$$\frac{c}{2}\delta_w B_{22}v_{,y} + \frac{c}{2}\delta_w D_{22}\psi_{,y} + \frac{c^2}{3}\delta_w D_{22}\varphi_{,y} + \frac{c}{2}\delta_w D_{26}\theta_{,y} + \frac{c}{2}D_{26}\varphi = 0 \qquad (3.13)$$

$$A_{55}\psi + \frac{c}{2}A_{55}\varphi + A_{55}w_{,y} + A_{55}(x_o\theta)_{,y} - \frac{c}{2}A_{55}\theta_{,y} = 0$$

$$B_{26}v_{,y} + D_{26}\psi_{,y} + \frac{c}{2}\delta_w D_{26}\varphi_{,y} + D_{66}\theta_{,y} + D_{66}\varphi$$
$$- \left[\frac{c}{2}A_{55}\psi + \frac{c^2}{3}A_{55}\varphi + \frac{c}{2}A_{55}w_{,y} + \frac{c}{2}A_{55}(x_o\theta)_{,y} - \frac{c^2}{3}A_{55}\theta_{,y}\right] = 0$$

In the equation, δ_w identifies the warping restraint. $\mathcal{P}$ and $\mathcal{T}$ denote the vertical force and twisting moment, respectively.

Nondimensionalized Governing Equations:

For the study of the free vibration characteristics of the beam, it is advisable to introduce nondimensional parameters. They are defined as

$$\tilde{x} = \frac{2}{c}x, \quad \tilde{y} = \frac{y}{l}, \quad \tilde{z} = \frac{z}{h}, \quad \tilde{t} = \omega_o t, \quad \omega_o = \frac{\omega}{l^2}$$

$$\tilde{v} = \frac{v}{h}, \quad \tilde{\psi} = \psi, \quad \tilde{\varphi} = \frac{c}{2}\varphi, \quad \tilde{w} = \frac{w}{l}, \quad \tilde{\theta} = \theta \qquad (3.14)$$

$$AR = \frac{2l}{c}, \quad \tilde{x}_o = \frac{2}{c}x_o,$$

where like the case of aircraft wings $\mathcal{AR}$ denotes the beam aspect ratio. The coefficients of matrices $\tilde{A}$, $\tilde{B}$, and $\tilde{D}$ are nondimensional counterparts of rigidity quantities, being defined as

$$(\tilde{A}_{ij}, \tilde{B}_{ij}, \tilde{D}_{ij}) = \int_{-1/2}^{1/2} \bar{Q}_{ij}(1, \tilde{z}, \tilde{z}^2) dz, \quad i,j = 1,2,3 \tag{3.15}$$

whereas the mass terms $\tilde{m}_1$, $\tilde{m}_2$, and $\tilde{m}_3$ are defined as

$$(\tilde{m}_1, \tilde{m}_2, \tilde{m}_3) = \int_{-1/2}^{1/2} \rho\ (1, \tilde{z}, \tilde{z}^2) dz, \quad i,j = 1,2,3 \tag{3.16}$$

In light of Eqs. (3.14-16), the governing equations become

$$\left(\tilde{A}_{22}\tilde{v}_{,\tilde{y}} + \tilde{B}_{22}\tilde{\psi}_{,\tilde{y}} + \delta_w \tilde{B}_{22}\tilde{\varphi}_{,\tilde{y}} + \tilde{B}_{26}\tilde{\theta}_{,\tilde{y}} + \mathcal{AR}\ \tilde{B}_{26}\tilde{\varphi}\right)_{,\tilde{y}}$$

$$= \tilde{m}_1\tilde{v}_{,\tilde{t}\tilde{t}} + \tilde{m}_2\tilde{\psi}_{,\tilde{t}\tilde{t}} + \tilde{m}_2\tilde{\varphi}_{,\tilde{t}\tilde{t}}$$

$$\left[\tilde{B}_{22}\tilde{v}_{,\tilde{y}} + \tilde{D}_{22}\tilde{\psi}_{,\tilde{y}} + \delta_w \tilde{D}_{22}\tilde{\varphi}_{,\tilde{y}} + \tilde{D}_{26}\tilde{\theta}_{,\tilde{y}} + \mathcal{AR}\ \tilde{D}_{26}\tilde{\varphi}\right]_{,\tilde{y}}$$

$$- \left(\frac{l}{h}\right)^2 \left[\tilde{A}_{55}\tilde{\psi} + \tilde{A}_{55}\tilde{\varphi} + \tilde{A}_{55}\tilde{w}_{,\tilde{y}} + \frac{1}{\mathcal{AR}}\tilde{A}_{55}\left((\tilde{x}_o\tilde{\theta})_{,\tilde{y}} - \tilde{\theta}_{,\tilde{y}}\right)\right]$$

$$= \tilde{m}_3\tilde{\psi}_{,\tilde{t}\tilde{t}} + \tilde{m}_2\tilde{v}_{,\tilde{t}\tilde{t}} + \tilde{m}_3\tilde{\varphi}_{,\tilde{t}\tilde{t}}$$

$$\left[\delta_w\tilde{B}_{22}\tilde{v}_{,\tilde{y}} + \delta_w\tilde{D}_{22}\tilde{\psi}_{,\tilde{y}} + \frac{4}{3}\delta_w\tilde{D}_{22}\tilde{\varphi}_{,\tilde{y}} + \delta_w\tilde{D}_{26}\tilde{\theta}_{,\tilde{y}} + \mathcal{AR}\ \tilde{D}_{26}\tilde{\varphi}\right]_{,\tilde{y}}$$

$$- \mathcal{AR}\left[\tilde{B}_{26}\tilde{v}_{,\tilde{y}} + \tilde{D}_{26}\tilde{\psi}_{,\tilde{y}} + \tilde{D}_{26}\tilde{\varphi}_{,\tilde{y}} + \tilde{D}_{66}\tilde{\theta}_{,\tilde{y}} + \mathcal{AR}\ \tilde{D}_{66}\tilde{\varphi}\right] \tag{3.17}$$

$$- \left(\frac{l}{h}\right)^2 \left[\tilde{A}_{55}\tilde{\psi} + \frac{4}{3}\tilde{A}_{55}\tilde{\varphi} + \tilde{A}_{55}\tilde{w}_{,\tilde{y}} + \frac{1}{\mathcal{AR}}\tilde{A}_{55}\left((\tilde{x}_o\tilde{\theta})_{,\tilde{y}} - \frac{4}{3}\tilde{\theta}_{,\tilde{y}}\right)\right]$$

$$= \frac{4}{3}\tilde{m}_3\tilde{\varphi}_{,\tilde{t}\tilde{t}} + \tilde{m}_2\tilde{v}_{,\tilde{t}\tilde{t}} + \tilde{m}_3\tilde{\psi}_{,\tilde{t}\tilde{t}}$$

$$\left(\frac{l}{h}\right)^2\left[\tilde{A}_{55}\tilde{\psi}+\tilde{A}_{55}\tilde{\varphi}+\tilde{A}_{55}\tilde{w}_{,\tilde{y}}+\frac{1}{AR}\tilde{A}_{55}\left((\tilde{x}_o\tilde{\theta})_{,\tilde{y}}-\tilde{\theta}_{,\tilde{y}}\right)\right]_{,\tilde{y}}$$
$$=\left(\frac{l}{h}\right)^2\tilde{m}_1\tilde{w}_{,\tilde{t}\tilde{t}}-\frac{1}{AR}\left(\frac{l}{h}\right)^2(1-\tilde{x}_o)\tilde{m}_1\tilde{\theta}_{,\tilde{t}\tilde{t}}$$

$$\left[\tilde{B}_{26}\tilde{v}_{,\tilde{y}}+\tilde{D}_{26}\tilde{\psi}_{,\tilde{y}}+\delta_w\tilde{D}_{26}\tilde{\varphi}_{,\tilde{y}}+\tilde{D}_{66}\tilde{\theta}_{,\tilde{y}}+AR\ \tilde{D}_{66}\tilde{\varphi}\right]_{,\tilde{y}}$$
$$-\left[\frac{1}{AR}\left(\frac{l}{h}\right)^2\tilde{A}_{55}\tilde{\psi}+\frac{4}{3}\frac{1}{AR}\left(\frac{l}{h}\right)^2\tilde{A}_{55}\tilde{\varphi}+\frac{1}{AR}\left(\frac{l}{h}\right)^2\tilde{A}_{55}\tilde{w}_{,\tilde{y}}\right.$$
$$\left.+\left(\frac{1}{AR}\right)^2\left(\frac{l}{h}\right)^2\tilde{A}_{55}(\tilde{x}_o\tilde{\theta})_{,\tilde{y}}-\left(\frac{4}{3}\right)\left(\frac{1}{AR}\right)^2\left(\frac{l}{h}\right)^2\tilde{A}_{55}\tilde{\theta}_{,\tilde{y}}\right]_{,\tilde{y}}$$
$$+\frac{\tilde{x}_o}{AR}\left(\frac{l}{h}\right)^2\left[\tilde{A}_{55}\tilde{\psi}+\tilde{A}_{55}\tilde{\varphi}+\tilde{A}_{55}\tilde{w}_{,\tilde{y}}+\frac{1}{AR}\tilde{A}_{55}(\tilde{x}_o\tilde{\theta})_{,\tilde{y}}-\frac{1}{AR}\tilde{A}_{55}\tilde{\theta}_{,\tilde{y}}\right]_{,\tilde{y}}$$
$$=\left[\tilde{m}_3+\left(\frac{1}{AR}\right)^2\left(\frac{l}{h}\right)^2\left(\frac{4}{3}-2\tilde{x}_o+\tilde{x}_o^2\right)\tilde{m}_1\right]\tilde{\theta}_{,\tilde{t}\tilde{t}}-\frac{1}{AR}\left(\frac{l}{h}\right)^2(1-\tilde{x}_o)\tilde{m}_1\tilde{w}_{,\tilde{t}\tilde{t}}$$

The transformed boundary conditions become:

At the root, $\tilde{y}=0$,

$$v=0,\qquad \tilde{\psi}=0,\qquad \tilde{\varphi}=0,\qquad \tilde{w}=0,\qquad \tilde{\theta}=0, \tag{3.18}$$

and at tip, $\tilde{y}=1$,

$$\tilde{A}_{22}\tilde{v}_{,\tilde{y}}+\tilde{B}_{22}\tilde{\psi}_{,\tilde{y}}+\delta_w\tilde{B}_{22}\tilde{\varphi}_{,\tilde{y}}+\tilde{B}_{26}\tilde{\theta}_{,\tilde{y}}+AR\tilde{B}_{26}\tilde{\varphi}=0$$

$$\tilde{B}_{22}\tilde{v}_{,\tilde{y}}+\tilde{D}_{22}\tilde{\psi}_{,\tilde{y}}+\delta_w\tilde{D}_{22}\tilde{\varphi}_{,\tilde{y}}+\tilde{D}_{26}\tilde{\theta}_{,\tilde{y}}+AR\tilde{D}_{26}\tilde{\varphi}=0$$

$$\delta_w\tilde{B}_{22}\tilde{v}_{,\tilde{y}}+\delta_w\tilde{D}_{22}\tilde{\psi}_{,\tilde{y}}+\frac{4}{3}\delta_w\tilde{D}_{22}\tilde{\varphi}_{,\tilde{y}}+\delta_w\tilde{D}_{26}\tilde{\theta}_{,\tilde{y}}+AR\ \tilde{D}_{26}\tilde{\varphi}=0 \tag{3.19}$$

$$\tilde{A}_{55}\tilde{\psi} + \tilde{A}_{55}\tilde{\varphi} + \tilde{A}_{55}\tilde{w}_{,\tilde{y}} + \frac{1}{\cancel{R}}\tilde{A}_{55}(\tilde{x}_o\tilde{\theta})_{,\tilde{y}} - \frac{1}{\cancel{R}}\tilde{A}_{55}\tilde{\theta}_{,\tilde{y}} = 0$$

$$\tilde{B}_{26}\tilde{v}_{,\tilde{y}} + \tilde{D}_{26}\tilde{\psi}_{,\tilde{y}} + \delta_w\tilde{D}_{26}\tilde{\varphi}_{,\tilde{y}} + \tilde{D}_{66}\tilde{\theta}_{,\tilde{y}} + \cancel{R}\ \tilde{D}_{66}\tilde{\varphi}$$
$$- \left[\frac{1}{\cancel{R}}\left(\frac{l}{h}\right)^2\tilde{A}_{55}\tilde{\psi} + \frac{4}{3}\frac{1}{\cancel{R}}\left(\frac{l}{h}\right)^2\tilde{A}_{55}\tilde{\varphi} + \frac{1}{\cancel{R}}\left(\frac{l}{h}\right)^2\tilde{A}_{55}\tilde{w}_{,\tilde{y}}\right.$$
$$\left. + \left(\frac{1}{\cancel{R}}\right)^2\left(\frac{l}{h}\right)^2\tilde{A}_{55}(\tilde{x}_o\tilde{\theta})_{,\tilde{y}} - \left(\frac{4}{3}\right)\left(\frac{1}{\cancel{R}}\right)^2\left(\frac{l}{h}\right)^2\tilde{A}_{55}\tilde{\theta}_{,\tilde{y}}\right] = 0$$

3.2.2 The Classical Beam Theory:

When

$$\psi = -w_{,y} - (x_0\theta)_{,y} \quad and \quad \varphi = \theta_{,y} \tag{3.20}$$

the transverse shear strains become zero, implying the adoption of Bernoulli-Euler's structural model.

Upon paralleling the steps described previously, the three governing equations expressed in terms of v, w, θ are obtained as

$$\left[A_{22}v_{,y} - B_{22}w_{,yy} + (\frac{c}{2} - x_o)B_{22}\theta_{,yy} + 2B_{26}\theta_{,y}\right]_{,y} = m_1\ddot{v}$$

$$\left[B_{22}v_{,y} - D_{22}w_{,yy} + (\frac{c}{2} - x_o)D_{22}\theta_{,yy} + 2D_{26}\theta_{,y}\right]_{,yy} + \mathcal{P}$$
$$= m_1\ddot{w} - (\frac{c}{2} - x_o)m_1\ddot{\theta} \tag{3.21}$$

$$(\frac{c}{2} - x_o)B_{22}v_{,yyy} - 2B_{26}v_{,yy} - (\frac{c}{2} - x_o)D_{22}w_{,yyyy} + 2D_{26}w_{,yyy}$$
$$+\delta_w(\frac{c^2}{3} - x_oc + x_o^2)D_{22}\theta_{,yyyy} + (1 - \delta_w)(c - 2x_o)D_{26}\theta_{,yyy} - 4D_{66}\theta_{,yy} + \mathcal{T}$$

$$= \left[m_3 + \left(\frac{c^2}{3} - x_o c + x_o^2 \right) m_1 \right] \ddot{\theta} - (\frac{c}{2} - x_o) m_1 \ddot{w}$$

whereas the associated boundary conditions are:

At $y = 0$,

$$v = 0, \qquad w = 0, \qquad w_{,y} = 0 \qquad \theta = 0, \qquad \theta_{,y} = 0 \tag{3.22}$$

and at $y = l$,

$$A_{22} v_{,y} - B_{22} w_{,yy} + (\frac{c}{2} - x_o) B_{22} \theta_{,yy} + 2B_{26} \theta_{,y} = 0$$

$$\left[B_{22} v_{,y} - D_{22} w_{,yy} + (\frac{c}{2} - x_o) D_{22} \theta_{,yy} + 2D_{26} \theta_{,y} \right]_{,y} = 0$$

$$B_{22} v_{,y} - D_{22} w_{,yy} + (\frac{c}{2} - x_o) D_{22} \theta_{,yy} + 2D_{26} \theta_{,y} = 0 \tag{3.23}$$

$$(\frac{c}{2} - x_o) B_{22} v_{,yy} - 2B_{26} v_{,y} - (\frac{c}{2} - x_o) D_{22} w_{,yyy} + 2D_{26} w_{,yy}$$
$$+ \delta_w (\frac{c^2}{3} - x_o c + x_o^2) D_{22} \theta_{,yyy} + (1 - \delta_w)(c - 2x_o) D_{26} \theta_{,yy} - 4D_{66} \theta_{,y} = 0$$

When the tangential inertia term is discarded, the original governing equations can be simplified. Toward this end, it is readily seen that the first equation $(3.21)_1$ becomes

$$v_{,y} = \frac{B_{22}}{A_{22}} w_{,yy} - (\frac{c}{2} - x_o) \frac{B_{22}}{A_{22}} \theta_{,yy} - \frac{2B_{26}}{A_{22}} \theta_{,y} \tag{3.24}$$

Substituting $v_{,y}$ into Eqs. (3.21-23) yields an eighth-order governing equation system expressed in terms of w and θ only,

$$- \left[\bar{D}_{22} w_{,yy} - (\frac{c}{2} - x_o) \bar{D}_{22} \theta_{,yy} - \bar{D}_{26} \theta_{,y} \right]_{,yy} + \mathcal{P}$$
$$= m_1 \ddot{w} - (\frac{c}{2} - x_o) m_1 \ddot{\theta} \tag{3.25}$$

$$-\left[\frac{c^2}{12}\delta_w D_{22}+(\delta_w D_{22}-\frac{B_{22}^2}{A_{22}})(\frac{c^2}{4}-x_o c+x_o^2)\right]\theta_{,yyyy}$$

$$-(1-\delta_w)(c-2x_o)D_{26}\theta_{,yyy}+\bar{D}_{66}\theta_{,yy}+(\frac{c}{2}-x_o)\bar{D}_{22}w_{,yyyy}-\bar{D}_{26}w_{,yyy}+\mathcal{T}$$

$$=\left[m_3+\left(\frac{c^2}{3}-x_o c+x_o^2\right)m_1\right]\ddot{\theta}-(\frac{c}{2}-x_o)m_1\ddot{w}$$

where $\bar{D}_{22}, \bar{D}_{26}$ and $\bar{D}_{66}$ are coupling rigidities defined as

$$\bar{D}_{22}=\left(D_{22}-\frac{B_{22}^2}{A_{22}}\right), \bar{D}_{26}=2\left(D_{26}-\frac{B_{22}B_{26}}{A_{22}}\right), \bar{D}_{66}=4\left(D_{66}-\frac{B_{26}^2}{A_{22}}\right) \quad (3.26)$$

In a similar way , the boundary conditions modify as

at $y=0$

$$w=0, \qquad w_{,y}=0, \qquad \theta=0, \qquad \theta_{,y}=0 \quad (3.27)$$

at $y=l$

$$\left[\bar{D}_{22}w_{,yy}-(\frac{c}{2}-x_o)\bar{D}_{22}\theta_{,yy}-\bar{D}_{26}\theta_{,y}\right]_{,y}=0$$

$$\bar{D}_{22}w_{,yy}-(\frac{c}{2}-x_o)\bar{D}_{22}\theta_{,yy}-\bar{D}_{26}\theta_{,y}=0$$

$$\left[\frac{c^2}{12}\delta_w D_{22}+(\delta_w D_{22}-\frac{B_{22}^2}{A_{22}})(\frac{c^2}{4}-x_o c+x_o^2)\right]\theta_{,yyy} \quad (3.28)$$

$$+(1-\delta_w)(c-2x_o)D_{26}\theta_{,yy}-\bar{D}_{66}\theta_{,y}-(\frac{c}{2}-x_o)\bar{D}_{22}w_{,yyy}+\bar{D}_{26}w_{,yy}=0$$

$$\left[\frac{c^2}{12}\delta_w D_{22}+(\delta_w D_{22}-\frac{B_{22}^2}{A_{22}})(\frac{c^2}{4}-x_o c+x_o^2)\right]\theta_{,yy}$$

$$+(1-\delta_w)(c-2x_o)D_{26}\theta_{,y}-(\frac{c}{2}-x_o)\bar{D}_{22}w_{,yy}=0$$

Moreover, if the elastic axis is located at the mid-chord, the governing equations become identical to the ones given by Librescu and Simovich [19].

$$-\left[\bar{D}_{22}w_{,yyyy}-\bar{D}_{26}\theta_{,yyy}\right]+\mathcal{P}=m_1\ddot{w}$$

$$-\left[\frac{c^2}{12}\delta_w D_{22}\theta_{,yyy} - \bar{D}_{66}\theta_{,yy} + \bar{D}_{26}w_{,yyy}\right] + \mathcal{T} = (m_3 + \frac{c^2}{12}m_1)\ddot{\theta} \tag{3.29}$$

The boundary conditions at $y = 0$ remain unchanged, being expressed as

$$w = 0, \qquad w_{,y} = 0, \qquad \theta = 0, \qquad \delta_w\theta_{,y} = 0 \tag{3.30}$$

whereas the boundary conditions at $y = l$ modify to

$$\bar{D}_{22}w_{,yyy} - \bar{D}_{26}\theta_{,yy} = 0, \qquad \bar{D}_{22}w_{,yy} - \bar{D}_{26}\theta_{,y} = 0$$

$$\frac{c^2}{12}\delta_w D_{22}\theta_{,yyy} - \bar{D}_{66}\theta_{,y} + \bar{D}_{26}w_{,yy} = 0, \qquad \delta_w D_{22}\theta_{,yy} = 0 \tag{3.31}$$

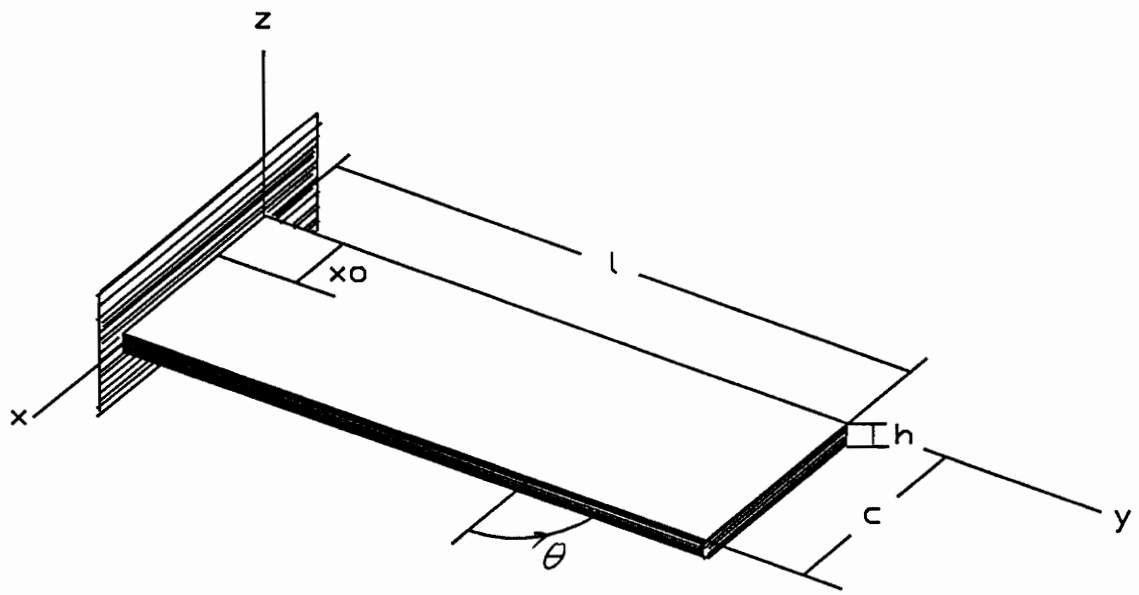

Figure 3.1 Coordinate system and geometry of cantilevered structure.

4. FREE VIBRATION ANALYSIS

4.1 Overview

With the recent advances in materials science, in general, and in fiber-reinforced composite materials, in particular, and as a result of their integration in the advanced structures of flight vehicles, it becomes a necessity to investigate the dynamic characteristics of structures composed of new materials. For this purpose, a number of investigations devoted to the study of free vibrations of cantilevered beams composed of fiber-reinforced composite materials have been accomplished. Besides shear deformation effects, bending-twist coupling plays an important role in anisotropic material structures.

In the following section, in order to analyze the dynamic characteristics of cantilevered beam-type structures, spatial discretization techniques are employed. To this end, approximate methods, such as the Rayleigh-Ritz, the Extended-Galerkin, and the Finite Element, are used, and then compared to each other to insure the accuracy of the results. Furthermore, a convergence study and accuracy analysis are performed for specially laminated structures to guarantee accurate solutions, comparing the results by these methods to exact solutions.

4.2 Variational Formulation

This section deals with the development of discretized models of cantilevered laminated structures. When the exact solution is not available, approximate solutions must be found. The variational formulation is applied to the system, which consists of simultaneous, coupled, partial differential equations of motion. Several

discretization techniques are applied to find approximate solutions for the vibration problem . Toward this end, the partial differential equations of motion will be reduced to an algebraic eigenvalue problem. Dealing with the free vibration problem, the loading terms are discarded.

4.2.1 Rayleigh-Ritz Formulation:

The following assumed mode shapes for $\tilde{v}, \tilde{\psi}, \tilde{\varphi}, \tilde{w}, \tilde{\theta}$ that satisfy the boundary conditions at $\tilde{y} = 0$ in Eq. (3.18) are chosen:

$$\begin{aligned}
\tilde{v}(\tilde{y},\tilde{t}) &= \sum_{k=1}^{n} C_{\bar{v}k}\bar{v}_k(\tilde{y})q_k(\tilde{t}) = \sum_{k=1}^{n} \hat{v}_k(\tilde{y})q_k(\tilde{t}) \\
\tilde{\psi}(\tilde{y},\tilde{t}) &= \sum_{k=1}^{n} C_{\bar{\psi}k}\bar{\psi}_k(\tilde{y})q_k(\tilde{t}) = \sum_{k=1}^{n} \hat{\psi}_k(\tilde{y})q_k(\tilde{t}) \\
\tilde{\varphi}(\tilde{y},\tilde{t}) &= \sum_{k=1}^{n} C_{\bar{\varphi}k}\bar{\varphi}_k(\tilde{y})q_k(\tilde{t}) = \sum_{k=1}^{n} \hat{\varphi}_k(\tilde{y})q_k(\tilde{t}) \\
\tilde{w}(\tilde{y},\tilde{t}) &= \sum_{k=1}^{n} C_{\bar{w}k}\bar{w}_k(\tilde{y})q_k(\tilde{t}) = \sum_{k=1}^{n} \hat{w}_k(\tilde{y})q_k(\tilde{t}) \\
\tilde{\theta}(\tilde{y},\tilde{t}) &= \sum_{k=1}^{n} C_{\bar{\theta}k}\bar{\theta}_k(\tilde{y})q_k(\tilde{t}) = \sum_{k=1}^{n} \hat{\theta}_k(\tilde{y})q_k(\tilde{t})
\end{aligned} \tag{4.1}$$

where $\bar{v}_k(\tilde{y}), \bar{\psi}_k(\tilde{y}), \bar{\varphi}_k(\tilde{y}), \bar{w}_k(\tilde{y}), \bar{\theta}_k(\tilde{y})$ are global admissible functions and $q(\tilde{t})$ are generalized coordinates. Upon substituting Eqs. (4.1) into the governing system equations (3.17), followed by their integration over the entire domain, we obtain the eigenvalue problem

$$([K] - \lambda[M])\{u\} = \{0\} \tag{4.2}$$

where $[K]$, $[M]$ are stiffness and mass matrices, and λ, u are the eigenvalues and eigenvectors of nodal displacements corresponding to an eigenvalue, respectively.

The natural frequencies are $\omega=\sqrt{\lambda}$ and the modes of bending and torsion are in the form of

$$W_r(\tilde{y}) = \sum_{k=1}^{n} \bar{w}_k(\tilde{y})\phi_{kr}, \quad \Theta_r(\tilde{y}) = \sum_{k=1}^{n} \bar{\theta}_k(\tilde{y})\phi_{kr}, \quad r = 1, 2, \ldots n \tag{4.3}$$

where ϕ_{kr} is the kth component of the eigenvector ϕ_r.

In detail, the coefficient elements in the mass matrix and stiffness matrix are

$$[M] = \begin{bmatrix} M^{\tilde{v}\tilde{v}} & M^{\tilde{v}\tilde{\psi}} & M^{\tilde{v}\tilde{\varphi}} & M^{\tilde{v}\tilde{w}} & M^{\tilde{v}\tilde{\theta}} \\ M^{\tilde{\psi}\tilde{v}} & M^{\tilde{\psi}\tilde{\psi}} & M^{\tilde{\psi}\tilde{\varphi}} & M^{\tilde{\psi}\tilde{w}} & M^{\tilde{\psi}\tilde{\theta}} \\ M^{\tilde{\varphi}\tilde{v}} & M^{\tilde{\varphi}\tilde{\psi}} & M^{\tilde{\varphi}\tilde{\varphi}} & M^{\tilde{\varphi}\tilde{w}} & M^{\tilde{\varphi}\tilde{\theta}} \\ M^{\tilde{w}\tilde{v}} & M^{\tilde{w}\tilde{\psi}} & M^{\tilde{w}\tilde{\varphi}} & M^{\tilde{w}\tilde{w}} & M^{\tilde{w}\tilde{\theta}} \\ M^{\tilde{\theta}\tilde{v}} & M^{\tilde{\theta}\tilde{\psi}} & M^{\tilde{\theta}\tilde{\varphi}} & M^{\tilde{\theta}\tilde{w}} & M^{\tilde{\theta}\tilde{\theta}} \end{bmatrix}$$

$$[K] = \begin{bmatrix} K^{\tilde{v}\tilde{v}} & K^{\tilde{v}\tilde{\psi}} & K^{\tilde{v}\tilde{\varphi}} & K^{\tilde{v}\tilde{w}} & K^{\tilde{v}\tilde{\theta}} \\ K^{\tilde{\psi}\tilde{v}} & K^{\tilde{\psi}\tilde{\psi}} & K^{\tilde{\psi}\tilde{\varphi}} & K^{\tilde{\psi}\tilde{w}} & K^{\tilde{\psi}\tilde{\theta}} \\ K^{\tilde{\varphi}\tilde{v}} & K^{\tilde{\varphi}\tilde{\psi}} & K^{\tilde{\varphi}\tilde{\varphi}} & K^{\tilde{\varphi}\tilde{w}} & K^{\tilde{\varphi}\tilde{\theta}} \\ K^{\tilde{w}\tilde{v}} & K^{\tilde{w}\tilde{\psi}} & K^{\tilde{w}\tilde{\varphi}} & K^{\tilde{w}\tilde{w}} & K^{\tilde{w}\tilde{\theta}} \\ K^{\tilde{\theta}\tilde{v}} & K^{\tilde{\theta}\tilde{\psi}} & K^{\tilde{\theta}\tilde{\varphi}} & K^{\tilde{\theta}\tilde{w}} & K^{\tilde{\theta}\tilde{\theta}} \end{bmatrix} \tag{4.4}$$

For the Rayleigh-Ritz formulation, $[M]$ and $[K]$ are symmetric.

Mass coefficients are defined by

$$M_{rs}^{\tilde{v}\tilde{v}} = \int_0^1 \tilde{m}_1 \bar{v}_r \bar{v}_s d\tilde{y}, \qquad M_{rs}^{\tilde{v}\tilde{\psi}} = \int_0^1 \tilde{m}_2 \bar{v}_r \bar{\psi}_s d\tilde{y}, \qquad M_{rs}^{\tilde{v}\tilde{\varphi}} = \int_0^1 \tilde{m}_2 \bar{v}_r \bar{\varphi}_s d\tilde{y}$$

$$M_{rs}^{\tilde{v}w} = M_{rs}^{\tilde{v}\tilde{\theta}} = 0$$

$$M_{rs}^{\tilde{\psi}\tilde{\psi}} = \int_0^1 \tilde{m}_3 \bar{\psi}_r \bar{\psi}_s d\tilde{y}, \qquad M_{rs}^{\tilde{\psi}\tilde{\varphi}} = \int_0^1 \tilde{m}_3 \bar{\psi}_r \bar{\varphi}_s d\tilde{y}, \qquad M_{rs}^{\tilde{\psi}\tilde{w}} = M_{rs}^{\tilde{\psi}\tilde{\theta}} = 0$$

$$M_{rs}^{\tilde{\varphi}\tilde{\varphi}} = \int_0^1 \frac{4}{3} \tilde{m}_3 \bar{\varphi}_r \bar{\varphi}_s d\tilde{y}, \qquad M_{rs}^{\tilde{\varphi}\tilde{w}} = M_{rs}^{\tilde{\varphi}\tilde{\theta}} = 0 \tag{4.5}$$

$$M_{rs}^{\tilde{w}\tilde{w}} = \int_0^1 \left(\frac{l}{h}\right)^2 \tilde{m}_1 \bar{w}_r \bar{w}_s d\tilde{y}, \qquad M_{rs}^{\tilde{w}\tilde{\theta}} = -\int_0^1 \frac{1}{AR} \left(\frac{l}{h}\right)^2 (1 - \tilde{x}_o)\, \tilde{m}_1 \bar{w}_r \bar{\theta}_s d\tilde{y}$$

$$M_{rs}^{\tilde{\theta}\tilde{\theta}} = \int_0^1 \left[\tilde{m}_3 + \left(\frac{1}{AR}\right)^2 \left(\frac{l}{h}\right)^2 \left(\frac{4}{3} - 2\tilde{x}_o + \tilde{x}_o^2\right) \tilde{m}_1\right] \bar{\theta}_r \bar{\theta}_s d\tilde{y}$$

The stiffness coefficients are defined by

$$K_{rs}^{\tilde{v}\tilde{v}} = \int_0^1 \tilde{A}_{22}\bar{v}_{r,\tilde{y}}\,\bar{v}_{s,\tilde{y}}\,d\tilde{y}, \qquad K_{rs}^{\tilde{v}\tilde{\psi}} = \int_0^1 \tilde{B}_{22}\bar{v}_{r,\tilde{y}}\,\bar{\psi}_{s,\tilde{y}}\,d\tilde{y}$$

$$K_{rs}^{\tilde{v}\tilde{\varphi}} = \int_0^1 \left[\delta_w \tilde{B}_{22}\bar{v}_{r,\tilde{y}}\,\bar{\varphi}_{s,\tilde{y}} + \mathcal{R}\,\tilde{B}_{26}\bar{v}_{r,\tilde{y}}\,\bar{\varphi}_s\right] d\tilde{y}$$

$$K_{rs}^{\tilde{v}\tilde{w}} = 0, \qquad K_{rs}^{\tilde{v}\tilde{\theta}} = \int_0^1 \tilde{B}_{26}\bar{v}_{r,\tilde{y}}\,\bar{\theta}_{s,\tilde{y}}\,d\tilde{y}$$

$$K_{rs}^{\tilde{\psi}\tilde{\psi}} = \int_0^1 \left[\tilde{D}_{22}\bar{\psi}_{r,\tilde{y}}\,\bar{\psi}_{s,\tilde{y}} + \left(\frac{l}{h}\right)^2 \tilde{A}_{55}\bar{\psi}_r\bar{\psi}_s\right] d\tilde{y}$$

$$K_{rs}^{\tilde{\psi}\tilde{\varphi}} = \int_0^1 \left[\delta_w \tilde{D}_{22}\bar{\psi}_{r,\tilde{y}}\,\bar{\varphi}_{s,\tilde{y}} + \mathcal{R}\,\tilde{D}_{26}\bar{\psi}_{r,\tilde{y}}\,\bar{\varphi}_s + \left(\frac{l}{h}\right)^2 \tilde{A}_{55}\bar{\psi}_r\bar{\varphi}_s\right] d\tilde{y}$$

$$K_{rs}^{\tilde{\psi}\tilde{w}} = \int_0^1 \left(\frac{l}{h}\right)^2 \tilde{A}_{55}\bar{\psi}_r\bar{w}_{s,\tilde{y}}\,d\tilde{y}$$

$$K_{rs}^{\tilde{\psi}\tilde{\theta}} = \int_0^1 \left[\tilde{D}_{26}\bar{\psi}_{r,\tilde{y}}\,\bar{\theta}_{s,\tilde{y}} + \frac{1}{\mathcal{R}}\left(\frac{l}{h}\right)^2 \tilde{A}_{55}\bar{\psi}_r\left(\left(\tilde{x}_o\bar{\theta}_s\right)_{,\tilde{y}} - \bar{\theta}_{s,\tilde{y}}\right)\right] d\tilde{y}$$

$$K_{rs}^{\tilde{\varphi}\tilde{\varphi}} = \int_0^1 \Bigg[\frac{4}{3}\,\delta_w \tilde{D}_{22}\bar{\varphi}_{r,\tilde{y}}\,\bar{\varphi}_{s,\tilde{y}} + \mathcal{R}\,\tilde{D}_{26}\bar{\varphi}_{r,\tilde{y}}\,\bar{\varphi}_s + \mathcal{R}\,\tilde{D}_{26}\bar{\varphi}_r\bar{\varphi}_{s,\tilde{y}} + \left(\mathcal{R}^2\,\tilde{D}_{66} + \frac{4}{3}\left(\frac{l}{h}\right)^2 \tilde{A}_{55}\right)\bar{\varphi}_r\bar{\varphi}_s\Bigg] d\tilde{y}$$

$$K_{rs}^{\tilde{\varphi}\tilde{w}} = \int_0^1 \left(\frac{l}{h}\right)^2 \tilde{A}_{55}\bar{\varphi}_r\bar{w}_{s,\tilde{y}}\,d\tilde{y} \tag{4.6}$$

$$K_{rs}^{\tilde{\varphi}\tilde{\theta}} = \int_0^1 \left[\delta_w \tilde{D}_{26}\bar{\varphi}_{r,\tilde{y}}\,\bar{\theta}_{s,\tilde{y}} + \mathcal{R}\,\tilde{D}_{66}\bar{\varphi}_r\bar{\theta}_{s,\tilde{y}} + \frac{1}{\mathcal{R}}\left(\frac{l}{h}\right)^2 \tilde{A}_{55}\bar{\varphi}_r\left(\left(\tilde{x}_o\bar{\theta}_s\right)_{,\tilde{y}} - \frac{4}{3}\,\bar{\theta}_{s,\tilde{y}}\right)\right] d\tilde{y}$$

$$K_{rs}^{\tilde{w}\tilde{w}} = \int_0^1 \left(\frac{l}{h}\right)^2 \tilde{A}_{55}\bar{w}_{r,\tilde{y}}\,\bar{w}_{s,\tilde{y}}\,d\tilde{y}$$

$$K_{rs}^{\tilde{w}\tilde{\theta}} = \int_0^1 \left[\frac{1}{\mathcal{R}}\left(\frac{l}{h}\right)^2 \tilde{A}_{55}\bar{w}_{r,\tilde{y}}\left(\left(\tilde{x}_o\bar{\theta}_s\right)_{,\tilde{y}} - \bar{\theta}_{s,\tilde{y}}\right)\right] d\tilde{y}$$

$$K_{rs}^{\tilde{\theta}\tilde{\theta}} = \int_0^1 \left[\tilde{D}_{66}\bar{\theta}_{r,\tilde{y}}\,\bar{\theta}_{s,\tilde{y}} - \frac{1}{\mathcal{R}^2}\left(\frac{l}{h}\right)^2 \tilde{A}_{55}\bar{\theta}_{r,\tilde{y}}\left(\left(\tilde{x}_o\bar{\theta}_s\right)_{,\tilde{y}} - \frac{4}{3}\tilde{\theta}_{s,\tilde{y}}\right)\right.$$

$$+\frac{1}{AR^2}\left(\frac{l}{h}\right)^2 \tilde{A}_{55}\left(\tilde{x}_o\bar{\theta}_r\right)_{,\tilde{y}}\left(\left(\tilde{x}_o\bar{\theta}_s\right)_{,\tilde{y}}-\bar{\theta}_{s,\tilde{y}}\right)\Bigg]d\tilde{y}$$

4.2.2 Extended-Galerkin Formulation:

Within the Extended-Galerkin method (Ref. [25]), the natural boundary conditions are retained in the variational formulation rather than only essential boundary conditions kept in the Rayleigh-Ritz method. In this case,

$$K_{rs}^{\tilde{v}\tilde{v}} = -\int_0^1 \tilde{A}_{22}\bar{v}_r\bar{v}_{s,\tilde{y}\tilde{y}}\,d\tilde{y} + \tilde{A}_{22}\bar{v}_r(1)\bar{v}_s(1)_{,\tilde{y}}$$

$$K_{rs}^{\tilde{v}\tilde{\psi}} = -\int_0^1 \tilde{B}_{22}\bar{v}_r\bar{\psi}_{s,\tilde{y}\tilde{y}}\,d\tilde{y} + \tilde{B}_{22}\bar{v}_r(1)\bar{\psi}_s(1)_{,\tilde{y}}$$

$$K_{rs}^{\tilde{v}\tilde{\varphi}} = -\int_0^1 \left[\delta_w\tilde{B}_{22}\bar{v}_r\bar{\varphi}_{s,\tilde{y}\tilde{y}} + AR\ \tilde{B}_{26}\bar{v}_r\bar{\varphi}_{s,\tilde{y}}\right]d\tilde{y} + \delta_w\tilde{B}_{22}\bar{v}_r(1)\bar{\varphi}_s(1)_{,\tilde{y}} + AR\,\tilde{B}_{26}\bar{v}_r(1)\bar{\varphi}_s(1)$$

$$K_{rs}^{\tilde{v}\tilde{w}} = 0$$

$$K_{rs}^{\tilde{v}\tilde{\theta}} = -\int_0^1 \tilde{B}_{26}\bar{v}_r\bar{\theta}_{s,\tilde{y}\tilde{y}}\,d\tilde{y} + \tilde{B}_{26}\bar{v}_r(1)\bar{\theta}_s(1)_{,\tilde{y}}$$

$$K_{rs}^{\tilde{\psi}v} = -\int_0^1 \tilde{B}_{22}\bar{\psi}_r\bar{v}_{s,\tilde{y}\tilde{y}}\,d\tilde{y} + \tilde{B}_{22}\bar{\psi}_r(1)\bar{v}_s(1)_{,\tilde{y}}$$

$$K_{rs}^{\tilde{\psi}\tilde{\psi}} = \int_0^1 \left[-\tilde{D}_{22}\bar{\psi}_r\bar{\psi}_{s,\tilde{y}\tilde{y}} + \left(\frac{l}{h}\right)^2 \tilde{A}_{55}\bar{\psi}_r\bar{\psi}_s\right]d\tilde{y} + \tilde{D}_{22}\bar{\psi}_r(1)\bar{\psi}_s(1)_{,\tilde{y}}$$

$$K_{rs}^{\tilde{\psi}\tilde{\varphi}} = \int_0^1 \left[-\delta_w\tilde{D}_{22}\bar{\psi}_r\bar{\varphi}_{s,\tilde{y}\tilde{y}} - AR\ \tilde{D}_{26}\bar{\psi}_r\bar{\varphi}_{s,\tilde{y}} + \left(\frac{l}{h}\right)^2 \tilde{A}_{55}\bar{\psi}_r\bar{\varphi}_s\right]d\tilde{y}$$

$$+\delta_w\tilde{D}_{22}\bar{\psi}_r(1)\bar{\varphi}_s(1)_{,\tilde{y}} + AR\ \tilde{D}_{26}\bar{\psi}_r(1)\bar{\varphi}_s(1)$$

$$K_{rs}^{\tilde{\psi}\tilde{w}} = \int_0^1 \left(\frac{l}{h}\right)^2 \tilde{A}_{55}\bar{\psi}_r\bar{w}_{s,\tilde{y}}\,d\tilde{y} \quad ,$$

$$K_{rs}^{\tilde{\psi}\tilde{\theta}} = \int_0^1 \left[-\tilde{D}_{26}\bar{\psi}_r\bar{\theta}_{s,\tilde{y}\tilde{y}} + \frac{1}{AR}\left(\frac{l}{h}\right)^2 \tilde{A}_{55}\bar{\psi}_r\left(\left(\tilde{x}_o\bar{\theta}_s\right)_{,\tilde{y}} - \bar{\theta}_{s,\tilde{y}}\right)\right]d\tilde{y} + \tilde{D}_{26}\bar{\psi}_r(1)\bar{\theta}_s(1)_{,\tilde{y}}$$

$$K_{rs}^{\tilde{\varphi}\tilde{v}} = \int_0^1 \left[-\delta_w \tilde{B}_{22} \bar{\varphi}_r \bar{v}_{s,\tilde{y}\tilde{y}} + \mathcal{R}\, \tilde{B}_{26} \bar{\varphi}_r \bar{v}_{s,\tilde{y}} \right] d\tilde{y} + \delta_w \tilde{B}_{22} \bar{\varphi}_r(1) \bar{v}_s(1)_{,\tilde{y}}$$

$$K_{rs}^{\tilde{\varphi}\tilde{\psi}} = \int_0^1 \left[-\delta_w \tilde{D}_{22} \bar{\varphi}_r \bar{\psi}_{s,\tilde{y}\tilde{y}} + \mathcal{R}\, \tilde{D}_{26} \bar{\varphi}_r \bar{\psi}_{s,\tilde{y}} + \left(\frac{l}{h}\right)^2 \tilde{A}_{55} \bar{\varphi}_r \bar{\psi}_s \right] d\tilde{y} + \delta_w \tilde{D}_{22} \bar{\varphi}_r(1) \bar{\psi}_s(1)_{,\tilde{y}}$$

$$K_{rs}^{\tilde{\varphi}\tilde{\varphi}} = \int_0^1 \left[-\frac{4}{3}\, \delta_w \tilde{D}_{22} \bar{\varphi}_r \bar{\varphi}_{s,\tilde{y}\tilde{y}} + \mathcal{R}^2\, \tilde{D}_{66} \bar{\varphi}_r \bar{\varphi}_s + \frac{4}{3} \left(\frac{l}{h}\right)^2 \tilde{A}_{55} \bar{\varphi}_r \bar{\varphi}_s \right] d\tilde{y}$$

$$+ \frac{4}{3}\, \delta_w \tilde{D}_{22} \bar{\varphi}_r(1) \bar{\varphi}_s(1)_{,\tilde{y}} + \mathcal{R}\, \tilde{D}_{26} \bar{\varphi}_r(1) \bar{\varphi}_s(1)$$

$$K_{rs}^{\tilde{\varphi}\tilde{w}} = \int_0^1 \left(\frac{l}{h}\right)^2 \tilde{A}_{55} \bar{\varphi}_r \bar{w}_{s,\tilde{y}}\, d\tilde{y},$$

$$K_{rs}^{\tilde{\varphi}\tilde{\theta}} = \int_0^1 \left[-\delta_w \tilde{D}_{26} \bar{\varphi}_r \bar{\theta}_{s,\tilde{y}\tilde{y}} + \mathcal{R}\, \tilde{D}_{66} \bar{\varphi}_r \bar{\theta}_{s,\tilde{y}} + \frac{1}{\mathcal{R}} \left(\frac{l}{h}\right)^2 \tilde{A}_{55} \bar{\varphi}_r \left(\left(\tilde{x}_o \bar{\theta}_s\right)_{,\tilde{y}} - \frac{4}{3}\, \bar{\theta}_{s,\tilde{y}} \right) \right] d\tilde{y}$$

$$+ \delta_w \tilde{D}_{26} \bar{\varphi}_r(1) \bar{\theta}_s(1)_{,\tilde{y}}$$

$$K_{rs}^{\tilde{w}\tilde{v}} = 0$$

$$K_{rs}^{\tilde{w}\tilde{\psi}} = -\int_0^1 \left(\frac{l}{h}\right)^2 \tilde{A}_{55} \bar{w}_r \bar{\psi}_{s,\tilde{y}}\, d\tilde{y} + \left(\frac{l}{h}\right)^2 \tilde{A}_{55} \bar{w}_r(1) \bar{\psi}_s(1)$$

$$K_{rs}^{\tilde{w}\tilde{\varphi}} = -\int_0^1 \left(\frac{l}{h}\right)^2 \tilde{A}_{55} \bar{w}_r \bar{\varphi}_{s,\tilde{y}}\, d\tilde{y} + \left(\frac{l}{h}\right)^2 \tilde{A}_{55} \bar{w}_r(1) \bar{\varphi}_s(1)$$

$$K_{rs}^{\tilde{w}\tilde{w}} = -\int_0^1 \left(\frac{l}{h}\right)^2 \tilde{A}_{55} \bar{w}_r \bar{w}_{s,\tilde{y}\tilde{y}}\, d\tilde{y} + \left(\frac{l}{h}\right)^2 \tilde{A}_{55} \bar{w}_r(1) \bar{w}_s,(1)_{\tilde{y}}$$

$$K_{rs}^{\tilde{w}\tilde{\theta}} = -\int_0^1 \left[\frac{1}{\mathcal{R}} \left(\frac{l}{h}\right)^2 \tilde{A}_{55} \bar{w}_r \left(\left(\tilde{x}_o \bar{\theta}_s\right)_{,\tilde{y}\tilde{y}} - \bar{\theta}_{s,\tilde{y}\tilde{y}} \right) \right] d\tilde{y}$$

$$+ \frac{1}{\mathcal{R}} \left(\frac{l}{h}\right)^2 \tilde{A}_{55} \bar{w}_r(1) \left(\left(\tilde{x}_o \bar{\theta}_s(1)\right)_{,\tilde{y}} - \bar{\theta}_s(1)_{,\tilde{y}} \right)$$

$$K_{rs}^{\tilde{\theta}\tilde{v}} = -\int_0^1 \tilde{B}_{26} \bar{\theta}_r \bar{v}_{s,\tilde{y}\tilde{y}}\, d\tilde{y} + \tilde{B}_{26} \bar{\theta}_r(1) \bar{v}_s(1)_{,\tilde{y}} \tag{4.7}$$

$$K_{rs}^{\tilde{\theta}\bar{\psi}} = \int_0^1 \left[-\tilde{D}_{26}\bar{\theta}_r\bar{\psi}_{s,\tilde{y}\tilde{y}} - \frac{1}{\mathcal{R}}\left(\frac{l}{h}\right)^2 \tilde{A}_{55}((\tilde{x}_o\bar{\theta}_r) - \bar{\theta}_r)\bar{\psi}_{s,\tilde{y}} \right] d\tilde{y}$$

$$+\tilde{D}_{26}\bar{\theta}_r(1)\bar{\psi}_{s,\tilde{y}}(1) + \frac{1}{\mathcal{R}}\left(\frac{l}{h}\right)^2 \tilde{A}_{55}\left(\tilde{x}_o\bar{\theta}_r(1) - \bar{\theta}_r(1)\right)\bar{\psi}_s(1)$$

$$K_{rs}^{\tilde{\theta}\bar{\varphi}} = \int_0^1 \left[-\delta_w\tilde{D}_{26}\bar{\theta}_r\bar{\varphi}_{s,\tilde{y}\tilde{y}} - \mathcal{R}\,\tilde{D}_{66}\bar{\theta}_r\bar{\varphi}_{s,\tilde{y}} - \frac{1}{\mathcal{R}}\left(\frac{l}{h}\right)^2 \tilde{A}_{55}(\tilde{x}_o\bar{\theta}_r - \frac{4}{3}\,\bar{\theta}_r)\bar{\varphi}_{s,\tilde{y}} \right] d\tilde{y}$$

$$+\delta_w\tilde{D}_{26}\bar{\theta}_r(1)\bar{\varphi}_s(1)_{,\tilde{y}} + \mathcal{R}\,\tilde{D}_{66}\bar{\theta}_r(1)\bar{\varphi}_s(1) + \frac{1}{\mathcal{R}}\left(\frac{l}{h}\right)^2 \tilde{A}_{55}\left(\tilde{x}_o\bar{\theta}_r(1) - \frac{4}{3}\bar{\theta}_r(1)\right)\bar{\varphi}_s(1)$$

$$K_{rs}^{\tilde{\theta}\bar{w}} = \int_0^1 \left[-\frac{1}{\mathcal{R}}\left(\frac{l}{h}\right)^2 \tilde{A}_{55}\left(\tilde{x}_o\bar{\theta}_r - \bar{\theta}_r\right) w_{s,\tilde{y}\tilde{y}} \right] d\tilde{y} + \frac{1}{\mathcal{R}}\left(\frac{l}{h}\right)^2 \tilde{A}_{55}\left(\tilde{x}_o\bar{\theta}_r(1) - \bar{\theta}_r(1)\right)\bar{w}_s(1)_{,\tilde{y}}$$

$$K_{rs}^{\tilde{\theta}\tilde{\theta}} = \int_0^1 \left[-\tilde{D}_{66}\bar{\theta}_r\bar{\theta}_{s,\tilde{y}\tilde{y}} + \frac{1}{\mathcal{R}^2}\left(\frac{l}{h}\right)^2 \tilde{A}_{55}\bar{\theta}_r((\tilde{x}_o\bar{\theta}_s)_{,\tilde{y}\tilde{y}} - \frac{4}{3}\bar{\theta}_{s,\tilde{y}\tilde{y}}) \right.$$

$$\left. -\frac{1}{\mathcal{R}^2}\left(\frac{l}{h}\right)^2 \tilde{A}_{55}\left(\tilde{x}_o\bar{\theta}_r\right)\left(\left(\tilde{x}_o\bar{\theta}_s\right)_{,\tilde{y}\tilde{y}} - \bar{\theta}_{s,\tilde{y}\tilde{y}}\right) \right] d\tilde{y}$$

$$+\tilde{D}_{66}\bar{\theta}_r(1)\bar{\theta}_s(1)_{,\tilde{y}} - \frac{1}{\mathcal{R}^2}\left(\frac{l}{h}\right)^2 \tilde{A}_{55}\bar{\theta}_r(1)\left(\left(\tilde{x}_o\bar{\theta}_s(1)\right)_{,\tilde{y}} - \frac{4}{3}\bar{\theta}_s(1)_{,\tilde{y}}\right)$$

$$+\frac{1}{\mathcal{R}^2}\left(\frac{l}{h}\right)^2 \tilde{A}_{55}\left(\tilde{x}_o\bar{\theta}_r(1)\right)\left(\left(\tilde{x}_o\bar{\theta}_s(1)\right)_{,\tilde{y}} - \bar{\theta}_s(1)_{,\tilde{y}}\right)$$

4.2.3 Finite Element Formulation:

The finite element formulation based on the first-order shear deformation theory makes use of linear or higher Lagrange interpolation functions for all mode shapes. Over a small domain e, we seek a finite element approximation of $\tilde{v}, \tilde{\psi}, \tilde{\varphi}, \tilde{w}, \tilde{\theta}$ in the form

$$\sum_{k=1}^{n} C_k\xi_k(\tilde{y})q_k(\tilde{t}) \tag{4.8}$$

where $\xi_k(\tilde{y})$ are local interpolation functions and $q_k(\tilde{t})$ are nodal displacements of the cantilevered structure at the nodal points. The elements of the mass and stiffness matrices, $M^e_{rs}, K^e_{rs}, K^e_{rs'}, K^e_{r's}$, and $K^e_{r's'}$, are

$$M^e_{rs} = \int_o^h \xi_r \xi_s d\tilde{y}, \quad K^e_{rs} = \int_o^h \xi_r \xi_s d\tilde{y}, \quad K^e_{rs'} = \int_o^h \xi_r \xi_{s,\tilde{y}}\, d\tilde{y}$$

$$K^e_{r's} = \int_o^h \xi_{r,\tilde{y}}\, \xi_s d\tilde{y}, \qquad K^e_{r's'} = \int_o^h \xi_{r,\tilde{y}}\, \xi_{s,\tilde{y}}\, d\tilde{y} \tag{4.9}$$

where r, s=1, 2 for linear elements, r, s=1, 2, 3 for quadratic ones, and r, s=1, 2, 3, 4 for cubic ones. Taking the same kind of interpolation functions for each variable $\bar{v}, \bar{\varphi}, \bar{\psi}, \bar{w}, \bar{\theta}$ and using linear interpolation functions ξ_1, ξ_2 given by

$$\xi_1 = 1 - \frac{\tilde{y}}{h^e}, \qquad \xi_2 = \frac{\tilde{y}}{h^e} \tag{4.10}$$

then, mass and stiffness elements for the finite mesh h^e are

$$M^e_{rs} = \frac{h^e}{6}\begin{bmatrix} 2 & 1 \\ 1 & 2 \end{bmatrix}, \quad K^e_{rs'} = \frac{1}{2}\begin{bmatrix} -1 & 1 \\ -1 & 1 \end{bmatrix}$$

$$K^e_{r's} = \frac{1}{2}\begin{bmatrix} -1 & -1 \\ 1 & 1 \end{bmatrix}, \quad K^e_{r's'} = \frac{1}{h^e}\begin{bmatrix} 1 & -1 \\ -1 & 1 \end{bmatrix} \tag{4.11}$$

Using quadratic interpolation functions ξ_1, ξ_2, ξ_3 given by

$$\xi_1 = \frac{2(\tilde{y} - \frac{h^e}{2})(\tilde{y} - h^e)}{h^{e2}}, \qquad \xi_2 = \frac{-4\tilde{y}(\tilde{y} - h^e)}{h^{e2}}, \qquad \xi_3 = \frac{2\tilde{y}(\tilde{y} - \frac{h^e}{2})}{h^{e2}} \tag{4.12}$$

the mass and stiffness elements for the finite mesh h^e are

$$M^e_{rs} = \frac{h^e}{30}\begin{bmatrix} 4 & 2 & -1 \\ 2 & 16 & 2 \\ -1 & 2 & 4 \end{bmatrix}, \quad K^e_{rs'} = \frac{1}{6}\begin{bmatrix} -3 & 4 & -1 \\ -4 & 0 & 4 \\ 1 & -4 & 3 \end{bmatrix} \tag{4.13}$$

$$K^e_{r's} = \frac{1}{6}\begin{bmatrix} -3 & -4 & 1 \\ 4 & 0 & -4 \\ -1 & 4 & 3 \end{bmatrix}, \quad K^e_{r's'} = \frac{1}{3h^e}\begin{bmatrix} 7 & -8 & 1 \\ -8 & 16 & -8 \\ 1 & -8 & 7 \end{bmatrix}$$

Using cubic interpolation functions $\xi_1, \xi_2, \xi_3, \xi_4$ given by

$$\xi_1 = \frac{-9(\tilde{y} - \frac{h^e}{3})(\tilde{y} - \frac{2h^e}{3})(\tilde{y} - h^e)}{2h^{e3}}, \qquad \xi_2 = \frac{27\tilde{y}(\tilde{y} - \frac{2h^e}{3})(\tilde{y} - h^e)}{2h^{e3}}$$

$$\xi_3 = \frac{-27\tilde{y}(\tilde{y} - \frac{h^e}{3})(\tilde{y} - h^e)}{2h^{e3}}, \qquad \xi_4 = \frac{9\tilde{y}(\tilde{y} - \frac{h^e}{3})(\tilde{y} - \frac{2h^e}{3})}{2h^{e3}} \tag{4.14}$$

then mass and stiffness matrices are

$$M^e_{rs} = \frac{h^e}{1680}\begin{bmatrix} 128 & 99 & -36 & 19 \\ 99 & 648 & -81 & -36 \\ -36 & -81 & 648 & 99 \\ 19 & -36 & 99 & 128 \end{bmatrix}, K^e_{rs'} = \frac{1}{80}\begin{bmatrix} -40 & 57 & -24 & 7 \\ -57 & 0 & 81 & -24 \\ 24 & -81 & 0 & 57 \\ -7 & 24 & -57 & 40 \end{bmatrix}$$

$$K^e_{r's} = \frac{1}{80}\begin{bmatrix} -40 & -57 & 24 & -7 \\ 57 & 0 & -81 & 24 \\ -24 & 81 & 0 & -57 \\ 7 & -24 & 57 & 40 \end{bmatrix}, K^e_{r's'} = \frac{1}{40h^e}\begin{bmatrix} 148 & -189 & 54 & -13 \\ -189 & 432 & -297 & 54 \\ 54 & -297 & 432 & -189 \\ -13 & 54 & -189 & 148 \end{bmatrix} \tag{4.15}$$

Assembling of element matrices of M^e and K^e in Eq. (4.5) yields global matrices M and K.

4.3 Exact Solutions of Special Composite Cantilevers

For the sake of comparison and assessment of accuracy of approximate solutions, the exact solutions of equations (3.29) based on the classical lamination theory are considered. For special cases of laminated cantilevers, the bending-twist coupling rigidity $\bar{D}_{26}$ vanishes. As a result the equations become decoupled, so we can find exact solutions for the free vibration problem. The decoupled equations

$$\bar{D}_{22} w_{,yyyy} = m_1 \ddot{w} \tag{4.16}$$

$$\frac{c^2}{12}\delta_w D_{22}\theta_{,yyyy} - \bar{D}_{66}\theta_{,yy} = (m_3 + \frac{c^2}{12}m_1)\ddot{\theta}$$

govern the pure bending and twist, respectively.

The associated boundary conditions at the fixed end $y = 0$ are

$$\begin{aligned} for\ bending: &\quad w = 0, \quad w_{,y} = 0, \\ for\ twist: &\quad \theta = 0, \quad \delta_w \theta_{,y} = 0 \end{aligned} \tag{4.17}$$

at the free end $y = l$, the boundary conditions reduce to

$$\begin{aligned} for\ bending: &\quad \bar{D}_{22} w_{,yyy} = 0, \quad \bar{D}_{22} w_{,yy} = 0 \\ for\ twist: &\quad \frac{c^2}{12} \delta_w D_{22} \theta_{,yyy} - \bar{D}_{66} \theta_{,y} = 0, \quad \delta_w D_{22} \theta_{,yy} = 0 \end{aligned} \tag{4.18}$$

Upon nondimensionalizing, equations (4.16-18) will be properly modified. The dynamic equation related to the bending becomes

$$\tilde{\bar{D}}_{22} \tilde{w}_{,\tilde{y}\tilde{y}\tilde{y}\tilde{y}} = \left(\frac{l}{h}\right)^2 \tilde{m}_1 \tilde{w}_{,\tilde{t}\tilde{t}} \tag{4.19}$$

and the boundary conditions are

$$\tilde{w} = 0, \quad \tilde{w}_{,\tilde{y}} = 0, \quad at \quad \tilde{y} = 0 \tag{4.20}$$

$$\tilde{\bar{D}}_{22} \tilde{w}_{,\tilde{y}\tilde{y}\tilde{y}} = 0, \quad \tilde{\bar{D}}_{22} w_{,\tilde{y}\tilde{y}} = 0 \quad at \quad \tilde{y} = 1$$

The dynamic equation related to the torsion becomes

$$\frac{1}{3}\left(\frac{1}{\mathcal{AR}}\right)^2 \delta_w \tilde{D}_{22} \tilde{\theta}_{,\tilde{y}\tilde{y}\tilde{y}\tilde{y}} - \tilde{\bar{D}}_{66} \tilde{\theta}_{,\tilde{y}\tilde{y}} = \left[\tilde{m}_3 + \frac{1}{3}\left(\frac{1}{\mathcal{AR}}\right)^2 \left(\frac{l}{h}\right)^2 \tilde{m}_1\right] \tilde{\theta}_{,\tilde{t}\tilde{t}} \tag{4.21}$$

and the associated boundary conditions are

$$\tilde{\theta} = 0, \quad \tilde{\theta}_{,\tilde{y}} = 0 \quad at \quad \tilde{y} = 0 \tag{4.22}$$

$$\frac{1}{3}\left(\frac{1}{\mathcal{AR}}\right)^2 \delta_w \tilde{D}_{22} \tilde{\theta}_{,\tilde{y}\tilde{y}\tilde{y}} - \tilde{\bar{D}}_{66} \tilde{\theta}_{,\tilde{y}} = 0, \quad \delta_w \tilde{\bar{D}}_{22} \tilde{\theta}_{,\tilde{y}\tilde{y}} = 0 \quad at \quad \tilde{y} = 1$$

where $\tilde{}$ denote nondimensionalized quantities.

For decoupled bending vibration, the natural frequencies are $\tilde{\omega}=\beta^2\sqrt{\frac{\tilde{\bar{D}}_{22}}{\tilde{m}_1}}$, the associated characteristic equation is

$$1+\cos\beta\cosh\beta=0 \tag{4.23}$$

and the natural modes of bending vibration are

$$\tilde{W}(\tilde{y})=(\sin\beta-\sinh\beta)(\sin\beta\tilde{y}-\sinh\beta\tilde{y})+(\cos\beta-\cosh\beta)(\cos\beta\tilde{y}-\cosh\beta\tilde{y}) \tag{4.24}$$

For torsional vibration, the eigenvalue problem becomes (Ref. [11])

$$\mu\tilde{\theta}_{,\tilde{y}\tilde{y}\tilde{y}\tilde{y}}-\tilde{\theta}_{,\tilde{y}\tilde{y}}-\nu^2\tilde{\theta}=0 \tag{4.25}$$

and the boundary conditions are

$$\tilde{\theta}=0, \qquad \tilde{\theta}_{,\tilde{y}}=0 \qquad at \qquad \tilde{y}=0 \tag{4.26a}$$

$$\mu\tilde{\theta}_{,\tilde{y}\tilde{y}\tilde{y}}-\tilde{\theta}_{,\tilde{y}}=0, \qquad \tilde{\theta}_{,\tilde{y}\tilde{y}}=0 \qquad at \qquad \tilde{y}=1 \tag{4.26b}$$

where

$$\mu=\frac{1}{3}\left(\frac{1}{AR}\right)^2\delta_w\left(\frac{\tilde{D}_{22}}{\tilde{\bar{D}}_{66}}\right), \qquad \nu^2=\left[\tilde{m}_3+\frac{1}{3}\left(\frac{1}{AR}\right)^2\left(\frac{l}{h}\right)^2 m_1\right]\tilde{\omega}^2 \tag{4.27}$$

The characteristic equation is

$$\mu\lambda^4-\lambda^2-\nu^2=0 \tag{4.28}$$

When the warping restraint effect is discarded, $\delta_w=0$ (implying $\mu=0$), and the eigenfrequency and mode equations yield simply

$$\omega_r=\frac{(2r-1)}{2}\pi\sqrt{\frac{\tilde{\bar{D}}_{66}}{\tilde{I}}}, \qquad \tilde{\Theta}_r=\sin\frac{(2r-1)}{2}\pi\tilde{y}, \qquad r=1,2,\ldots,n \tag{4.29}$$

where

$$\tilde{I} = \tilde{m}_3 + \frac{1}{3}\left(\frac{1}{AR}\right)^2\left(\frac{l}{h}\right)^2 m_1 \tag{4.30}$$

When the warping restraint term is included ($\delta_w = 1$), the solution of the characteristic equation (4.28) is

$$\lambda_{1,2,3,4} = \pm\sqrt{\frac{1 \pm \sqrt{1+4\mu\nu^2}}{2\mu}} \tag{4.31}$$

The relationship between $\lambda_1 = \sqrt{\frac{1+\sqrt{1+4\mu\nu^2}}{2\mu}}$ and $\lambda_4 = -\sqrt{\frac{1-\sqrt{1+4\mu\nu^2}}{2\mu}}$ is

$$\lambda_1 = \sqrt{\lambda_4^2 + 1/\mu} \tag{4.32}$$

and the one between λ_4 and ν is

$$\nu = \lambda_4\sqrt{1+\mu\lambda_4^2} \tag{4.33}$$

The general solution for the torsional mode $\Theta(\tilde{y})$ is assumed to be

$$\tilde{\Theta}(\tilde{y}) = C_1\cos\lambda_4\tilde{y} + C_2\sin\lambda_4\tilde{y} + C_3\cosh\lambda_1\tilde{y} + C_4\sinh\lambda_1\tilde{y} \tag{4.34}$$

Substituting equation (4.34) into the boundary conditions (4.26) yields

$$\begin{bmatrix} 1 & 0 & 1 & 0 \\ 0 & \lambda_4 & 0 & \lambda_1 \\ -\lambda_4^2\cos\lambda_4 & -\lambda_4^2\sin\lambda_4 & \lambda_1^2\cosh\lambda_1 & \lambda_1^2\sinh\lambda_1 \\ \lambda_4\lambda_1^2\sin\lambda_4 & -\lambda_4\lambda_1^2\cos\lambda_4 & \lambda_4^2\lambda_1\sinh\lambda_1 & \lambda_4^2\lambda_1\cosh\lambda_1 \end{bmatrix} \begin{Bmatrix} C_1 \\ C_2 \\ C_3 \\ C_4 \end{Bmatrix} = 0 \tag{4.35}$$

The argument of nontriviality of the solution requires that the determinant of the coefficient matrix in Eq. (4.35) must be zero, wherefrom one obtains

$$(\lambda_1^2 - \lambda_4^2)\lambda_1^2\lambda_4^2\sinh\lambda_1\sin\lambda_4 + (\lambda_1^4 + \lambda_4^4)\lambda_1\lambda_4\cos\lambda_4 + 2\lambda_1^3\lambda_4^3 = 0 \tag{4.36}$$

The natural frequencies are given as

$$\omega = \sqrt{\frac{\nu^2}{\tilde{I}}} \tag{4.37}$$

in conjunction with equations (4.27), (4.30), and (4.32-33).

To find natural modes of torsional vibration, in conjunction with the boundary conditions (4.26a), one obtains

$$C_3 = -C_1, \qquad C_4 = -(\lambda_4/\lambda_1)C_2 \tag{4.38}$$

and as a result the solution takes the form

$$\tilde{\Theta}(\tilde{y}) = C_1(\cos\lambda_4\tilde{y} - \cosh\lambda_1\tilde{y}) + C_2(\sin\lambda_4\tilde{y} - (\lambda_4/\lambda_1)\sinh\lambda_1\tilde{y}) \tag{4.39}$$

Using the boundary conditions (4.26b), we arrive at

$$C_1 = \frac{-(\lambda_4^2\sin\lambda_4 + \lambda_4\lambda_1\sinh\lambda_1)}{\lambda_4^2\cos\lambda_4 + \lambda_1^2\cosh\lambda_1}, \quad or \quad C_1 = \frac{\lambda_1^2\cos\lambda_4 + \lambda_4^2\cosh\lambda_1}{\lambda_1^2\sin\lambda_4 - \lambda_4\lambda_1\sinh\lambda_1} \tag{4.40}$$

Finally, Eq. (4.39) in conjunction with Eqs. (4.38), (4.40) becomes

$$\begin{aligned}\tilde{\Theta}(\tilde{y}) =&(\lambda_4^2\sin\lambda_4 + \lambda_4\lambda_1\sinh\lambda_1)(\cosh\lambda_1\tilde{y} - \cos\lambda_4\tilde{y}) \\ &+(\lambda_4^2\cos\lambda_4 + \lambda_1^2\cosh\lambda_1)(\sin\lambda_4\tilde{y} - (\frac{\lambda_4}{\lambda_1})\sinh\lambda_1\tilde{y})\end{aligned} \tag{4.41}$$

4.4 Numerical Results

Consider the case of a cantilevered composite structure composed of laminae exhibiting similar material properties and constant thicknesses. For the graphite/epoxy material the elastic properties are as follows:

$$E_1 = 18.5 \times 10^6\ psi, \quad E_2 = 1.6 \times 10^6\ psi, \quad \nu_{12} = .35$$

$$G_{12} = .832 \times 10^6\ psi, \quad G_{23} = .332 \times 10^6\ psi, \quad G_{13} = .332 \times 10^6\ psi$$

$$\rho = .056\ lb/in^3, \qquad t = .0053\ in$$

where E_1 and E_2 denote the in-plane Young's moduli parallel and perpendicular to the fiber direction, respectively, and ν_{12} is the major Poisson's ratio. G_{12} is the in-plane shear modulus, while G_{23} and G_{13} are transverse shear moduli, ρ mass density, and t the layer thickness. The elastic axis is chosen to be $x_o = 0.5c$ (see Figure 3.1) through all subsequent chapters.

4.4.1. Consideration of Convergence and Accuracy:

The convergence and the accuracy are two basic requirements to be proved when dealing with approximate solutions. Two sets of admissible functions are chosen for the Rayleigh-Ritz and Extended-Galerkin methods. One is in the form of a polynomial series, another is in the form of trigonometric functions. As a result, the displacements, $\tilde{v}_r, \tilde{\psi}_r, \tilde{\varphi}_r, \tilde{w}_r, \tilde{\theta}_r$ are in the form:

$$x^r, \qquad \sin\frac{(2r-1)}{2}\pi \qquad r = 1, 2, \ldots n$$

Quadratic and cubic elements are used in the finite element method.

In Figures 4.1-2, convergence consideration on free vibration of cantilevered composite structures is modeled as per the FSDT with the warping restraint included. The natural frequencies are plotted versus the number of terms n in the approximating series. Convergence of the frequencies of bending and torsional vibration is tested comparing results by the finite element method using quadratic and cubic interpolation functions and the Rayleigh-Ritz and Extended-Galerkin methods using polynomial and trigonometric functions. From the comparison between the results of these three methods, a very slow convergence rate is observed on two solutions, the Rayleigh-Ritz formulation using trigonometric functions and the quadratic finite element formulation. The cubic finite element formulation gives reasonably better convergence than the quadratic finite element and the Rayleigh-Ritz formulation using trigonometric functions. More terms, however,

are needed to achieve the same convergence rate of the Rayleigh-Ritz solutions using polynomial functions. The Rayleigh-Ritz solutions using polynomial functions result in fast convergence with a fewer number of terms than others in the free vibration problem of cantilevered composite structure. Once this fact is found, the Rayleigh-Ritz method with polynomial admissible functions will be used extensively to find natural vibration frequencies.

In addition, it should be noted that for self-adjoint problems, the Extended-Galerkin method is equivalent to the Rayleigh-Ritz method, thus both methods would produce identical numerical results. However, for non self-adjoint problems, the Rayleigh-Ritz formulation is no longer applicable. For such problems the Extended-Galerkin method (EGM) is more convenient than the classical Galerkin method.

In Figures 4.3-4, convergence consideration for cantilevered composite structures modeled as per first-order transverse shear deformation theory and classical lamination theory with or without warping restraint is given. For all cases where transverse shear deformation and the warping restraint effect were incorporated, good convergence has been achieved. It is also illustrated that for cantilevered structures taking into account the warping restraint effect, faster convergence is achieved than for free warping models.

Furthermore, the accuracy of the free vibration results by the Rayleigh-Ritz method is checked through a comparison with exact solutions for special laminates. Exact solutions for the non shear-deformable beam model can be obtained for specific types of laminates such as cross-ply, anti-symmetric angle [29], specially orthotropic laminates [30,31], and sublaminates [32] where the coupling rigidity $\bar{D}_{26}$ is considered identically zero. No bending-twist coupling exists, and as a

result, exact solutions are easier to obtain. For example, A, B, D, stiffness matrix elements of the cross-ply laminate become:

$$\begin{bmatrix} A_{11} & A_{12} & 0 \\ A_{21} & A_{22} & 0 \\ 0 & 0 & A_{66} \end{bmatrix}, \quad \begin{bmatrix} B_{11} & B_{12} & 0 \\ B_{21} & B_{22} & 0 \\ 0 & 0 & B_{66} \end{bmatrix}, \quad \begin{bmatrix} D_{11} & D_{12} & 0 \\ D_{21} & D_{22} & 0 \\ 0 & 0 & D_{66} \end{bmatrix}$$

For an antisymmetric angle-ply laminate,

$$\begin{bmatrix} A_{11} & A_{12} & 0 \\ A_{21} & A_{22} & 0 \\ 0 & 0 & A_{66} \end{bmatrix}, \quad \begin{bmatrix} 0 & 0 & B_{16} \\ 0 & 0 & B_{26} \\ B_{16} & B_{26} & 0 \end{bmatrix}, \quad \begin{bmatrix} D_{11} & D_{12} & 0 \\ D_{21} & D_{22} & 0 \\ 0 & 0 & D_{66} \end{bmatrix}$$

and for a specially orthotropic laminate,

$$\begin{bmatrix} A_{11} & A_{12} & 0 \\ A_{21} & A_{22} & 0 \\ 0 & 0 & A_{66} \end{bmatrix}, \quad \begin{bmatrix} 0 & 0 & 0 \\ 0 & 0 & 0 \\ 0 & 0 & 0 \end{bmatrix}, \quad \begin{bmatrix} D_{11} & D_{12} & 0 \\ D_{21} & D_{22} & 0 \\ 0 & 0 & D_{66} \end{bmatrix}$$

Tables 4.1-2 show the comparison between the exact solutions and the output from the Rayleigh-Ritz method for cross-ply and specially orthotropic laminate, respectively. An excellent agreement is seen between the two sets of results.

4.4.2. Free Vibration Results:

In this section, computational results will be presented for free vibration of anisotropic cantilevered composite structures. To investigate the nonclassical effects on the structure, the first-order shear deformable beam structural model is considered along with its classical lamination counterpart. The effects of bending-twist coupling, warping restraint, and transverse shear deformation on natural frequencies will be emphasized. Ply angle is measured clockwise from the x-coordinate. The effect of the (nondimensional) geometric quantities, as, e.g., aspect ratio (AR), and span-to-thickness ratio (l/h) are considered.

In Figure 4.5, the variation of the first bending vibration frequency versus aspect ratio (AR) and span-to-thickness ratio (l/h) is presented for the laminate

$[90/\pm 45/0]_{S4}$. While keeping the chord length constant, the span length increases along the coordinate. As a result, the span-to-thickness ratio and the beam aspect ratio increase at the same time. In other words, the structure become more slender and more narrow. Figure 4.5 reveals that the effects of transverse shear flexibility and warping inhibition on the lowest frequencies are small excepting the case labeled as FSDT free warping. However, in Figure 4.6, these effects become apparent in higher frequencies (1st torsional frequencies).

To infer information about the thickness effect only, the number of layers is allowed to increase, and as a result, l/h decreases but AR remains the same. A moderate aspect ratio ($AR = 8$) is chosen in the first example and a low aspect ratio ($AR = 4$) is considered in the second one. From Figures 4.7-10, it is observed that the difference between the frequencies predicted by the CLT and FSDT diminishes for large l/h. The torsional frequencies are also influenced by transverse shear deformation due to the bending-twist coupling. The warping restraint effect is practically immaterial for the moderate aspect ratio ($AR = 8$), but its effect becomes apparent for the low aspect ratio ($AR = 4$). It is seen that the effect of transverse shear deformation increases as (l/h) decreases.

On the other hand, in order to infer information about the effect of AR, it is assumed that the beam length changes as the number of layer increases. As a result, AR changes but l/h remains the same. A moderate span-to-thickness ratio ($l/h = 70.8$) is chosen for the first case depicted in Figures 4.11-12. Further comparisons for thick ($l/h = 11.8$) structures are displayed in Figures 4.13-14. As the aspect ratio of the cantilevered structure decreases, the discrepancy between the estimations of natural frequencies based on the free warping and warping restraint becomes larger. The torsional frequencies are strongly affected by the warping restraint.

From the results, it is concluded that the effects of transverse shear deformation and warping restraint should be accounted for in the modeling of cantilevered structures constituted of composite materials.

4.4.3. Parametric Study for Shear Correction Factor:

The sensitivity of natural frequencies with the change of transverse shear correction factor is shown in Figures 4.15-18. For a numerical example, with the stacking sequence $[90/\pm 45/0]_{S4}$, the shear correction factor, K^2, is chosen as either 5/6 or 2/3. Variations of frequencies are observed with respect to geometric parameters (both span-to-thickness ratio and aspect ratio parameters are considered in Figures 4.15-16, and only span-to-thickness ratio is considered in Figures 4.17-18).

It is seen that first-order transverse shear deformation theory with $K^2 = 2/3$ predicts lower natural frequencies than in the case when $K^2 = 5/6$. In Figure 4.15, no sensitivity with the variation of K^2 is seen in the first bending frequencies for $AR = 4$ and $l/h = 35.4$. Torsional frequencies are slightly influenced by the change of shear correction factor in Figure 4.16.

For a better understanding of the parametric sensitivity with respect to laminate thickness, variations of natural frequencies are plotted versus span-to-thickness ratio in Figures 4.17-18. Only the number of laminae increases, i.e., the total thickness of the laminate increases while the other parameters remain unchanged. As a result, in this case the span-to-thickness ratio decreases while aspect ratio remains unchanged. From the results shown in the figures, it is concluded that a more accurate evaluation of K^2 should be done, especially for thick structures.

4.4.4. Changes of Natural Mode Shapes:

Mode changes corresponding to variation of ply orientation, θ, along with stacking sequence $[90/\pm\theta/0]_{S4}$ are plotted in Figures 4.19-21. The structural model is based on FSDT taking into account the warping restraint effect. The ply angle θ varies in the range $0^o \leq \theta \leq 90^o$ with increments of 15^o. Bending-twist coupling appears to increase as θ varies far away from 0^o or 90^o. In consequence, variation of θ reveals the effect of the coupling on mode shapes. First bending vibration modes are least affected by the coupling. Although torsional mode shapes are similar, their magnitudes become significantly small in the coupling region. It indicates that the torsional mode is greatly influenced by the coupling, while bending modes are slightly changed.

Natural mode shapes for the laminated cantilever are projected in Figures 4.22-26. To investigate the effect of bending-twist coupling on mode shapes, two different stacking sequences are chosen as $[90/\pm 15/0_2/-15/45/90]_4$ and $[90_3/0]_{S4}$, respectively. The coupling is high in the former stacking sequence, but small in the latter one. Mode shapes of the FSDT model are compared to those of the CLT counterpart with and without account of warping restraint. It is seen that the existence of the coupling between bending and torsion is obvious in torsional modes. Furthermore, the effect of the coupling is more apparent for the FSDT model without consideration of warping restraint. Unlike the coupled mode shapes of $[90/\pm 15/0_2/-15/45/90]_4$, in Figures 4.25-26 bending and torsional modes are uncoupled for $[90_3/0]_{S4}$ excepting the case labeled as FSDT free warping.

Comparison of the free vibration associated with the stacking sequences ($[90/\pm 15/0_2/-15/45/90]_4$, $[90_3/0]_{S4}$) reveals that the mode shapes are more distorted within the transverse shear deformation model in the presence of bending-twist coupling. It is concluded that transverse shear deformation, warping restraint and bending-twist coupling change the modes shapes as well as natural frequencies. The coupling effect on mode shapes is more severe when transverse shear deformation is accounted for and cross-section warping is considered.

Table 4.1 Rayleigh-Ritz and exact solutions of the natural frequencies for cross-ply laminate ($l = 15\ in,\ c = 3\ in$) based on CLT.

	$[(90_3/0)_{S2}]$ Warping			$[(90_3/0)_{S2}]$ Free warping		
	Exact	RRM	%Error	Exact	RRM	%Error
ω_1	6.3496	6.3496	——	6.3496	6.3496	——
ω_2	26.3622	26.3622	——	22.8101	22.9698	.7001
ω_3	39.7920	39.7920	——	39.7920	39.7920	——
ω_4	86.6251	86.6252	.0001	68.4303	68.8992	.6852
ω_5	111.4187	111.4189	.0002	111.4187	111.4189	.0002
ω_6	167.7652	167.7654	.0001	114.0505	114.7656	.6270

	$[(90_3/0)_{S8}]$ Warping			$[(90_3/0)_{S8}]$ Free warping		
	Exact	RRM	%Error	Exact	RRM	%Error
ω_1	24.6138	24.6139	.0004	24.6138	24.6139	.0004
ω_2	104.3196	104.3197	.0001	90.6990	91.3474	.7149
ω_3	154.2522	154.2525	.0002	154.2522	154.2525	.0002
ω_4	341.5002	341.5006	.0001	272.0969	274.0451	.7160
ω_5	431.9106	431.9114	.0002	431.9106	431.9114	.0002
ω_6	657.6123	657.6131	.0001	453.4948	456.7504	.7179

unit: rad/sec

Table 4.2 Rayleigh-Ritz and exact solutions of the natural frequencies for specially orthotropic laminate ($l = 15\ in,\ c = 3\ in$) based on CLT.

	[(0/±15)s(0/∓15)s]			[(0/±30)s(0/∓30)s]		
	Exact	RRM	%Error	Exact	RRM	%Error
ω_1	4.3976	4.3976	——	5.1757	5.1757	——
ω_2	27.5593	27.5593	——	32.4357	32.4357	——
ω_3^{FW}	37.0043	37.3124	.8326	49.8141	50.2288	.8325
ω_3^{WR}	.1987	39.1988	.0003	52.3635	52.3638	.0006
ω_4	77.1667	77.1667	——	90.8209	90.8210	.0001
ω_5^{FW}	111.0219	112.9335	.8293	149.4422	150.6814	.8292
ω_5^{WR}	120.4296	120.4297	.0001	160.0551	160.0557	.0004
ω_6	151.2160	151.2185	.0017	177.9728	177.9761	.0019

	[(0/±45)s(0/∓45)s]				[(0/±75)s(0/∓75)s]		
	Exact	RRM	%Error		Exact	RRM	%Error
ω_1	6.9383	6.9383	——	ω_1	10.7542	10.7542	——
ω_2	43.4813	43.4813	——	ω_2^{FW}	37.0043	37.3124	.8326
ω_3^{FW}	55.1136	55.5726	.8328	ω_2^{WR}	43.0625	43.0625	——
ω_3^{WR}	58.5966	58.5976	.0002	ω_3	67.3953	67.3953	——
ω_4	121.7490	121.7490	——	ω_4^{FW}	111.0129	11.9335	.8293
ω_5^{FW}	165.3407	166.7123	.2247	ω_4^{WR}	142.2653	142.2653	——
ω_5^{WR}	180.4859	180.4860	.0001	ω_5	188.7087	188.7087	——
ω_6	238.5795	238.5836	.0017	ω_6^{FW}	185.0215	186.5342	.8176
				ω_6^{WR}	277.7692	277.7692	——

^{FW} Free warping ^{WR} Warping restraint unit: rad/sec

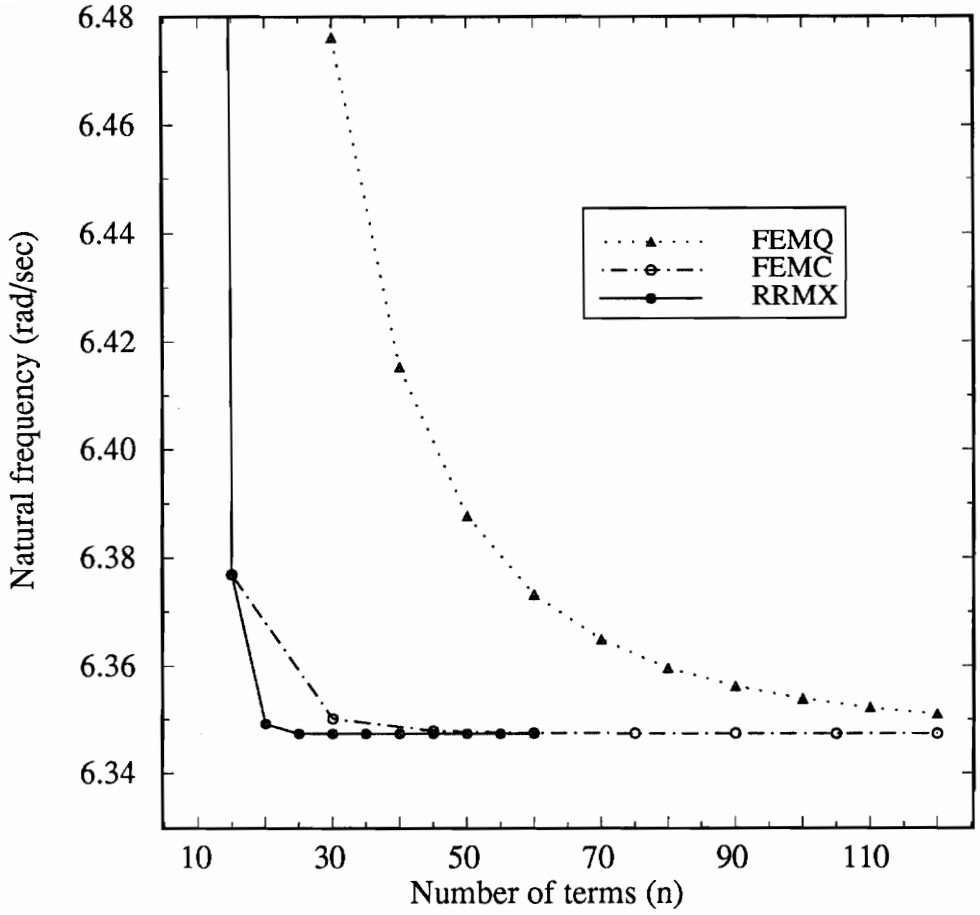

Figure 4.1 First bending frequencies computed via the Rayleigh-Ritz method using polynomial admissible functions (RRMX) and the finite element method using quadratic (FEMQ) and cubic (FEMC) interpolation functions for the laminate $[90_3/0]_{S2}$ ($l = 15\ in$, $c = 3\ in$) based on the FSDT and incorporation of the warping restraint.

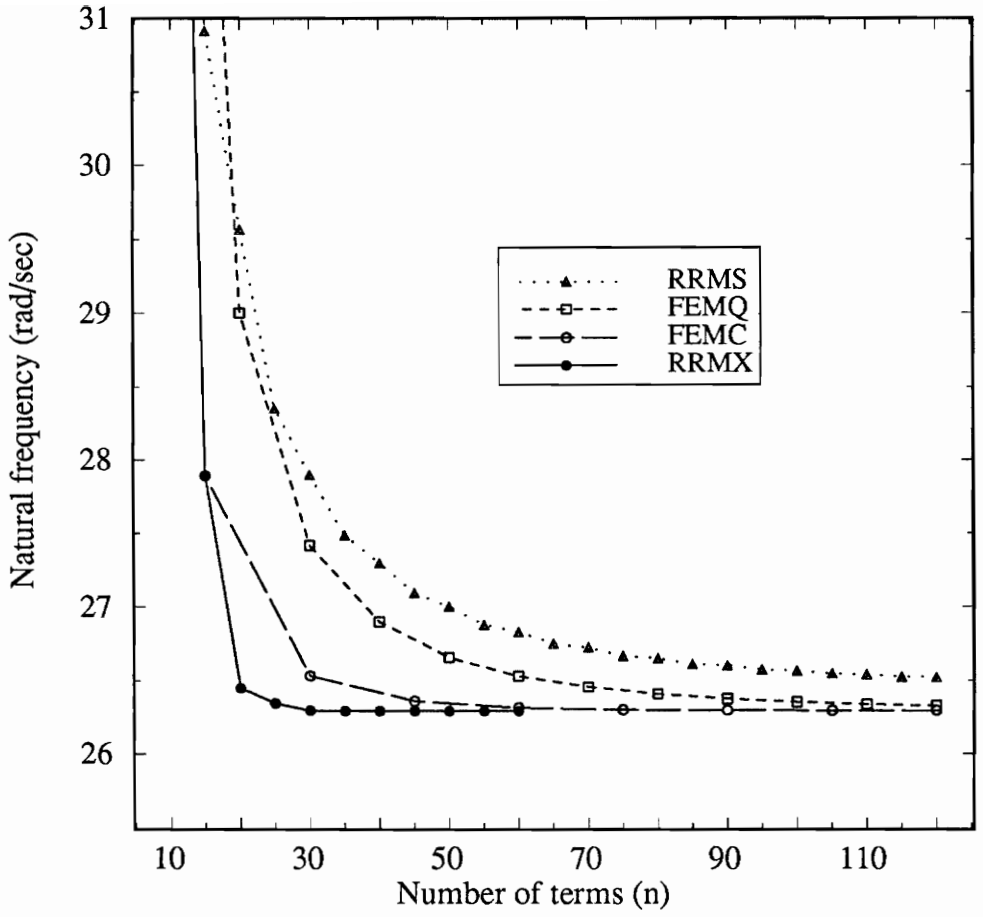

Figure 4.2 First torsional frequencies computed via the Rayleigh-Ritz method using polynomial (RRMX) and trigonometric (RRMS) admissible functions and the finite element method using quadratic (FEMQ) and cubic (FEMC) interpolation functions for the laminate $[90_3/0]_{S2}$ ($l = 15\ in,\ c = 3\ in$) based on the FSDT and incorporation of the warping restraint.

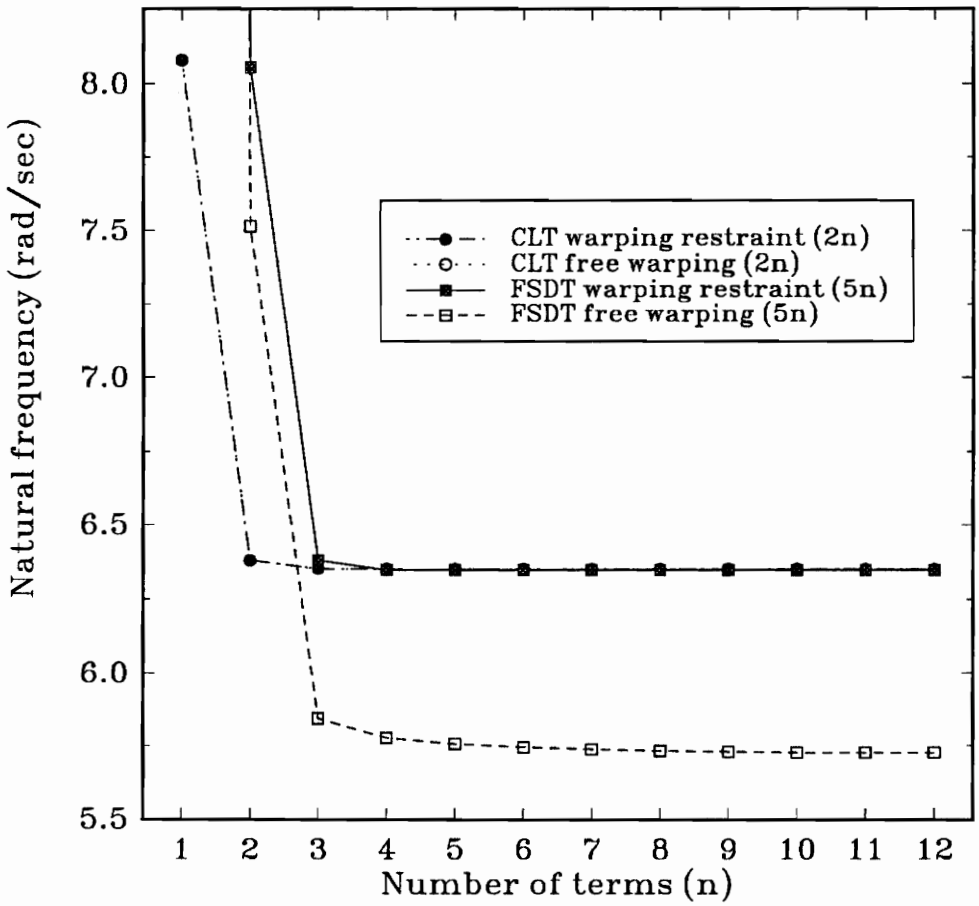

Figure 4.3 Convergence of the first bending frequencies computed via Rayleigh-Ritz method using polynomial admissible function for the laminate $[90_3/0]_{S2}$ ($l = 15\ in,\ c = 3\ in$) based on four different structural models (i.e. FSDT, CLT with/without warping restraint).

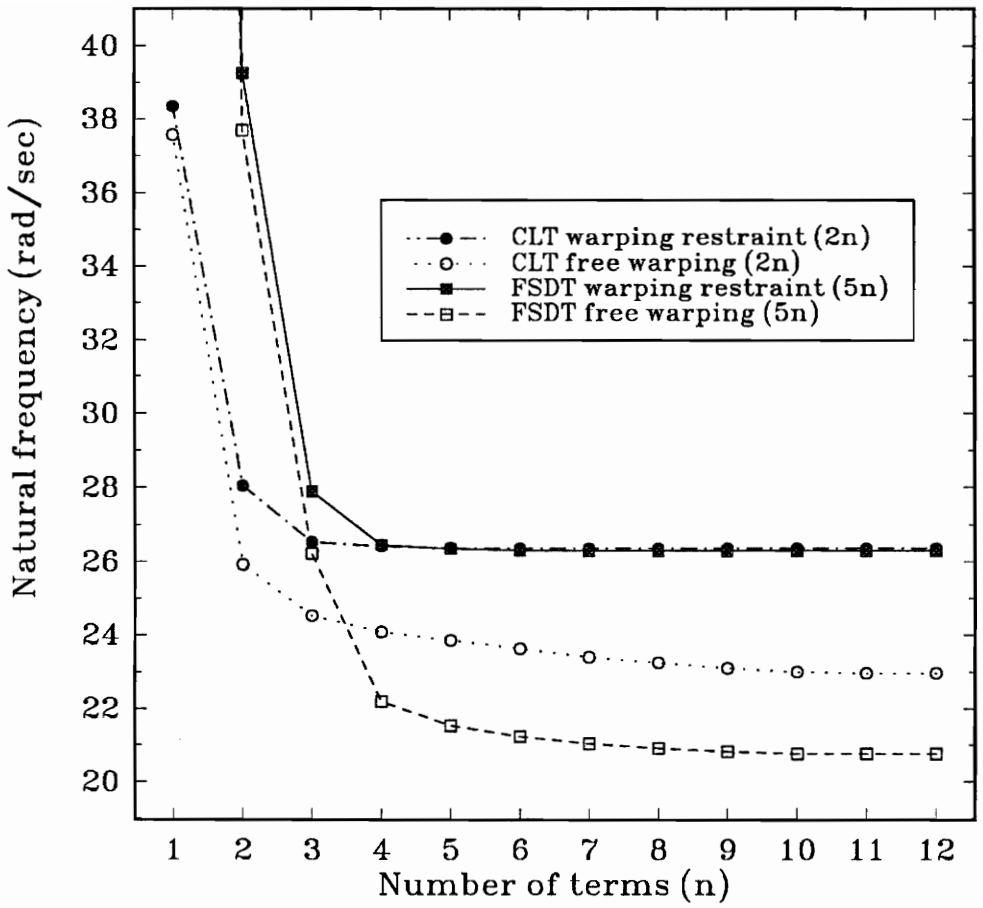

Figure 4.4 Convergence of the first torsional frequencies computed via Rayleigh-Ritz method using polynomial admissible function for the laminate $[90_3/0]_{S2}$ ($l = 15\ in,\ c = 3\ in$) based on four different structural models (i.e. FSDT, CLT with/without warping restraint).

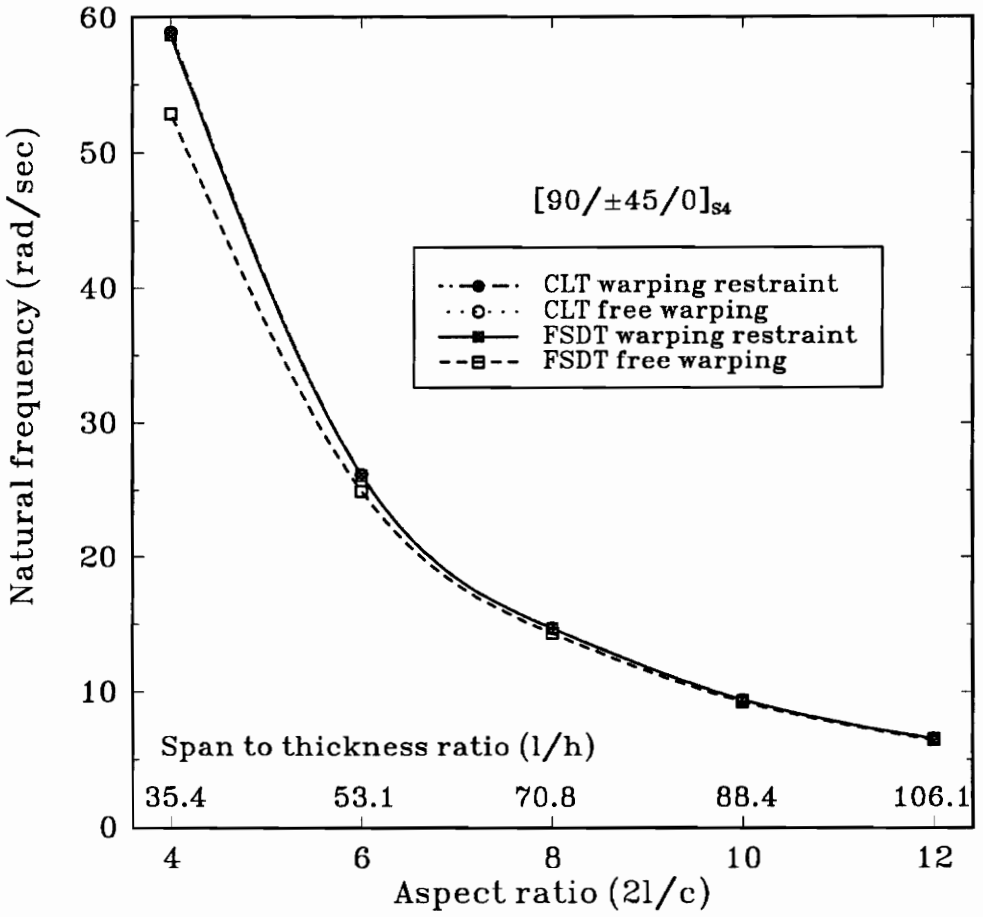

Figure 4.5 Variation of first bending vibration frequency versus aspect ratio and span-to-thickness ratio for laminate $[90/\pm 45/0]_{S4}$ ($c = 3\ in$, $l = 6, 9, 12, 15, 18\ in$) taking into account transverse shear deformation and warping restraint effects.

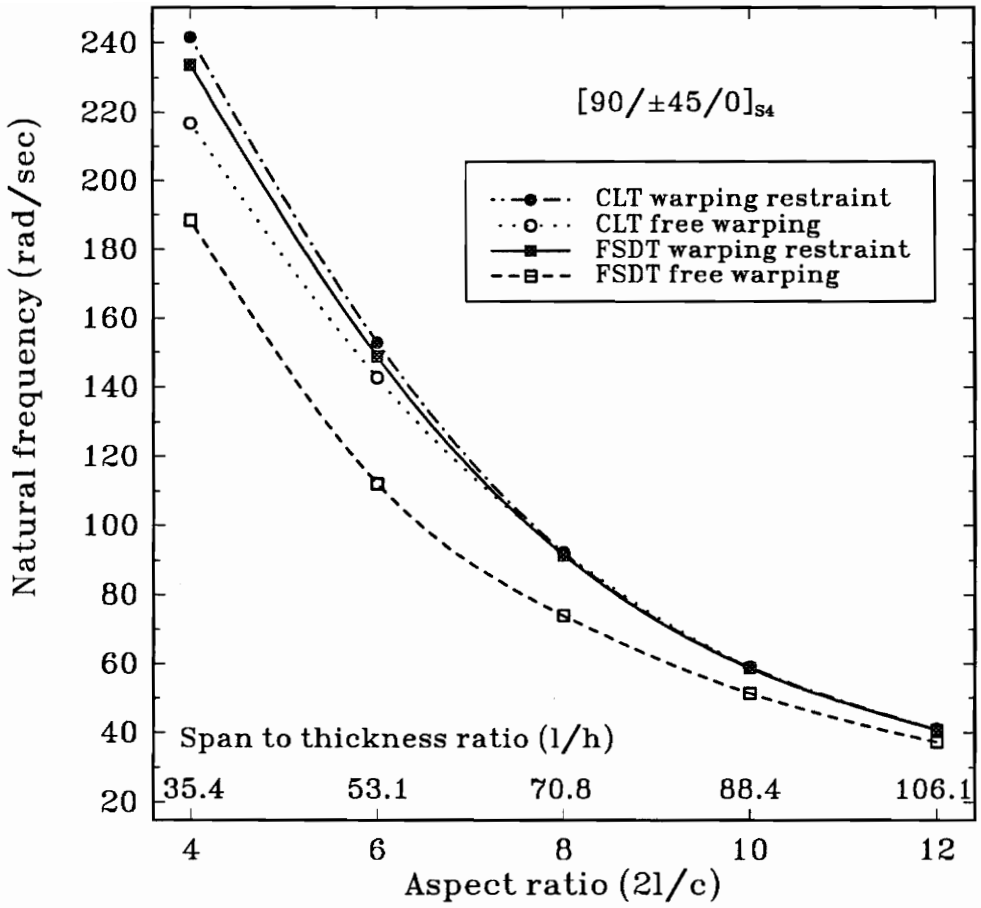

Figure 4.6 Variation of first torsional vibration frequency versus aspect ratio and span-to-thickness ratio for laminate $[90/\pm 45/0]_{S4}$ ($c = 3\ in$, $l = 6, 9, 12, 15, 18\ in$) taking into account transverse shear deformation and warping restraint effects.

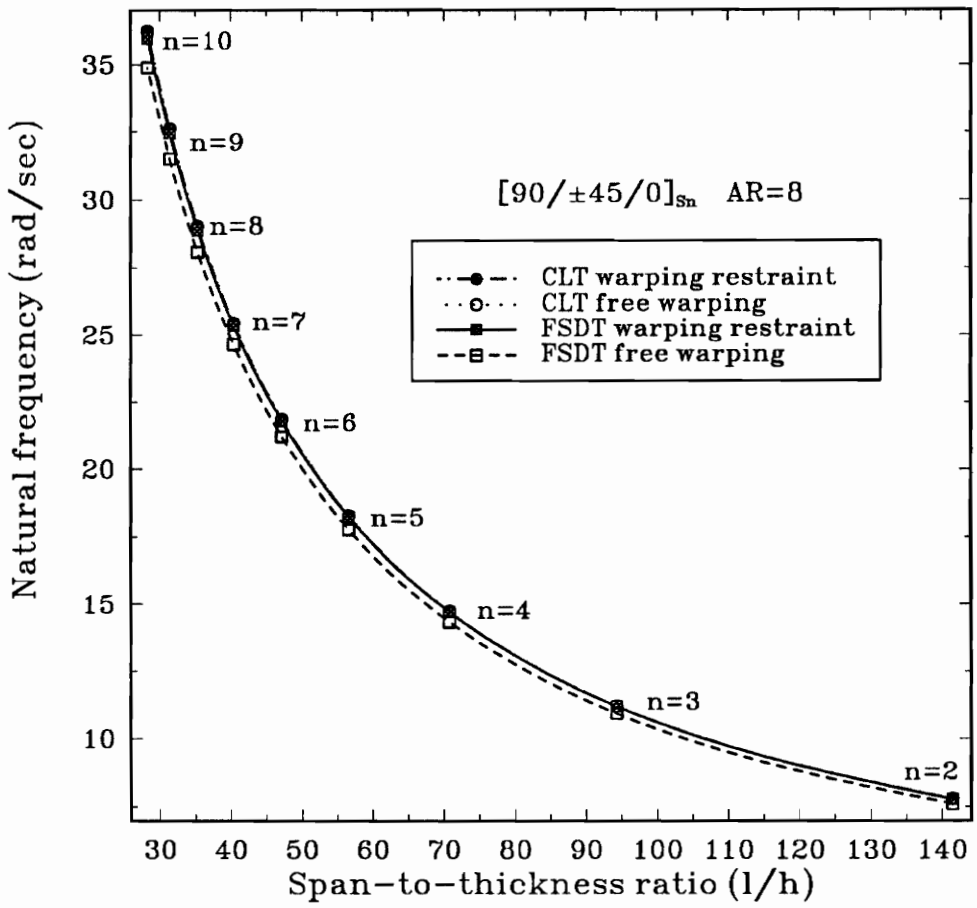

Figure 4.7 Variation of first bending vibration frequency versus span-to-thickness ratio for laminate $[90/\pm 45/0]_{Sn}$ with moderate aspect ratio $\mathcal{AR} = 8$ ($c = 3\ in$, $l = 12\ in$) taking into account transverse shear deformation and warping restraint effects.

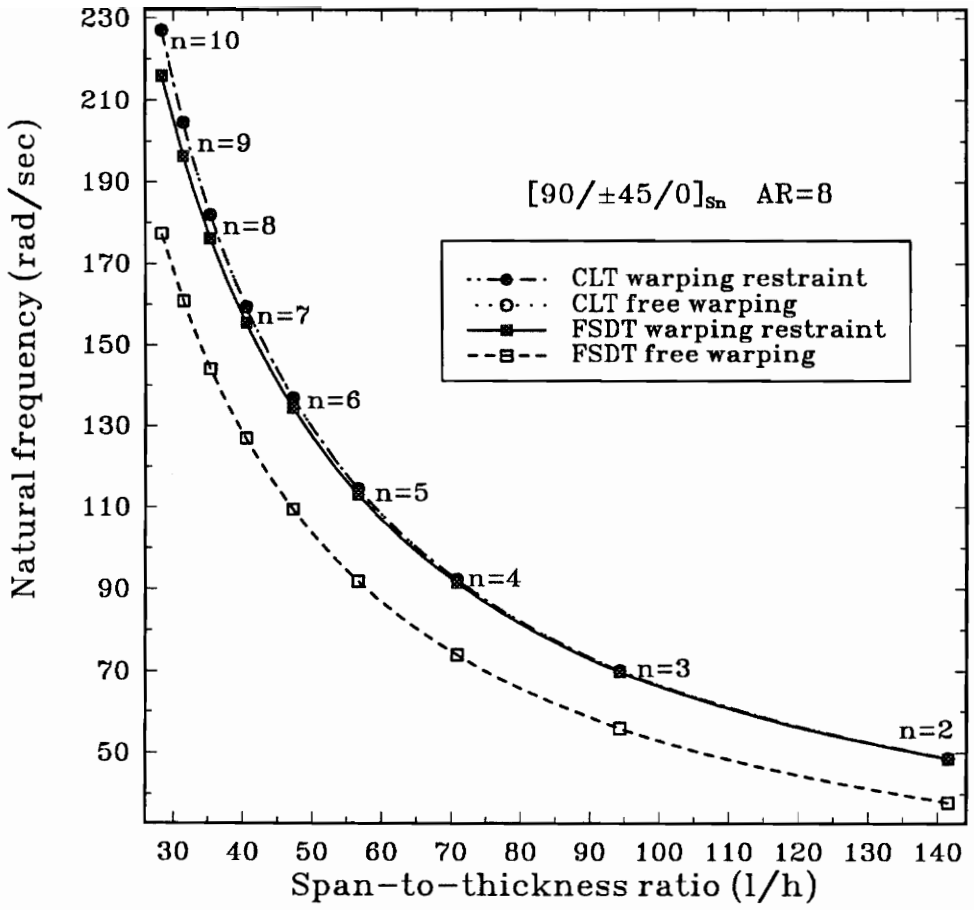

Figure 4.8 Variation of first torsional vibration frequency versus span-to-thickness ratio for laminate $[90/\pm 45/0]_{Sn}$ with moderate aspect ratio $AR = 8$ ($c = 3\ in$, $l = 12\ in$) taking into account transverse shear deformation and warping restraint effects.

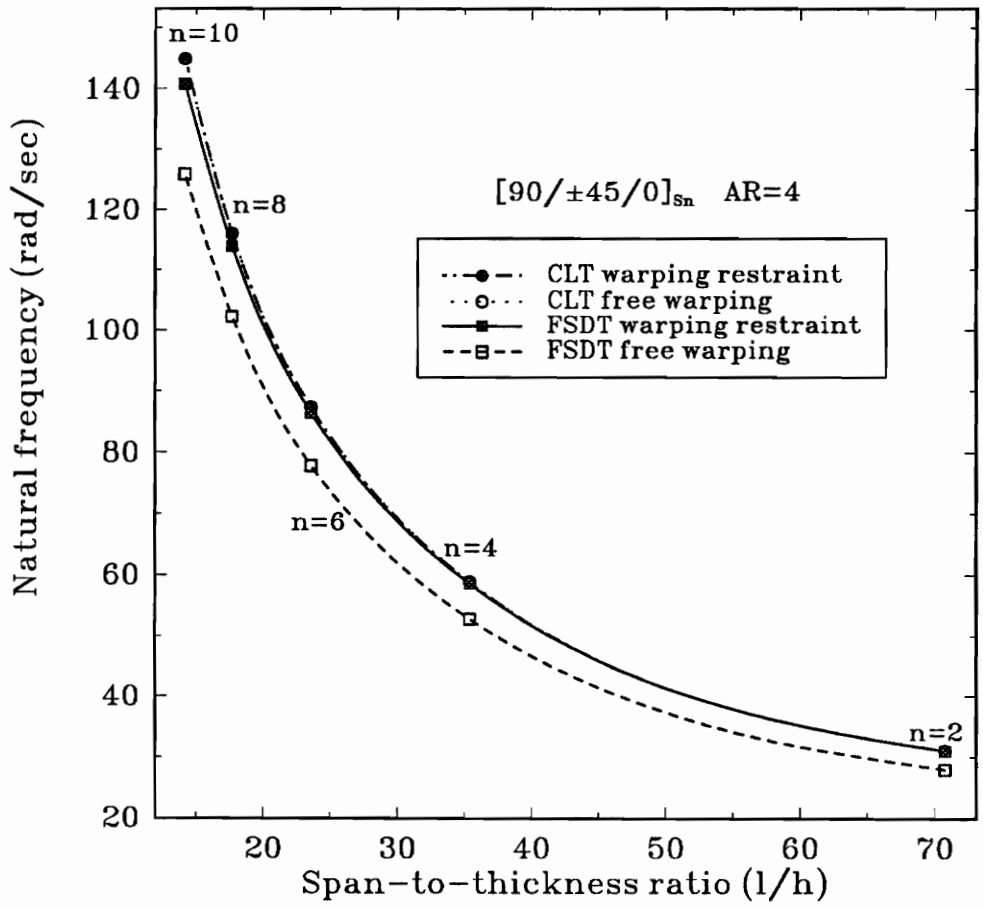

Figure 4.9 Variation of first bending vibration frequency versus span-to-thickness ratio for laminate $[90/\pm 45/0]_{Sn}$ with low aspect ratio $\mathcal{AR} = 4$ ($c = 3\ in$, $l = 6\ in$) taking into account transverse shear deformation and warping restraint effects.

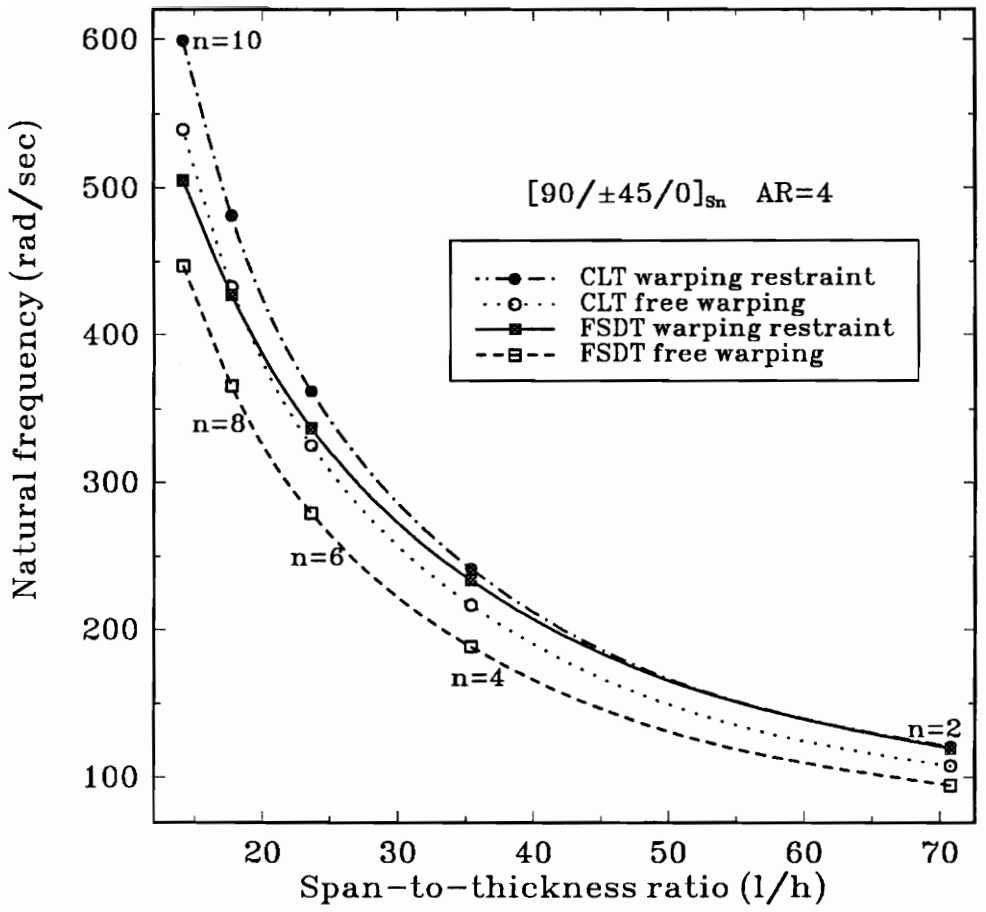

Figure 4.10 Variation of first torsional vibration frequency versus span-to-thickness ratio for laminate $[90/\pm 45/0]_{Sn}$ with low aspect ratio $\mathcal{AR} = 4$ ($c = 3$ *in*, $l = 6$ *in*) taking into account transverse shear deformation and warping restraint effects.

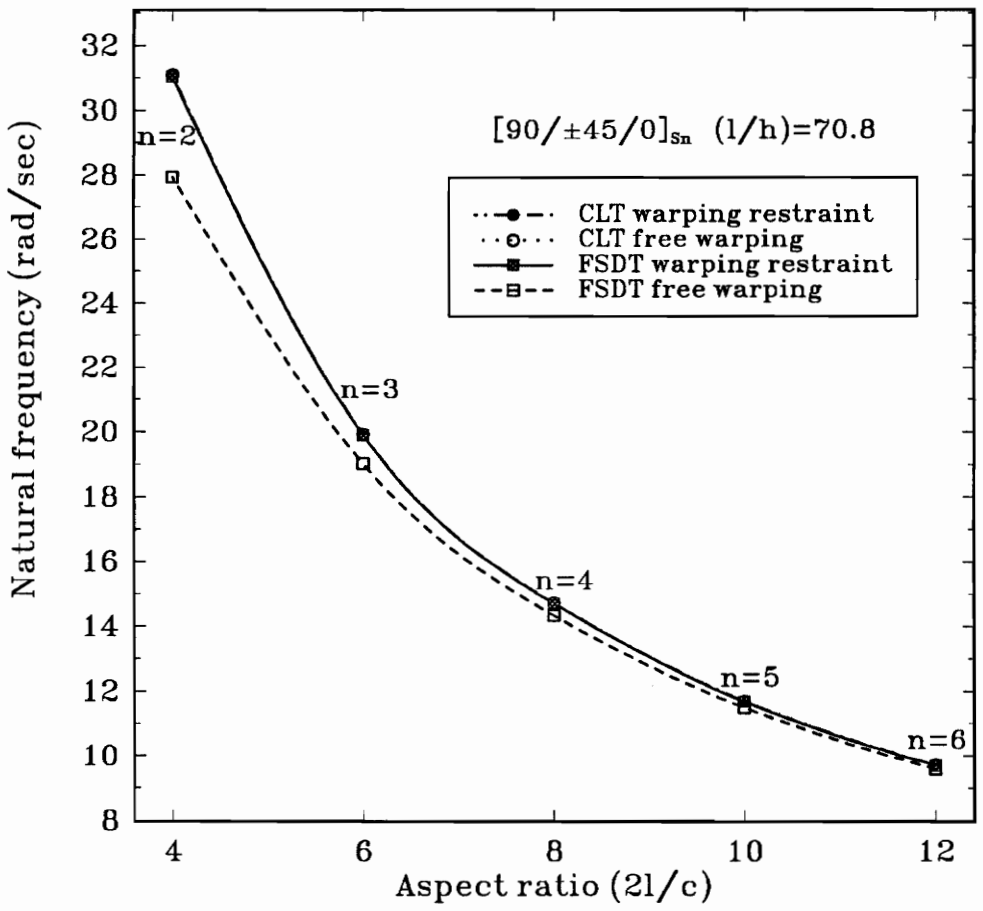

Figure 4.11 Variation of first bending vibration frequency versus aspect ratio for laminate $[90/\pm 45/0]_{Sn}$ with moderate span-to-thickness ratio ($l/h = 70.8$) taking into account transverse shear deformation and warping restraint effects.

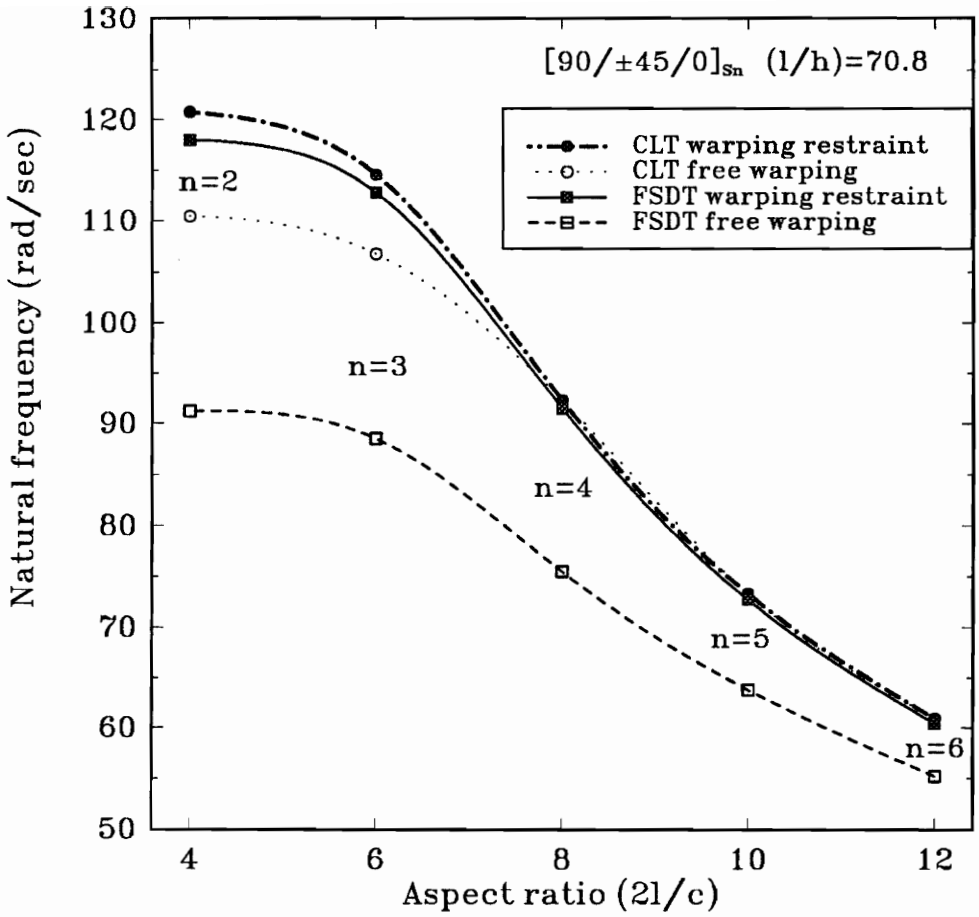

Figure 4.12 Variation of first torsional vibration frequency versus aspect ratio for laminate $[90/\pm 45/0]_{Sn}$ with moderate span-to-thickness ratio ($l/h = 70.8$) taking into account transverse shear deformation and warping restraint effects.

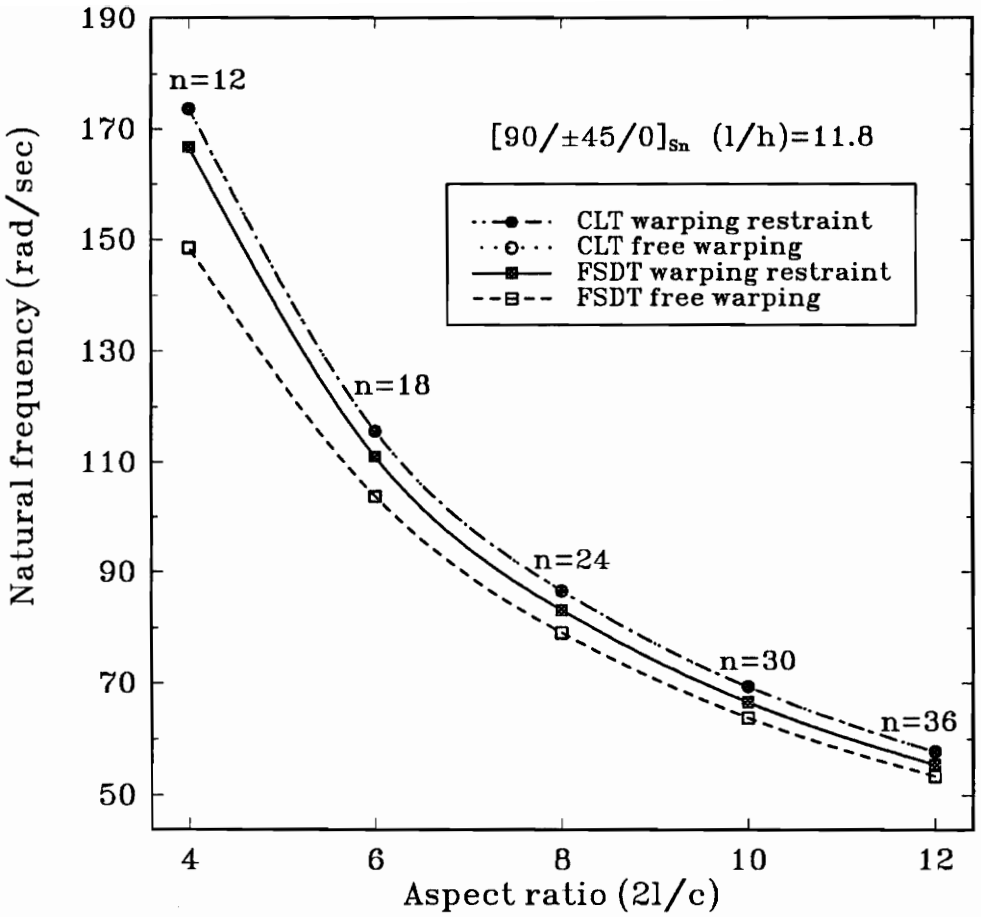

Figure 4.13 Variation of first bending vibration frequency versus aspect ratio for laminate $[90/\pm 45/0]_{Sn}$ with low span-to-thickness ratio ($l/h = 11.8$) taking into account transverse shear deformation and warping restraint effects.

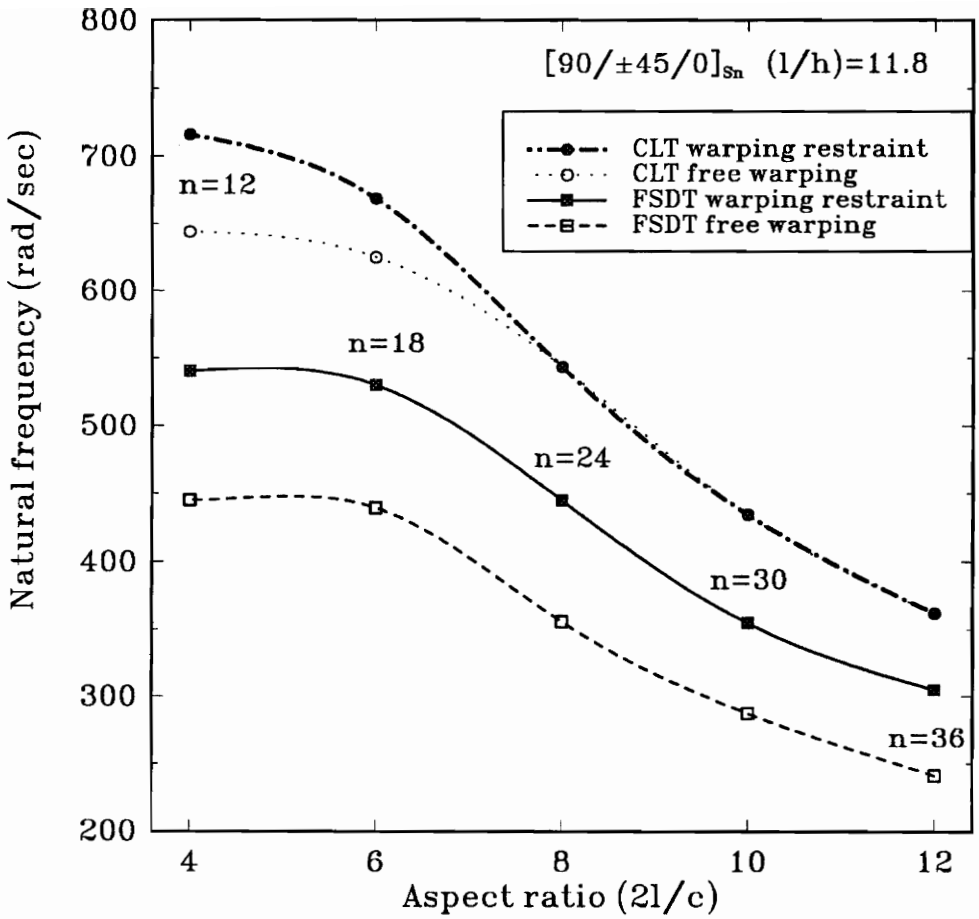

Figure 4.14 Variation of first torsional vibration frequency versus aspect ratio for laminate $[90/\pm 45/0]_{Sn}$ with low span-to-thickness ratio ($l/h = 11.8$) taking into account transverse shear deformation and warping restraint effects.

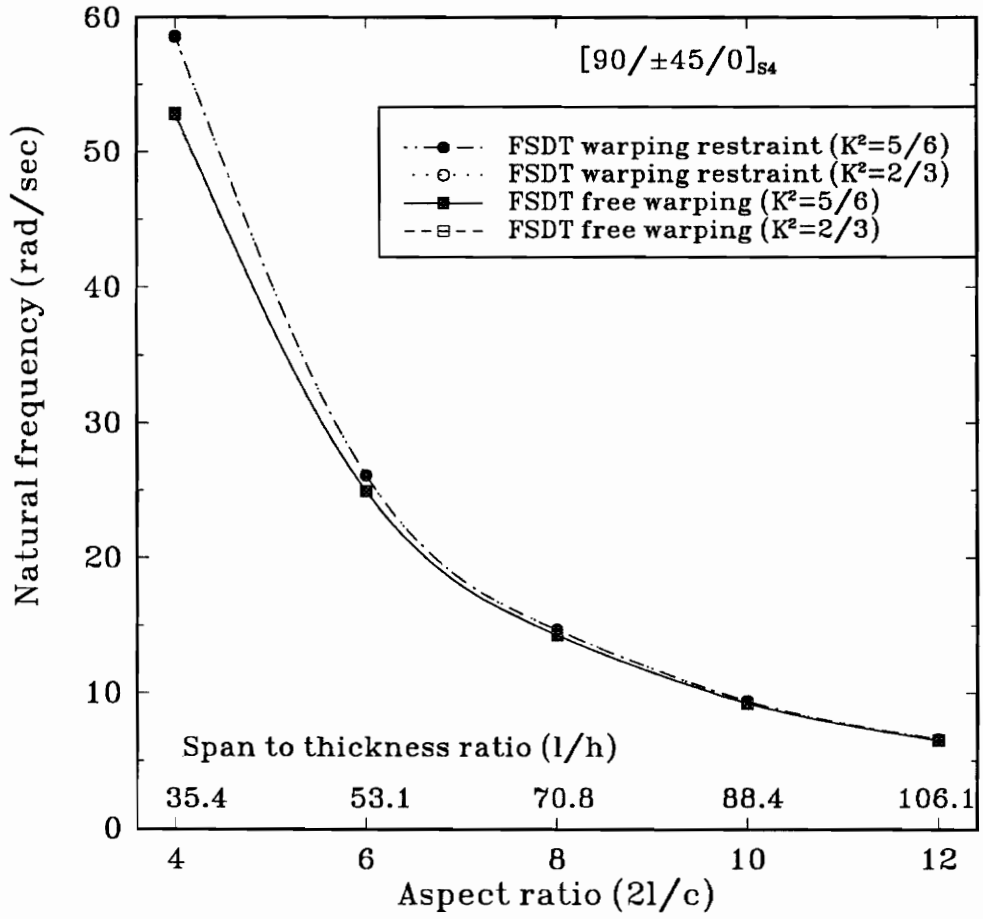

Figure 4.15 Parametric study for transverse shear correction factor in first bending frequency for laminate $[90/\pm\theta/0]_{S4}$ ($c = 3\ in,\ l = 6, 9, 12, 15, 18\ in$) taking into account warping restraint effect.

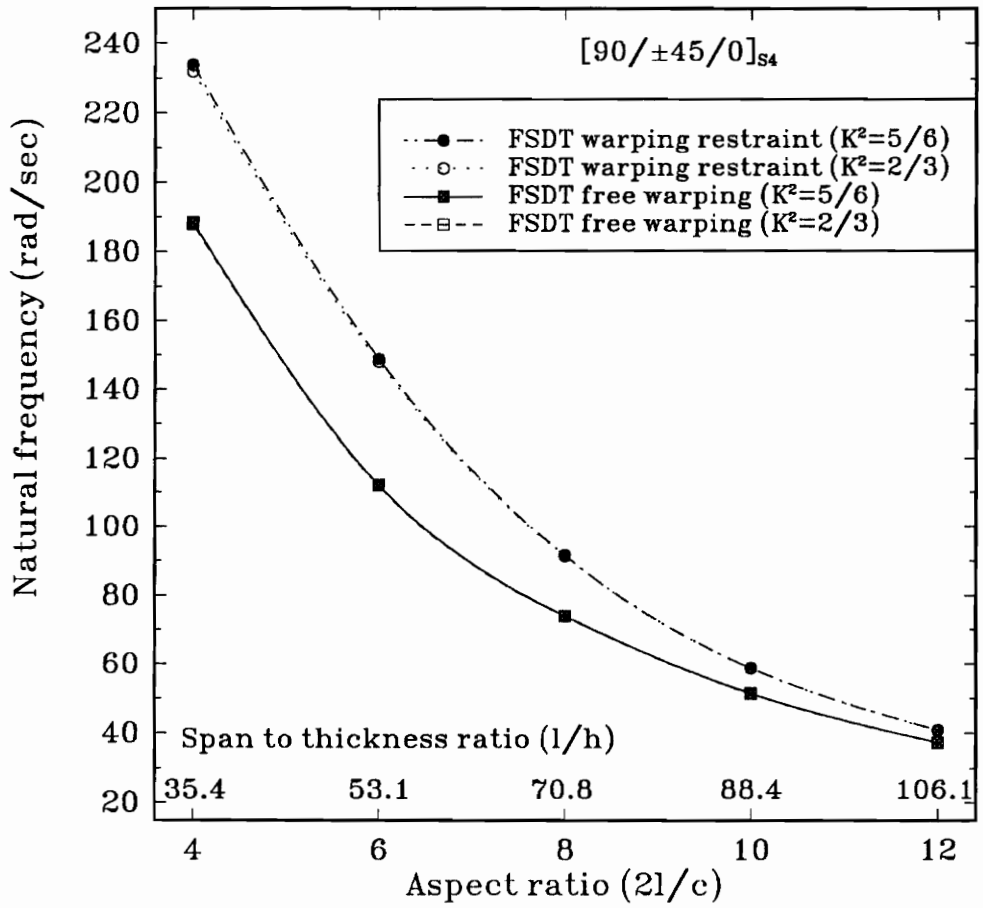

Figure 4.16 Parametric study for transverse shear correction factor in first torsional frequency for laminate $[90/\pm\theta/0]_{S4}$ ($c = 3\ in,\ l = 6, 9, 12, 15, 18\ in$) taking into account warping restraint effect.

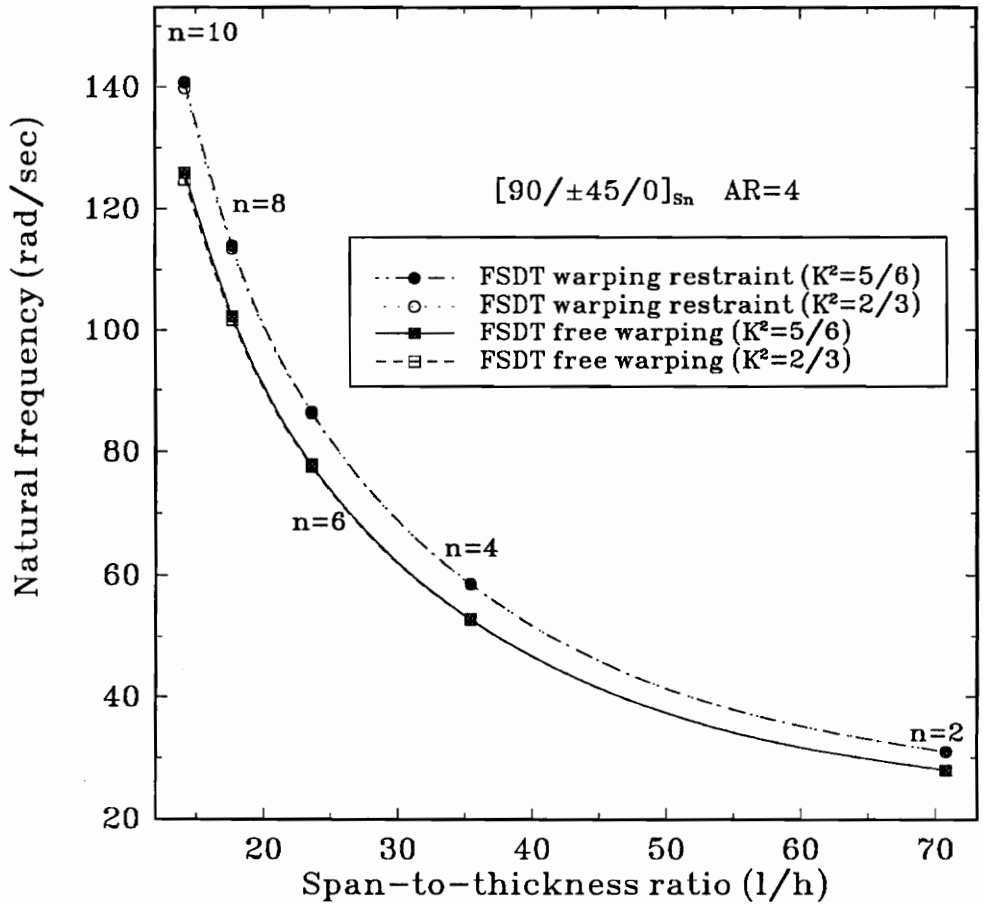

Figure 4.17 Parametric study for transverse shear correction factor in first bending frequency for laminate $[90/\pm\theta/0]_{S4}$ with low aspect ratio $AR = 4$ ($c = 3\ in,\ l = 6\ in$) taking into account warping restraint effect.

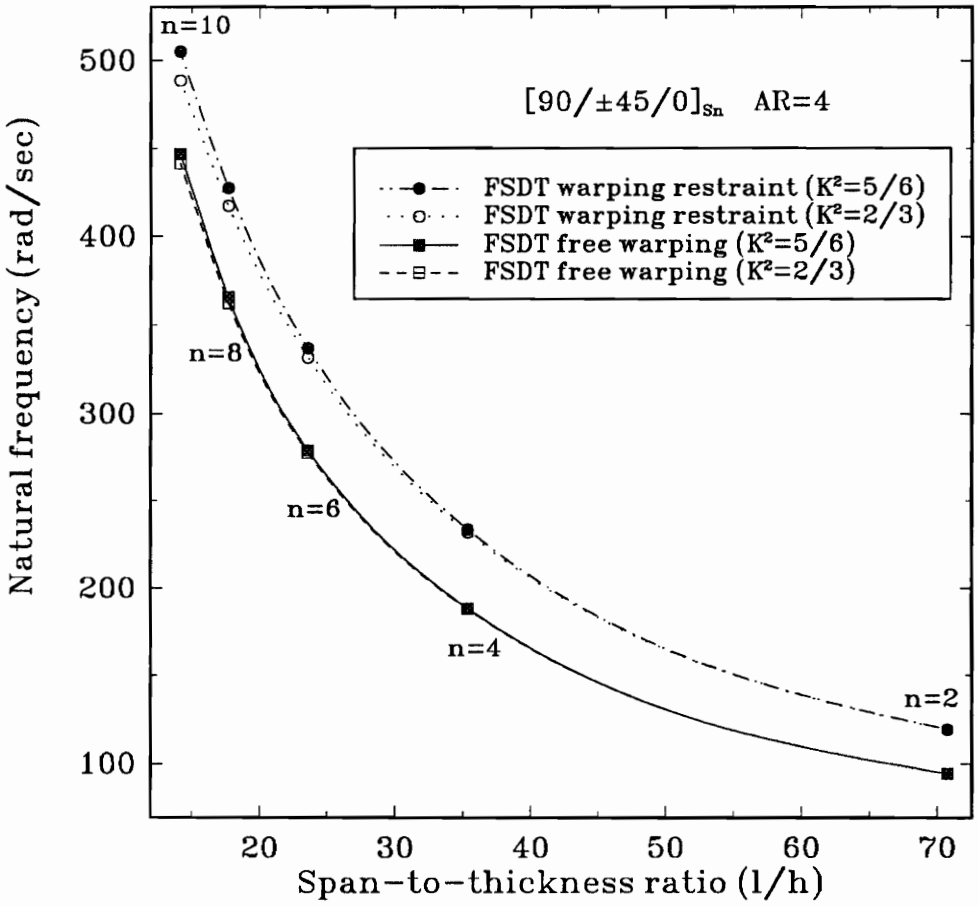

Figure 4.18 Parametric study for transverse shear correction factor in first torsional frequency for laminate $[90/\pm\theta/0]_{S4}$ with low aspect ratio $\mathcal{AR} = 4$ ($c = 3\ in,\ l = 6\ in$) taking into account warping restraint effect.

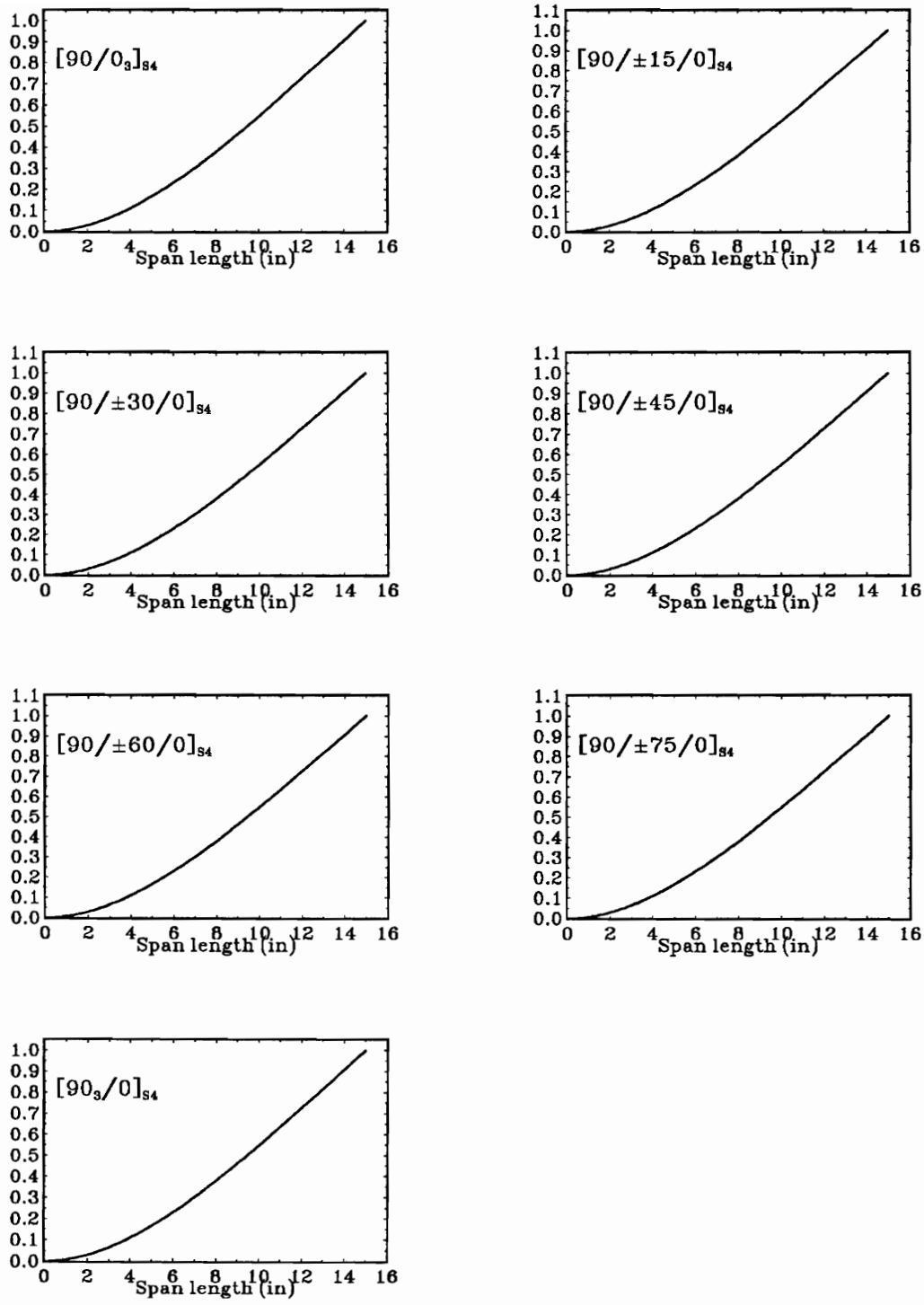

Figure 4.19 First bending modes $W_1(y)$ of laminate $[90/\pm\theta/0]_{S4}$ ($l = 15\ in$, $c = 3\ in$, based on the FSDT, warping restraint effect being incorporated) with change of ply orientation θ.

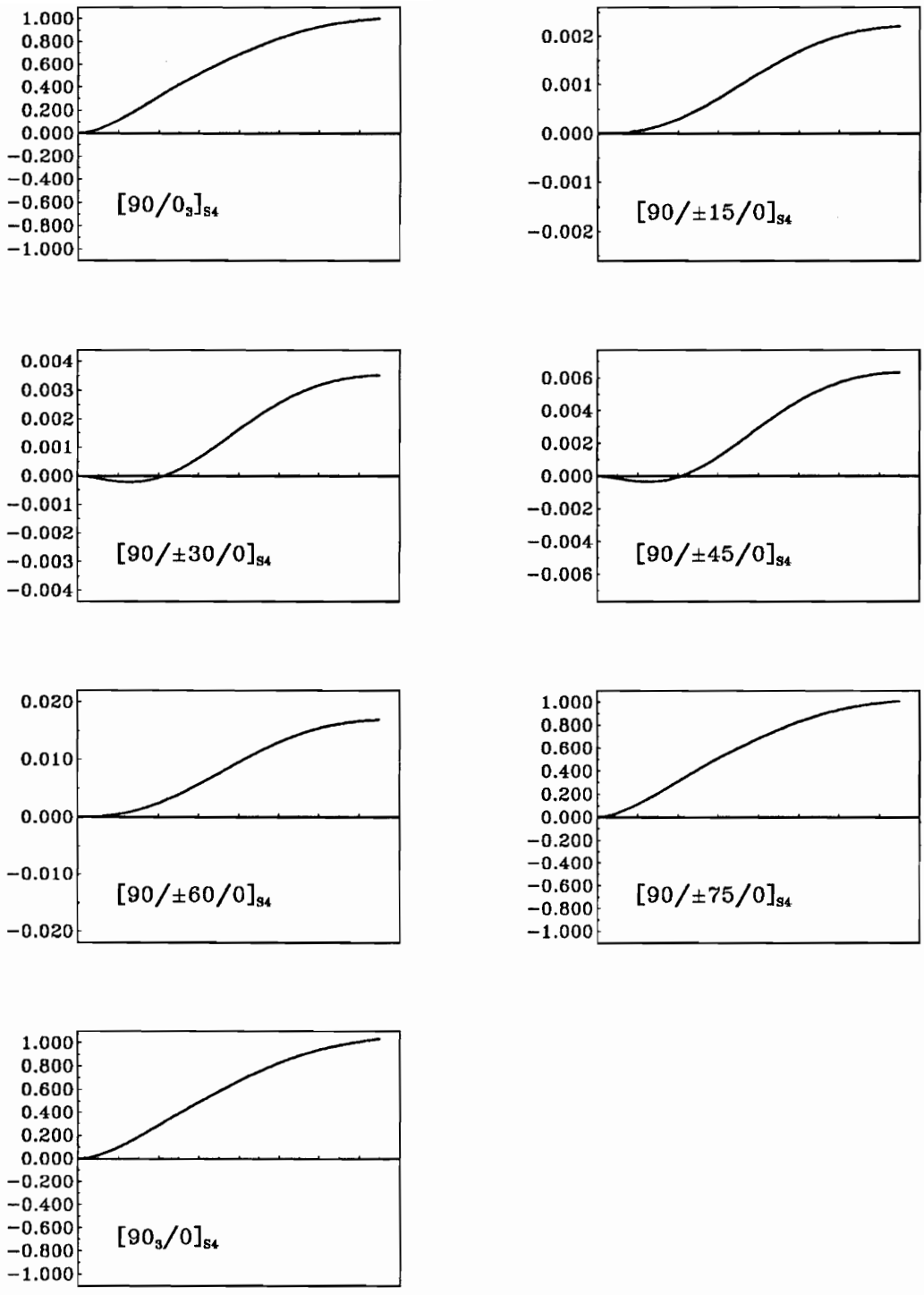

Figure 4.20 First torsional modes $\Theta_1(y)$ of laminate $[90/\pm\theta/0]_{S4}$ ($l = 15\ in,\ c = 3\ in$, based on the FSDT and incorporating warping restraint effect) with change of the ply angle θ.

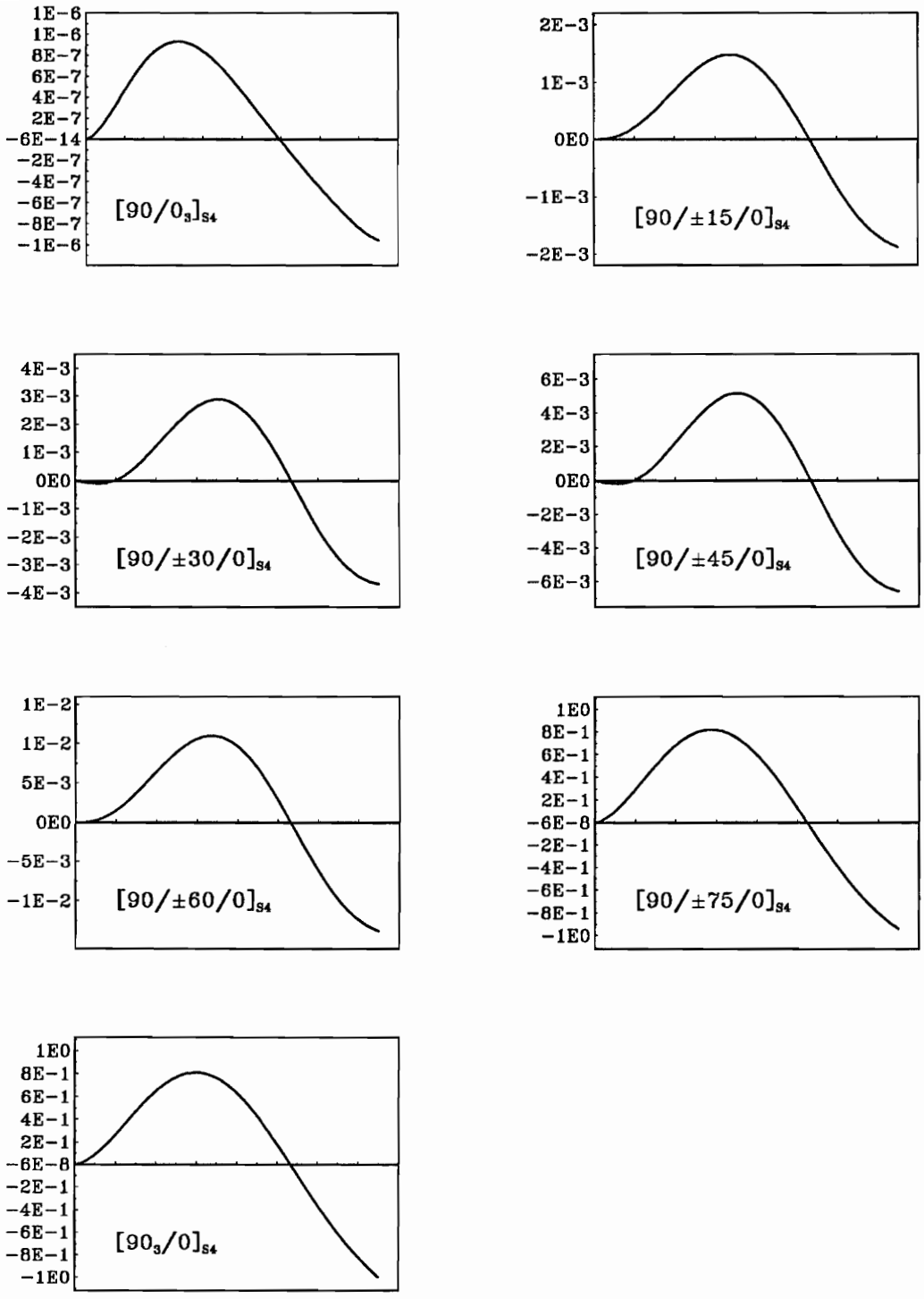

Figure 4.21 Second torsional modes $\Theta_2(y)$ of laminate $[90/\pm\theta/0]_{S4}$ ($l = 15\ in,\ c = 3\ in$, based on the FSDT with the incorporation of the warping restraint) with change of the ply angle θ.

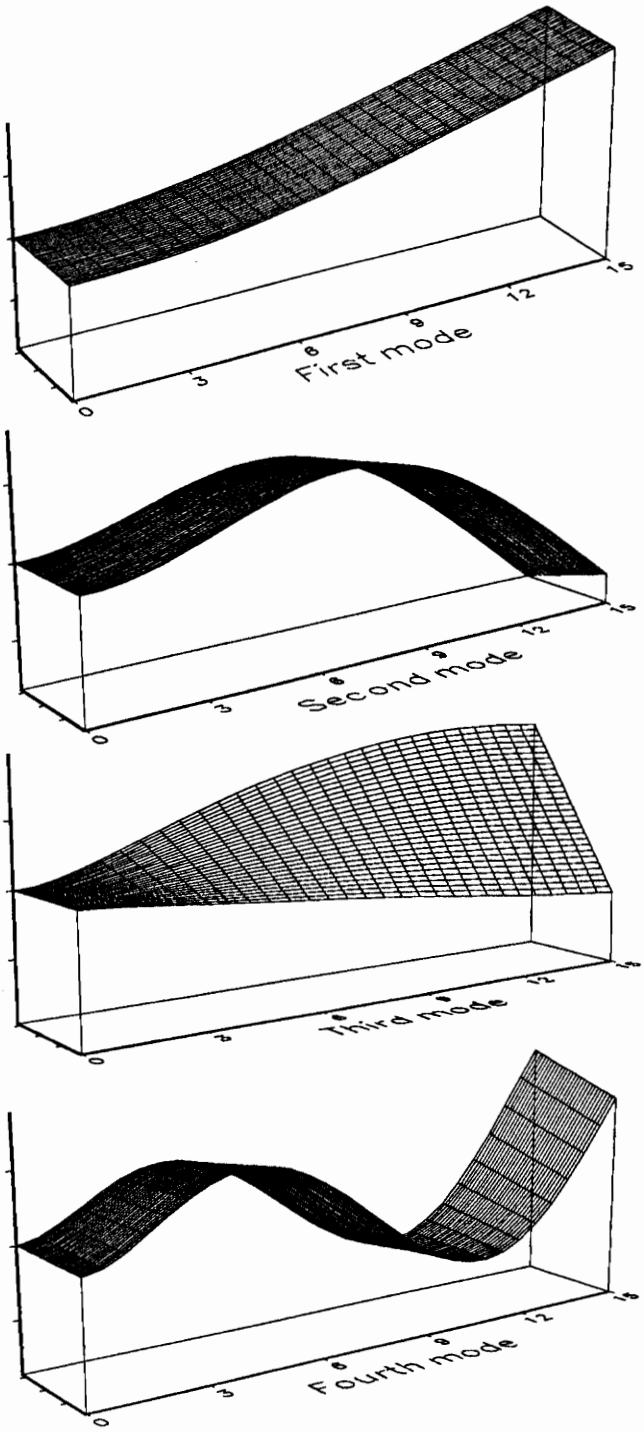

Figure 4.22 Natural mode shapes for laminate $[90/\pm 15/0_2/-15/45/90]_4$ ($l = 15\ in,\ c = 3\ in$) based on the FSDT with the incorporation of the warping restraint.

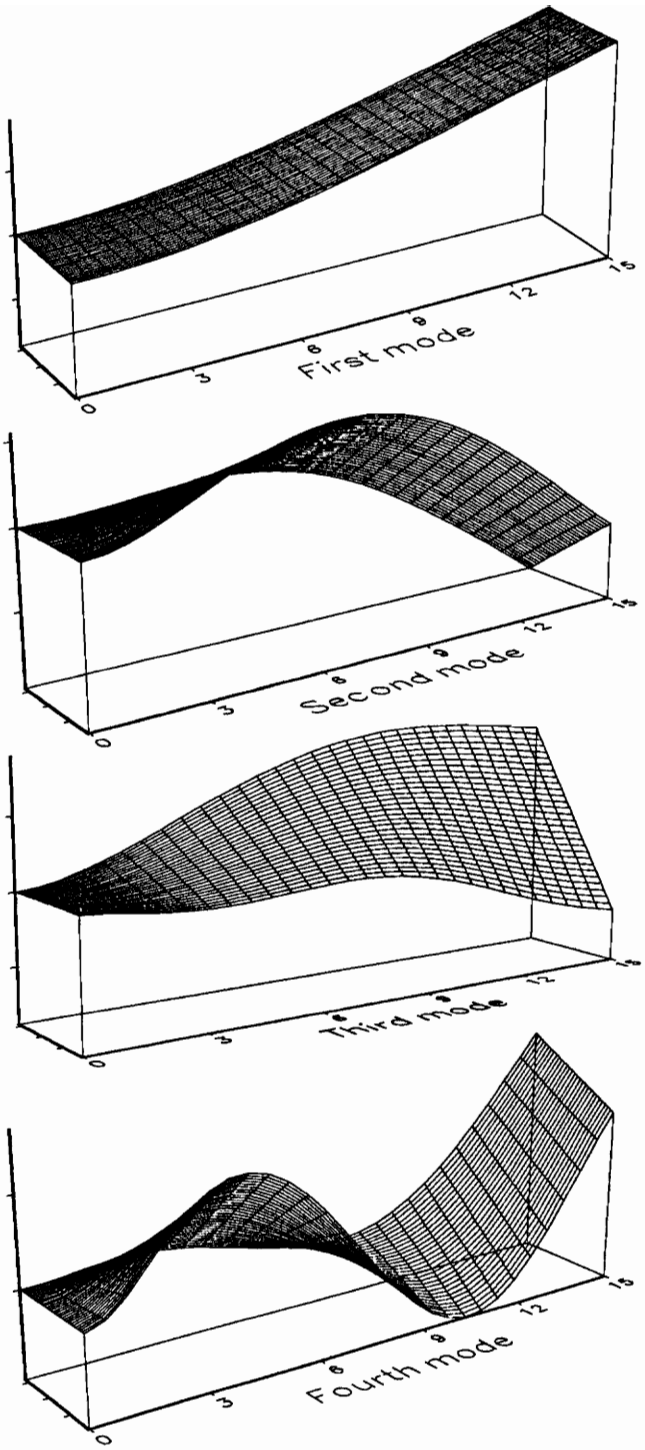

Figure 4.23 Natural mode shapes for laminate $[90/\pm 15/0_2/-15/45/90]_4$ ($l = 15\ in,\ c = 3\ in$) based on the FSDT and consideration of the free warping.

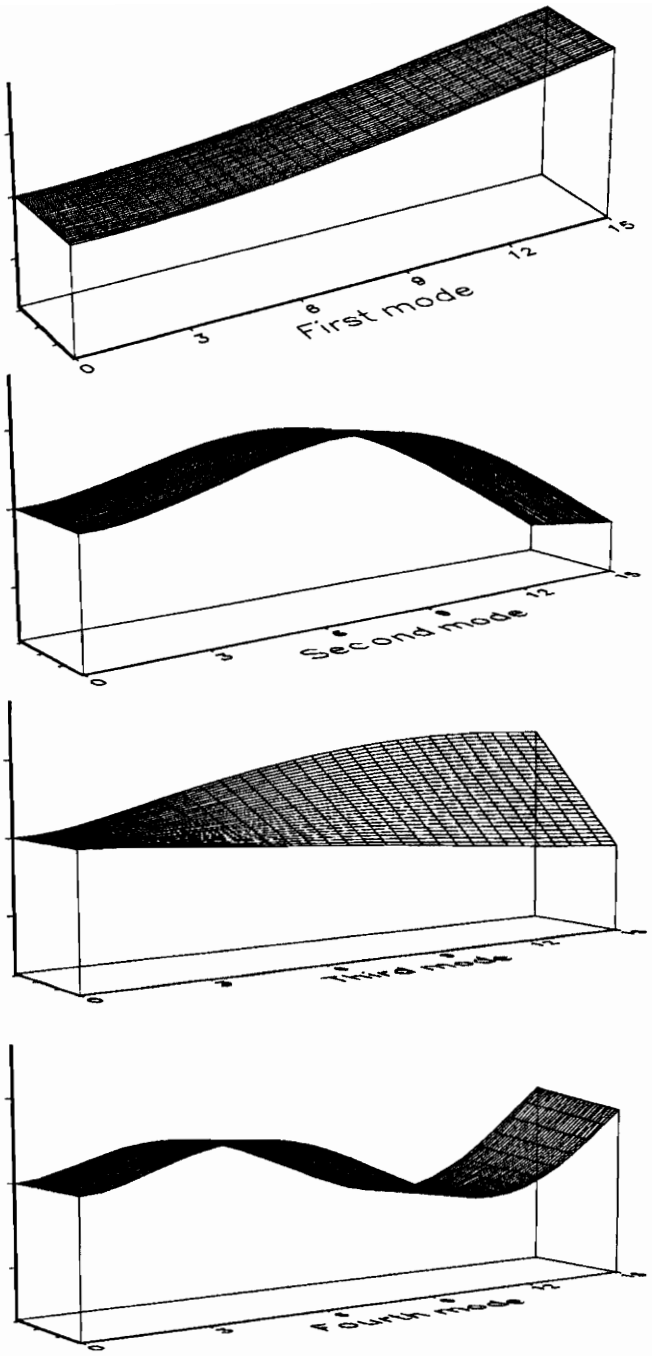

Figure 4.24 Natural mode shapes for laminate $[90/\pm 15/0_2/-15/45/90]_4$ ($l = 15\ in,\ c = 3\ in$) based on CLT with/without incorporation of the warping restraint.

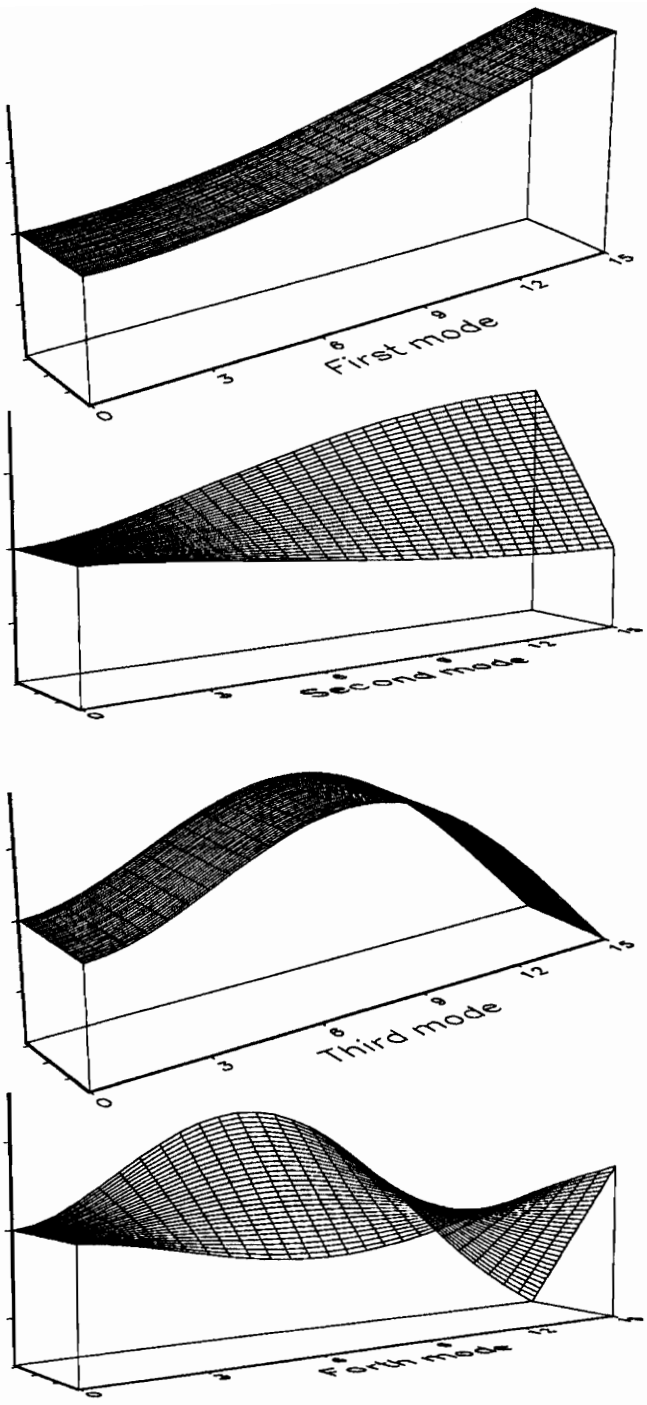

Figure 4.25 Natural mode shapes for laminate $[90_3/0]_{S4}$ ($l = 15\ in,\ c = 3\ in$) based on the FSDT and consideration of the warping restraint (Same results are obtained for CLT with/without incorporation of the warping restraint).

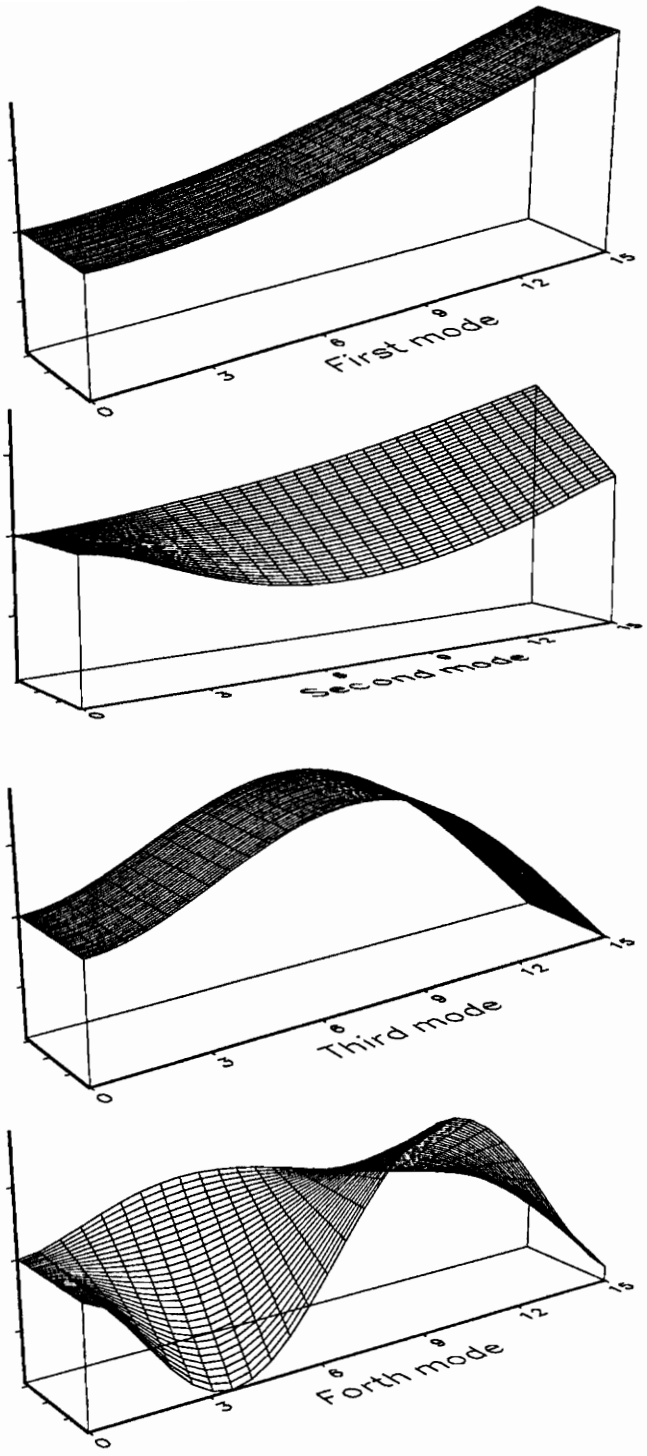

Figure 4.26 Natural mode shapes for laminate $[90_3/0]_{S4}$ ($l = 15\ in,\ c = 3\ in$) based on the FSDT with consideration of the free warping.

5. PASSIVE VIBRATION CONTROL

5.1 Overview

The advance of composite materials and their increased use in aircraft wing structures has resulted lately in the development of an efficient design technique in which elastic tailoring has provided new ways of vibration control. For enhancement of dynamic characteristics of anisotropic composite structures, the tailoring technique can provide a means of passive vibration control. For instance, as shown in Ref. [20], for swept-wing aircraft the bending deformations tend to reduce or increase twist angles, which can constitute beneficial or detrimental effects on stability performance of aircraft wings.

Furthermore, the significant effects of warping restraint and bending-twist coupling must be included in the tailoring of cantilevered composite structures. For this reason structural tailoring of laminated composite cantilevers was performed by incorporating the coupling and the warping constraint effects [11-13]. Within the tailoring technique, elastic constants, stacking sequences, ply angles, and thickness of each layer were considered as design variables.

From the point of view of the design, the structural tailoring technique, yielding modification of the behavior of a system without any control forces, seems to provide the best means for passive vibration control of cantilevered composite structures.

5.2.1 Structural Tailoring Results:

The structural tailoring technique is applied by operating on the ply orientation, θ, in the given stacking sequence. Figures 5.1-6 reveal the power of the structural tailoring technique on the free vibration analysis of cantilevered composite structures. Variations of first bending and torsional frequencies are plotted versus ply orientation θ. The geometry of the composite cantilever is given by $l = 6\ in,\ c = 3\ in$ or $l = 12\ in,\ c = 3\ in$. In Figures 5.1-2, eight constituent layers are considered. Further, the number of laminae increases by a factor of two. In Figures 5.3-6, sixteen layers are considered.

The plots reveal the effect of the tailoring technique towards the enhancement of the free vibration response of the structure. As seen in Figure 5.1, for a thin ($l/h = 141.5$) and low-aspect-ratio ($\mathcal{AR} = 4$) structure, of lamination scheme: $[90/\pm\theta/0/90/\mp\theta/0]_S$, the first bending frequency for $\theta = 90^0$ becomes three times larger than the one corresponding to the poor design $[0/\pm\theta/90]_{S2}$ ($\theta = 0$). Figures 5.3 and 5.5 show the bending frequencies raised up to 84% for both cases of $l = 12\ in,\ c = 3\ in$, and $l = 6\ in,\ c = 3\ in$ for the sixteen-layer laminate. For the eight-layer laminate, two stacking sequences, $[90/\pm\theta/0]_2$ and $[0/\pm\theta/90]_2$, give the same results for both bending and torsional vibration.

To check the influence of bending-stretching coupling on the natural frequencies, asymmetric stacking sequences are also considered, together with the symmetric ones. For this purpose, two stacking sequences, $[90/\pm\theta/0]_S$ and $[90/\pm\theta/0]_2$, are shown for the eight-layer structure in Figures 5.1-2. In similar fashion, stacking sequences $[90/\pm\theta/0/90/\mp\theta/0]_S$ and $[90/\pm\theta/0/90/\mp\theta/0]_2$ are considered for the sixteen-layer structure in Figures 5.3-6. It turns out that bending-stretching coupling has a detrimental effect on structural tailoring. In practical design, for

evident reasons, symmetric laminates have been largely used. The results found here by using the tailoring technique validate the use of symmetric laminates also from the structural tailoring point of view.

For all cases, the bending frequencies increase as θ rotates toward 90^o. It implies that by placing more layers with plies in the spanwise direction, we can achieve higher bending natural frequencies. Unlike bending ones, higher torsional frequencies are obtained at different ply orientations with respect to the change of span length. For low aspect ratios, a higher torsional stiffness is predicted when the θ-layers are oriented around 45^o. The tailored beam structures follow the same pattern. For a moderate aspect ratio ($\mathcal{AR} = 8$), the ply angle θ rending higher torsional frequencies shifts to the right for different stacking sequences. Higher torsional natural frequencies for the laminate $[90/\pm\theta/0/90/\mp\theta/0]_S$ are obtained at $\theta = 53^o$ and for $[0/\pm\theta/90]_{S2}$ at $\theta = 60^o$.

To investigate the trend, various aspect ratios of beams are considered. Figures 5.7-8 display the variation of natural frequencies versus ply orientation for $c = 3in$ and various values of l. For all the cases, higher bending frequencies are predicted when the ply angles are near 90^o. As the beam aspect ratio increases, θ shifts toward 90^o yielding higher torsional frequencies of the beam. It implies that structural tailoring for both bending and torsional vibration can be done simultaneously.

Some conclusions on passive vibration control using structural tailoring technique are in order:

The results obtained (see Figures 5.1-6) reveal that for cantilevered laminates the tailoring technique is very effective. In this sense, it was shown that the free vibration characteristics of the structure can be dramatically improved via the application of the tailoring technique. It should be emphasized that such

an enhancement via the tailoring technique is achieved without weight penalties. These high capabilities are important in the practical application to vibration control.

5.2.2 Nonclassical Effects on Structural Tailoring:

In this section, the nonclassical effects of bending-twist coupling, transverse shear flexibility and warping restraint, characterizing the anisotropic composite cantilevers, will be investigated.

To infer information about the effect of bending-twist coupling on structural tailoring, the laminate $[90/\pm\theta/0]_{S2}$ structure based on CLT is considered. The bending-twist elastic coupling is induced through the coupling rigidity $\bar{D}_{26}$ in Eq. (3.29). The tailoring results based on CLT are compared to those of the hypothetical models characterized by $\bar{D}_{26} = 0$, wherein coupling is not considered although it exists.

As seen in Figure 5.9, bending frequencies are not affected by bending-twist coupling. However, the bending-twist coupling in cantilevered composite structure causes large changes in torsional frequencies (Figure 5.10). The coupling effect becomes broader when the warping restraint exists. Within the presence of the warping restraint, the bending and twist stiffnesses are coupled in the range $7^o \leq \theta \leq 70^o$, while in its absence, the coupling occurs in the range $16^o \leq \theta \leq 65^o$. High torsional frequencies are obtained near the points where coupling begins. If the coupling parameter $\bar{D}_{26}$ is not considered, the ply orientation is tailored at $\theta = 45^o$. The artificial discarding of cross-coupling may lead to erroneous results in the torsional vibration problem.

In summary, bending-twist cross-coupling plays an important role in the dynamic response characteristics. For an isotropic material structure, torsional vibration is independent of bending. However, for a composite cantilevered structure,

bending deformation interacts with the torsional deformation, leading to changes of torsional natural frequencies.

To investigate the effect of transverse shear deformation with respect to laminate thickness changes, thirty-two layers are used in Figures 5.11-12; later, in Figures 5.13-14 and 5.15-16, the number of laminae increases by factor of two and three, respectively. The effects of transverse shear deformation and warping restraint appear to be more significant in the uncoupled range. The effect of warping restraint based on CLT is not readily seen when the elastic coupling between bending and torsion is present. This is different for FSDT, where the effect of warping restraint is apparent. The coupling range decreases as the laminate thickness doubles, but remain the same after doubling. This is observed by comparing Figures 5.14 and 5.16. The coupling range $12^o \leq \theta \leq 61^o$ changes to $15^o \leq \theta \leq 59^o$. As has been seen in Figures 5.12 and 5.16, the first torsional frequencies predicted by both FSDT and CLT with consideration of the warping restraint effect are always higher than their free warping model counterparts. However, when $l/h = 22.1$ and $\mathcal{AR} = 10$ (see Figure 5.16) the effect of transverse shear deformation becomes more prominent than that of the warping restraint.

5.2.3 Parametric Study for Shear Correction Factor in Structural Tailoring:

In Figures 5.17-20, parametric studies on the influence of the transverse shear correction factor are performed. The shear correction factor, K^2, is chosen to be either 5/6 or 2/3. The span-to-thickness ratio changes with respect to the changes of laminate thickness while the aspect ratio is fixed to be $\mathcal{AR} = 10$. The discrepancy between the results for these two different K^2 increases as the laminate thickness increases. It is also seen that the higher frequencies are more influenced by the shear correction factor. In conclusion, it is suggested that further study of the shear correction factor is needed for accurate analysis of the composite laminate, especially for thick structures.

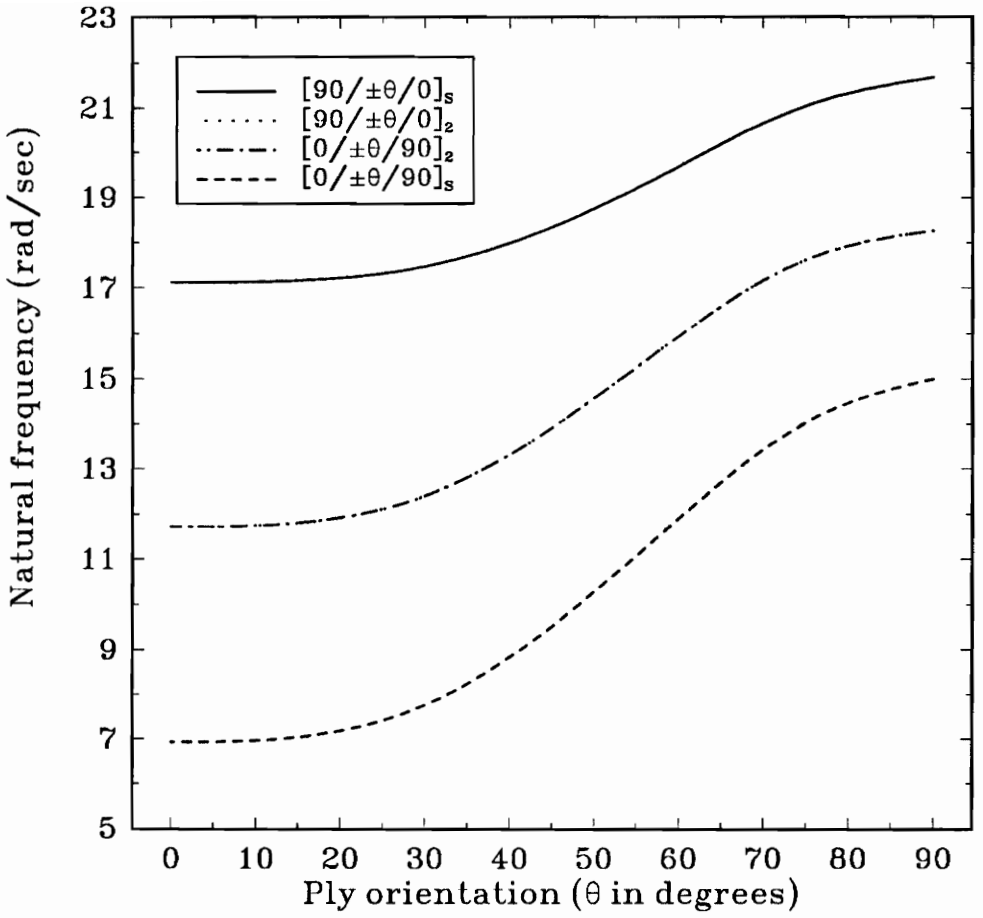

Figure 5.1 Variation of first bending frequencies versus ply orientation as design variable for eight-layer laminate ($l = 6$ *in*, $c = 3$ *in*) based on the FSDT with consideration of the warping restraint effect.

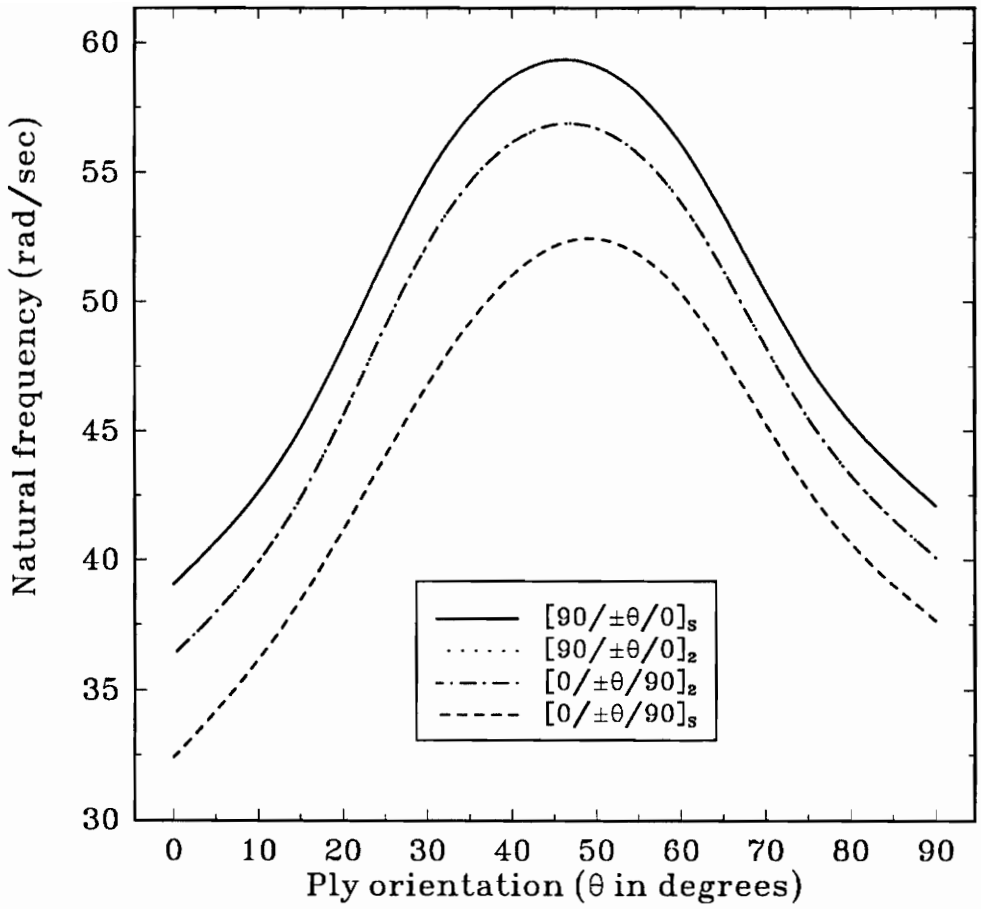

Figure 5.2 Variation of first torsional frequencies versus ply orientation as design variable for eight-layer laminate ($l = 6\ in$, $c = 3\ in$) based on the FSDT with consideration of the warping restraint effect.

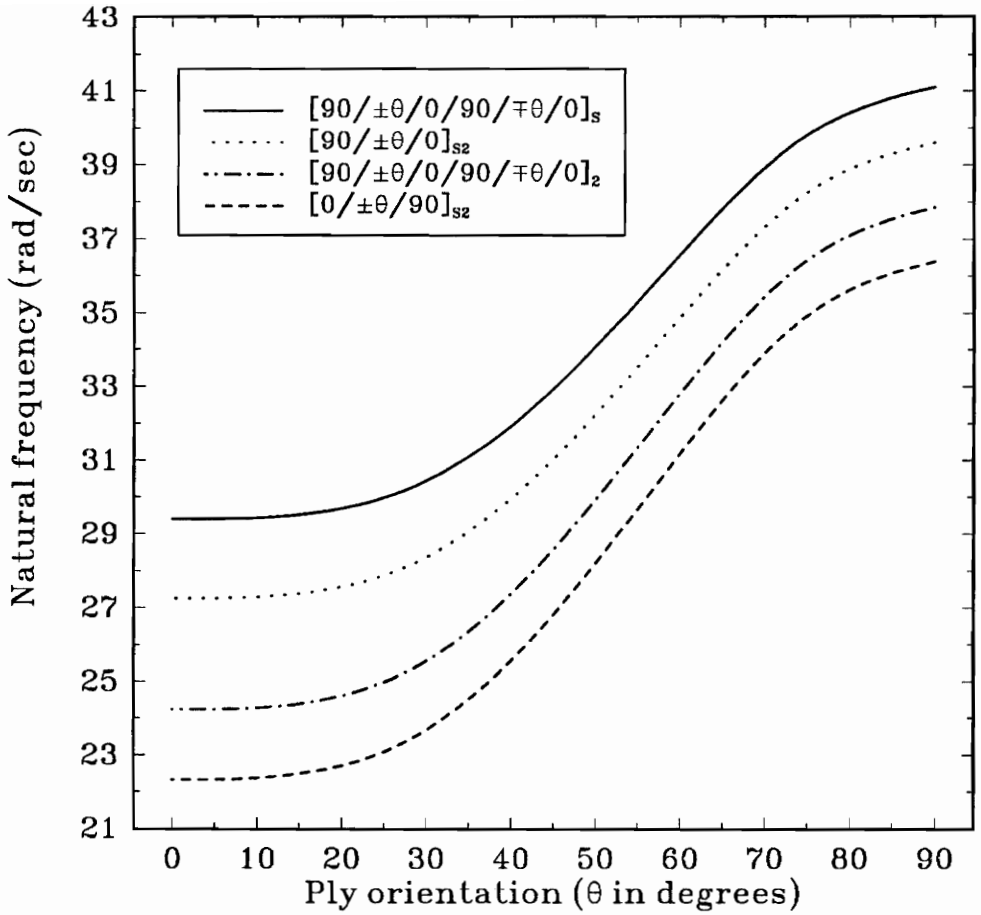

Figure 5.3 Variation of first bending frequencies versus ply orientation as design variable for sixteen-layer laminate ($l = 6\ in,\ c = 3\ in$) based on the FSDT with consideration of the warping restraint effect.

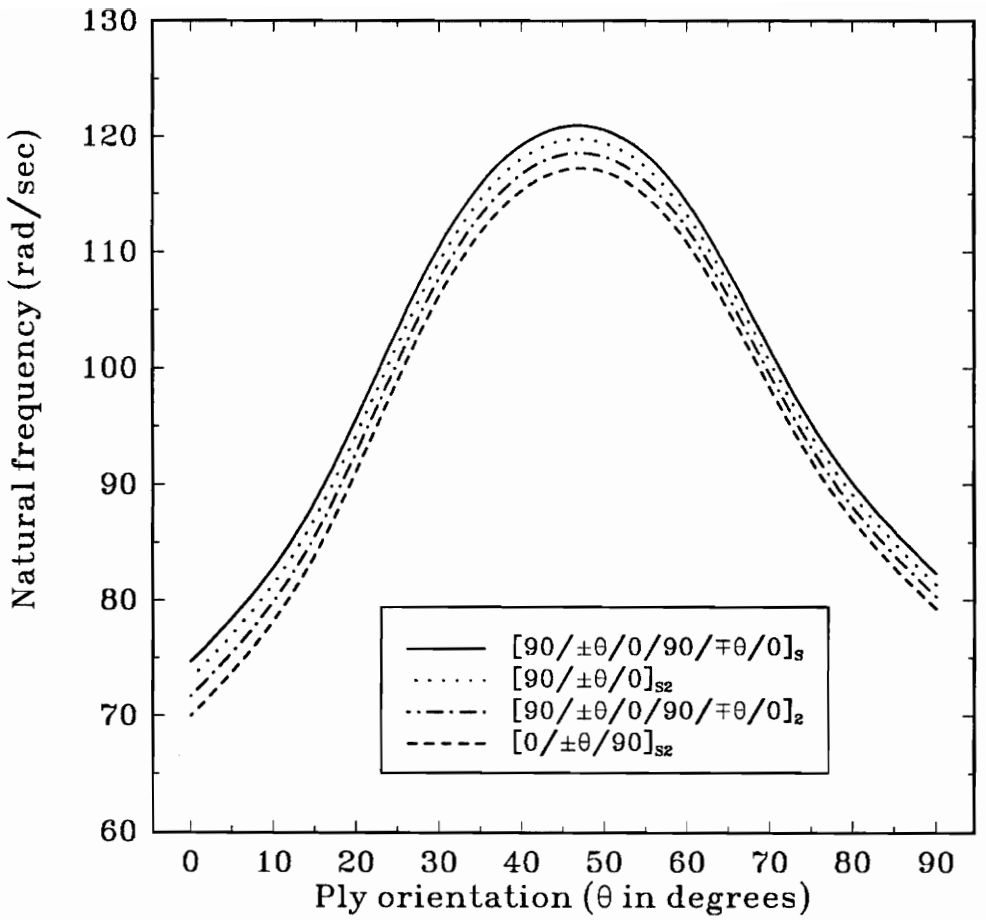

Figure 5.4 Variation of first torsional frequencies versus ply orientation as design variable for sixteen-layer laminate ($l = 6\ in,\ c = 3\ in$) based on the FSDT with consideration of the warping restraint effect.

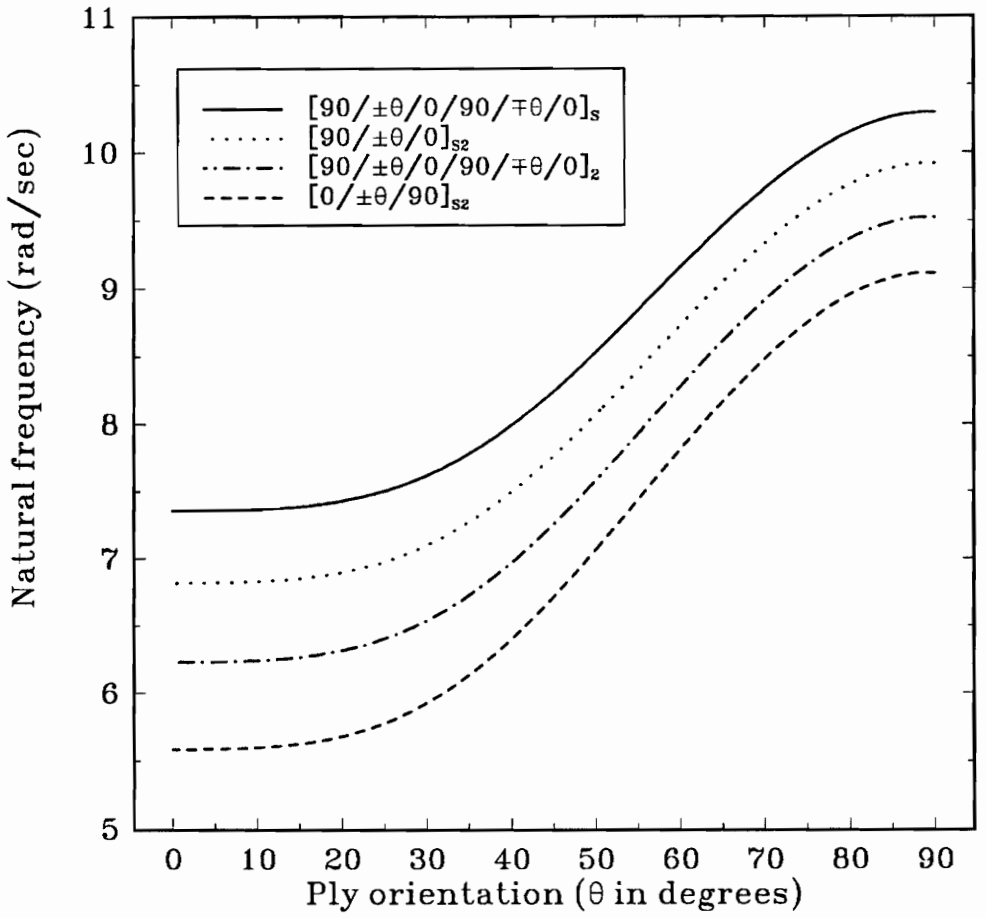

Figure 5.5 Variation of first bending frequencies versus ply orientation as design variable for sixteen-layer laminate ($l = 12\ in,\ c = 3\ in$) based on the FSDT with consideration of the warping restraint effect.

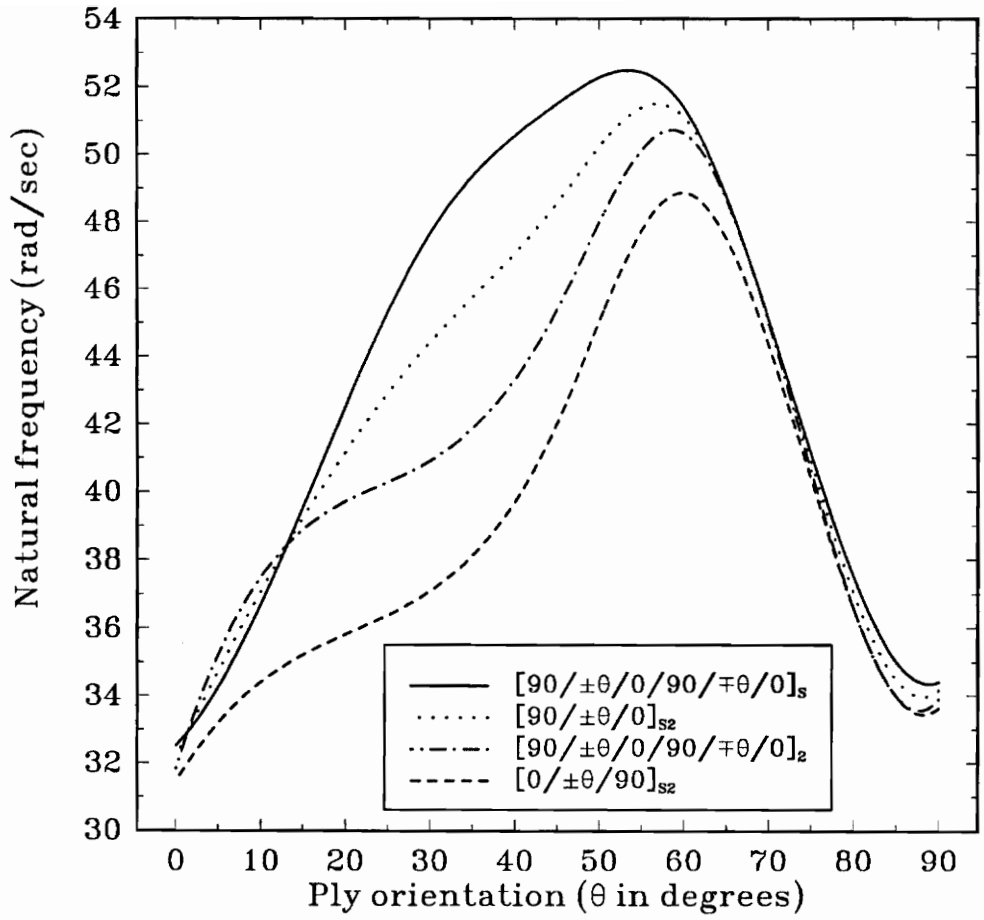

Figure 5.6 Variation of first torsional frequencies versus ply orientation as design variable for sixteen-layer laminate ($l = 12\ in,\ c = 3\ in$) based on the FSDT with consideration of the warping restraint effect.

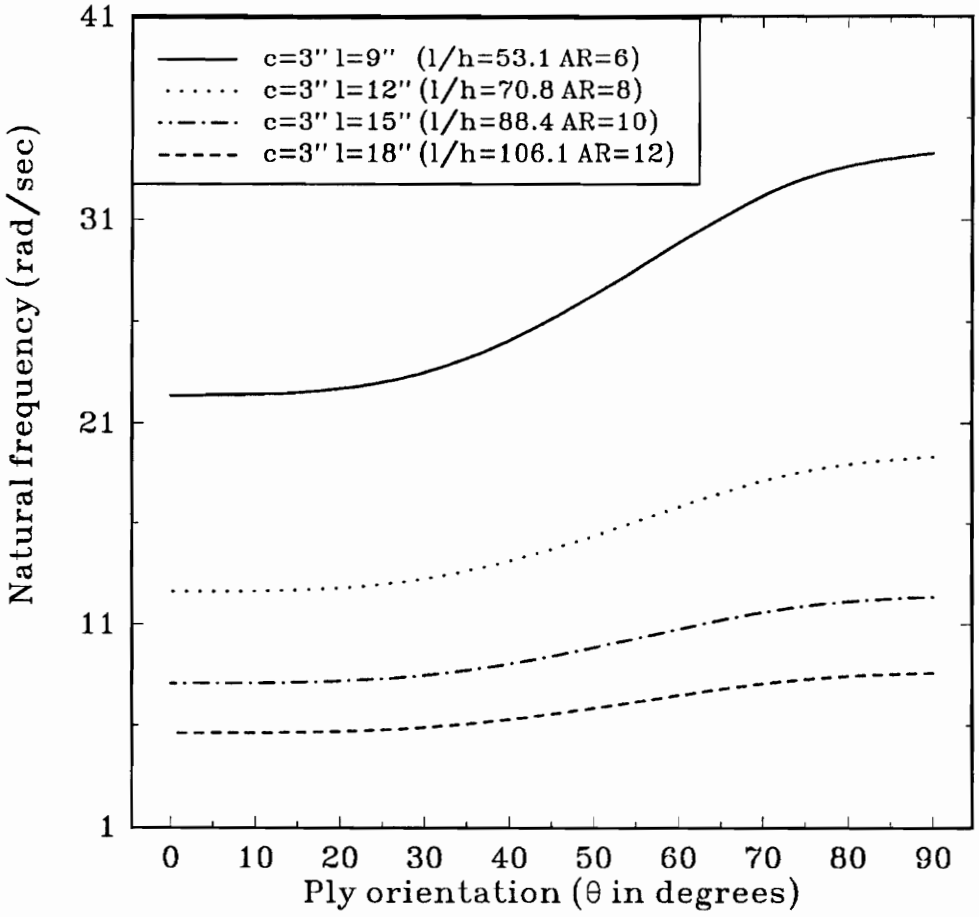

Figure 5.7 Variation of first bending frequencies versus ply orientation for various aspect ratios of laminate $[90/\pm\theta/0]_{S4}$ based on the FSDT with consideration of the warping restraint effect.

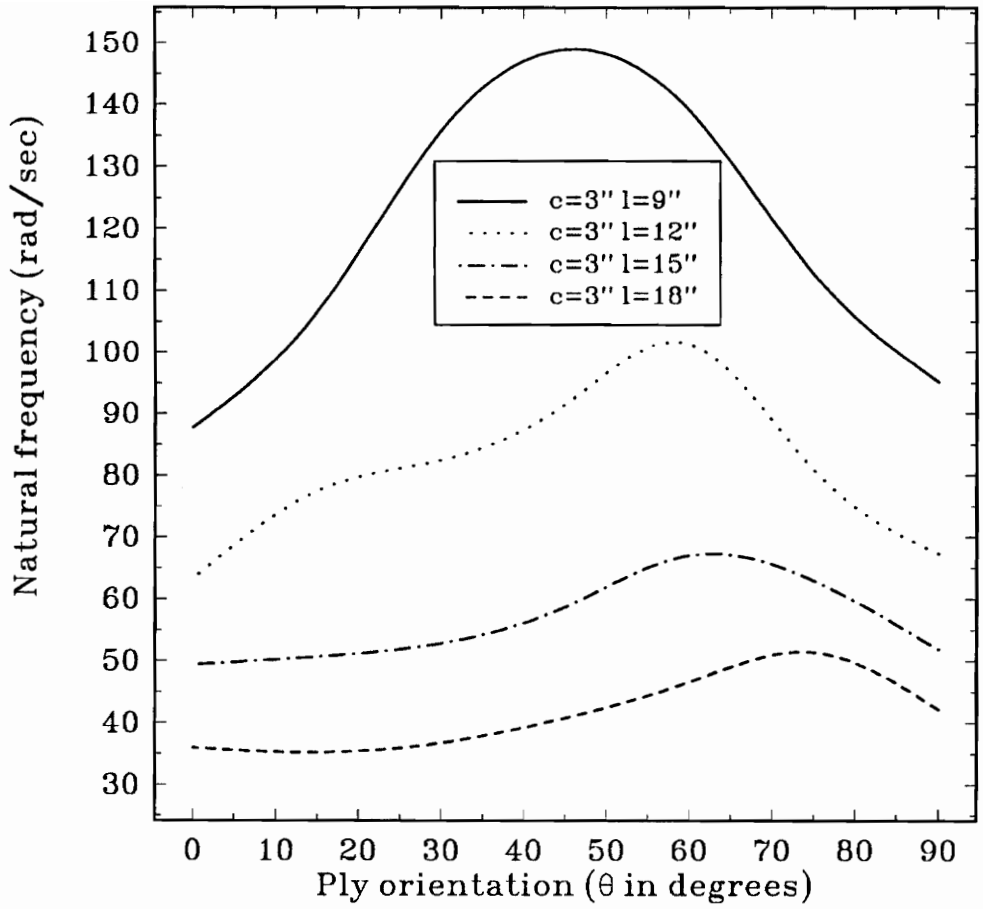

Figure 5.8 Variation of first torsional frequencies versus ply orientation for various aspect ratios of laminate $[90/\pm\theta/0]_{S4}$ based on the FSDT with consideration of the warping restraint effect.

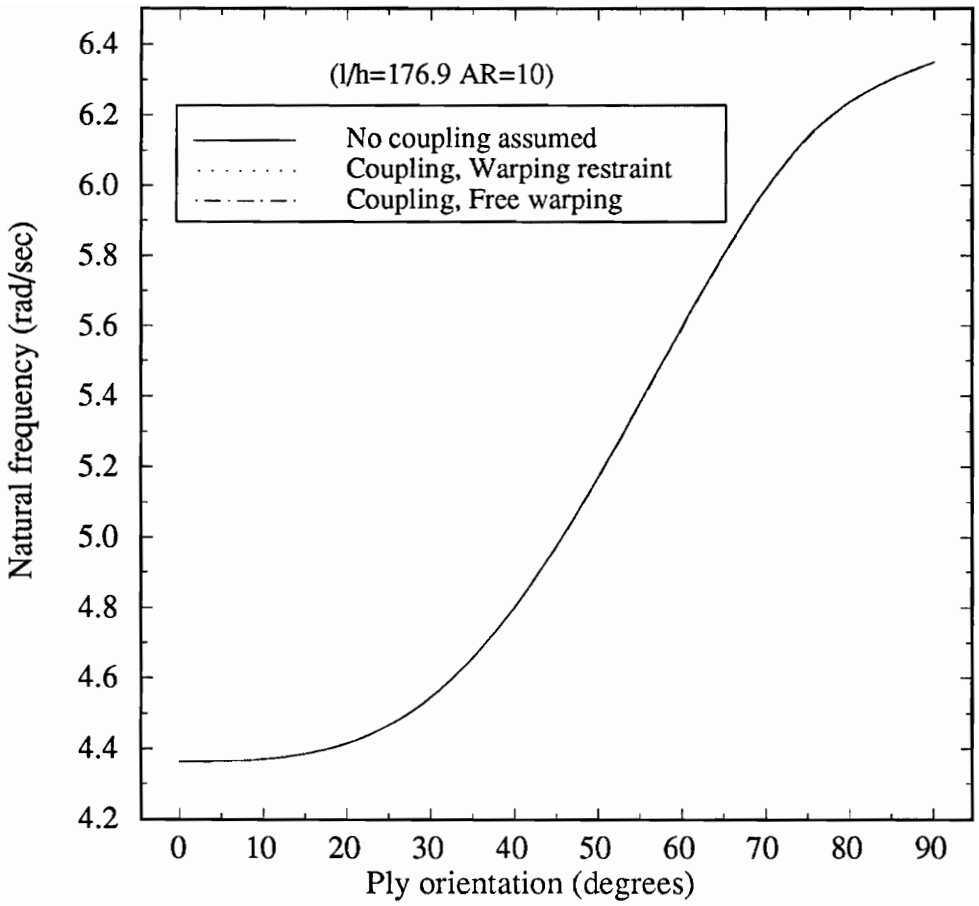

Figure 5.9 Effects of bending-twist coupling and warping restraint on the first bending frequency of laminate $[90/\pm\theta/0]_{S2}$ ($l = 15\ in,\ c = 3\ in$) based on CLT.

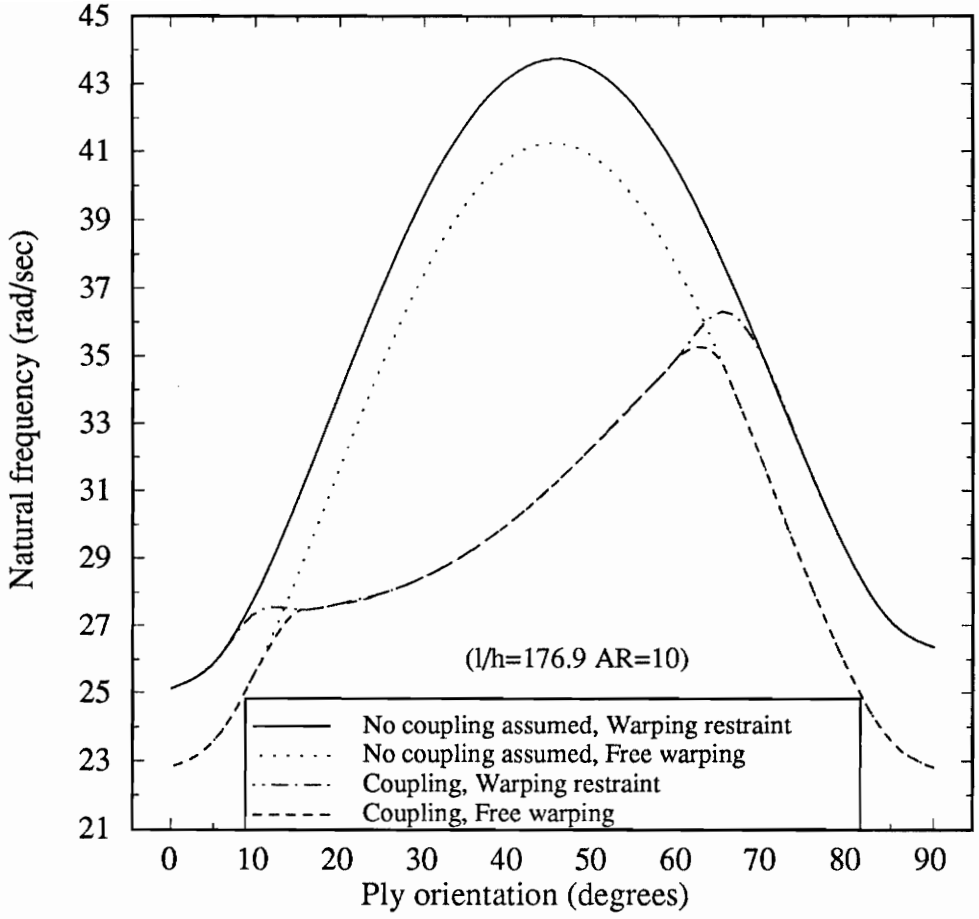

Figure 5.10 Effects of bending-twist coupling and warping restraint on the first torsional frequency of laminate $[90/\pm\theta/0]_{S2}$ ($l = 15\ in,\ c = 3\ in$) based on CLT.

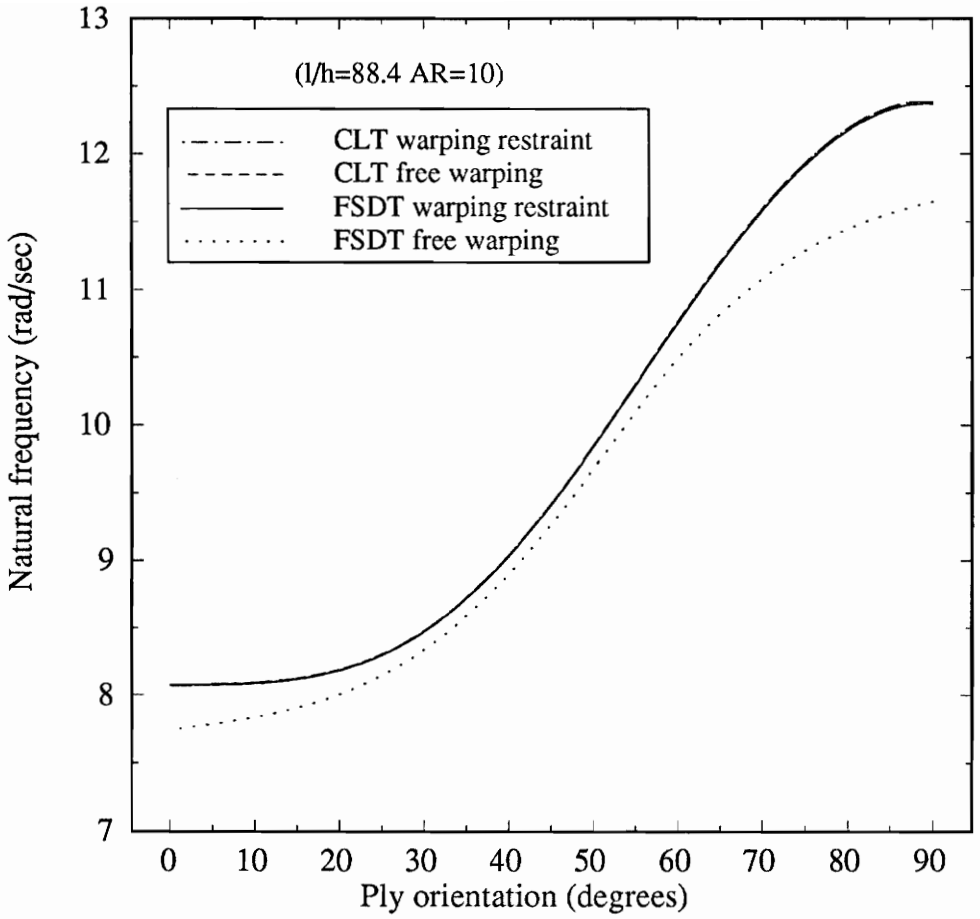

Figure 5.11 Effects of transverse shear deformation and warping restraint on the first bending frequencies of 32-layer laminate $[90/\pm\theta/0]_{S4}$ ($l = 15\ in,\ c = 3\ in$).

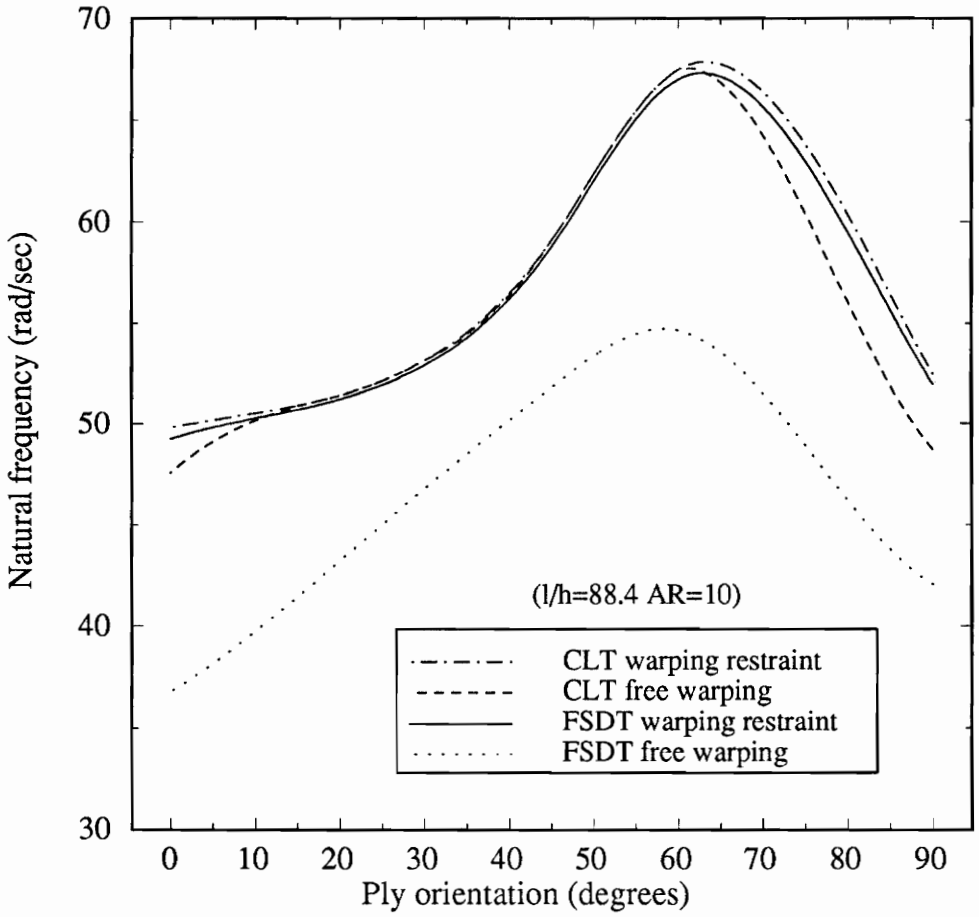

Figure 5.12 Effects of transverse shear deformation and warping restraint on the first torsional frequencies of 32-layer laminate $[90/\pm\theta/0]_{S4}$ $(l = 15\ in,\ c = 3\ in)$.

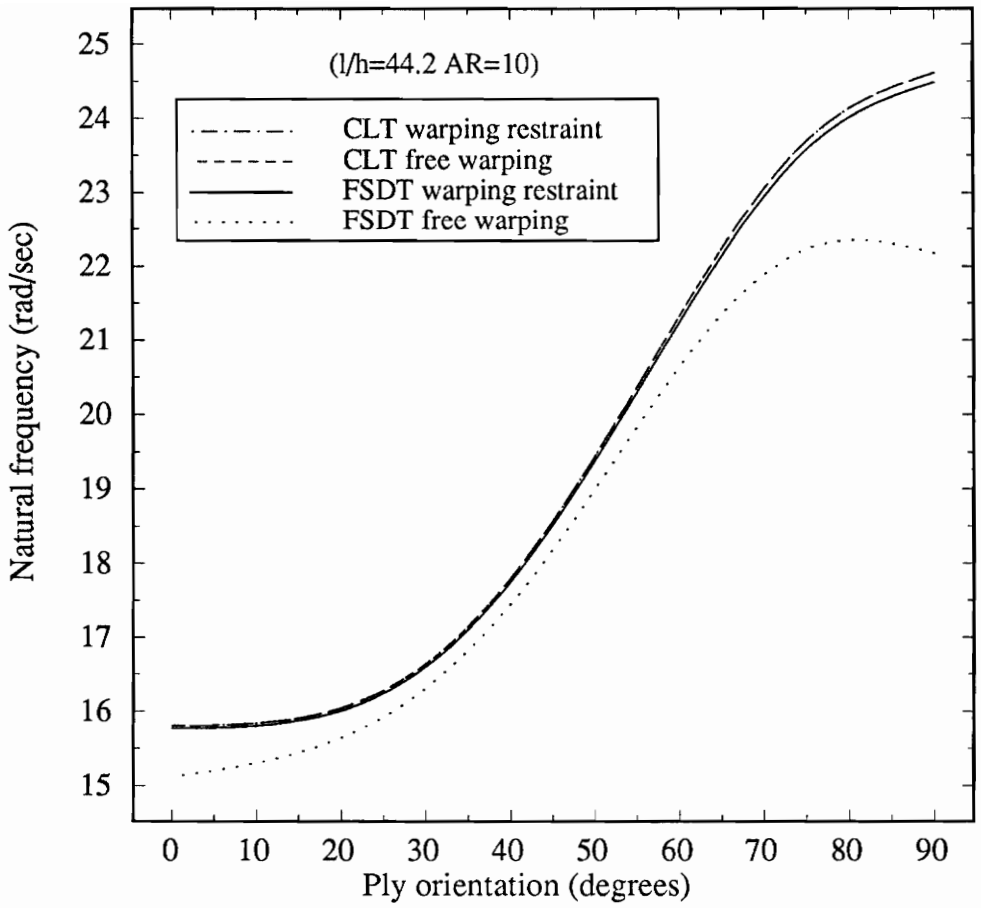

Figure 5.13 Effects of transverse shear deformation and warping restraint on the first bending frequencies of 64-layer laminate $[90/\pm\theta/0]_{S8}$ ($l = 15\ in,\ c = 3\ in$).

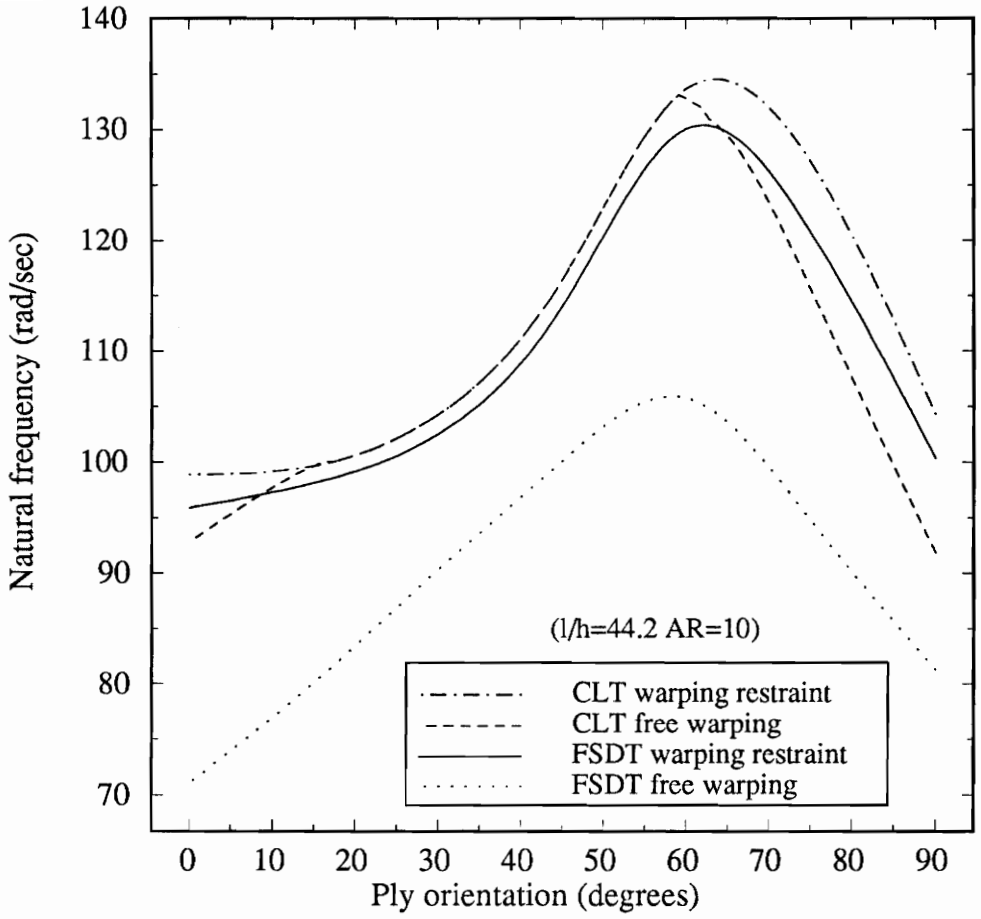

Figure 5.14 Effects of transverse shear deformation and warping restraint on the first torsional frequencies of 64-layer laminate $[90/\pm\theta/0]_{S8}$ ($l = 15\ in,\ c = 3\ in$).

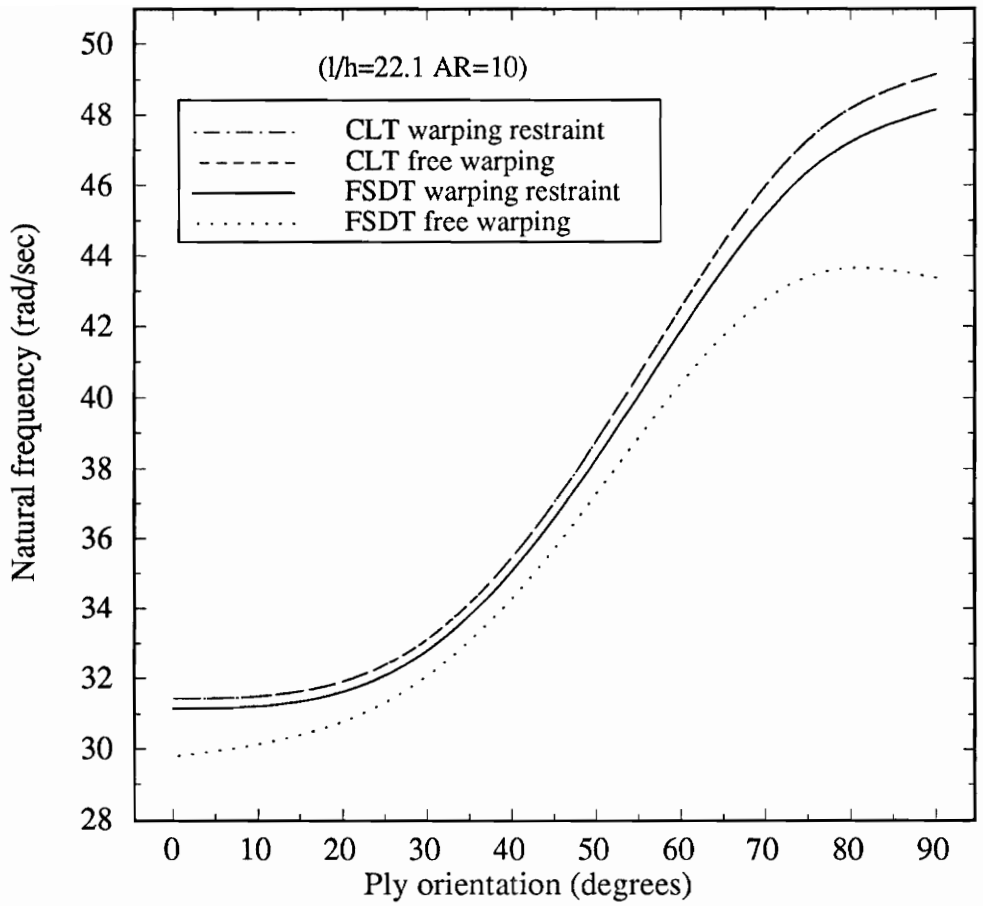

Figure 5.15 Effects of transverse shear deformation and warping restraint on the first bending frequencies of 128-layer laminate $[90/\pm\theta/0]_{S16}$ $(l = 15\ in,\ c = 3\ in)$.

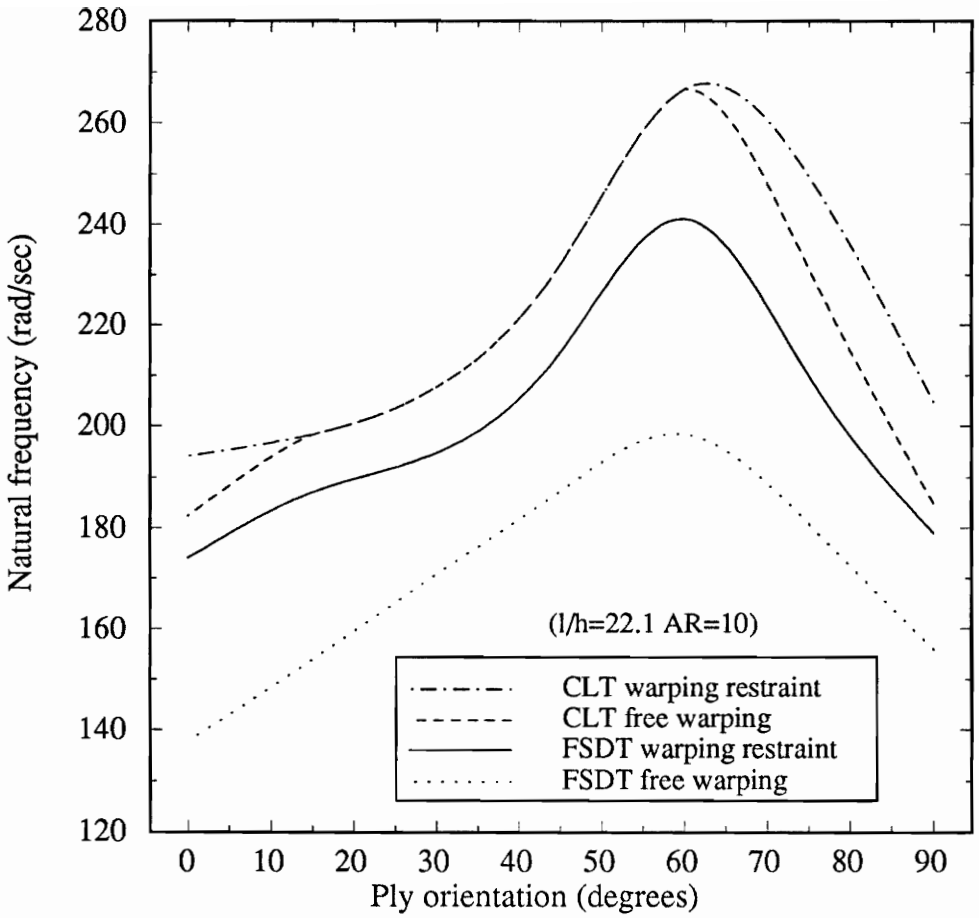

Figure 5.16 Effects of transverse shear deformation and warping restraint on the first torsional frequencies of 128-layer laminate $[90/\pm\theta/0]_{S16}$ $(l = 15\ in,\ c = 3\ in)$.

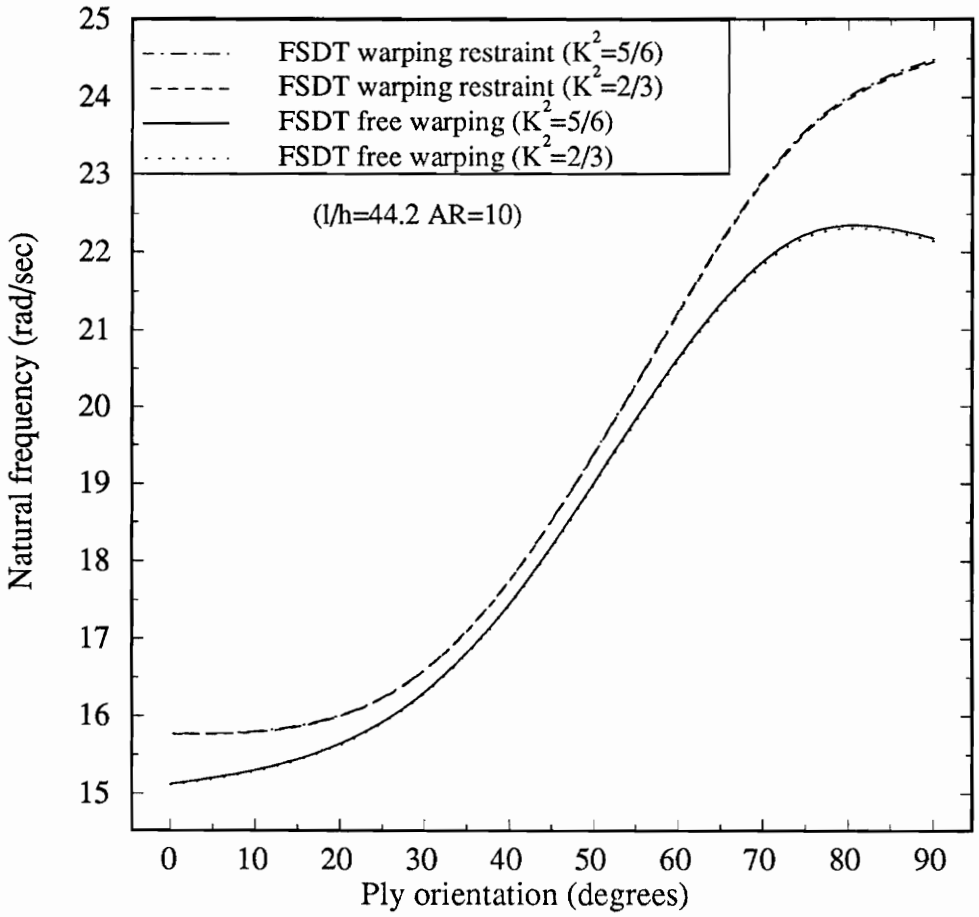

Figure 5.17 Parametric study for transverse shear correction factors in structural tailoring (first bending frequencies plotted for 64-layer laminate $[90/\pm\theta/0]_{S8}$ with $l = 15\ in,\ c = 3\ in$).

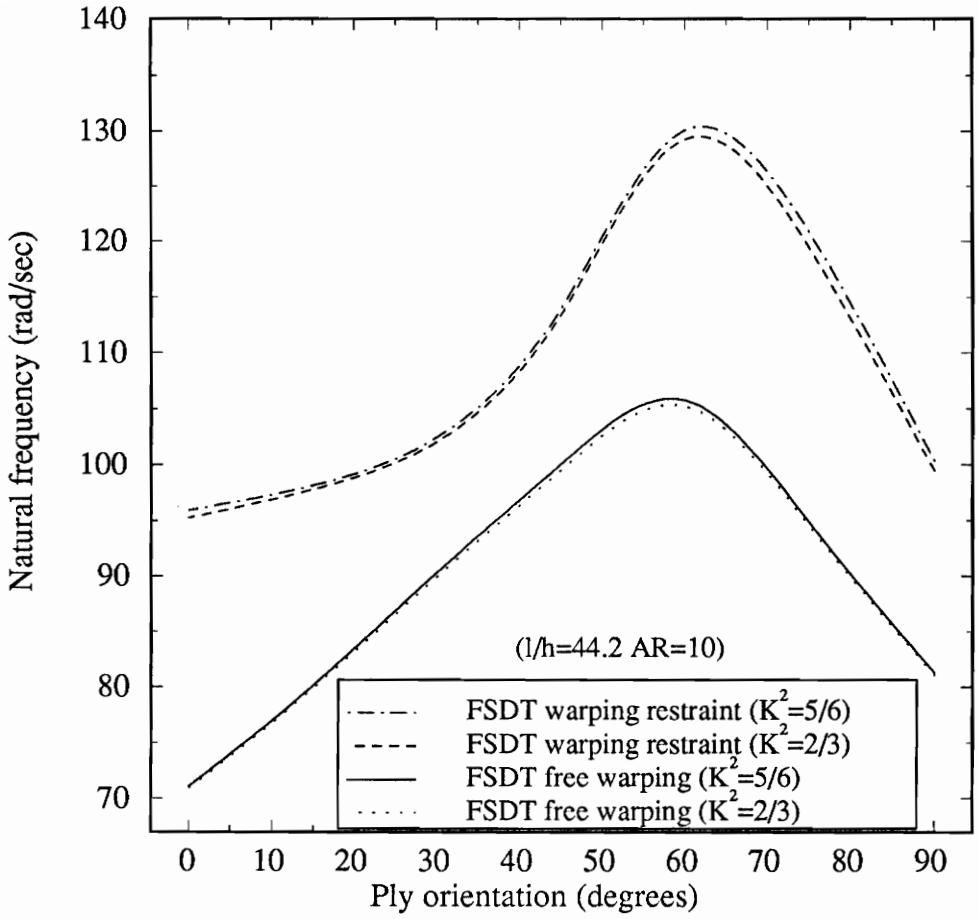

Figure 5.18 Parametric study for transverse shear correction factors in structural tailoring (first torsional frequencies plotted for 64-layer laminate $[90/\pm\theta/0]_{S8}$ with $l = 15\ in,\ c = 3\ in$).

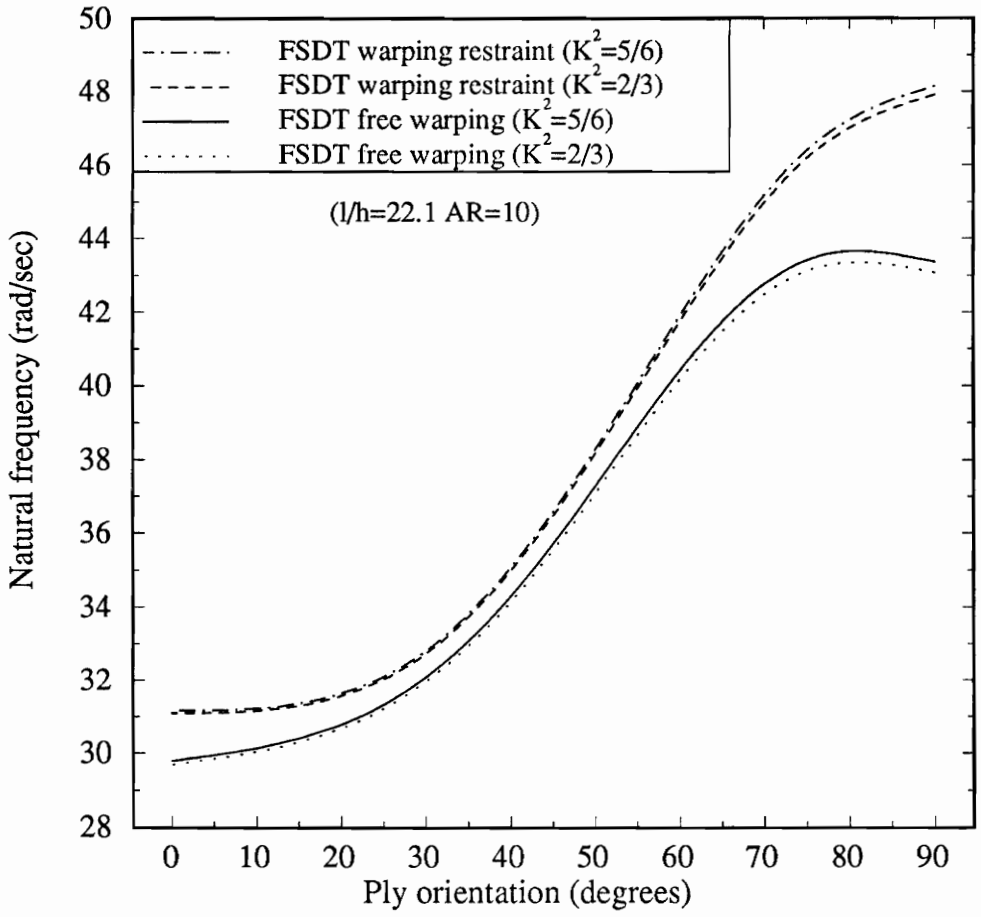

Figure 5.19 Parametric study for transverse shear correction factors in structural tailoring (first bending frequencies plotted for 128-layer laminate $[90/\pm\theta/0]_{S16}$ with $l = 15\ in,\ c = 3\ in$).

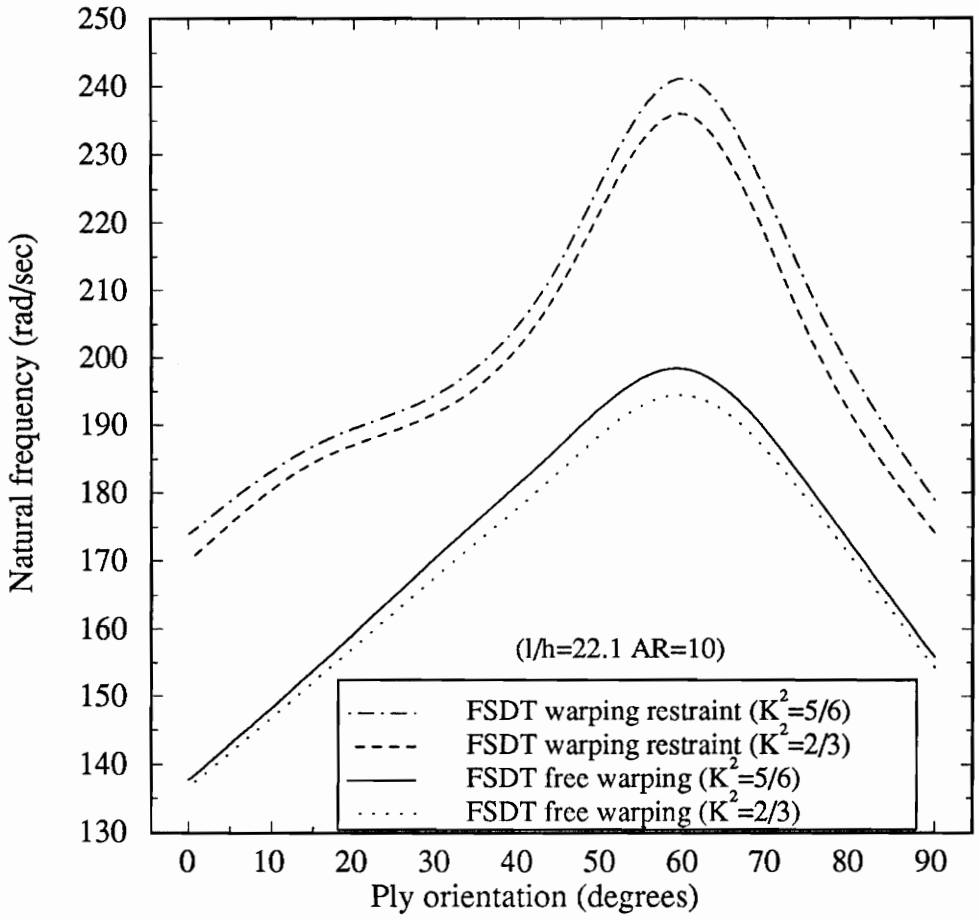

Figure 5.20 Parametric study for transverse shear correction factors in structural tailoring (first torsional frequencies plotted for 128-layer laminate $[90/\pm\theta/0]_{S16}$ with $l = 15\ in,\ c = 3\ in$).

6. STRUCTURAL OPTIMIZATION

6.1 Overview

Herein the optimum design procedure is aimed at maximizing the natural frequencies of cantilevered composite structures. In contrast to a number of previous works, transverse shear deformation and warping restraint are taken into consideration. Even though many optimization techniques have been developed in the design of composite structures, they experience severe limitation in application. For example, typical linear integer programming can not be applied if the exact solution is not readily available. Therefore, this technique is no longer applicable to the eigenvalue problems set up by variational formulation. In addition, their results are not a true optimum because ply orientations are preassigned and specific stacking sequences such as symmetric and cross-ply are considered for the design problem.

The optimization technique based on nonlinear real programming presented here has no such limitations and can deal with all cases of stacking sequences. In this technique, the ply orientation is treated as a real number, and does not need to be transformed to an integer variable. Certainly this approach is more complex than integer programing; however, it is more powerful. Moreover, this technique has many applications. For example, it is quite useful for parameter estimation in which a certain design variable can be found for the design of robust structures with respect to damage and uncertainty.

6.2 Structural Optimization Technique

The problem is to find the ply orientations in a consequential stacking sequence rendering maximum a natural frequency in bending and torsion for laminated composite structures. The objective function considered here is neither explicit nor linear since a variational formulation has been applied to obtain the natural frequencies. In the optimization process, computation begins with starting values of ply orientations. Iteration is carried out until the optimum is achieved.

The optimization process starts with reduced stiffnesses Q_{ij} in terms of engineering constants,

$$
\begin{gathered}
Q_{11} = \frac{E_1}{1-\nu_{12}\nu_{21}}, \qquad Q_{22} = \frac{E_2}{1-\nu_{12}\nu_{21}}, \\
Q_{12} = \frac{\nu_{12}E_2}{1-\nu_{12}\nu_{21}} = \frac{\nu_{21}E_1}{1-\nu_{12}\nu_{21}}, \qquad Q_{66} = G_{12}, \\
Q_{44} = G_{23}, \qquad Q_{55} = G_{13}.
\end{gathered} \tag{6.1}
$$

The constitutive equations in Eqs. (3.4-5) are represented by stress-strain relationships in structural coordinates. The reduced stiffnesses expressed in principal material coordinates, $1, 2, 3$ axes, need to be transformed into the ones corresponding to laminate coordinates, x, y, z axes. Here

$$
\begin{aligned}
\bar{Q}_{11} &= Q_{11}\cos^4\theta + 2(Q_{12}+2Q_{66})\sin^2\theta\cos^2\theta + Q_{22}\sin^4\theta, \\
\bar{Q}_{22} &= Q_{22}\sin^4\theta + 2(Q_{12}+2Q_{66})\sin^2\theta\cos^2\theta + Q_{22}\cos^4\theta, \\
\bar{Q}_{12} &= (Q_{11}+Q_{22}-4Q_{66})\cos^2\theta\sin^2\theta + Q_{12}(\sin^4\theta+\cos^4\theta), \\
\bar{Q}_{16} &= (Q_{11}-Q_{12}-2Q_{66})\sin\theta\cos^3\theta + (Q_{12}-Q_{22}+2Q_{66})\sin^3\theta\cos\theta, \\
\bar{Q}_{26} &= (Q_{11}-Q_{12}-2Q_{66})\sin^3\theta\cos\theta + (Q_{12}-Q_{22}+2Q_{66})\sin\theta\cos^3\theta, \\
\bar{Q}_{66} &= (Q_{11}+Q_{22}-2Q_{12}-2Q_{66})\sin^2\theta\cos^2\theta + Q_{66}(\sin^4\theta+\cos^4\theta), \\
\bar{Q}_{44} &= Q_{44}\cos^2\theta + Q_{55}\sin^2\theta, \qquad \bar{Q}_{55} = Q_{44}\sin^2\theta + Q_{55}\cos^2\theta.
\end{aligned} \tag{6.2}
$$

With the material invariants in Eq. (6.3), transformed reduced stiffnesses are expressed in Table 6.1:

$$
\begin{aligned}
U_1 &= \frac{1}{8}(3Q_{11} + 3Q_{22} + 2Q_{12} + 4Q_{66}) \\
U_2 &= \frac{1}{2}(Q_{11} - Q_{22}) \\
U_3 &= \frac{1}{8}(Q_{11} + Q_{22} - 2Q_{12} - 4Q_{66}) \\
U_4 &= \frac{1}{8}(Q_{11} + Q_{22} + 6Q_{12} - 4Q_{66}) \\
U_5 &= \frac{1}{8}(Q_{11} + Q_{22} - 2Q_{12} + 4Q_{66}) \\
U_{10} &= \frac{1}{2}(Q_{55} + Q_{44}) \\
U_{11} &= \frac{1}{2}(Q_{55} - Q_{44})
\end{aligned}
\tag{6.3}
$$

Table 6.1 Transformed reduced stiffness in terms of material invariants.

	constant	$cos2\theta$	$sin2\theta$	$cos4\theta$	$sin4\theta$
$\bar{Q}_{11}$	U_1	U_2	0	U_3	0
$\bar{Q}_{22}$	U_1	$-U_2$	0	U_3	0
$\bar{Q}_{12}$	U_4	0	0	$-U_3$	0
$\bar{Q}_{66}$	U_5	0	0	$-U_3$	0
$\bar{Q}_{16}$	0	0	$-\frac{1}{2}U_2$	0	$-U_3$
$\bar{Q}_{26}$	0	0	$-\frac{1}{2}U_2$	0	U_3
$\bar{Q}_{44}$	U_{10}	$-U_{11}$	0	0	0
$\bar{Q}_{55}$	U_{10}	U_{11}	0	0	0

Finally, structural stiffnesses, A_{ij}, B_{ij}, and D_{ij} in Eq.. (3.8), are expressed in terms of the invariants and out-of-plane coordinate z, and ply orientation θ.

$$
\begin{aligned}
\{A_{11}, B_{11}, D_{11}\} =& U_1 \int_{-h/2}^{h/2} \{1, z, z^2\} dz + U_2 \int_{-h/2}^{h/2} \{1, z, z^2\} \cos 2\theta dz \\
&+ U_3 \int_{-h/2}^{h/2} \{1, z, z^2\} \cos 4\theta dz
\end{aligned}
$$

$$\{A_{22}, B_{22}, D_{22}\} = U_1 \int_{-h/2}^{h/2} \{1, z, z^2\} dz - U_2 \int_{-h/2}^{h/2} \{1, z, z^2\} \cos 2\theta dz$$
$$+ U_3 \int_{-h/2}^{h/2} \{1, z, z^2\} \cos 4\theta dz \tag{6.4}$$

$$\{A_{12}, B_{12}, D_{12}\} = U_4 \int_{-h/2}^{h/2} \{1, z, z^2\} dz - U_3 \int_{-h/2}^{h/2} \{1, z, z^2\} \cos 4\theta dz$$

$$\{A_{66}, B_{66}, D_{66}\} = U_5 \int_{-h/2}^{h/2} \{1, z, z^2\} dz - U_3 \int_{-h/2}^{h/2} \{1, z, z^2\} \cos 4\theta dz$$

$$\{A_{16}, B_{16}, D_{16}\} = -\frac{1}{2} U_2 \int_{-h/2}^{h/2} \{1, z, z^2\} \sin 2\theta dz - U_3 \int_{-h/2}^{h/2} \{1, z, z^2\} \sin 4\theta dz$$

$$\{A_{26}, B_{26}, D_{26}\} = -\frac{1}{2} U_2 \int_{-h/2}^{h/2} \{1, z, z^2\} \sin 2\theta dz + U_3 \int_{-h/2}^{h/2} \{1, z, z^2\} \sin 4\theta dz$$

$$\{A_{44}, B_{44}, D_{44}\} = U_{10} \int_{-h/2}^{h/2} \{1, z, z^2\} dz + U_{11} \int_{-h/2}^{h/2} \{1, z, z^2\} \cos 2\theta dz$$

$$\{A_{55}, B_{55}, D_{55}\} = U_{10} \int_{-h/2}^{h/2} \{1, z, z^2\} dz - U_{11} \int_{-h/2}^{h/2} \{1, z, z^2\} \cos 2\theta dz$$

The invariants are calculated from given elastic constants and the location of each layer is expressed in the z coordinate. Therefore, ply orientations of all the layers play a role in optimum design. For numerical calculation, nonlinear real programming (Ref. [37]) incorporating a sequential quadratic programming method is used. In this method, a quadratic programming subproblem is solved at each iteration.

6.3 Numerical Examples

For optimization examples, sixteen layers are used to design composite cantilevers. Similar material properties to the ones in the previous chapters are considered. Without any constraints on design variables, an unconstrained optimization technique is applied.

Maximum bending frequencies are always obtained for the all 90^o-layer laminate. It indicates that most bending stiffness comes from the layers with the fibers placed in the spanwise direction. Besides, all 0^o layers giving lowest torsional frequencies is the worst case of design practice for both bending and torsional vibration. Next, the optimization process focuses on maximizing torsional frequencies.

To check the effect of geometry on the optimum design, various aspect ratios (AR) are considered in Table 6.2. The structure is optimized with respect to the first torsional frequency. Before proceeding to the discussion of the results, it should be pointed out that solutions for all design variables are calculated with the convergence limit 0.01^o. Later, decimal points are rounded off, then shown to be integer values. In the table, different optimization results are obtained as the geometry of the structure changes. For a high-aspect-ratio structure, the optimum is achieved when most ply orientations rotate to near $90^o s$. The same trend mentioned above is noticed in maximizing torsional frequencies, especially for high aspect ratio. In other words, the similar results can be obtained for maximum frequencies for both bending and torsional vibration for high-aspect-ratio structures. This means that the bending stiffness becomes critical for torsional as well as bending vibration for cantilevered structures with high aspect ratio. The first torsional frequencies corresponding to the optimum ply orientations are shown in Figure 6.1 and compared to those by structural tailoring. As seen, there is still margin to improve dynamic characteristics by structural optimization.

In the next example, four cases of modeling approximation are considered to see how optimization results are influenced by nonclassical characteristics of the composite cantilever. Transverse shear flexibility, characterizing composite structures, and warping restraint due to the rigidity of the root of the cantilever

are taken into consideration. A structural model based on FSDT with warping restraint is assumed to be the actual plant while others are assumed to be the nominal ones. Table 6.3 shows optimum results for symmetric laminates and asymmetric ones as well. Percentage errors of optimum results induced by assumed modeling errors are shown by comparing the results based on the nominal plant to the actual one. More than 5% error is seen for CLT free warping model and 10% for FSDT free warping model for both symmetric and asymmetric laminates. One conclusion reached from the study was that optimization should be based on an accurate model, including the effects of transverse shear deformation and warping restraint.

Some comments on the optimization process are stated as follows: Linear integer programming is not adequate for solving the problem at hand, therefore nonlinear real programming can be suggested for structural optimization.

Table 6.2 Optimum ply orientations for 1st torsional frequencies based on the FSDT and incorporation of warping restraint effect.

l	c	l/h	AR	*Optimum Stacking Sequence*	*Highest 1st Torsional Freq.*
6	3	70.7	4	$[42/90/43/40/63/90/60/49]_S$	132.1100
9	3	106.1	6	$[56/90/47/45/56/90/68/33]_S$	82.1093
12	3	141.5	8	$[81/60/\text{-}59/\text{-}59/\text{-}61/\text{-}60/69/61]_S$	57.0164
15	3	176.9	10	$[83/67/\text{-}68/\text{-}67/\text{-}77/\text{-}59/78/90]_S$	39.9607
18	3	212.3	12	$[90/78/\text{-}80/51/89/\text{-}78/63/\text{-}32]_S$	28.3200
21	3	247.6	14	$[89/80/\text{-}71/\text{-}82/90/\text{-}33/90/21]_S$	21.2509
24	3	283.0	16	$[88/\text{-}86/83/83/80/90/87/7]_S$	15.9382

Table 6.3 Percentage errors of the optimum first torsional frequencies by modeling approximation.

Symmetric laminate ($l = 6\ in, c = 3\ in$)

Mathematical Modeling	*Optimum Stacking Sequence*	*Highest 1st Torsional Freq.*	*% Error*
$(CLT)_W$	$[46/72/45/31/52/84/56/49]_S$	133.8100	1.2868
$(CLT)_{FW}$	$[49/75/46/33/51/86/58/46]_S$	124.7923	5.5391
$\mathbf{(FSDT)_W}$	$[42/90/43/40/63/90/60/49]_S$	132.1100	—
$(FSDT)_{FW}$	$[42/90/43/40/63/90/60/49]_S$	116.5147	11.8048

$_W$: warping restraint $_{FW}$: free warping

Asymmetric laminate ($l = 6\ in, c = 3\ in$)

Mathematical Modeling	*Optimum Stacking Sequence*	*Highest 1st Torsional Freq.*	*% Error*
$(CLT)_W$	$[52/74/49/38/59/81/57/53$ $53/66/82/59/38/49/74/45]_T$	133.0104	1.2943
$(CLT)_{FW}$	$[44/78/42/26/45/86/58/47$ $50/51/79/51/26/42/72/45]_T$	124.1407	5.4604
$\mathbf{(FSDT)_W}$	$[44/90/44/46/54/90/56/49$ $50/56/\text{-}84/54/46/44/\text{-}54/44]_T$	131.3108	—
$(FSDT)_{FW}$	$[90/82/34/\text{-}45/24/60/69/73$ $65/64/57/31/\text{-}55/42/90/90]_T$	115.1786	12.2855

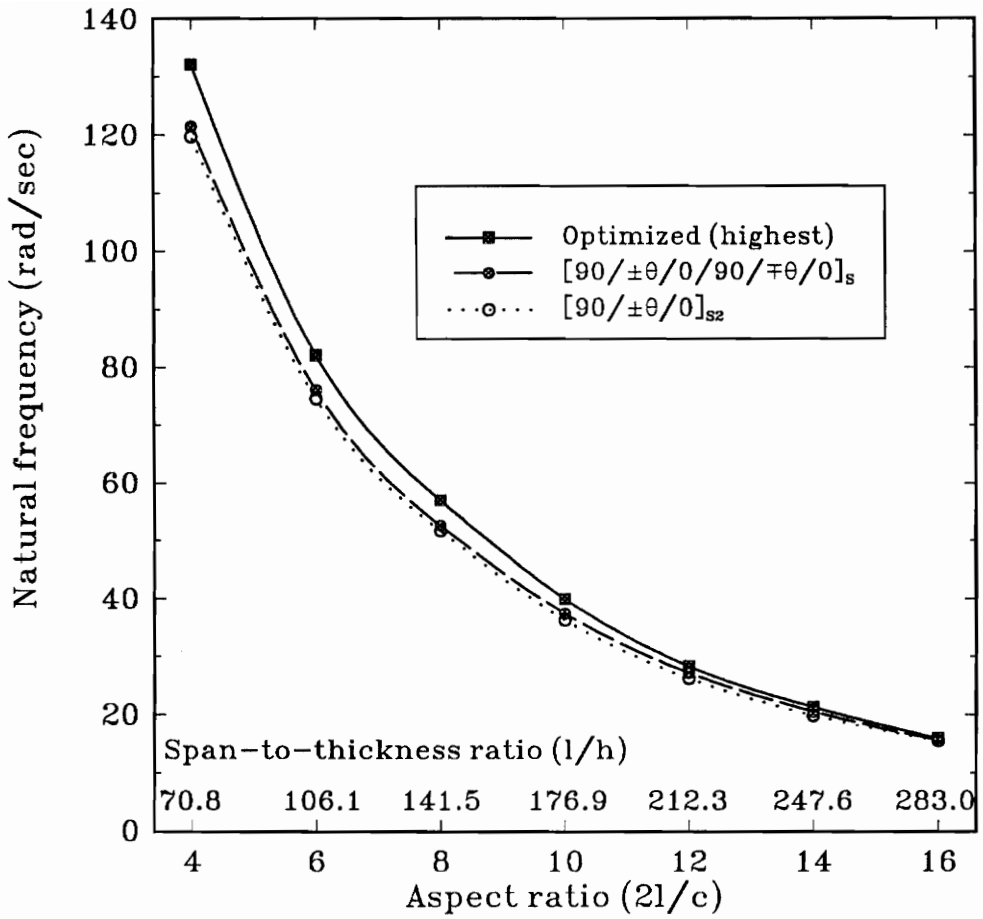

Figure 6.1 Optimum torsional frequencies compared to the ones obtained by structural tailoring.

7. ANALYSIS OF STRUCTURES WITH PARAMETER UNCERTAINTIES

7.1 Overview

Laminated composite structures are in general anisotropic, in the sense that the constituent layers exhibit anisotropic properties. These properties may vary with temperature, moisture, and time during the fabrication process. Moreover, inaccuracies in the evaluation of elastic constants, layer thicknesses and ply orientations can often occur. Quite often, structural uncertainties over an entire system are interpreted in a stochastic sense. The influence of random uncertainty upon dynamic behavior of composite structures has been of practical interest to analysts and designers. The probabilistic tools are necessary to quantify the effects of the random uncertainties. Centered-mean second-moment method and first-order perturbation technique are employed during the probabilistic discretization process of uncertain distributed-parameter structural systems. As a result, random properties are put into sequential stiffness and mass matrices. Therefore a stochastic eigenvalue problem is formulated to provide first and second moments of statistics, i.e., mean and variance.

7.2 Variation of Structural Properties

For the study of variation of structural properties, the relationship between the elements of elastic stiffness of composite laminate S and the coefficients of random variables, $x_1, x_2, \ldots, x_n$ are expressed by

$$S = f(x_1, x_2, \ldots, x_n), \qquad i = 1, \ldots, n \tag{7.1}$$

where by S we denote the set of laminate stiffness matrices A, B, D, and x_i denotes the set of random variables, $E_1, E_2, \nu_{12}, G_{12}, G_{23}, G_{13}, \rho, \theta_k$, $t_k = z_k - z_{k-1}$, respectively. The notations used for statistical description are:

μ_{x_i} = mean value of the ith component random variable.

Var_{x_i} = variance, which is the second moment about the mean of the ith component random variables. In mathematical notation for discrete variable, this is

$$Var_{x_i} = \sum_{j=1}^{N} \frac{x_i - \mu_{x_i}}{N-1}$$

where N is the number of samples.

σ_{x_i} = standard deviation, defined as the square root of the variance.

$Cov_{x_i x_j}$ = covariance of the ith and jth component random variables, defined as

$Cov_{x_i x_j} = \wp_{x_i x_j} \sigma_{x_i} \sigma_{x_j}$ (if $i = j$, then $Cov_{x_i x_j} \equiv Var_{x_i}$)

$\wp_{x_i x_j}$ = coefficient of correlation between ith and jth component random variables.

To evaluate the variation of the elastic stiffness, Taylor series up to second order about the mean of each random variable yields:

$$S(x_1, x_2, \ldots, x_n) = S[\mu_{x_1}, \mu_{x_2}, \ldots, \mu_{x_n}] \tag{7.2}$$

$$+ \sum_{i=1}^{n} \frac{\partial S}{\partial x_i}[x_i - \mu_{x_i}] + \frac{1}{2} \sum_{i=1}^{n} \sum_{j=1}^{n} \frac{\partial^2 S}{\partial x_i \partial x_j}[x_i - \mu_{x_i}][x_j - \mu_{x_j}]$$

Taking linear operation of expectation and variance on both sides of the equation, respectively, and truncating up to second order, one obtains

$$\mu_S = S[\mu_{x_1}, \mu_{x_2}, \ldots, \mu_{x_3}] + \frac{1}{2} \sum_{i=1}^{n} \sum_{j=1}^{n} \frac{\partial^2 S}{\partial x_i \partial x_j} Cov_{x_i x_j} \tag{7.3}$$

$$Var_S = \sum_{i=1}^{n} \sum_{j=1}^{n} \frac{\partial S}{\partial x_i} \frac{\partial S}{\partial x_j} Cov_{x_i x_j} \tag{7.4}$$

From the previous chapter, the eigenvalue problem was expressed in the form:

$$(K - \lambda M)\phi = 0 \tag{7.5}$$

Here matrices K and M are perturbed due to variation of elastic stiffness matrices A, B, D. Upon expanding K and M in Taylor series up to second order, one obtains

$$K(x_1, x_2, \ldots, x_m) = K[\mu_{x_1}, \mu_{x_2}, \ldots, \mu_{x_m}] \tag{7.6}$$
$$+ \sum_{i=1}^{m} \frac{\partial K}{\partial x_i}[x_i - \mu_{x_i}] + \frac{1}{2}\sum_{i=1}^{m}\sum_{j=1}^{n} \frac{\partial^2 K}{\partial x_i \partial x_j}[x_i - \mu_{x_i}][x_j - \mu_{x_j}]$$

where $i = 1, \ldots, m$, and

$$M(x_1, x_2, \ldots, x_m) = M[\mu_{x_1}, \mu_{x_2}, \ldots, \mu_{x_m}] \tag{7.7}$$
$$+ \sum_{i=1}^{m} \frac{\partial M}{\partial x_i}[x_i - \mu_{x_i}] + \frac{1}{2}\sum_{i=1}^{m}\sum_{j=1}^{n} \frac{\partial^2 M}{\partial x_i \partial x_j}[x_i - \mu_{x_i}][x_j - \mu_{x_j}]$$

The perturbed eigenvalues and eigenvectors are expressed similarly as

$$\lambda(x_1, x_2, \ldots, x_m) = \lambda[\mu_{x_1}, \mu_{x_2}, \ldots, \mu_{x_m}] \tag{7.8}$$
$$+ \sum_{i=1}^{m} \frac{\partial \lambda}{\partial x_i}[x_i - \mu_{x_i}] + \frac{1}{2}\sum_{i=1}^{m}\sum_{j=1}^{m} \frac{\partial^2 \lambda}{\partial x_i \partial x_j}[x_i - \mu_{x_i}][x_j - \mu_{x_j}]$$

$$\phi(x_1, x_2, \ldots, x_m) = \phi[\mu_{x_1}, \mu_{x_2}, \ldots, \mu_{x_m}] \tag{7.9}$$
$$+ \sum_{i=1}^{m} \frac{\partial \phi}{\partial x_i}[x_i - \mu_{x_i}] + \frac{1}{2}\sum_{i=1}^{m}\sum_{j=1}^{m} \frac{\partial^2 \phi}{\partial x_i \partial x_j}[x_i - \mu_{x_i}][x_j - \mu_{x_j}]$$

The mean values and variances of eigenvalues and eigenvectors are

$$\mu_\lambda = \lambda[\mu_{x_1}, \mu_{x_2}, \ldots, \mu_{x_3}] + \frac{1}{2}\sum_{i=1}^{m}\sum_{j=1}^{m} \frac{\partial^2 \lambda}{\partial x_i \partial x_j} Cov_{x_i x_j} \tag{7.10}$$

$$Var_\lambda = \sum_{i=1}^{m}\sum_{j=1}^{m} \frac{\partial \lambda}{\partial x_i}\frac{\partial \lambda}{\partial x_j} Cov_{x_i x_j} \tag{7.11}$$

$$\mu_\phi = \phi[\mu_{x_1}, \mu_{x_2}, \ldots, \mu_{x_3}] + \frac{1}{2}\sum_{i=1}^{m}\sum_{j=1}^{m}\frac{\partial^2\phi}{\partial x_i \partial x_j}Cov_{x_i x_j} \tag{7.12}$$

$$Var_\phi = \sum_{i=1}^{m}\sum_{j=1}^{m}\frac{\partial\phi}{\partial x_i}\frac{\partial\phi}{\partial x_j}Cov_{x_i x_j} \tag{7.13}$$

For small variation of random variables about their means, a perturbation technique can be successfully applied to evaluate first and second derivatives of eigenvalues and eigenvectors with respect to random variables x_i. For the sake of simplicity, we introduce the notation:

$$K^o \equiv K(\mu_{x_1}, \mu_{x_2}, \ldots, \mu_{x_n}), \quad K_i^I \equiv \frac{\partial K}{\partial x_i}, \quad K_{ij}^{II} \equiv \frac{\partial^2 K}{\partial x_i \partial x_j}$$

$$\epsilon_i \equiv x_i - \mu_{x_i} \tag{7.14}$$

Substituting Eqs. (7.6) and (7.7) into Eq. (7.5),

$$[K^o + \sum_{i=1}^{m} K_i^I \epsilon_i + \frac{1}{2}\sum_{i=1}^{m}\sum_{j=1}^{m} K_{ij}^{II}\epsilon_i\epsilon_j][\phi^o + \sum_{i=1}^{m}\phi_i^I\epsilon_i + \frac{1}{2}\sum_{i=1}^{m}\sum_{j=1}^{m}\phi_{ij}^{II}\epsilon_i\epsilon_j] =$$

$$[M^o + \sum_{i=1}^{m} M_i^I \epsilon_i + \frac{1}{2}\sum_{i=1}^{m}\sum_{j=1}^{m} M_{ij}^{II}\epsilon_i\epsilon_j][\lambda^o + \sum_{i=1}^{m}\lambda_i^I\epsilon_i + \frac{1}{2}\sum_{i=1}^{m}\sum_{j=1}^{m}\lambda_{ij}^{II}\epsilon_i\epsilon_j]$$

$$[\phi^o + \sum_{i=1}^{m}\phi_i^I\epsilon_i + \frac{1}{2}\sum_{i=1}^{m}\sum_{j=1}^{m}\phi_{ij}^{II}\epsilon_i\epsilon_j] \tag{7.15}$$

and collecting and equating terms up to second power of ϵ_i results in

$$\epsilon_i^0 \qquad (K^o - \lambda^o M^o)\phi^o = 0 \tag{7.16}$$

$$\epsilon_i^1 \qquad (K^o - \lambda^o M^o)\phi_i^I + (K^I - \lambda^o M_i^I)\phi^o - \lambda_i^I M^o \phi^o = 0 \tag{7.17}$$

$$\epsilon_i^2 \qquad (K^o - \lambda^o M^o)\phi_{ij}^{II} + (K^I - \lambda^o M_i^I)\phi_i^I - \lambda_i^I M^o \phi^o = 0 \tag{7.18}$$

Premultipling all terms in Eq. (7.17) by ϕ^o, λ_i^I are obtained as follows:

$$\lambda_i^I = \frac{\phi^{oT}(K_i^I - \lambda^o M_i^I)\phi^o}{\phi^{oT} M^o \phi^o} \tag{7.19}$$

Finally, the mean and standard deviation of natural frequencies are obtained from the statistics of eigenvalues

$$\sigma_\omega = \frac{1}{2\sqrt{\lambda}}\sigma_\lambda \tag{7.20}$$

7.3 Numerical Examples

Uncertain material properties, fiber orientations, lamina thicknesses and mass density are treated as Gaussian random variables. We describe uncertainty in terms of coefficient of variation (C.O.V.) defined as the ratio of the standard deviation to the mean of random variable. Statistics for graphite/epoxy material properties are given in terms of mean value and standard deviation.

7.3.1 Stochastic Variation of Natural Frequencies:

Figure 7.1 shows the fluctuation of fundamental natural frequencies due to uncertain material properties for the laminate $[90/\pm 45/0]_{S4}$. The theoretical model is based upon the FSDT while taking into account the warping restraint to the root of the cantilever. Material properties, E_1, E_2, ν_{12}, G_{12}, G_{23}, G_{13} are interpreted as Gaussian random variables where the coefficients of variation are 6%. The mean values are shown in Table 7.1. No correlation is involved in random parameters due to independent sampling, which is one of the characteristics of Monte Carlo simulation. Bold letters $\mathbf{E}, \mathbf{G}$ are used when all Young's moduli and shear moduli are random. The geometric parameters, i.e. the span length, chord length and total thickness of the structure l, c and h, are assumed deterministic, without uncertainties. Figure 7.2 shows the convergence of the mean values of natural frequencies for the same structure, but based on two different theoretical models, FSDT and CLT with and without warping restraint. The solution by Monte Carlo simulation is compared to the result by the Stochastic Rayleigh-Ritz method where 40 terms are taken for FSDT and 16 terms are taken for CLT.

This approach validates the solution procedure by the Stochastic Rayleigh-Ritz formulation while verifying the solution by Monte Carlo simulation. From the results, Monte Carlo solutions fully converge at 1000 simulations. However, this procedure is extremely prohibitive because of the consumed time.

In Figure 7.3, the convergence of C.O.V.'s of natural frequencies computed by Monte Carlo simulation is presented. Stochastic Rayleigh-Ritz solutions are presented and are in good agreement with the results estimated by Monte Carlo simulation. Although the two methods compare very well in accuracy, the Stochastic Rayleigh-Ritz method proves to be much simpler and efficient toward estimating the effects of structural uncertainties. In the same figure, the C.O.V.'s of natural frequencies are compared for four different cases of modeling. In the presence of uncertain material properties and ply orientations, the effect of transverse shear deformation and warping restraint in the free vibration problem is revealed. The CLT model has higher C.O.V.'s no matter if the warping restraint exists or not. On the other hand, the FSDT model with free warping gives a lower C.O.V. than the other cases. For a thin structure along with CLT, good results are obtained on estimating the uncertainty effect. However, for thick structures, we may overestimate the C.O.V.'s without consideration of transverse flexibility.

As a second example, C.O.V.'s for material properties, layer thickness, mass density, and standard deviation of fiber orientation are given in Table 7.1. The C.O.V.'s of natural vibration frequencies for the laminate $[90/\pm 75/0]_{S4}$ with $\mathcal{AR} = 10$ are shown in Table 7.2. To estimate the sensitivity of natural frequencies to the random variables, the variation of frequencies to each random variable will be calculated. Later, more variables are treated together to emphasize their combined effect. The bending frequencies are dominated by the in-plane Young's modulus parallel to the fiber direction, the torsional frequencies by layer thickness.

This comes from the fact that axial and transversal rigidities provide most of the bending stiffness. An interesting result is that for a certain stacking sequence with specific geometry of the structure, the torsional frequencies can be most affected by a local geometric parameter, layer thickness, rather than elastic moduli.

In the design process, one question arises as to how much the design variable θ affects the overall uncertainty of the structure. Note that θ, which is mostly used as a design variable in structural tailoring, influences torsion more than bending. Based on the results obtained within the structural optimization, it has already been seen that torsional frequencies are quite sensitive to stacking sequence and geometric parameters. In torsional vibration, the in-plane shear modulus G_{12} gives more variation than E_1. The influence of transverse shear deformation introduced by G_{23}, G_{13} is insignificant.

When considering multi-random variables, the combined effects are revealed. Now, uncertainties of the elastic moduli E_1 and G_{12} are taken into consideration. This yields little effect on bending frequencies; however, more effect on torsional frequencies is shown when more random variables are considered. It is seen that the torsional vibration problem is much more complex than the bending one when parameter uncertainties exist in the structure.

Figure 7.4 shows the effect of the material properties fluctuation on the first bending and torsional frequencies. In Figure 7.5, the effect of ply orientation uncertainty on natural frequencies is illustrated. The C.O.V.'s of natural frequencies increase linearly as the standard deviation of stacking sequence increases. Also, correlated and uncorrelated random variables are compared. When all layers are correlated, the C.O.V.'s increase significantly, even for small correlation.

7.3.2 Reliability Analysis:

In Figure 7.1, while running 1000 samples in Monte Carlo simulation, the fundamental natural frequency can deviate up to 7.54% from its mean value based on the FSDT warping restraint model. The extreme deviation is three times greater than the calculated $C.O.V. = 2.35\%$, which brings a concern on the safety of the structure during its operation. We introduce the reliability to measure the safety of structures in terms of probability of survival. To figure out which uncertain parameters play a major role in structural safety, various kinds of uncertainties are considered:

- geometric uncertainty
  - layer thickness ρ interfering with other parameter uncertainties and affecting
    weight of structure
- material property uncertainties
  - elastic moduli $E_1, E_2, \nu_{12}, G_{12}, G_{23}, G_{13}$ affecting structural stiffness
  - mass density ρ affecting weight of structure
- design parameter uncertainty
  - ply angle θ affecting dynamic characteristics, yielding changes of natural frequencies

Reliability of the composite structure due to uncertain elastic moduli, layer thickness, ply orientation and mass density are calculated and shown, respectively, in Figures 7.6-9. The fundamental natural frequency, ω_{un}, of the structure with parameter uncertainties is normalized with respect to the one, ω_{wun}, without the uncertainties. The structure is subjected to an external oscillatory load whose frequency ω_e is within the range 0 to ω_{wun}. The structure is safe when its fundamental natural frequency is beyond ω_e. From the result, it is seen that uncertainty of face layers plays a dominant role in the fluctuation of the natural frequencies

for the laminate $[90/\pm 45/0]_S$. The combined effects of all uncertain parameters on structural reliability is depicted on Figure 7.10. In conclusion, among other uncertain parameters, uncertain elastic moduli have a significant effect on structural safety.

7.3.3 Structural Tailoring With Parameter Uncertainties:

In the previous chapter, considerable efforts have been made to find higher natural frequencies by structural tailoring. Here, again we apply the structural tailoring techniques to reduce the effects of the uncertainties. A positive outcome of structural tailoring is that the composite laminated structure can be designed as to feature robustness to uncertainties. Robustness is defined as a structure not being sensitive to parameter variations.

To illustrate the beneficial effect of structural tailoring on reliability performance, four different stacking sequences are chosen along with θ varying from 0 to 90 degrees. Natural frequencies (in small figures at the right corner) and their variations are shown in Figures 7.11-12. From the results, it is seen that the natural frequencies of cantilevered structures laminated with $\theta = 90^o$ are least sensitive to uncertain material properties for both bending and torsion. The robust structure is laminated with stacking sequence $[0/\pm\theta/90]_{S2}$ and the vulnerable one is stacked with $[90/\pm\theta/0/90/\mp\theta/0]_S$.

From the previous results on structural tailoring, the stacking sequence $[90/\pm\theta/0/90/\mp\theta/0]_2$ gave higher natural frequencies than other stacking sequences. However, from the reliability point of view, this stacking sequence is not desirable any more when uncertainties exist. We had designed certain stacking sequences yielding higher natural frequencies without consideration of parameter uncertainties. In consequence, the structure can result in a large range of frequency variation. To minimize the unavoidable effect of uncertainties on structural reliability,

the stacking sequence which is less sensitive to uncertainties while providing higher natural frequency has to be selected.

Figure 7.13 shows the effect of laminate thickness h on the uncertainties of natural frequencies using FSDT with incorporation of the warping restraint effect. As laminate thickness increases by a factor of two, C.O.V.s of bending frequencies decrease about one-third over the entire range of θ. The same amount of C.O.V. decrease can result for torsional frequencies when bending-twist coupling exists in the laminated cantilever. On the other hand, the thickness effect on C.O.V.'s of torsional frequencies is insignificant when bending and torsional vibrations become decoupled.

Maintaining the thickness of the composite unchanged while changing the thickness of each lamina, one can increase correspondingly the number of layers. The effect of number of the layers on the C.O.V.'s is presented in Figures 7.14-15 in the presence of uncertainties of elastic moduli E_1, E_2. Figures 7.16-17 reveal that an increasing number of layer exhibiting thickness uncertainty will reduce the C.O.V.'s. It implies that the uncertainty effects diminish for larger number of layers.

Table 7.1 Material properties and statistics for graphite/epoxy laminate.

Random Variable	*Mean*	*Standard Deviation*	*Coefficient of Variation*
E_1 (psi)	18.5000x10^6	2.7750x10^6	0.15
E_2 (psi)	1.6000x10^6	0.2400x10^6	0.15
ν_{12}	0.3500	0.0525	0.15
G_{12} (psi)	0.8320x10^6	0.1248x10^6	0.15
G_{23} (psi)	0.3320x10^6	0.0498x10^6	0.15
G_{13} (psi)	0.3320x10^6	0.0498x10^6	0.15
θ $(degree)$		2.500	–
t (in)	0.0053	0.0008	0.15
ρ (lb/in^3)	0.0560	0.0084	0.15

Table 7.2 Coefficients of variation of the first natural frequencies of laminate $[90/\pm 75/0]_{S4}$ ($l = 15\ in$, $c = 3\ in$, modeled as per the FSDT with warping restraint) with uncertain moduli of elasticity, Poisson's ratio, thickness, mass density, and fiber orientation.

Random Variable(s)	*Correlation*	*Coefficient of Variation (%)*	
		Bending Frequency	*Torsional Frequency*
E_1	—	4.7531	0.6075
E_2	—	0.1068	0.0927
G_{12}	—	0.0188	0.8607
G_{23}	—	0.0020	0.0212
G_{13}	—	0.0033	0.0349
θ	—	0.3075	0.4920
t	—	1.3760	1.3359
ρ	—	1.3258	1.3216
t, ρ	—	1.9108	1.8792
$\mathbf{E}$	—	4.7543	0.6145
$\mathbf{G}$	—	0.0192	0.8616
$\mathbf{E}, \nu_{12}$	—	4.8075	0.8832
$\mathbf{E}, G_{12}$	—	4.7544	1.0575
$\mathbf{E}, G_{12}, \nu_{12}$	—	4.8075	1.2332
$\mathbf{E}, \mathbf{G}$	—	4.7544	1.0583
$\mathbf{E}, \mathbf{G}, \nu_{12}$	—	4.8075	1.2339
$\mathbf{E}, \mathbf{G}, \nu_{12}, t$	—	5.0006	1.8186
$\mathbf{E}, \mathbf{G}, \nu_{12}, \rho$	—	4.9870	1.8081
$\mathbf{E}, \mathbf{G}, \nu_{12}, \theta$	—	4.8173	1.3284
$\mathbf{E}, \mathbf{G}, \nu_{12}, t, \rho$	—	5.1733	2.2481
$\mathbf{E}, \mathbf{G}, \nu_{12}, t, \theta$	—	5.0100	1.8839
$\mathbf{E}, \mathbf{G}, \nu_{12}, \rho, \theta$	—	4.9964	1.8738
$\mathbf{E}, \mathbf{G}, \nu_{12}, t, \rho, \theta$	—	5.1825	2.3013

Table 7.3 Effect of coefficients of correlation on the first natural frequencies of laminate $[90/\pm 75/0]_{S4}$ ($l = 15\ in$, $c = 3\ in$, modeled as per the FSDT with warping restraint) with uncertain moduli of elasticity, Poisson's ratio, thickness, mass density, and fiber orientation.

Random Variables	*Coefficient of Correlation*	*Coefficient of Variation (%)*	
		Bending Frequency	*Torsional Frequency*
$\mathbf{E}, \mathbf{G}, \nu_{12}$	—	4.8075	1.2339
$\mathbf{E}, \mathbf{G}, \nu_{12}$	0.1 (each layer)	4.8788	1.2142
$\mathbf{E}, \mathbf{G}, \nu_{12}$	0.2 (each layer)	4.9490	1.1942
$\mathbf{E}, \mathbf{G}, \nu_{12}$	0.02 (all layers)	7.4959	1.7613
$\mathbf{E}, \mathbf{G}, \nu_{12}$	0.05 (all layers)	10.2861	2.3392
$\mathbf{E}, \mathbf{G}, \nu_{12}, t$	—	5.0006	1.8186
$\mathbf{E}, \mathbf{G}, \nu_{12}, t$	0.1 (each layer)	5.0691	1.8053
$\mathbf{E}, \mathbf{G}, \nu_{12}, t$	0.2 (each layer)	5.1368	1.7919
$\mathbf{E}, \mathbf{G}, \nu_{12}, t$	0.02 (all layers)	7.7737	2.6646
$\mathbf{E}, \mathbf{G}, \nu_{12}, t$	0.05 (all layers)	10.6568	3.5762
$\mathbf{E}, \mathbf{G}, \nu_{12}, \theta$	—	4.8173	1.3284
$\mathbf{E}, \mathbf{G}, \nu_{12}, \theta$	0.1 (each layer)	4.8885	1.3101
$\mathbf{E}, \mathbf{G}, \nu_{12}, \theta$	0.2 (each layer)	4.9586	1.2916
$\mathbf{E}, \mathbf{G}, \nu_{12}, \theta$	0.02 (all layers)	7.5100	1.9090
$\mathbf{E}, \mathbf{G}, \nu_{12}, \theta$	0.05 (all layers)	10.3049	2.5424
$\mathbf{E}, \mathbf{G}, \nu_{12}, t, \theta$	—	5.0100	1.8839
$\mathbf{E}, \mathbf{G}, \nu_{12}, t, \theta$	0.1 (each layer)	5.0784	1.8711
$\mathbf{E}, \mathbf{G}, \nu_{12}, t, \theta$	0.2 (each layer)	5.1459	1.8582
$\mathbf{E}, \mathbf{G}, \nu_{12}, t, \theta$	0.02 (all layers)	7.7873	2.7644
$\mathbf{E}, \mathbf{G}, \nu_{12}, t, \theta$	0.05 (all layers)	10.6750	3.7123
$\mathbf{E}, \mathbf{G}, \nu_{12}, t, \rho, \theta$	—	5.1825	2.3013
$\mathbf{E}, \mathbf{G}, \nu_{12}, t, \rho, \theta$	0.1 (each layer)	5.2486	2.2908
$\mathbf{E}, \mathbf{G}, \nu_{12}, t, \rho, \theta$	0.2 (each layer)	5.3140	2.2802
$\mathbf{E}, \mathbf{G}, \nu_{12}, t, \rho, \theta$	0.02 (all layers)	8.0361	3.3992
$\mathbf{E}, \mathbf{G}, \nu_{12}, t, \rho, \theta$	0.05 (all layers)	11.0073	4.5763

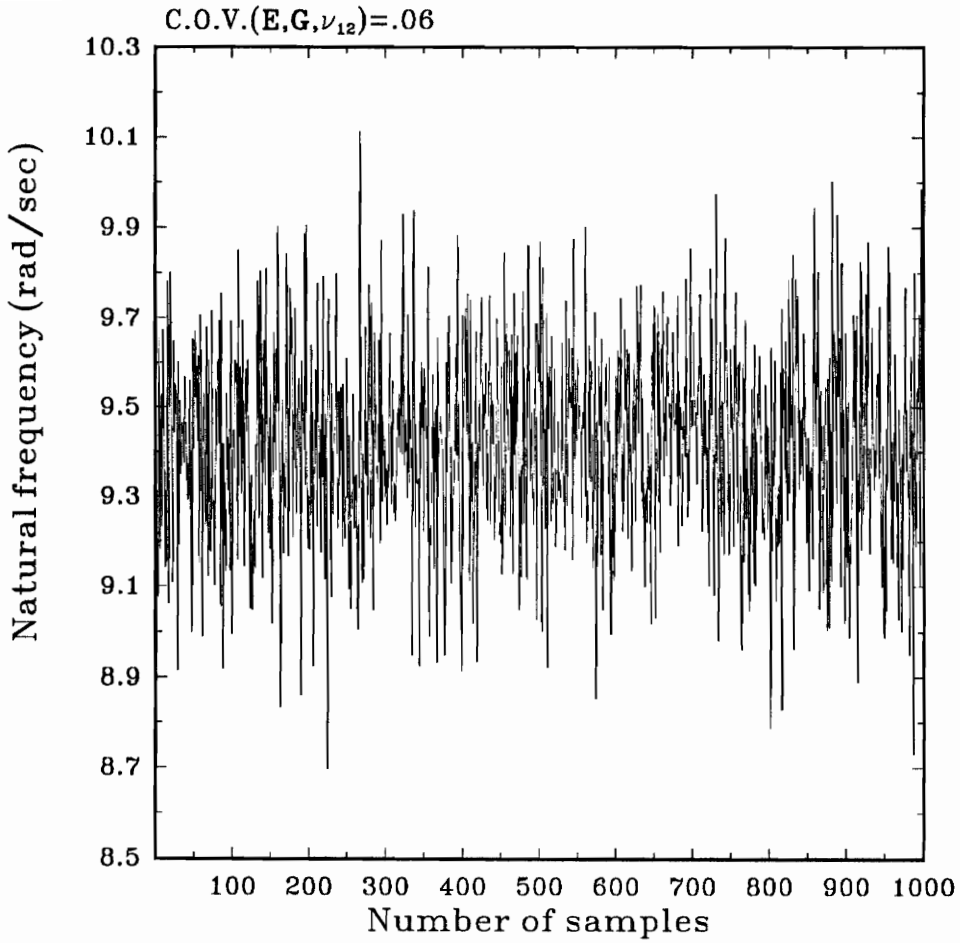

Figure 7.1 Fluctuation of fundamental natural frequency of laminate $[90/\pm 45/0]_{S4}$ ($l = 15\ in,\ c = 3\ in$, modeled as per the FSDT with warping restraint) due to uncertain material properties.

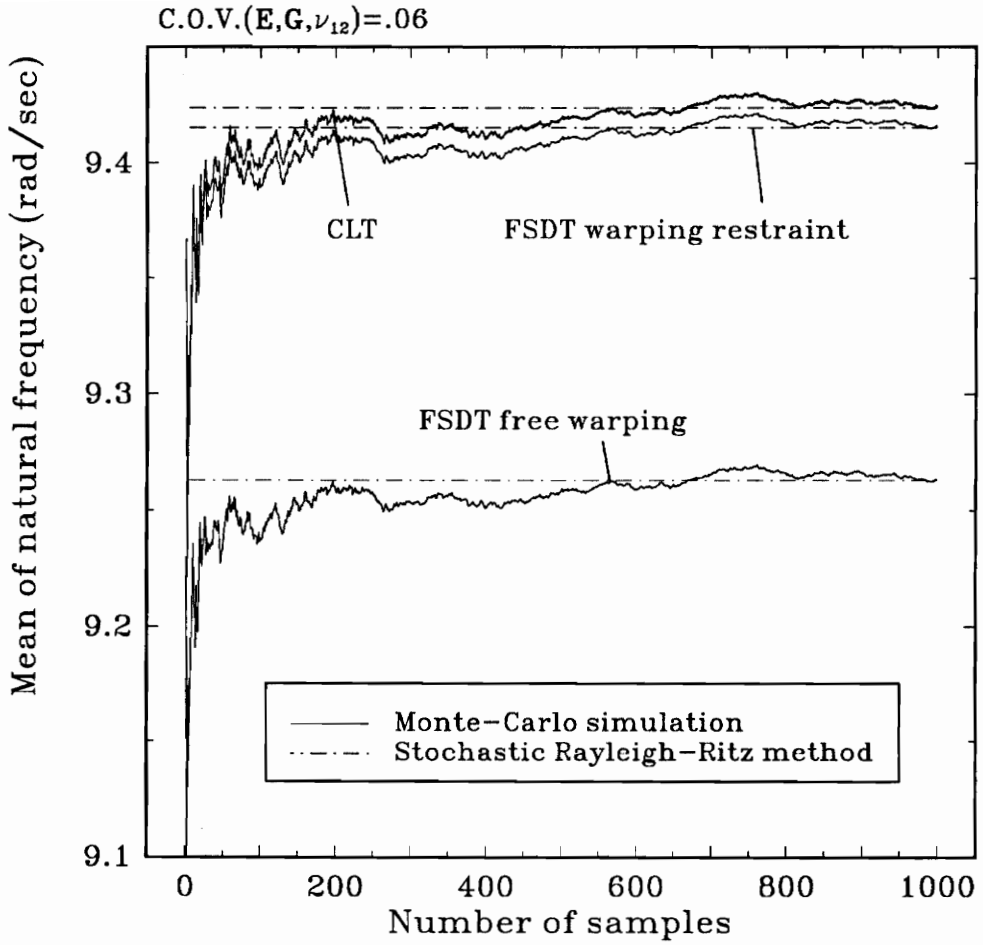

Figure 7.2 Comparison of the mean value of fundamental natural frequency for laminate $[90/\pm 45/0]_{S4}$ ($l = 15\ in,\ c = 3\ in$) in the presence of uncertain material properties.

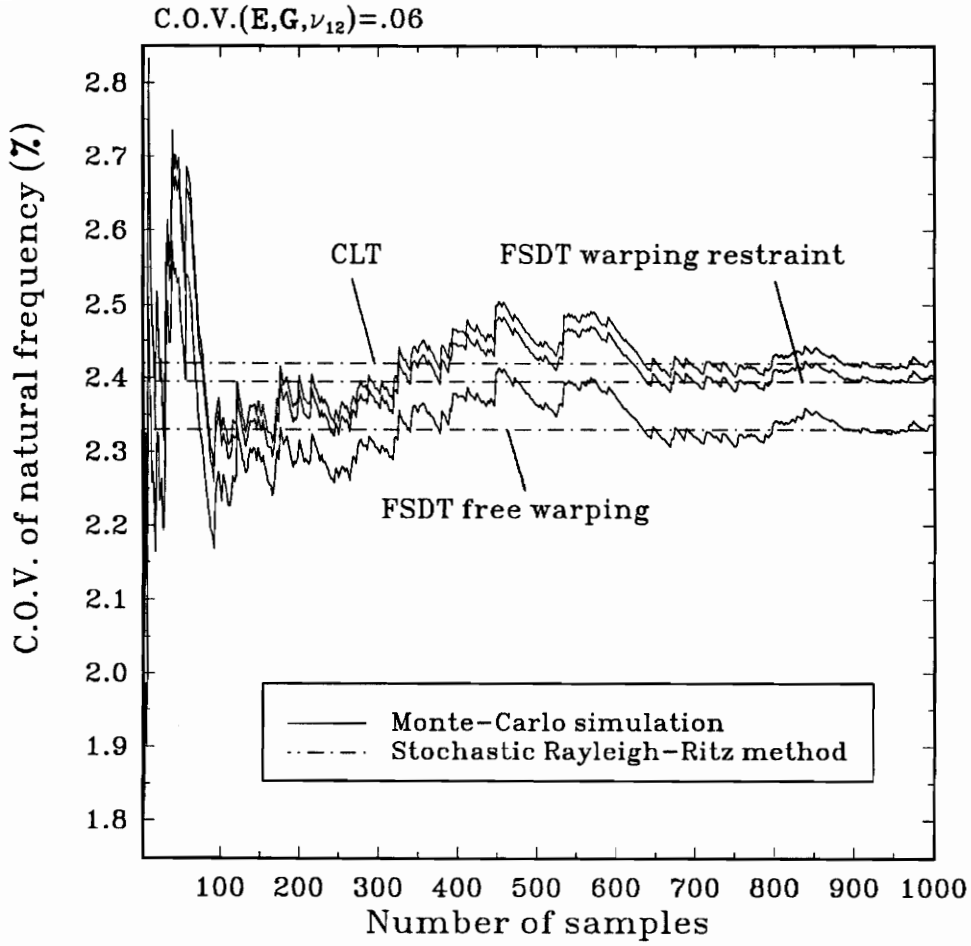

Figure 7.3 Comparison of coefficients of variation of fundamental natural frequency for laminate $[90/\pm 45/0]_{S4}$ ($l = 15\ in,\ c = 3\ in$) in the presence of uncertain material properties.

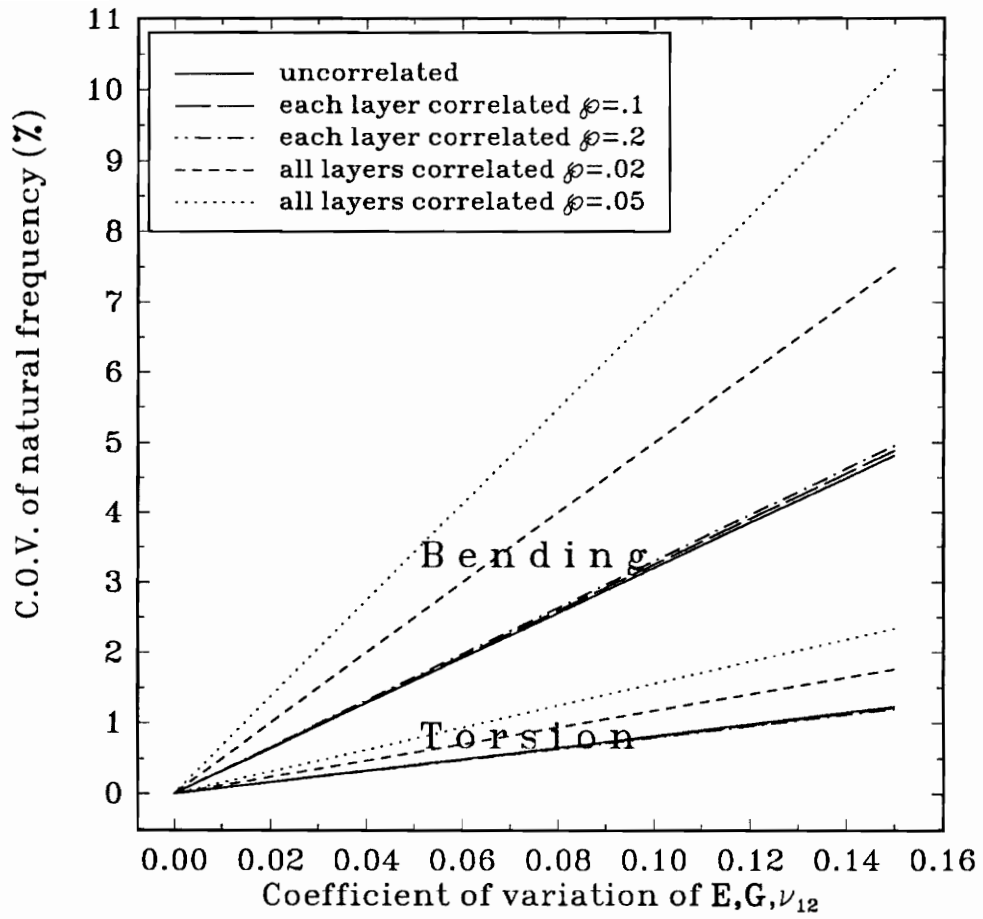

Figure 7.4 Coefficients of correlation of the first natural frequencies of laminate $[90/\pm 75/0]_{S4}$ ($l = 15\ in$, $c = 3\ in$, modeled as per the FSDT with incorporation of the warping restraint) according to the increased uncertainties of material properties.

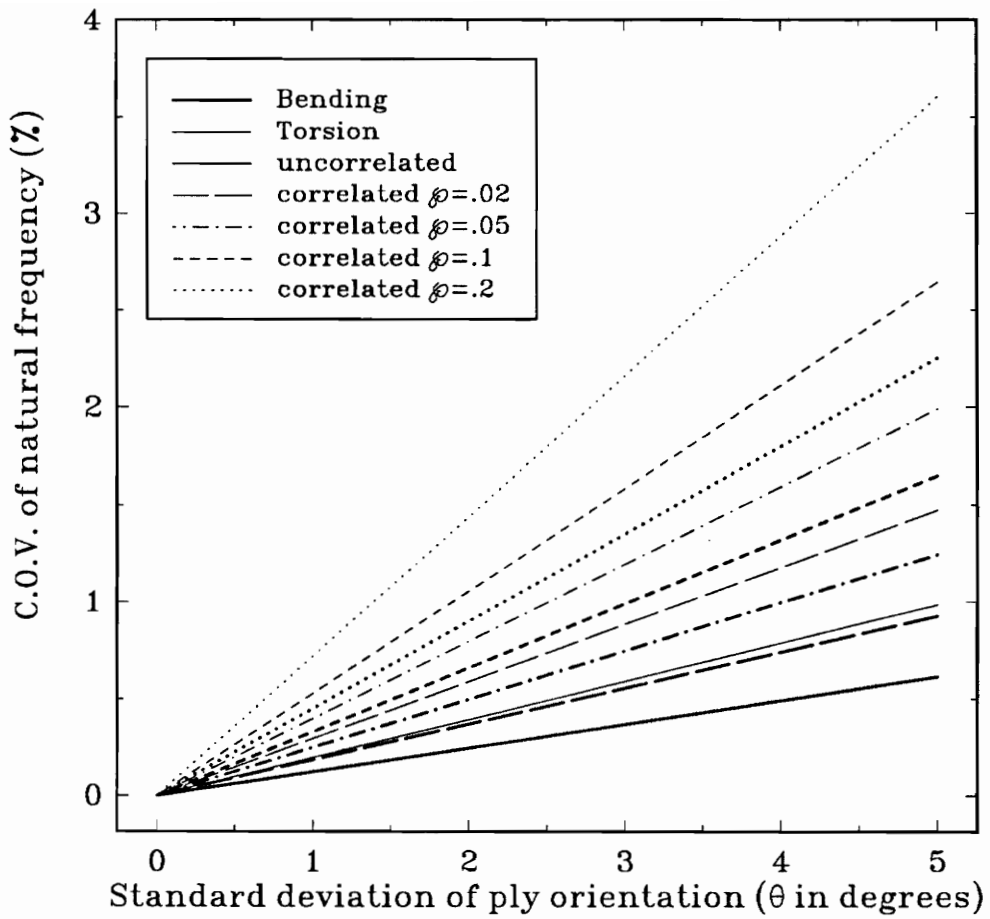

Figure 7.5 Coefficients of correlation of the first natural frequencies of laminate $[90/\pm 75/0]_{S4}$ ($l = 15\ in$, $c = 3\ in$, modeled as per the FSDT with incorporation of the warping restraint) according to the increased uncertainty of ply orientation.

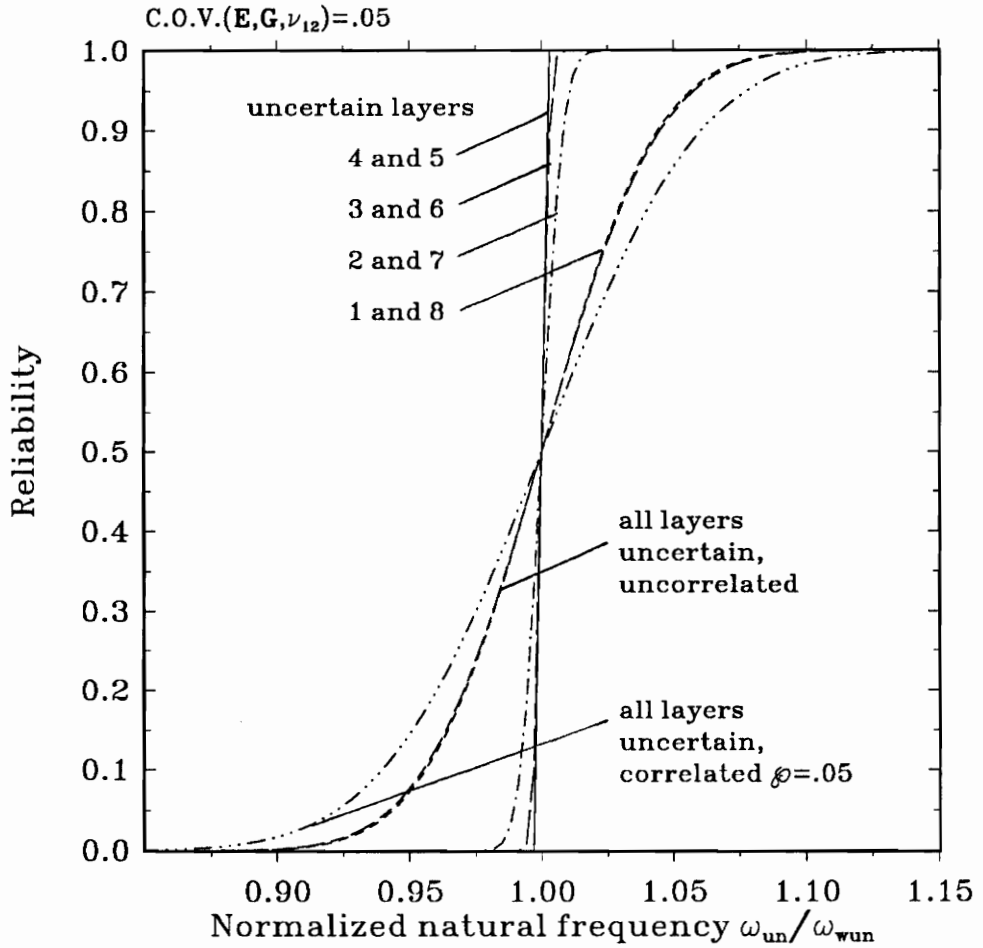

Figure 7.6 Reliability of laminate $[90/\pm 45/0]_S$ ($l = 9\ in,\ c = 3\ in$, modeled as per FSDT with incorporation of the warping restraint) under an external oscillatory load. The uncertainties concern the elastic moduli.

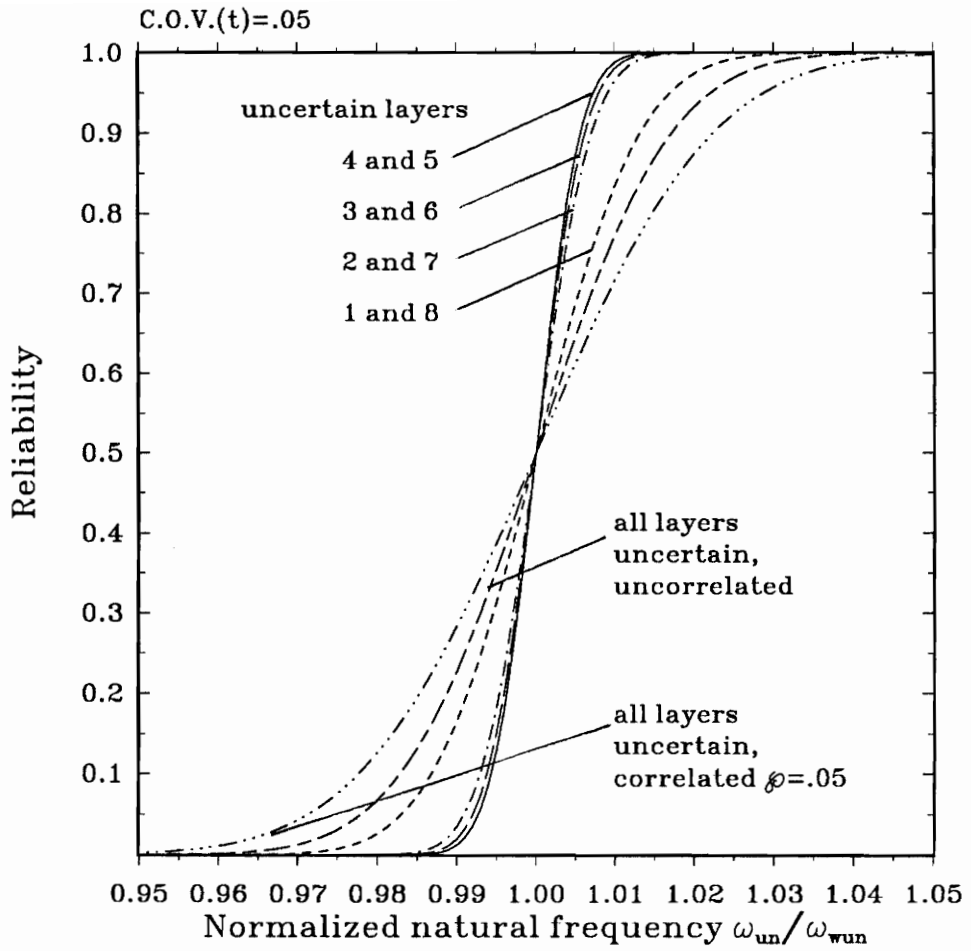

Figure 7.7 Reliability of laminate $[90/\pm 45/0]_S$ ($l = 9\ in,\ c = 3\ in$, modeled as per the FSDT with incorporation of the warping restraint) under an external oscillatory load. The uncertainty concerns the lamina thickness.

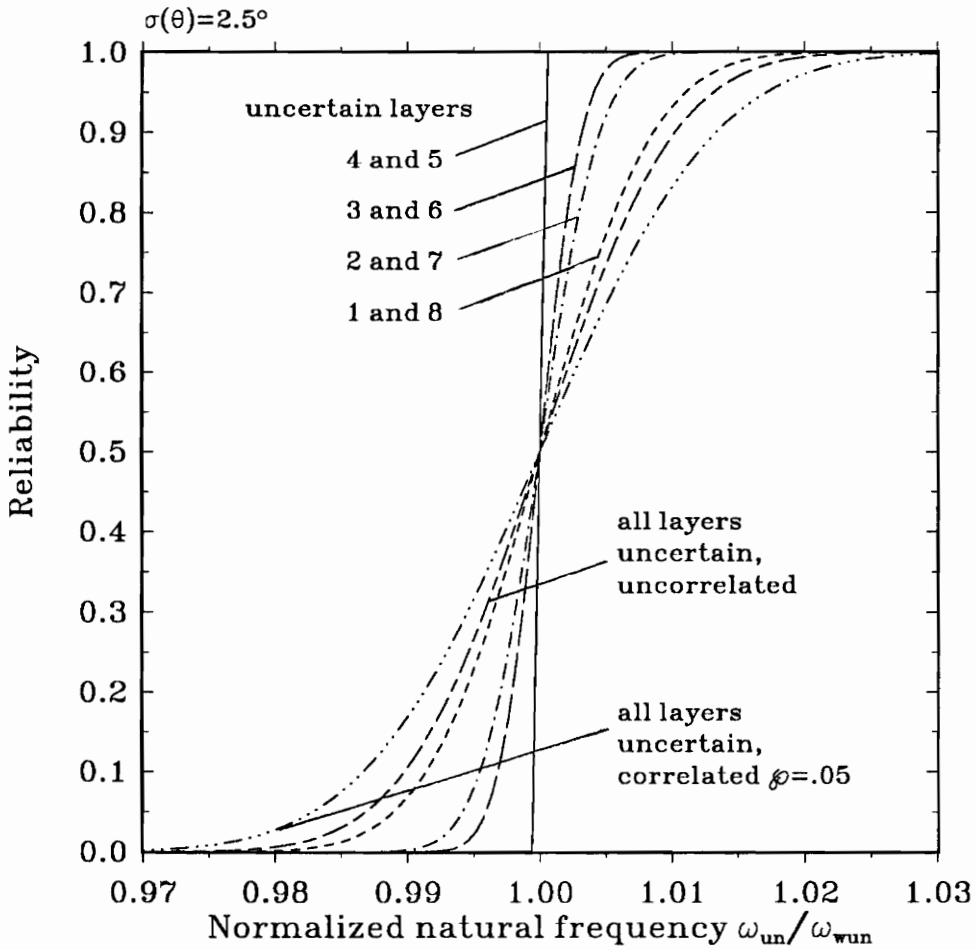

Figure 7.8 Reliability of laminate $[90/\pm 45/0]_S$ ($l = 9\ in,\ c = 3\ in$, modeled as per the FSDT with incorporation of the warping restraint) under an external oscillatory load. The uncertainty concerns the ply orientation.

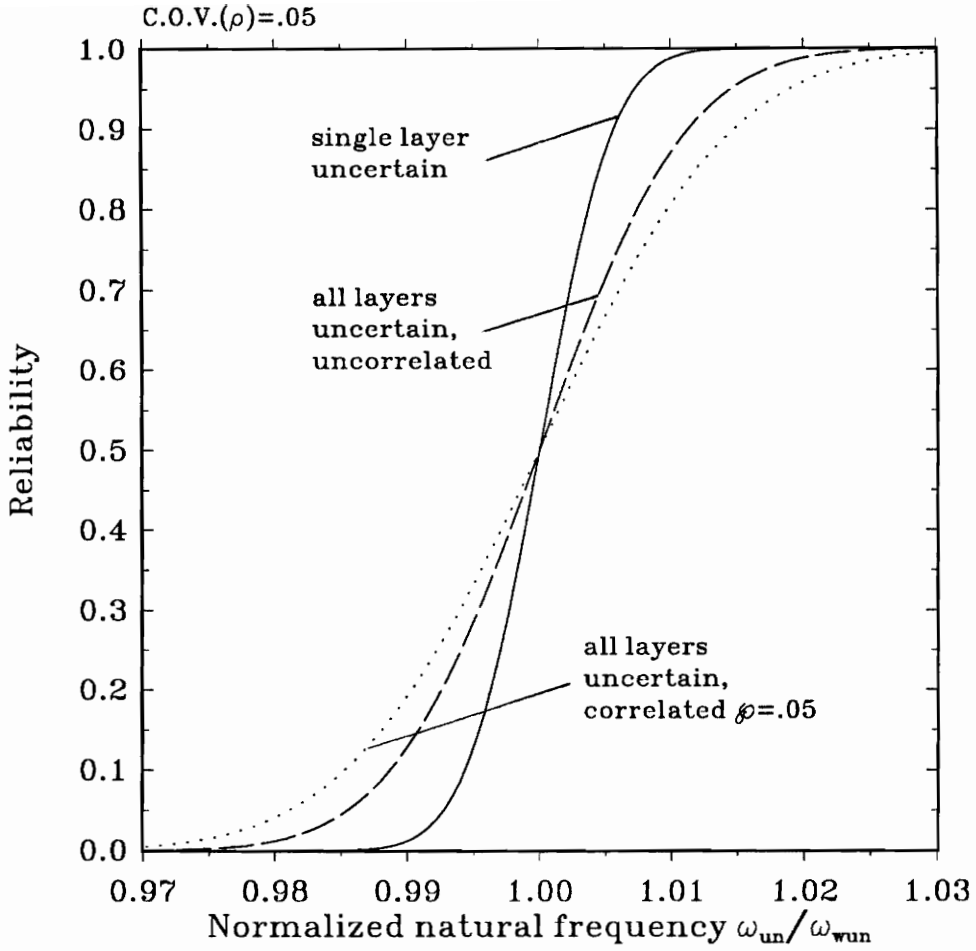

Figure 7.9 Reliability of laminate $[90/\pm 45/0]_S$ ($l = 9\ in,\ c = 3\ in$, modeled as per the FSDT with incorporation of warping restraint) under an external oscillatory load. The uncertainty concerns the mass density.

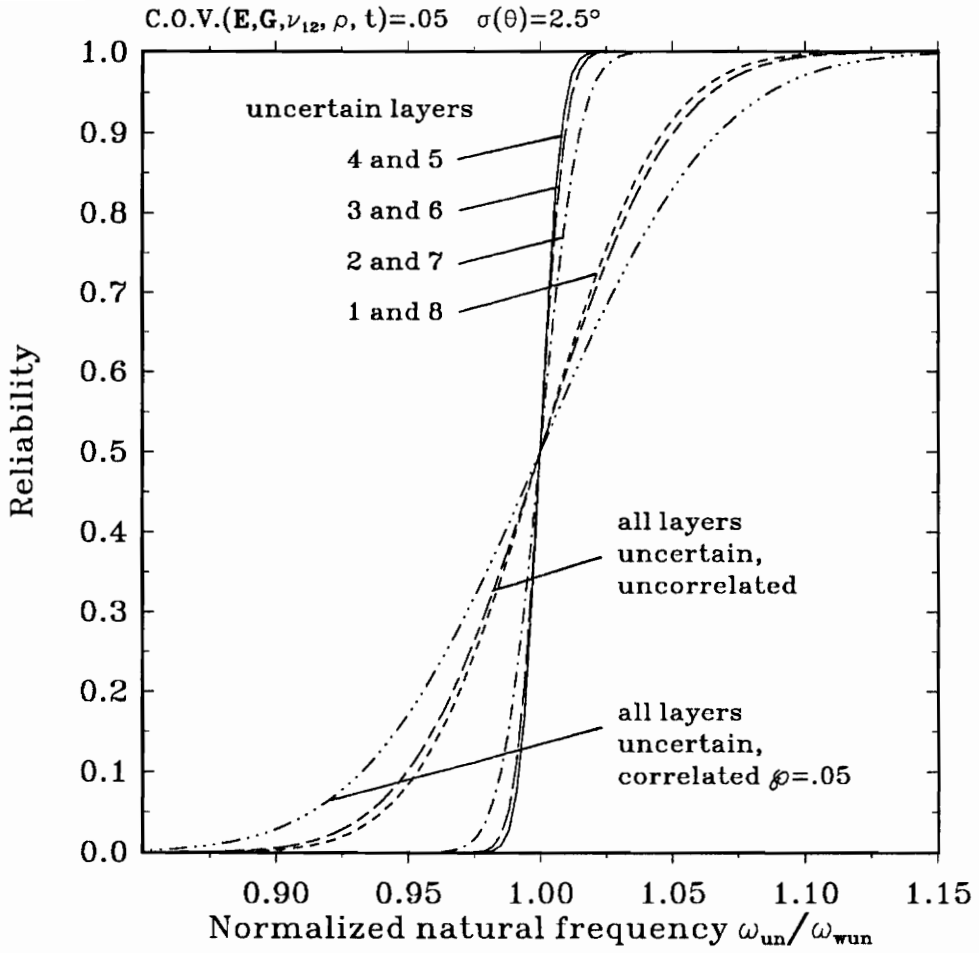

Figure 7.10 Reliability of laminate $[90/\pm 45/0]_S$ ($l = 9\ in,\ c = 3\ in$, modeled as per the FSDT with incorporation of the warping restraint) under an external oscillatory load. The uncertainties concern all variables.

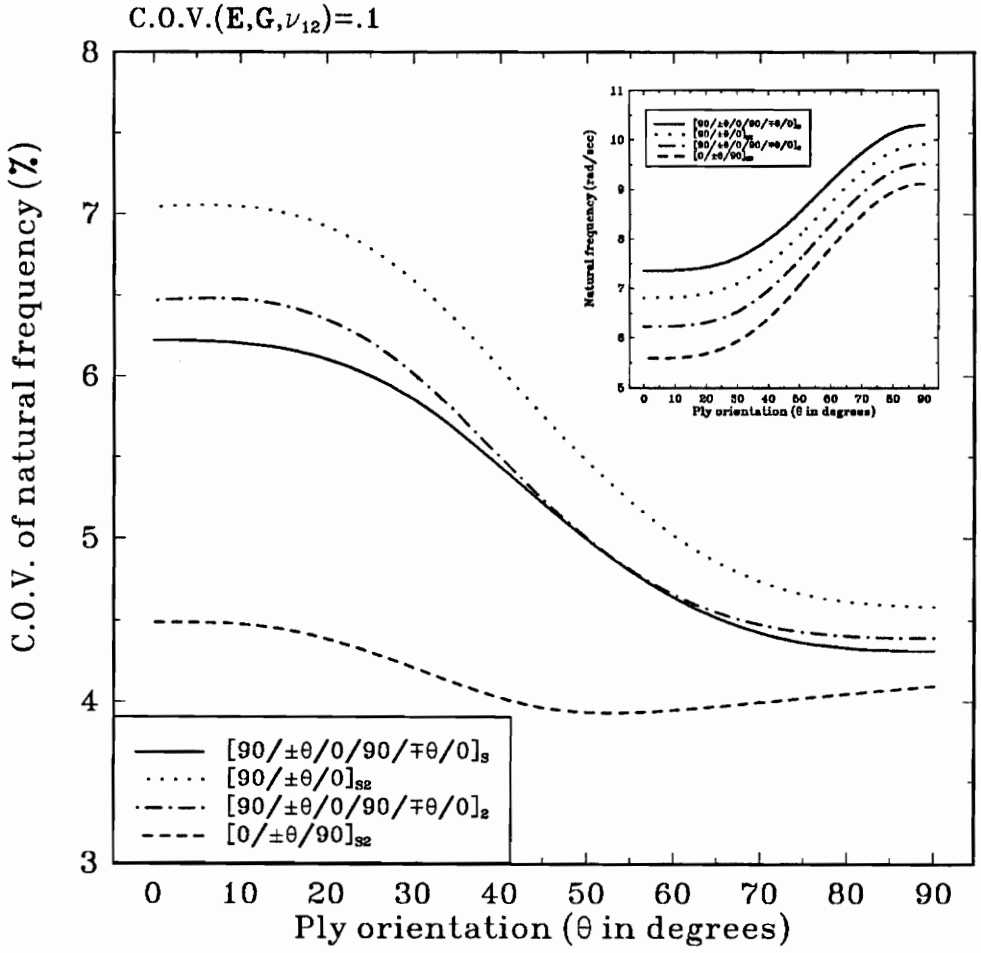

Figure 7.11 Coefficients of variation of the first bending frequencies versus ply orientation for structurally tailored laminate (l = 12 in, c = 3 in, modeled as per the FSDT with incorporation of the warping restraint). The uncertainties concern the material properties.

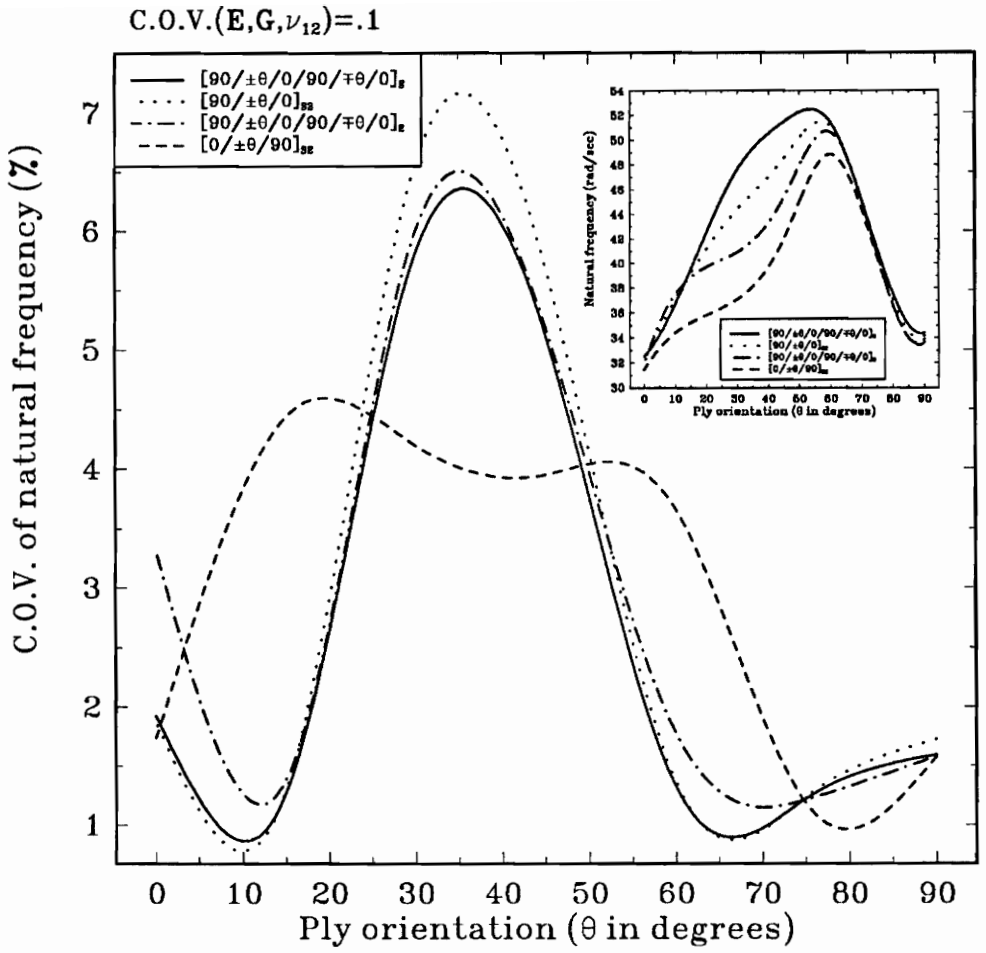

Figure 7.12 Coefficients of variation of the first torsional frequencies versus ply orientation for structurally tailored laminate (l = 12 in, c = 3 in, modeled as per FSDT with incorporation of the warping restraint). The uncertainties concern the material properties.

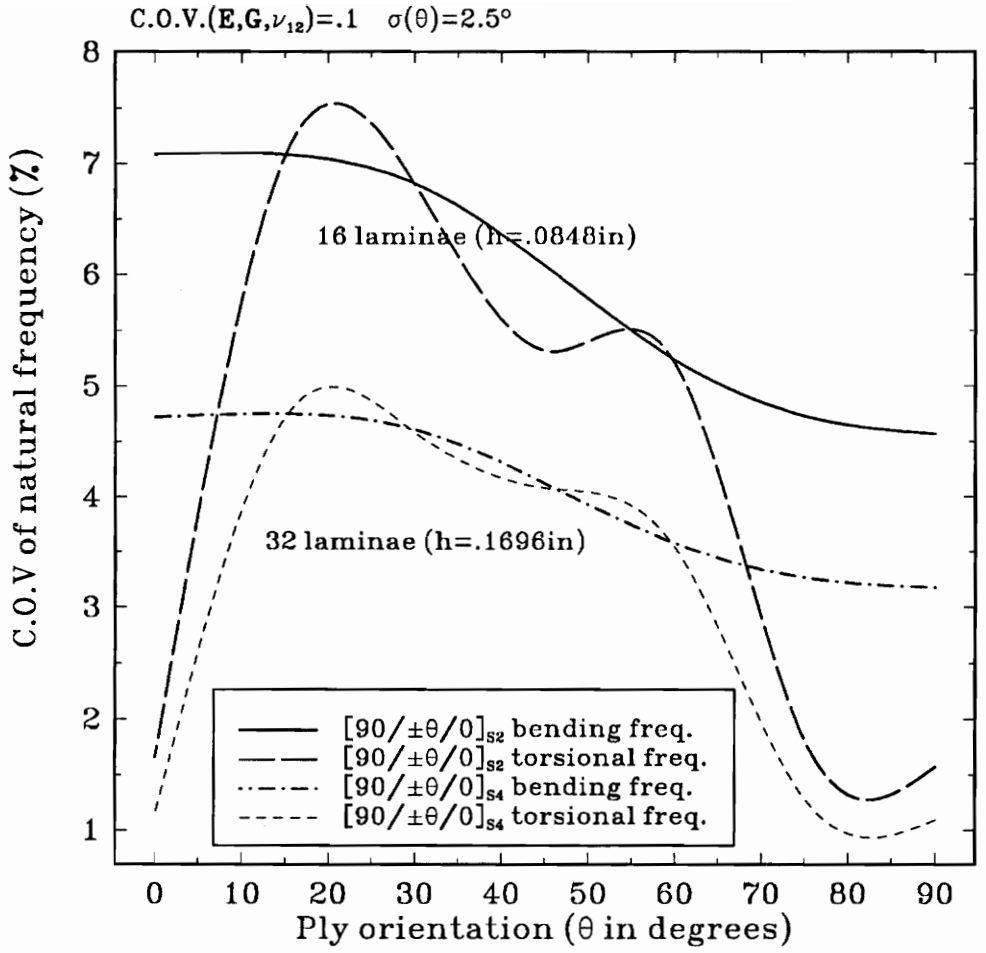

Figure 7.13 Effect of the thickness of laminate on the coefficient of variation of the first natural frequencies for laminate $[90/\pm\theta/0]_{Sn}$ ($l = 15\ in,\ c = 3\ in,\ t = .0053\ in,\ n = 2, 4$, modeled as per the FSDT with incorporation of the warping restraint). The uncertainties concern material properties and ply orientations of all layers.

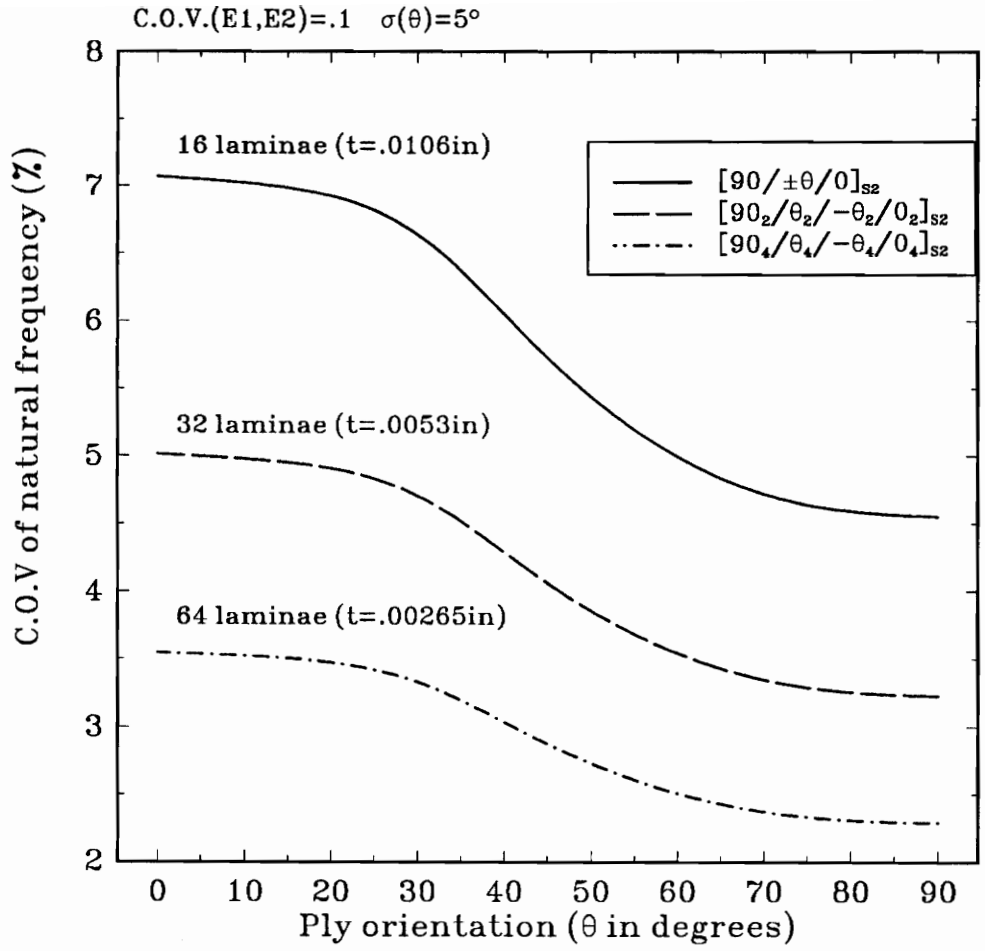

Figure 7.14 Effect of the number of layers on the coefficient of variation of the first bending frequency for laminate $[90_n/+\theta_n/-\theta_n/0_n]_{S2}$ ($l = 15\ in$, $c = 3\ in$, $h = .1696\ in$, $n = 1, 2, 4$, modeled as per the FSDT with incorporation of the warping restraint). The uncertainties concern material properties and ply orientations of all layers.

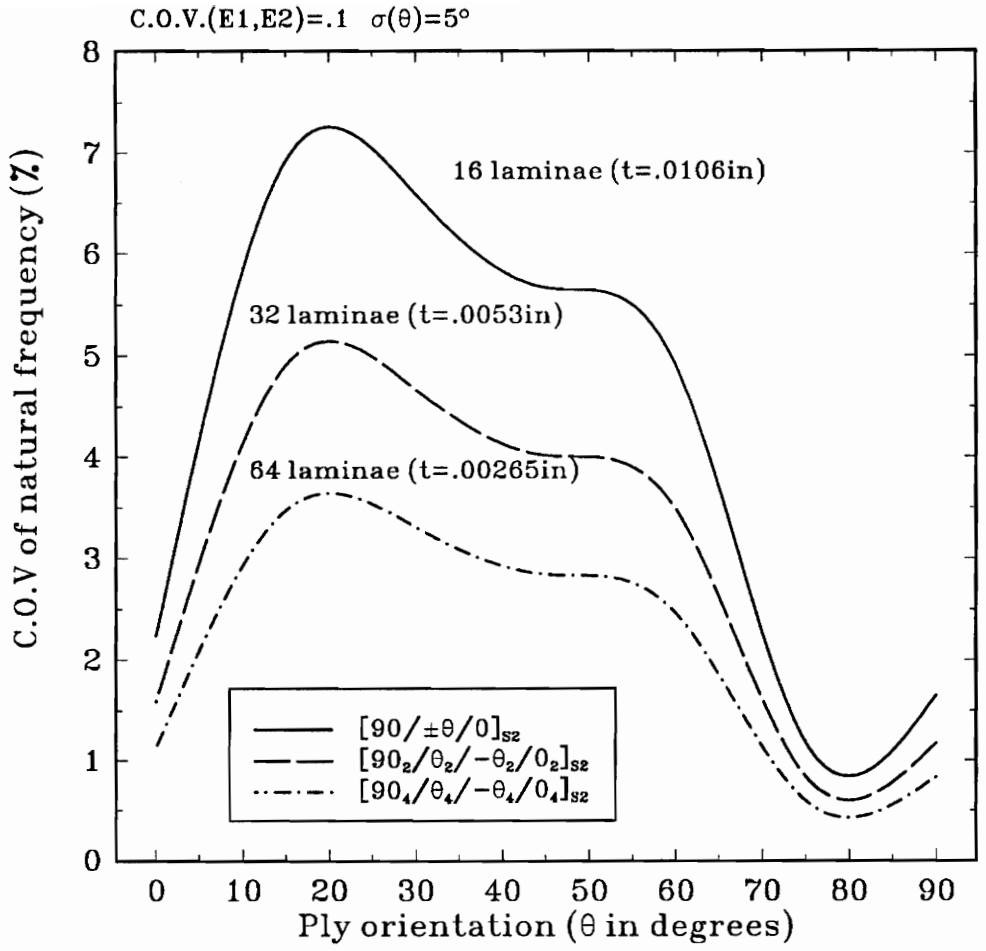

Figure 7.15 Effect of the number of layers on the coefficient of variation of the first torsional frequency for laminate $[90_n/ + \theta_n/ - \theta_n/0_n]_{S2}$ ($l = 15\ in$, $c = 3\ in$, $h = .1696\ in$, $n = 1, 2, 4$, modeled as per the FSDT with incorporation of the warping restraint). The uncertainties concern material properties and ply orientations of all layers.

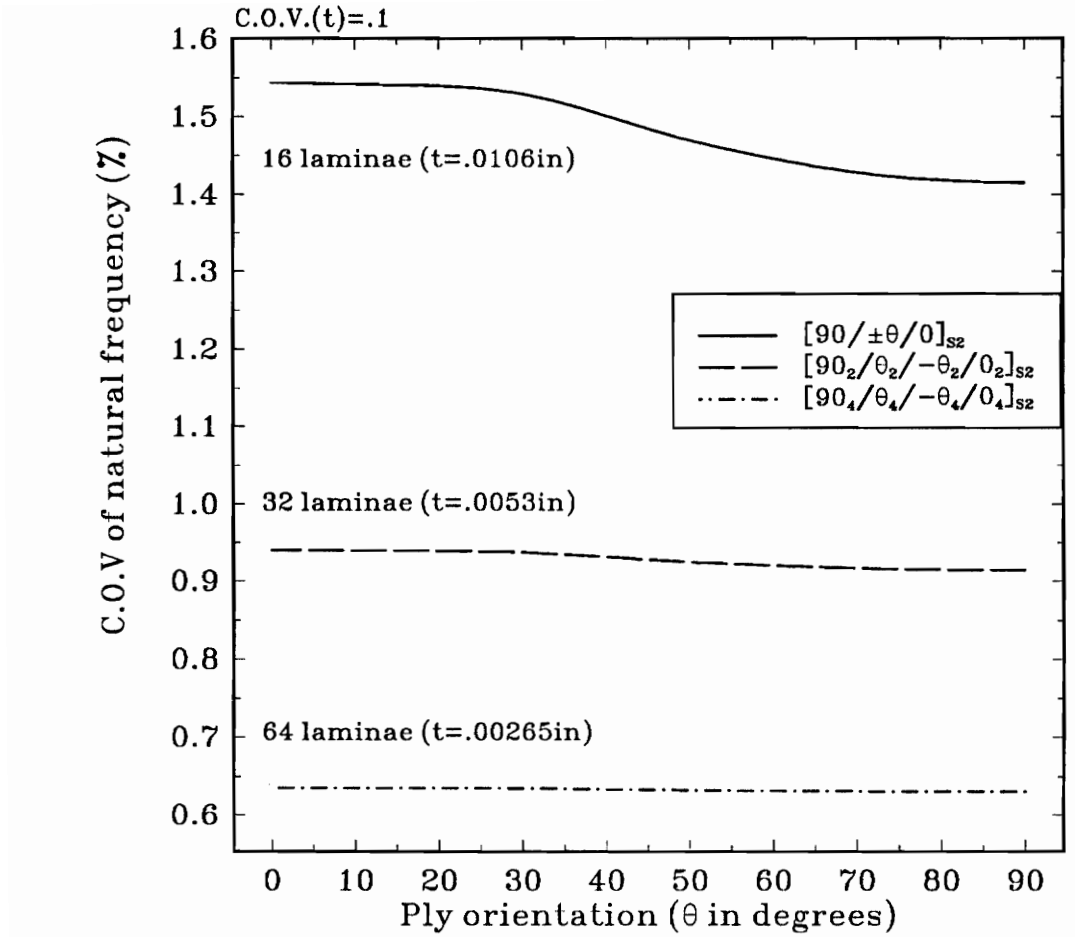

Figure 7.16 Effect of the number of layers on the coefficient of variation of the first bending frequency for laminate $[90_n/+\theta_n/-\theta_n/0_n]_{S2}$ ($l = 15\ in$, $c = 3\ in$, $h = .1696\ in$, $n = 1, 2, 4$ modeled as per the FSDT with incorporation of the warping restraint). The uncertainty concerns layer thickness.

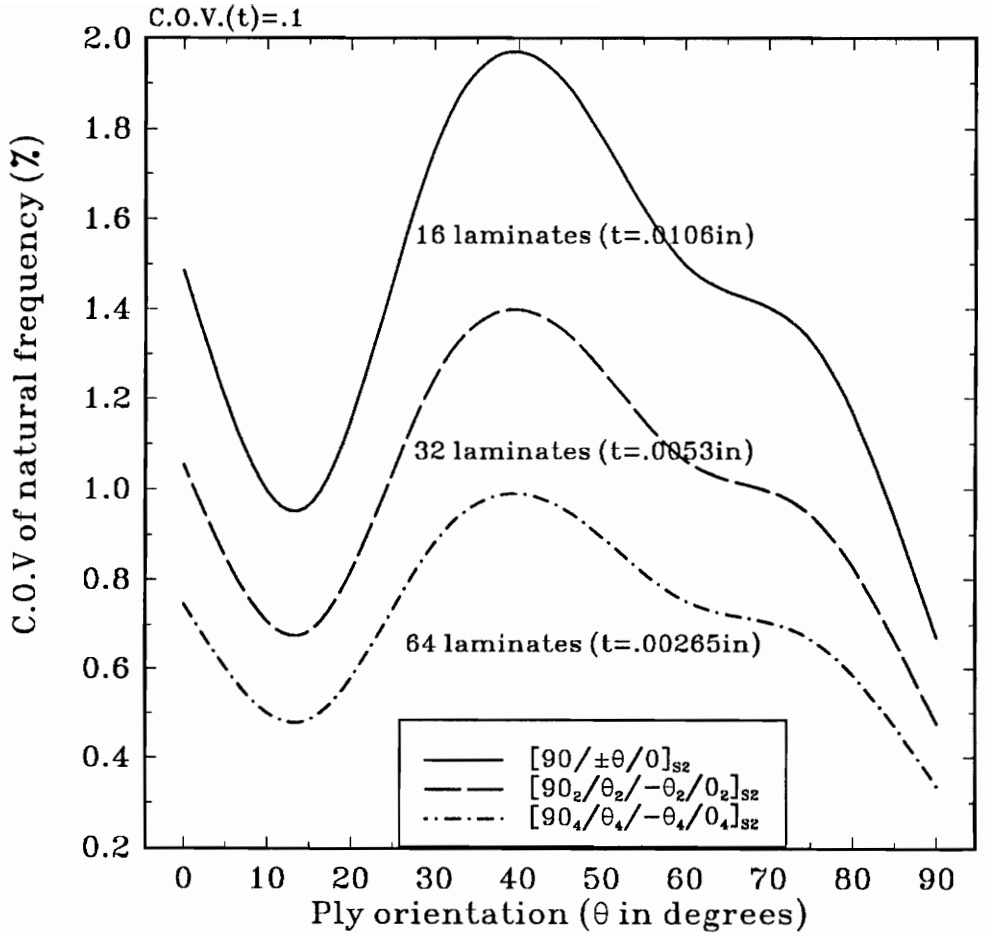

Figure 7.17 Effect of the number of layers on the coefficient of variation of the first torsional frequency for laminate $[90_n/ + \theta_n/ - \theta_n/0_n]_{S2}$ ($l = 15\ in$, $c = 3\ in$, $h = .1696\ in$, $n = 1, 2, 4$, modeled as per the FSDT with the incorporation of the warping restraint). The uncertainty concerns layer thickness.

8. ANALYSIS OF DAMAGED STRUCTURES

8.1 Overview

This chapter is devoted to an analysis of the damage effect on the dynamic behavior of cantilevered composite structures. When structures experience damage, their dynamic characteristics deteriorates. Flight structures are quite vulnerable to damage. Many military aircraft wings and helicopter blades, as well as marine and terrestrial constructions experience various degrees of damage during their service life. The presence of damage results in a decrease of natural frequencies of the structure, and consequently in an overall deterioration from the aeroelastic and dynamic response points of view. Without their consideration in the design process the structures can be exposed to dangerous situations during their operation. It is well known that an accurate estimation is essential for an accurate prediction of the aeroelastic stability of an airplane. In addition, in order to construct flight structures operating safely within their flight envelope even in the presence of damage, the natural frequency drop should be considered in the preliminary design. The damage occurs mostly in the skin layers, and then can propagate toward contiguous inner layers, and in the spanwise direction as well. Herein, we will consider such damages distributed in the spanwise direction.

8.2 Modeling of Structural Damage

Damage is characterized by its size, location and intensity. The intensity of the damage is interpreted as a reduction of elastic stiffness. In order to model the structural damage, we introduce the following parameters:

l_d = location of the damage in the spanwise direction
(in terms of the damaged element number)

k_d = location of the damage in the thickness direction
(in terms of the damaged layer number counted from the top)

$\mathbf{C}$ = set of nominal elastic moduli including $\mathbf{E}$ and $\mathbf{G}$ (undamaged)

$\bar{\mathbf{C}}$ = set of actual elastic moduli including $\bar{\mathbf{E}}$ and $\bar{\mathbf{G}}$ (damaged)

$M_d = \frac{\{\mathbf{C}-\bar{\mathbf{C}}\}}{\mathbf{C}}$ reduction of elastic moduli, or intensity of damage
(1 - elastic moduli reduced 100%, all damaged 0 - undamaged)

A = area of the upper bounding surface of the beam (see Figure 8.1)

$\bar{A}$ = damaged area of the upper bounding surface of the beam

$s_d = \frac{\bar{A}}{A}$ size of damage (=1 - when whole span is damaged; =0 - undamaged)

8.3 Numerical Examples

In this section, numerical results are presented for the free vibration problem of a cantilevered composite structure experiencing damage and uncertainties. The structural model is based on FSDT, the warping restraint effect being taken into consideration. The material properties of the cantilevered composite structure considered in this study are the same as in the previous chapter. The case of a symmetrically damaged panel is investigated. Skin-layer damage is considered first. Later, this study is extended to the multiple-layer damage problem.

8.3.1 Damage Effect on Free Vibration:

Panel damage geometry is illustrated in Figure 8.1, where ten separate elements are used to manifest the influence of damage location on free vibration characteristics. The influence of the location of the damaged panel on the fundamental natural frequency of the composite cantilever is presented in Figure

8.2. The natural frequency is normalized with respect to that of the undamaged structure. Figure 8.3 shows the influence of propagation of panel damage in the thickness direction. It is found that the damage at the face layers has significant a effect on the natural frequencies for the laminate $[90/\pm 45/0]_{S2}$. The damage effect increases a little after the propagation of the damage through the third inner layer. In order to investigate the effect of propagation in the spanwise direction, the damage is initiated from the root or tip of the cantilever in Figures 8.4-5. It is found that the effect becomes more severe when the damaged area is towards the root of the cantilevered beam and diminishes when it is towards the tip. In addition, for a stronger intensity of damage, the damage effect is exacerbated.

8.3.2 Safety Analysis:

Safety analysis associated with dynamic behavior of damaged structure is presented. In the framework of safety analysis for the damaged structure, probabilistic failure in the presence of uncertainty is considered in the design process. An external oscillatory load is applied as a driving force for the study of failure. When the excitation frequency approaches the natural frequencies, violent vibration happens, resulting in failure of the structure. In this study, the failure occurs when the fundamental natural frequency of the structure is within the range of the excitation frequency. Elastic constants, $\mathbf{E}$, $\mathbf{G}$, and Poisson's ratio, ν_{12}, mass density, ρ, each layer thickness, t, as well as ply orientation, θ, are treated as Gaussian random variables. Uncertainty is represented in terms of C.O.V.'s or standard deviation σ. C.O.V.$(\mathbf{E}, \mathbf{G}, \nu_{12}, \rho, t) = .1$ and $\sigma(\theta) = 2.5^o$ are assumed.

In Figure 8.6, the probabilistic failure of a damaged structure is compared to the undamaged one with respect to the intensity of damage. The stacking sequence, $[90/\pm 45/0]_{S2}$, is considered and it is assumed that the whole span of external layers is damaged. In Figures 8.4-5, it is seen that when the damage

becomes intense the damage effect is exacerbated. Here, similar results are obtained for the structure with damaged composite skins. The effect of the spanwise location of damage on structural safety is depicted in Figure 8.7. Again, the entire span is divided into ten elements and top and bottom layers about the mid-plane are taken for symmetric configuration of the damage. As seen in the figure, the damage near the root can jeopardize the safe operation of the structure.

Probabilistic failure due to propagation of the damaged composite skins is shown Figure 8.8. Even though half the span from the tip of the external layers is damaged, the structure can survive. It implies that an aircraft wing, one of the typical cantilevered structures, can still carry dynamic load although damage occurs, especially for tip damage. Skin-layer and all-layer damage are considered along with undamaged ones for various intensities of the damage in Figure 8.9. If the oscillatory load drives the structure below the frequency of 11 rad/sec, the structure can operate in confidence of full safety. However, if the whole span of the external layers is damaged up to 50%, under the same driving frequency, the chance of survival is only 65%. It is concluded that the safety of a damaged structure depends highly upon the location, size and intensity of the damage.

8.3.3 Structural Tailoring With Possible Damage Effect:

In the previous chapter, structural tailoring was applied to the structure with parameter uncertainties. In this section, the structural tailoring technique is extended to the structure with possible damage. To prevent the failure of the structure due to damage, structural tailoring is essentially needed. To decrease the possible damage effect, laminate ply orientations are considered as tailoring parameters in design. Four different stacking sequences are taken for the application of structural tailoring with damage.

In Figures 8.10-11, vibration frequencies of damaged structures are compared to those of the undamaged ones (shown in the small graphs at the right corner). It is noticeable that, for a certain stacking sequence, the vibration frequencies decrease a little even for relatively large magnitude and size of damage at composite skins. It implies that we can enhance the dynamic characteristics as well as damage tolerance by taking into account possible damage effect in structural tailoring.

Figures 8.12-13 show percentage of frequency reduction of the tailored structures with occurrence of damage. Significant reductions of frequencies are noticed when the θ of face layers are 90 degrees, i.e. when the fibers are parallel to the spanwise direction. On the other hand, the composite structure whose face layers are characterized by the angle $\theta = 0^o$ experiences strong tolerance to damage. From these numerical results, it appears that the dynamic behavior of a damaged structure depends highly on the stacking sequence as well as the damage configuration characterized by its location, and size and intensity.

To study damage with structural tailoring, various simple stacking sequences are presented for the study of reliability. Probabilistic failure curves are plotted in Figures 8.14-15. Comparing failure of the damaged structure (see Figure 8.14) to that of the undamaged one (see Figure 8.15), structural tailoring has been revealed from the safety point of view. The mean of natural frequencies and their variations to parameter uncertainties are almost the same for two stacking sequences, $[0/90_3]_{2S}$ and $[90/0]_{4S}$. However, they differ significantly after the structure experiences damage. The existence of damage slightly affects the safety of cantilevers laminated with $[0/90_3]_{2S}$. However, for laminate $[90/0]_{4S}$, the overall dynamic performance deteriorates significantly after damage, yielding failure of the structure. It is concluded that the damage effect on the structure can be alleviated using the structural tailoring technique.

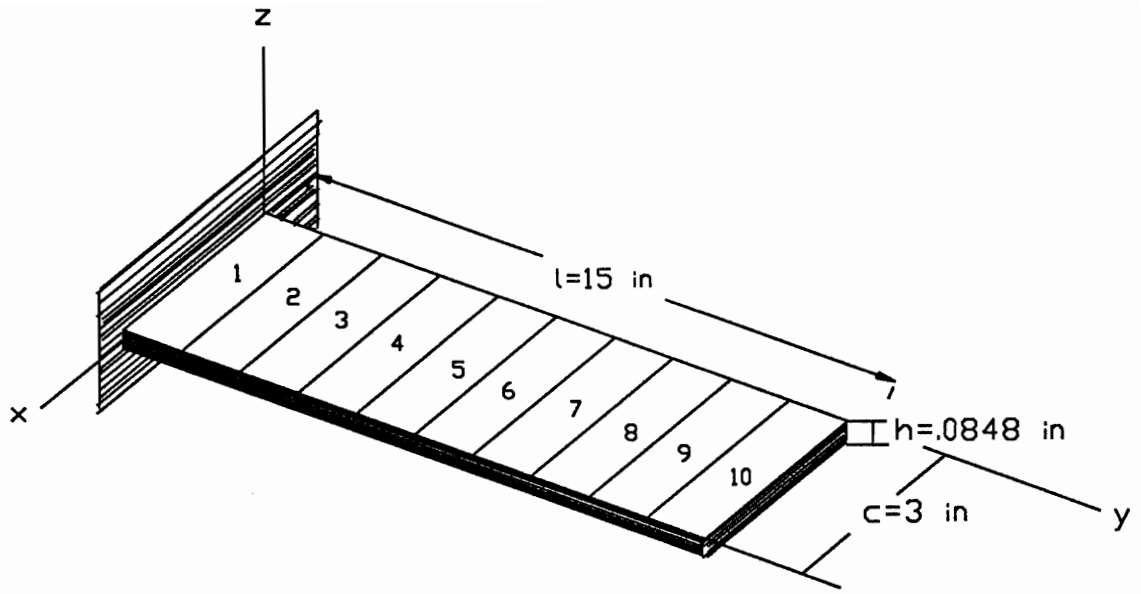

Figure 8.1 Description of the damaged panel geometry.

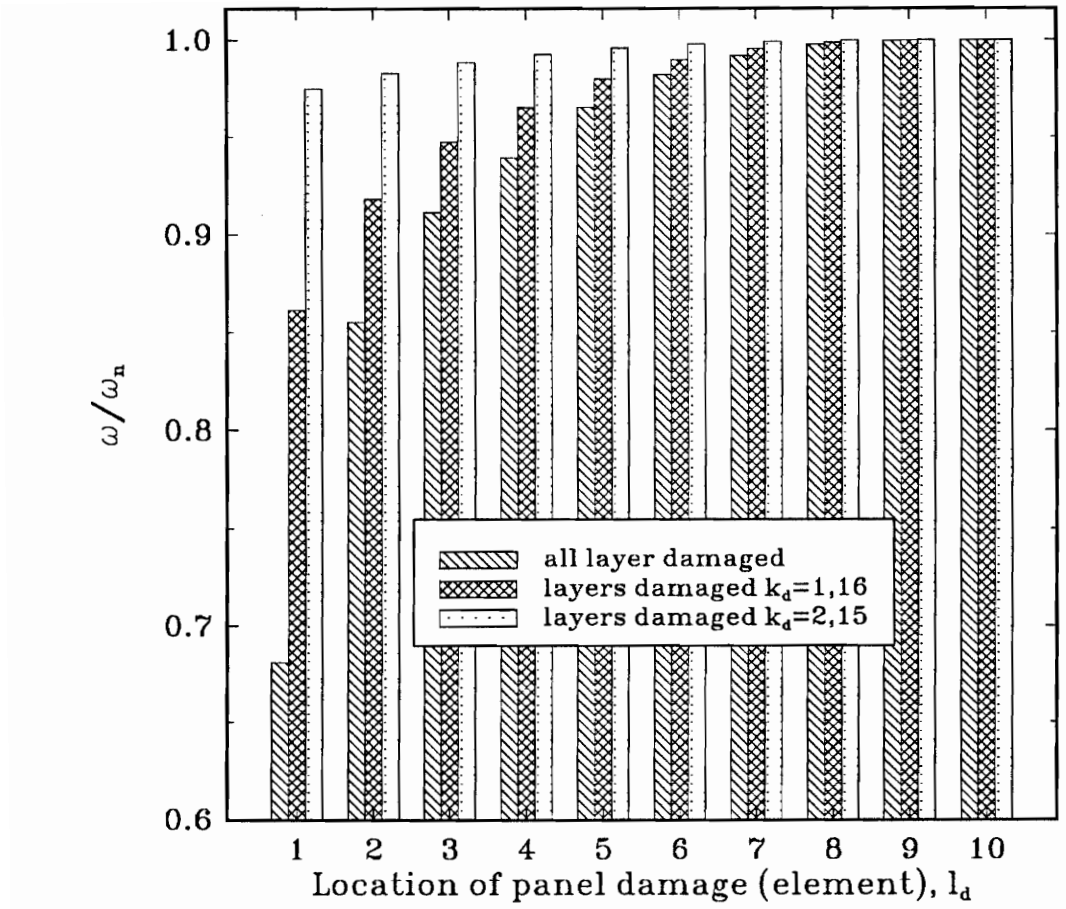

Figure 8.2 Influence of location of the damage on the fundamental natural frequencies for the laminate $[90/\pm 45/0]_{S2}$ ($l = 15\ in$, $c = 3\ in$, 10% of span experiences 80% drop of elasticity moduli).

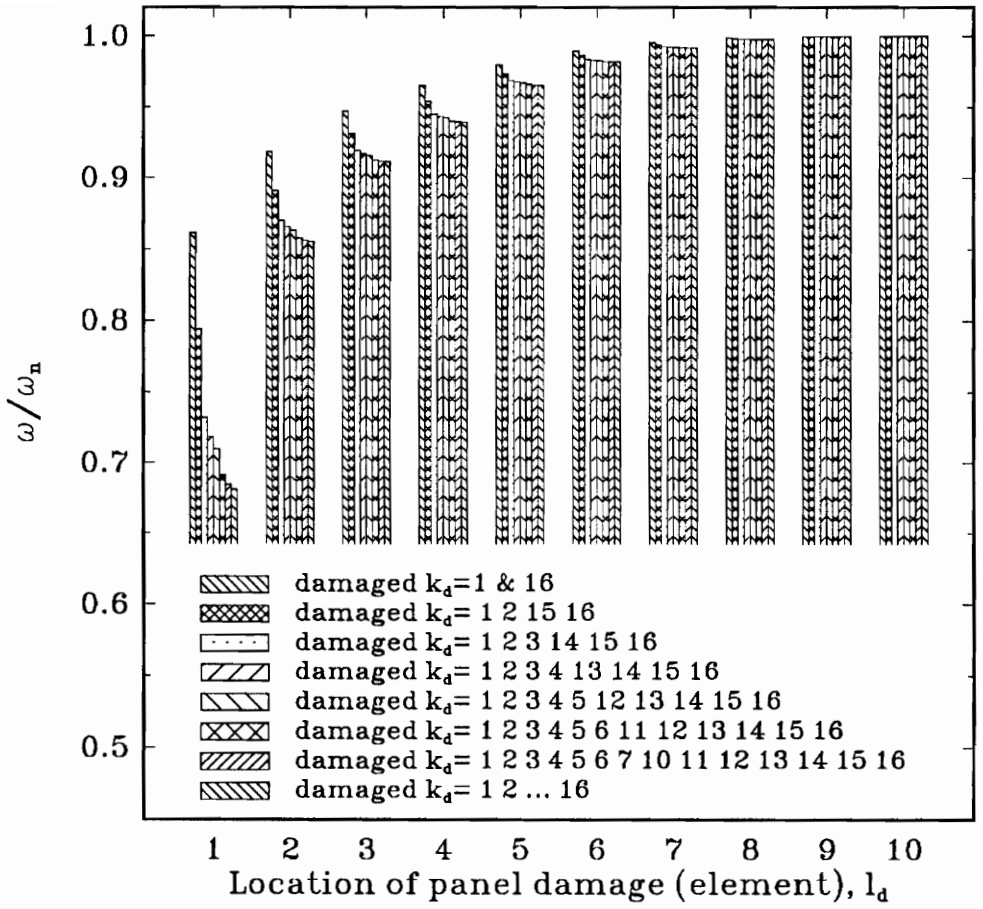

Figure 8.3 Fundamental natural frequency drop for the laminate $[90/\pm 45/0]_{S2}$ ($l = 15\ in,\ c = 3\ in$) with propagation of damage in the thickness direction (10% of span experiences 80% drop of elasticity moduli).

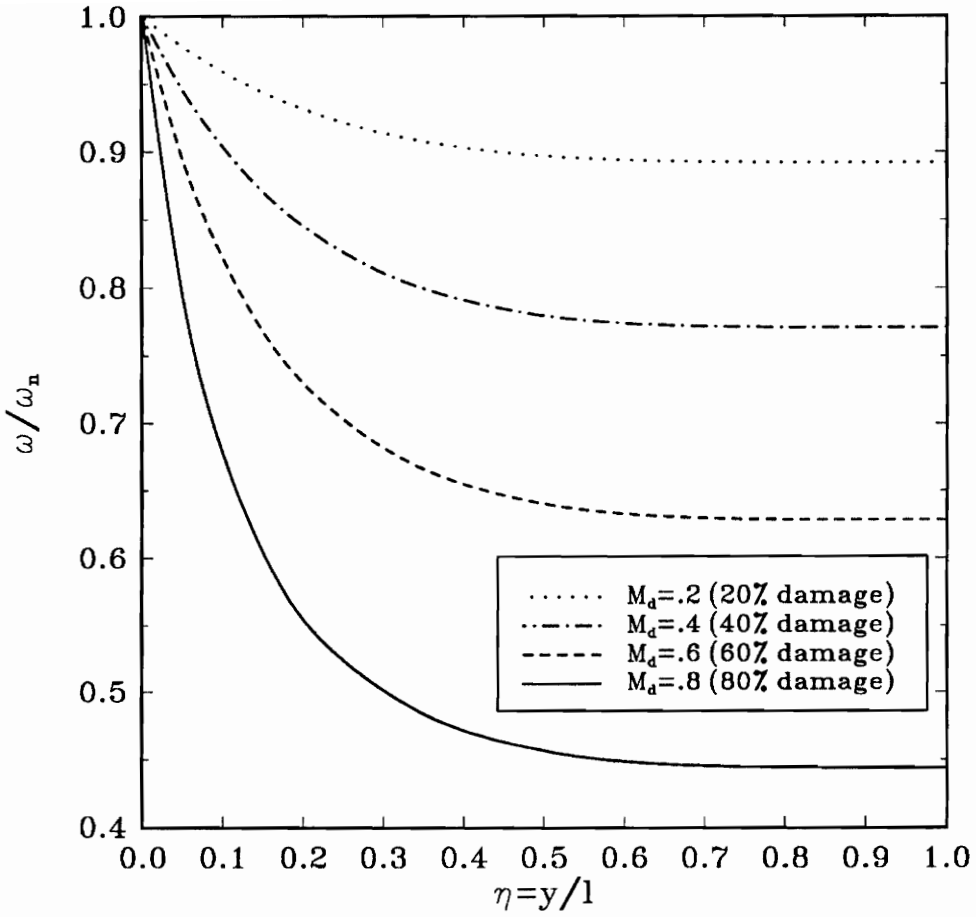

Figure 8.4 Reduced fundamental frequencies for laminate $[87/67/-68/-67/77/-59/78/90]_{S2}$ ($l = 15\ in,\ c = 3\ in$) with various intensities of damage (all layers damaged) propagated from root to tip.

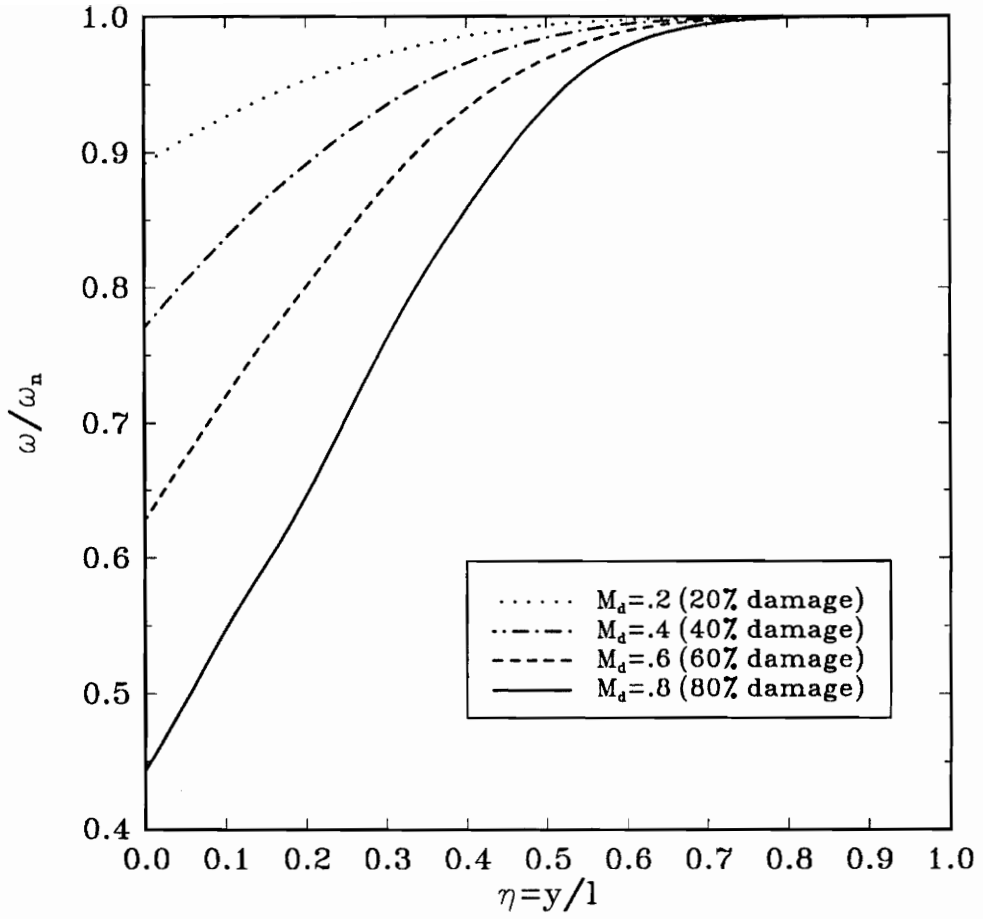

Figure 8.5 Reduced fundamental frequencies for laminate $[87/67/-68/-67/77/-59/78/90]_{S2}$ ($l = 15\ in,\ c = 3\ in$) with various intensities of damage (all layers damaged) propagated from tip to root.

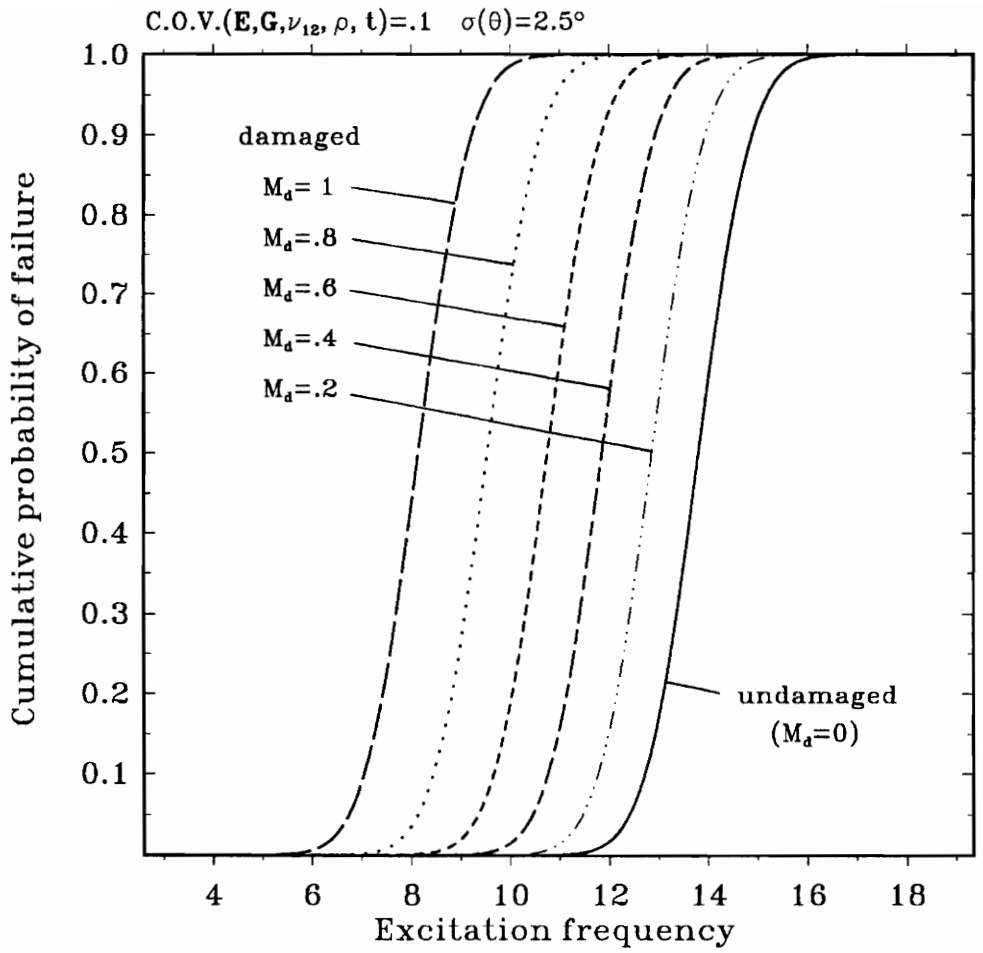

Figure 8.6 Probabilistic failure of the laminate $[90/\pm 45/0]_{S2}$ ($l = 9\ in$, $c = 3\ in$) with various intensities of damage at composite skins (whole span damaged) under an external oscillatory load.

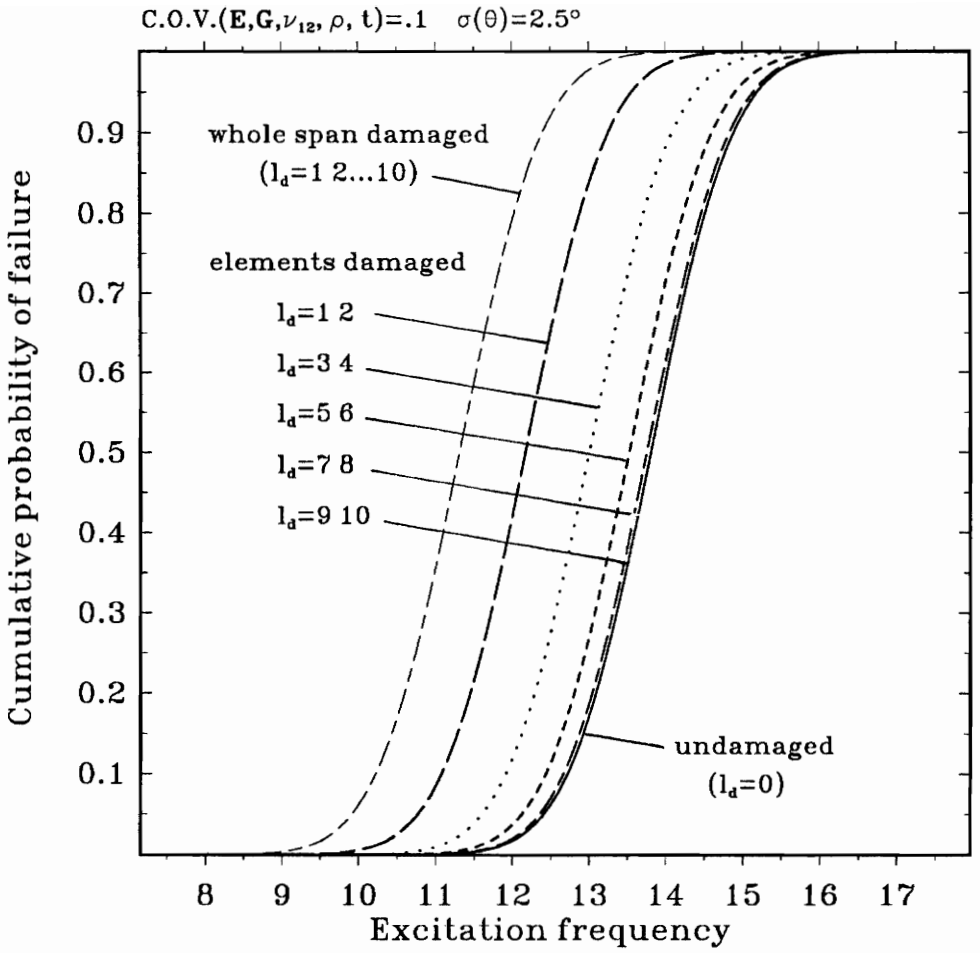

Figure 8.7 Probabilistic failure of the laminate $[90/\pm 45/0]_{S2}$ ($l = 9\ in$, $c = 3\ in$) with partly damaged composite skins (the damaged panel experiences 50% drop of elasticity moduli) under an external oscillatory load.

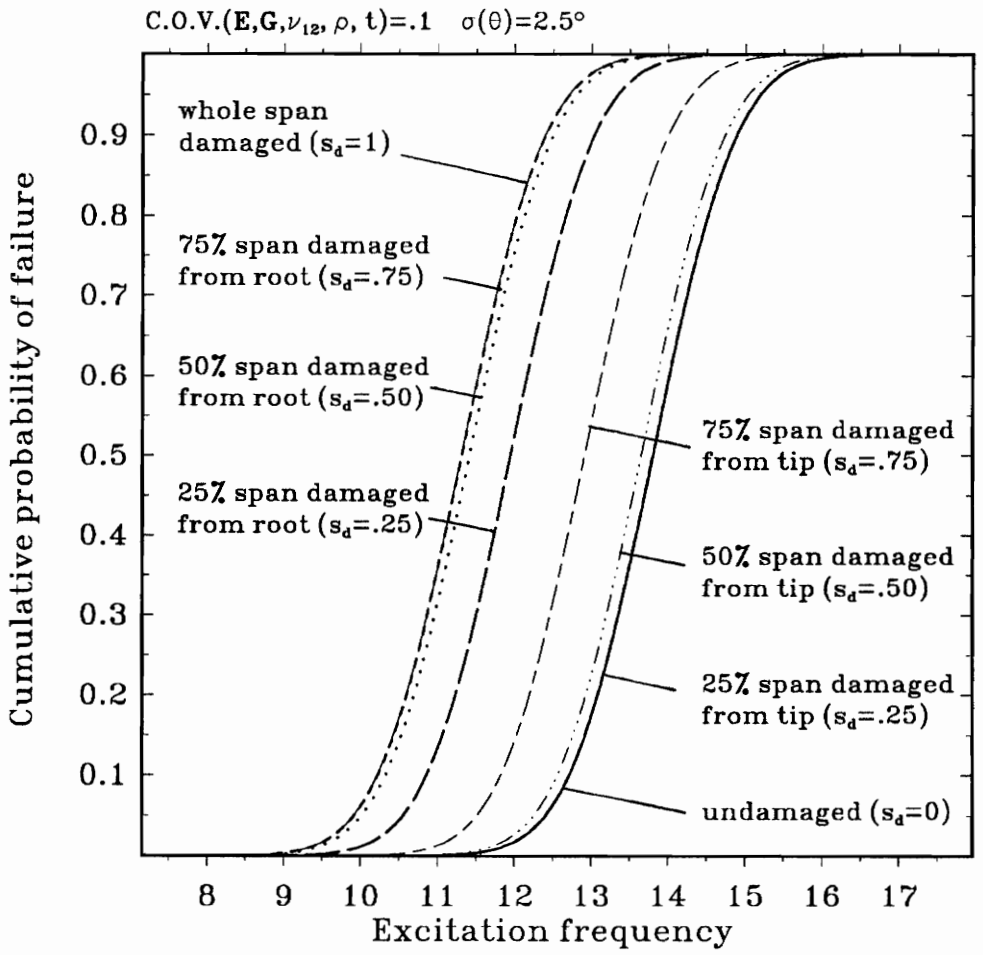

Figure 8.8 Probabilistic failure of the laminate $[90/\pm 45/0]_{S2}$ ($l = 9\ in$, $c = 3\ in$) with propagation of damaged composite skins (the damaged panel experiences 50% drop of elasticity moduli) under an external oscillatory load.

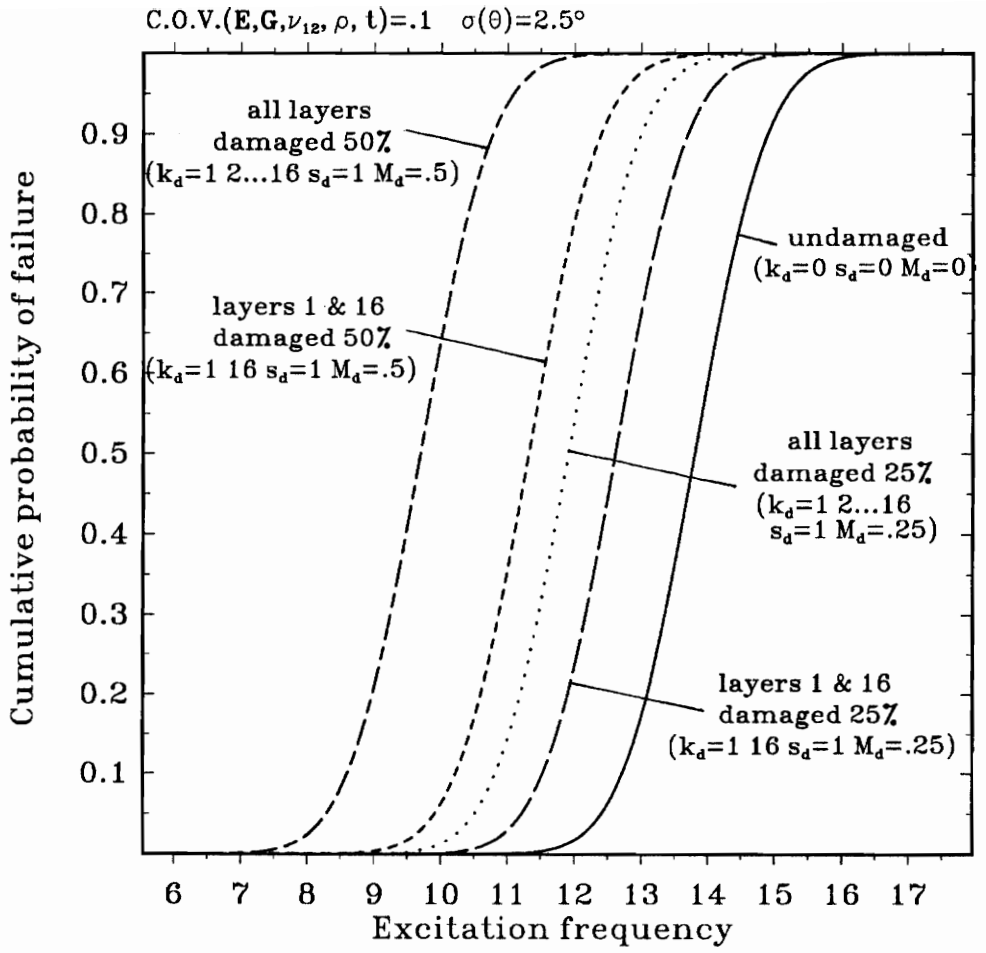

Figure 8.9 Probabilistic failure of the laminate $[90/\pm 45/0]_{S2}$ ($l = 9\,in$, $c = 3\,in$) with damage (whole span damaged) under an external oscillatory load.

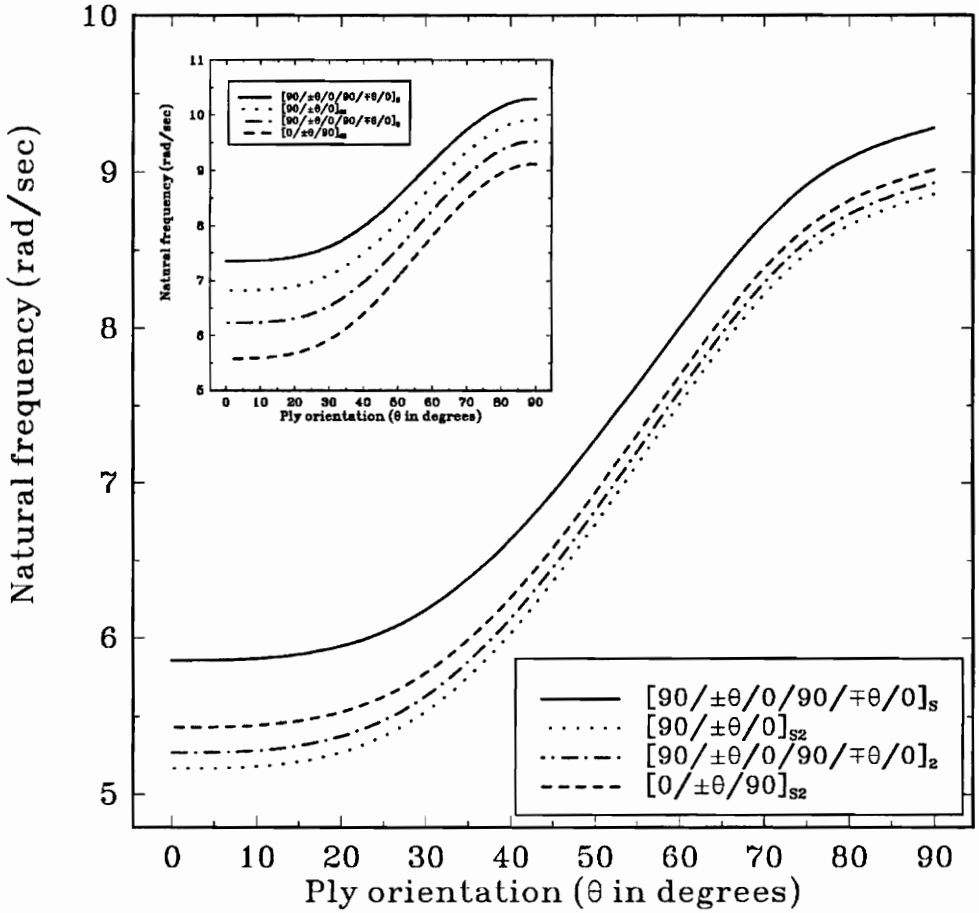

Figure 8.10 Variation of the first bending frequencies versus ply orientation as design variable for laminated cantilever ($l = 12\ in$, $c = 3\ in$) with damaged skins (whole span damaged 50%).

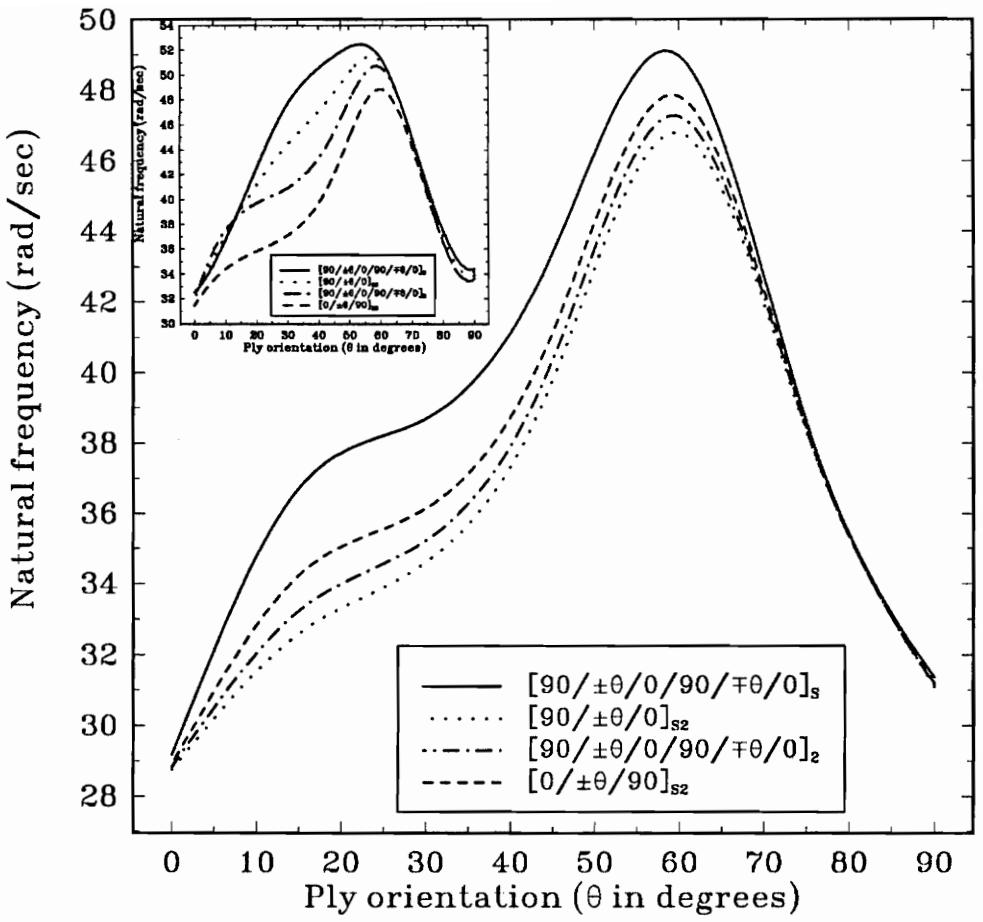

Figure 8.11 Variation of the first torsional frequencies versus ply orientation as design variable for laminated cantilever ($l = 12\ in,\ c = 3\ in$) with damaged skins (whole span damaged 50%).

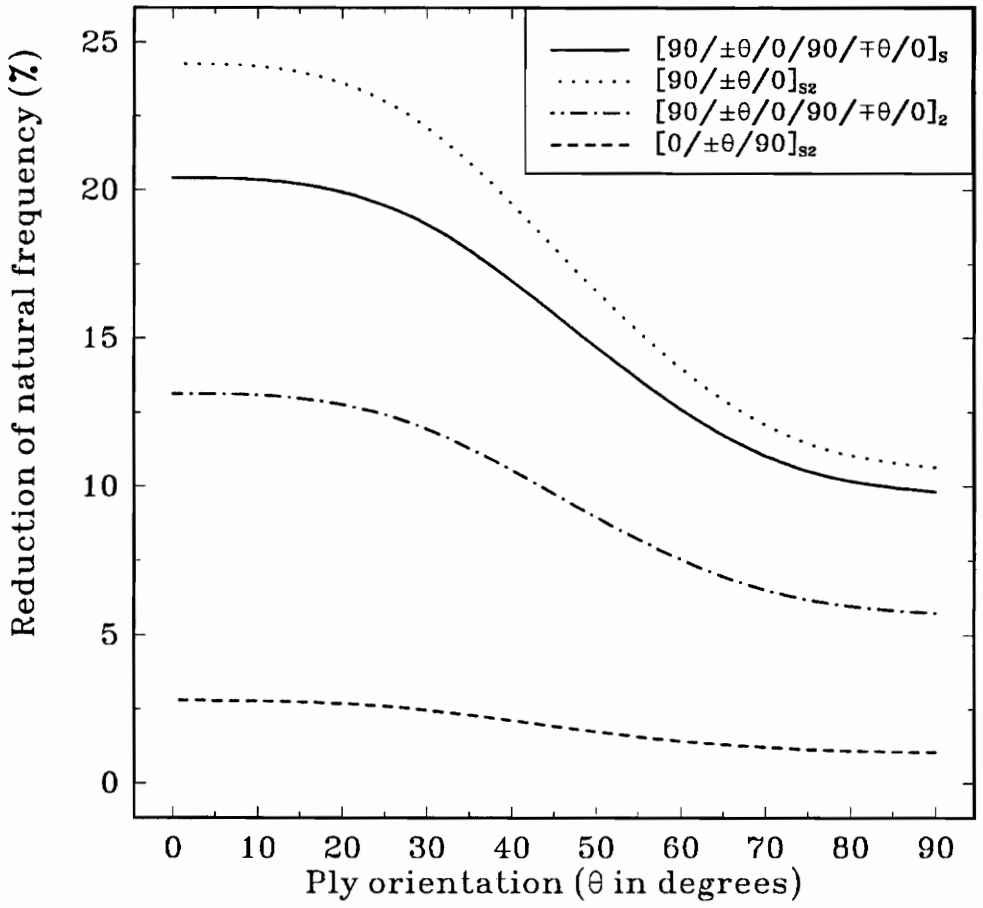

Figure 8.12 Reduction of the first bending frequencies for laminated cantilever ($l = 12\ in,\ c = 3\ in$) with damaged skins (whole span damaged 50%).

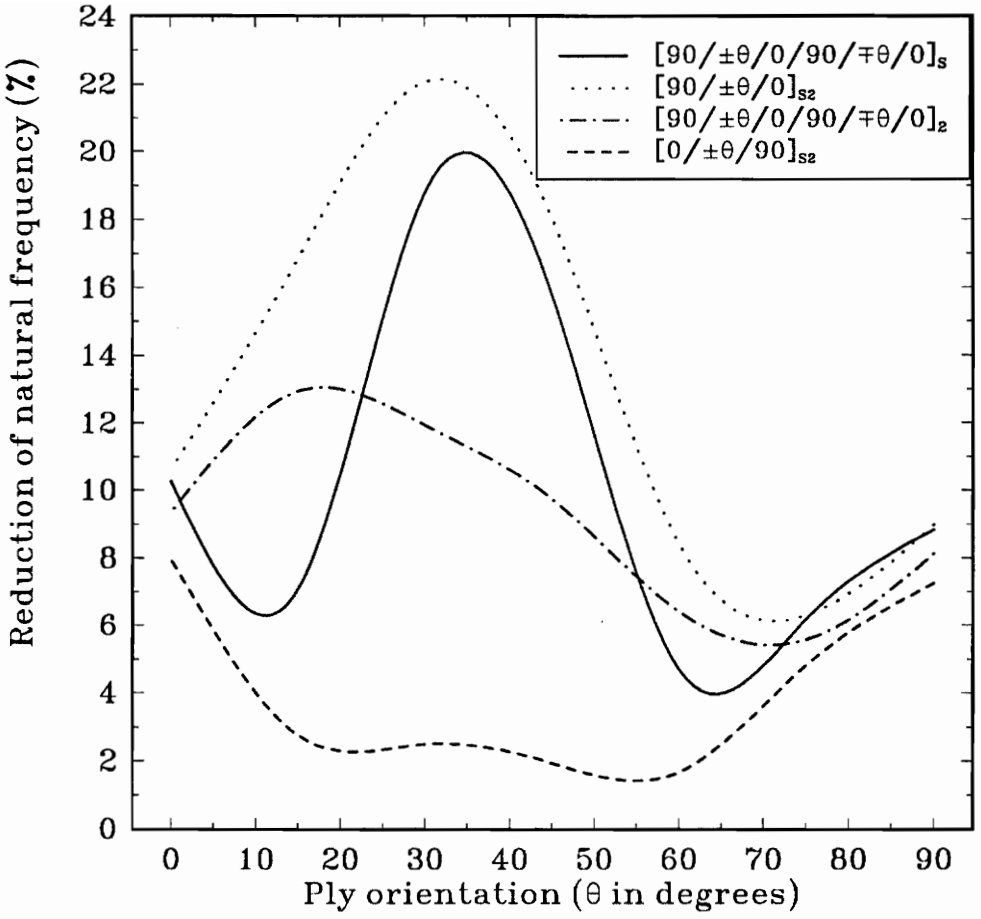

Figure 8.13 Reduction of the first torsional frequencies for laminated cantilever ($l = 12\ in,\ c = 3\ in$) with damaged skins (whole span damaged 50%).

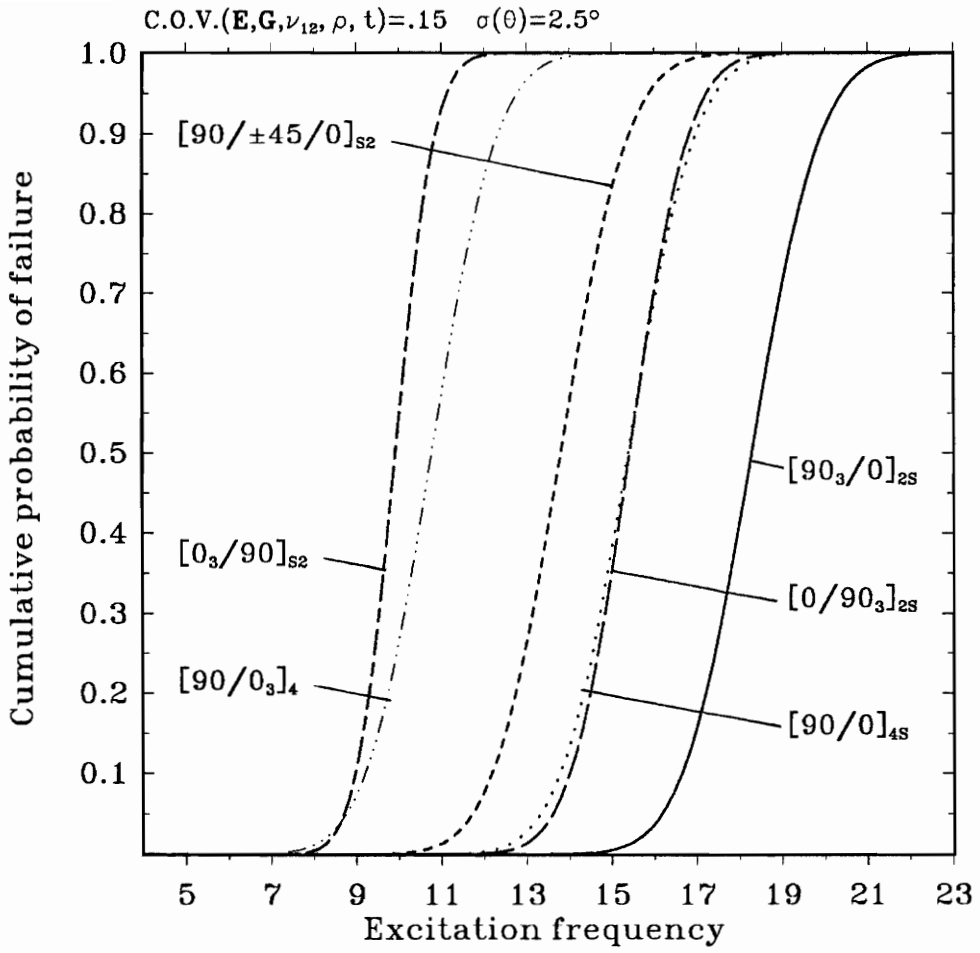

Figure 8.14 Probabilistic failure of structurally tailored laminate (l = 9 in, c = 3 in) with parameter uncertainties under an external oscillatory load.

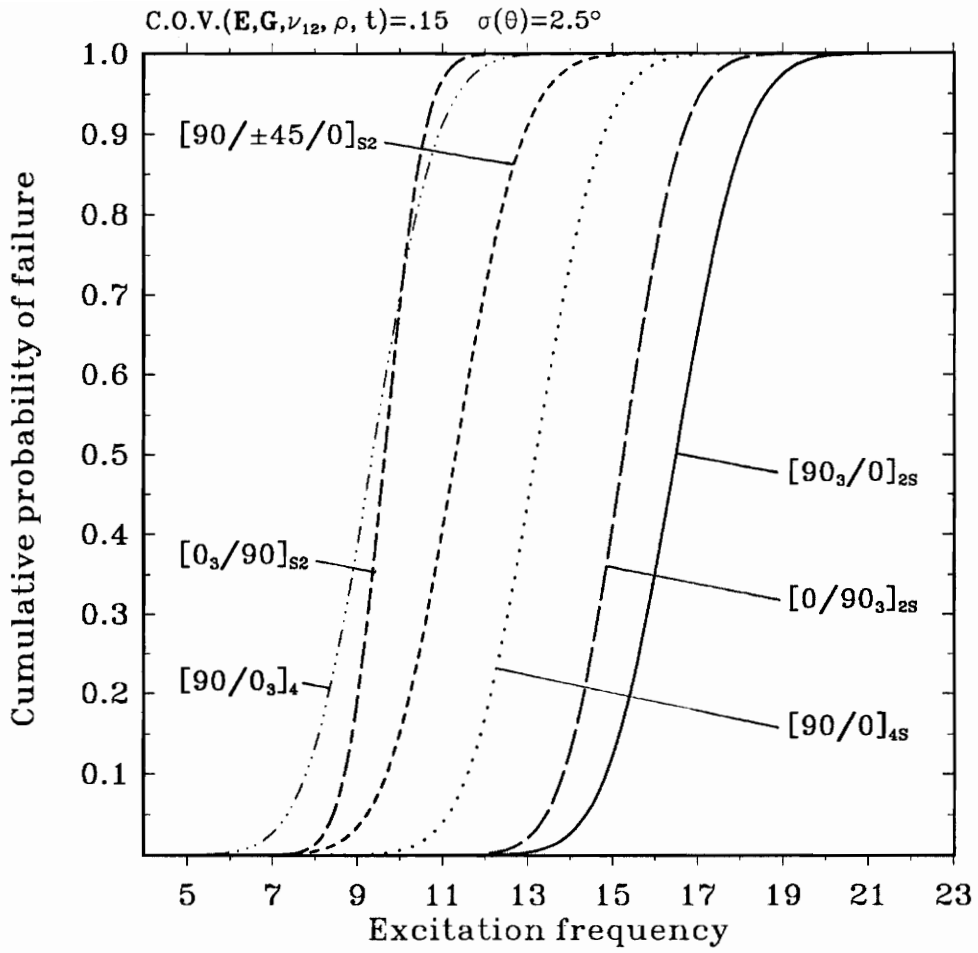

Figure 8.15 Probabilistic failure of structurally tailored laminate (l = 9 in, c = 3 in) with damaged composite skins (whole span damaged 50%) under an external oscillatory load.

9. DESIGN OF ROBUST STRUCTURES

9.1 Overview

A great deal of research work in connection with optimum design of laminated composite structures has been developed in recent years. Weight saving design for maximum buckling loads or constrained natural frequencies has been introduced in the optimum design of mechanical structures, in general, and of aeronautical space structures in particular. However, the structural damages which can occur during the operational life and parameter uncertainties have drastically affected the design practices.

Damage has drawn much attention to structural designers. Now it becomes one of the most important issues confronting aeronautical design. Structural damage yields a deterioration of the dynamic behavior of flight structures, and can result in catastrophic failures accompanied by loss of lives. Despite the necessary requirement of implementation of the damage and uncertainties into structural design explicitly, the literature in the field appears to be rather scarce.

The analysis of the effects of uncertainties in structural dynamics was described in the previous chapter using the *Stochastic Rayleigh-Ritz method.* Furthermore, it is required for the designer to find a way of reducing the effects of damage and unavoidable uncertainties on the structure. Here a systematic design methodology aiming at constructing robust structures to damage and uncertainties is presented.

Robustness is a design concept of structures based on the idea of enhancing their behavior or rendering them insensitive to parameter uncertainties and accidental damages occurring during their service life.

The present chapter is devoted to finding optimum design variables such as material properties, fiber orientations and proper stacking sequence as to render the structures still reliable in the presence of damage and parameter uncertainties.

9.2 Reliability-Based Design

In order to establish a probability of failure, consider a structure subject to oscillatory external loads. The structure is said to be safe if its lowest natural frequency ω_f (fundamental frequency) is beyond the excitation frequency range ω_e, i.e.

$$\omega_f > \omega_e \tag{9.1}$$

The boundary which falls into either failure or survival is called limit state. A function I known as the performance function can be characterized such that

$$\begin{aligned} I(\mathbf{x}) > 0 &= \textit{the safe state, and} \\ I(\mathbf{x}) < 0 &= \textit{the failure state} \end{aligned} \tag{9.2}$$

The limit-state equation $I(\mathbf{x}) = 0$ is referred to as the failure surface. $\mathbf{x} = (x_1, x_2, \ldots, x_n)$ is a set of design variables such as material elastic constants, mass density, layer thicknesses, and ply orientations. These variables are uncertain in a random sense, and as a result the dependent properties, i.e. natural frequencies, are also uncertain. In the design problem, the performance index is given as follows and new design points $x_1^*, x_2^*, \ldots, x_n^*$ are calculated by an iterative approach:

$$I(\mathbf{x}^*) = \omega_f^2(x_1^*, x_2^*, \ldots, x_n^*) - \omega_e^2 \tag{9.3}$$

or expressed as

$$I(\mathbf{x}^*) = \lambda_f(x_1^*, x_2^*, \ldots, x_n^*) - \lambda_e \tag{9.4}$$

New design points are calculated as

$$x_i^* = \mu_{x_i} - \alpha\beta\sigma_i \tag{9.5}$$

where

$$\alpha_i = \frac{\sigma_i \frac{\partial I}{\partial x_i}|_{\mu_{x_i}}}{\sqrt{\sum (\sigma_i \frac{\partial I}{\partial x_i})^2}} \tag{9.6}$$

α and β are called the alpha-value (Ref. [61]) and the safety index, respectively. The alpha-value α_i is used to measure the significance of the uncertain random variable x_i on the uncertainty of the dependent variable ω_f. Larger values of α_i imply that the uncertainty of the fundamental natural frequency ω_f is more influenced by the random variable x_i. The safety index is a unit distance from the average point to the limit state of failure criteria. Larger values of β_i imply smaller probability of failure.

The performance function is neither explicit nor linear; therefore, iterative solutions are obtained by adopting the optimization technique developed in chapter 6. Iteration steps are repeated through Eqs.(9.4-9.6) until x_i^* converges. In the end, new stacking sequences are generated to decrease the effects of the uncertainties while keeping the fundamental natural frequency unchanged. The derivative of the performance index is equivalent to the sensitivity of eigenvalues evaluated at the mean values, i.e.

$$\frac{\partial I}{\partial x_i}\Big|_{\mu_{x_i}} = \frac{\partial \lambda_f}{\partial x_i}\Big|_{\mu_{x_i}} \tag{9.7}$$

We will start with equation (4.2) in the eigenvalue problem for the sensitivity analysis of eigenvalues

$$(K - \lambda M)\phi = 0 \tag{9.8}$$

For a small variation of stiffness and mass matrices for Eq. (9.6), one obtains

$$\{(K + \delta K) - (\lambda + \delta\lambda)(M + \delta M)\}(\phi + \delta\phi) = 0 \tag{9.9}$$

Neglecting second order terms, we have

$$K\phi - \lambda M\phi - \lambda\delta M\phi + \delta K\phi - \delta\lambda M\phi + k\delta\phi - \lambda M\delta\phi = 0 \tag{9.10}$$

where $K\phi - \lambda M\phi = 0$; therefore

$$(-\lambda\delta M + \delta K - \delta\lambda M)\phi = (K - \lambda M)\delta\phi \tag{9.11}$$

Premultiplying both sides of the above equation by ϕ^T, and in light of the fact that its right hand side vanishes, one obtains

$$\phi^T\delta K\phi - \lambda\phi^T\delta M\phi = \phi^T\delta\lambda M\phi \tag{9.12}$$

and finally,

$$\delta\lambda = \frac{\phi^T(\delta K - \lambda\delta M)\phi}{\phi^T M\phi} \tag{9.13}$$

For sensitivity

$$\frac{\partial\lambda}{\partial x_i} = \frac{\phi^T\left(\frac{\partial K}{\partial x_i} - \lambda\frac{\partial M}{\partial x_i}\right)\phi}{\phi^T M\phi} \tag{9.14}$$

This result is identical to the ones derived by the mean-centered second-order moment method with first-order perturbation technique in Eq. (7.19). Considering ${\phi^o}^T M^o\phi^o = 1$ by normalization, Eq. (9.14) becomes:

$$\frac{\partial\lambda}{\partial x_i} = \phi^T\left(\frac{\partial K}{\partial x_i} - \lambda\frac{\partial M}{\partial x_i}\right)\phi \tag{9.15}$$

and in a more detailed form:

$$\frac{\partial\lambda_j}{\partial x_i} = \phi_j^T\left(\frac{\partial K}{\partial x_i} - \lambda_j\frac{\partial M}{\partial x_i}\right)\phi_j \tag{9.16}$$

Using the chain rule in tensorial notation, we have

$$\frac{\partial K}{\partial x_i} = \frac{\partial K}{\partial A_{kl}}\frac{\partial A_{kl}}{\partial x_i} + \frac{\partial K}{\partial B_{kl}}\frac{\partial B_{kl}}{\partial x_i} + \frac{\partial K}{\partial D_{kl}}\frac{\partial D_{kl}}{\partial x_i} \tag{9.17}$$

$$\frac{\partial M}{\partial x_i} = \frac{\partial M}{\partial A_{kl}} \frac{\partial A_{kl}}{\partial x_i} + \frac{\partial M}{\partial B_{kl}} \frac{\partial B_{kl}}{\partial x_i} + \frac{\partial M}{\partial D_{kl}} \frac{\partial D_{kl}}{\partial x_i} \tag{9.18}$$

where A, B, D are the laminated composite stiffnesses, $k = 1, 2, 6$, $l = 1, 2, 6$ and random variables

$$x_i = E_1, E_2, \nu_{12}, G_{12}, G_{23}, G_{23}, \rho, t, \theta_k \tag{9.19}$$

Correlated normal random variables may be treated for the design; however, they need to be uncorrelated for iteration. The correlated variables can be decoupled by transformation as follows (Ref. [62]):

1) Consider a random field characterized by mean matrix μ and covariance matrix **Cov**. Covariance matrix is expressed in the form of

$$\mathbf{Cov} = \begin{bmatrix} \sigma_{x_i}^2 & \wp_{x_i x_j} \sigma_{x_i} \sigma_{x_j} \\ \wp_{x_i x_j} \sigma_{x_i} \sigma_{x_j} & \sigma_{x_j}^2 \end{bmatrix}, \qquad i, j = 1, \ldots, n \tag{9.20}$$

where σ_{x_i} is the standard deviation of each random variable x_i, given by its square root of variance, and $\wp_{x_i x_j}$ is the coefficient of correlation between the ith and jth component random variables.

2) Find eigenvalues λ and modal matrix Φ (a set of normalized eigenvectors ϕ corresponding to eigenvalues λ) of the given covariance matrix.

3) Premultiply transpose of modal matrix Φ to mean of correlated values μ.

4) Mean of uncorrelated normal variables

$$\mu^i = \Phi^T \mu, \quad or \quad \begin{Bmatrix} \mu_{x_1}^i \\ \mu_{x_2}^i \\ \vdots \\ \mu_{x_n}^i \end{Bmatrix} = \begin{bmatrix} \Phi_{11} & \Phi_{12} & \ldots & \Phi_{1n} \\ \Phi_{21} & \Phi_{22} & \ldots & \Phi_{2n} \\ \vdots & \vdots & \ddots & \vdots \\ \Phi_{n1} & \Phi_{n2} & \ldots & \Phi_{nn} \end{bmatrix}^T \begin{Bmatrix} \mu_{x_1} \\ \mu_{x_2} \\ \vdots \\ \mu_{x_n} \end{Bmatrix} \tag{9.21}$$

5) Standard deviations of uncorrelated normal variables

$$\sigma^i = \sqrt{\lambda}, \quad or \quad \begin{Bmatrix} \sigma_{x_1}^i \\ \sigma_{x_2}^i \\ \vdots \\ \sigma_{x_n}^i \end{Bmatrix} = \begin{Bmatrix} \sqrt{\lambda_{x_1}} \\ \sqrt{\lambda_{x_2}} \\ \vdots \\ \sqrt{\lambda_{x_n}} \end{Bmatrix} \tag{9.22}$$

Note that this transformation is valid only for normal variables. For correlated nonnormal variables, see the appendix of Ref. [49].

If some of the variables are nonnormal, equivalent normal distributions may be applied by transformation as follows (Ref [62]):

1) Calculate probability density $f_{x_i}(x_i)$, and cumulative probability functions $F_{x_i}(x_i)$ of the variables x_i.
2) Obtain the inverse normal function for the argument $G^{-1}[F_{x_i}(x_i^*)]$.
3) Calculate the normal density function $g\{G^{-1}[F_{x_i}(x_i^*)]\}$.
4) Calculate the standard deviation for a normally distributed variable

$$\sigma_i^N = \frac{g\{G^{-1}[F_{x_i}(x_i^*)]\}}{f_{x_i}(x_i^*)} \tag{9.23}$$

5) Calculate the mean

$$\mu_i^N = x_i^* - \sigma_i^N G^{-1}[F_{x_i}(x_i^*)] \tag{9.24}$$

9.3 Numerical Examples

A sixteen-layer $[90/\pm 45/0]_{S2}$ laminate with uncertain material properties is treated for design, where uncertainties are described in terms of C.O.V.'s or standard deviations. The structural model is based on either FSDT or CLT, while warping restraint is accounted for in both theories. The statistics (means and standard deviations) of material properties are shown in Tables 9.1. All random variables are assumed to be statistically independent and normally distributed.

9.3.1 Design Results:

The results of the reliability-based design are shown in Table 9.1 and Figures 9.1-2, where the robust structure to uncertainty is constructed by changing the material properties. The first and subsequent iteration solutions are summarized in

Table 9.1. For both models based on CLT and FSDT, fast convergence is achieved with a few iterations. It is seen that the in-plane Young's modulus has been significantly changed. On the other hand, the remaining variables are revealed to be insignificant in the design of a robust, thin structure to uncertainties.

To measure the stochastic importance of each design variable in bending vibration, alpha-values are shown in Figure 9.1. It reveals that the uncertain elastic constant E_1 plays a dominant role on the uncertainties of the bending vibration frequencies. Variation of shear moduli including those for in-plane and the transverse shear turns out to be insignificant for the design of robust structures, especially for thin structures.

For the concern of safety, probabilistic failure curves based on the first bending vibration frequencies are shown in the presence of damage and uncertainties in the structure. In Figure 9.2, probabilistic failures of robust structures are compared to the original ones. Without changing material properties, the structures can be constructed to be robust to uncertainty, which is shown in Figure 9.3. Construction of robust structures to uncertainties has been done by increasing the number of laminae with a slight change of the stacking sequence, while keeping the thickness of the laminate and material properties unchanged. The probabilistic curve of the robust structure is more steep than the original one which does not account for the uncertainty effects. This implies that the uncertainty range of natural frequencies decreases.

Even with lowered material properties, the structure can be made robust to damage (in Figure 9.4) as well as uncertainty. The fiber ply angle $\theta = 0^o$ is placed on the top and bottom of the laminate, and then the optimization technique developed in chapter 6 is applied to seek the ply orientation with the stacking sequence yielding the same fundamental frequencies as the original structure.

Structures are constructed to be robust to damage with the original material properties, which are shown in Figure 9.5. The robust structures to damage are compared to the original ones, by requesting that the same fundamental frequencies can be obtained for both the robust and original structures before damage. After the occurrence of the damage, the dynamic characteristics of the original structure are significantly deteriorated. However, the robust structure can still withstand a large amount of damage at face layers.

From the above numerical results, several conclusions can be obtained:

A cost-effective design of robust structures to uncertainties is possible by changing material properties. The robust structure to uncertainties is also shown to be more tolerant to damage when the structural tailoring technique is applied. The design of robust structures to damage without changing material properties, while applying the structural tailoring technique, is proven to be best for alleviating the damage effect. The damage effect can be drastically reduced by applying structural tailoring technique; however, the effect of uncertainty decreases in small amounts. Furthermore, the effect of damage is much more significant than those of uncertainties, therefore damage must be the primary concern in design.

9.3.2 Effect of Transverse Shear Deformation on Design

To investigate the importance of transverse shear deformation on the design of robust structures, a transversely isotropic structure is considered. Consideration of such a case is useful for analyzing only the effect of transverse shear deformation. For a transversely isotropic body, the transformed reduced matrix $\bar{Q}$ can be expressed, in terms of the engineering constants, as:

$$\bar{Q}_{11} = \bar{Q}_{22} \rightarrow \frac{E}{1-\nu^2}, \qquad \bar{Q}_{12} = \bar{Q}_{21} \rightarrow \frac{\nu E}{1-\nu^2}$$

$$\bar{Q}_{66} \rightarrow G_{12} \equiv \frac{E}{2(1+\nu)}, \qquad \bar{Q}_{44} = \bar{Q}_{55} = G'$$

where

$$E_1 = E_2 \to E, \quad G_{13} = G_{23} \to G', \quad \nu_{12} \to \nu$$

Now we have three variables, E, G', ν, representing the material properties. The results obtained using the first-order transverse shear deformation theory (FSDT) are compared with their classical counterparts (CLT). For convenience, the natural frequencies are nondimensionalized with respect to the first bending frequency of the cantilever with $l/h = 5, \mathcal{AR} = 4$.

In Figures 9.6-7, the bending frequencies are shown to be affected greatly by the ratio E/G' for both undamaged and damaged structures. The ratio E/G' is used as a measure of transverse shear flexibility. The difference between the bending frequencies predicted by the CLT and FSDT increases as the ratio E/G' increases. Furthermore, such a discrepancy is found to be greater for higher modes. As the beam becomes slender (i.e. as the l/h ratio is increased), the difference between the frequencies predicted by the CLT and FSDT becomes smaller (a similar trend was shown for a thin composite structure in the previous section). The same trends are followed in the uncertain natural frequencies due to parameter variations of material properties E, G', ν and layer thickness, t, and mass density, ρ. Figures 9.8-9 show the standard deviations of natural frequencies. For torsional vibration, there is only a slight influence of the transverse shear flexibility. Herein, in contrast to anisotropic structures, there is no coupling between bending and torsion, and as a result shear deformation occurs in bending modes only.

The stochastic importance of transverse shear rigidity, G', in bending vibration is revealed by presenting alpha-values in Figure 9.10. For a short and thick structure ($l/h = 5$, $\mathcal{AR} = 4$) the alpha-value for G' drastically increases as the ratio E/G' increases. It is concluded that in the case of thick structures which experience a large amount of transverse shear deformation, its effect should be considered in the design of robust structures to damage and uncertainties.

Table 9.1 New material properties designed for constructing robust structure to uncertainties (C.O.V.($\mathbf{E}, \mathbf{G}, \nu_{12}$) = .1).

Material properties and statistics for graphite/epoxy laminate

Random Variable	*Mean*	*Standard Deviation*	*Coefficient of Variation*
E_1 (psi)	18.500x10^6	1.8500x10^6	0.1
E_2 (psi)	1.600x10^6	0.1600x10^6	0.1
ν_{12}	0.350	0.0350	0.1
G_{12} (psi)	0.832x10^6	0.0832x10^6	0.1
G_{23} (psi)	0.332x10^6	0.0332x10^6	0.1
G_{13} (psi)	0.332x10^6	0.0332x10^6	0.1

Newly designed material properties using classical lamination theory

Design Variable	*Starting Point*	*Number of Iteration (safety index β=3)* 1	2	3	4
E_1 $(10^6 psi)$	18.5000	13.0410	12.9965	12.9963	12.9963
E_2 $(10^6 psi)$	1.6000	1.5910	1.5905	1.5907	1.5907
ν_{12}	0.3500	0.3313	0.3368	0.3368	0.3368
G_{12} $(10^6 psi)$	0.8320	0.8278	0.8276	0.8276	0.8276

Newly designed material properties using transverse shear deformation theory

Design Variable	*Starting Point*	*Number of Iteration (safety index β=3)* 1	2	3	4
E_1 $(10^6 psi)$	18.5000	13.0400	12.9962	12.9961	12.9961
E_2 $(10^6 psi)$	1.6000	1.5913	1.5908	1.5909	1.5909
ν_{12}	0.3500	0.3313	0.3368	0.3368	0.3368
G_{12} $(10^6 psi)$	0.8320	0.8278	0.8275	0.8276	0.8276
G_{23} $(10^6 psi)$	0.3320	0.3320	0.3320	0.3320	0.3320
G_{13} $(10^6 psi)$	0.3320	0.3320	0.3320	0.3320	0.3320

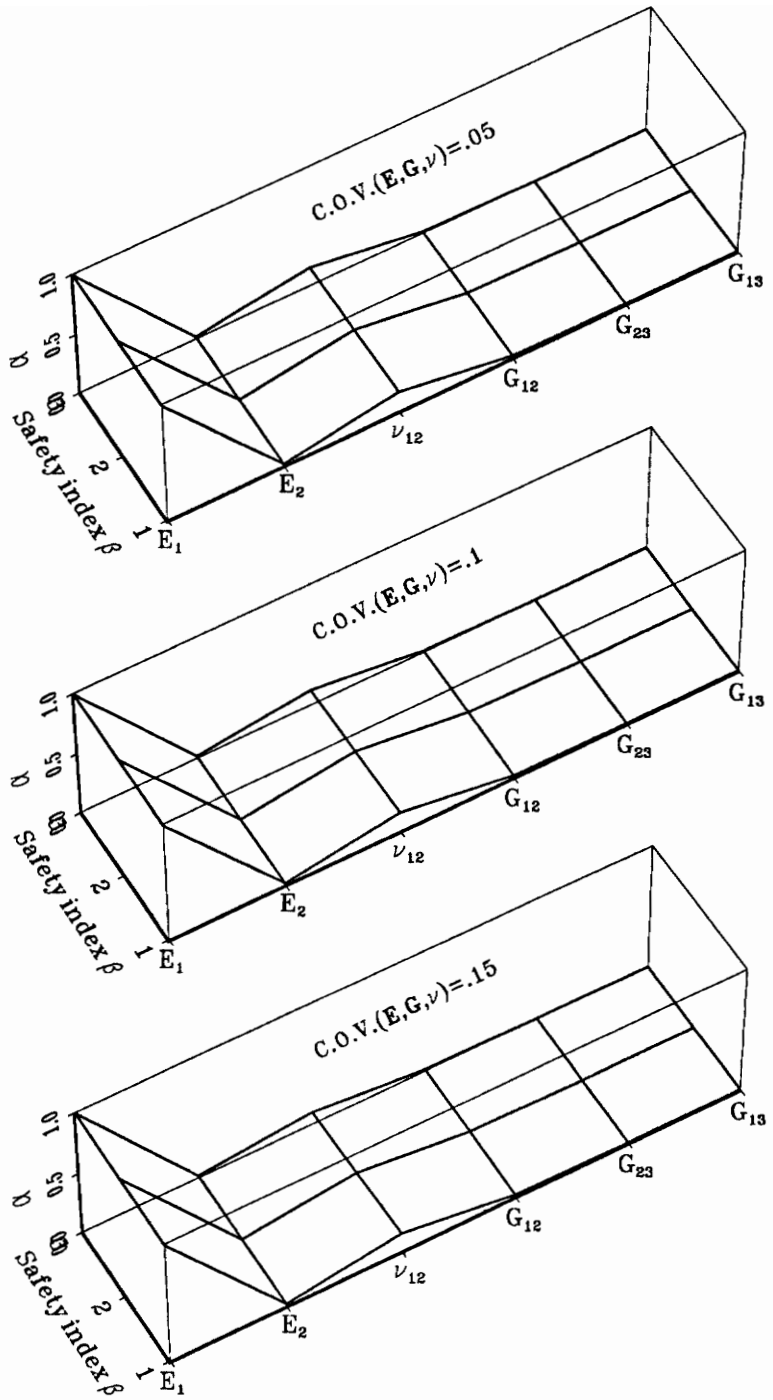

Figure 9.1 Alpha-value of random variables for the laminate $[90/\pm 45/0]_{S2}$ $(l = 9\ in,\ c = 3\ in)$.

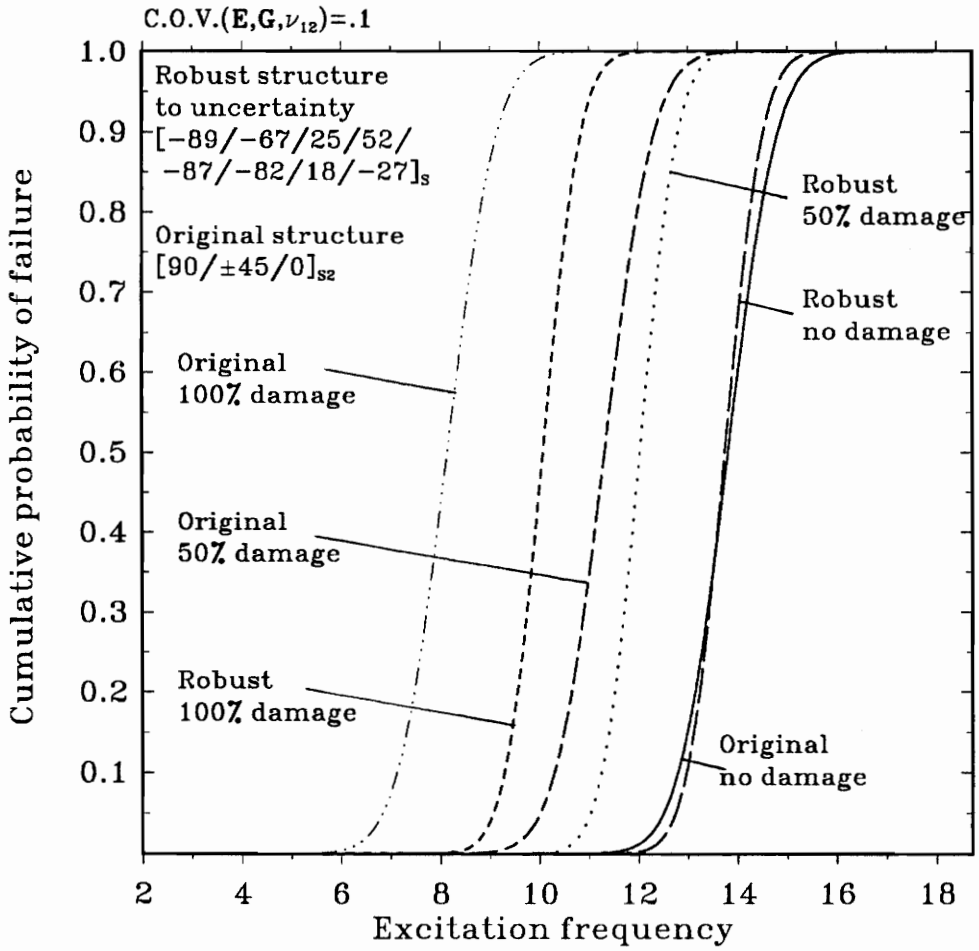

Figure 9.2 Probabilistic failure of original and robust structures (l = 9 in, c = 3 in) to uncertainties (C.O.V.($\mathbf{E}, \mathbf{G}, \nu_{12}$) = .1) with damaged composite skins (whole span of 1st and 16th layers are damaged up to 100 %) according to newly designed material properties.

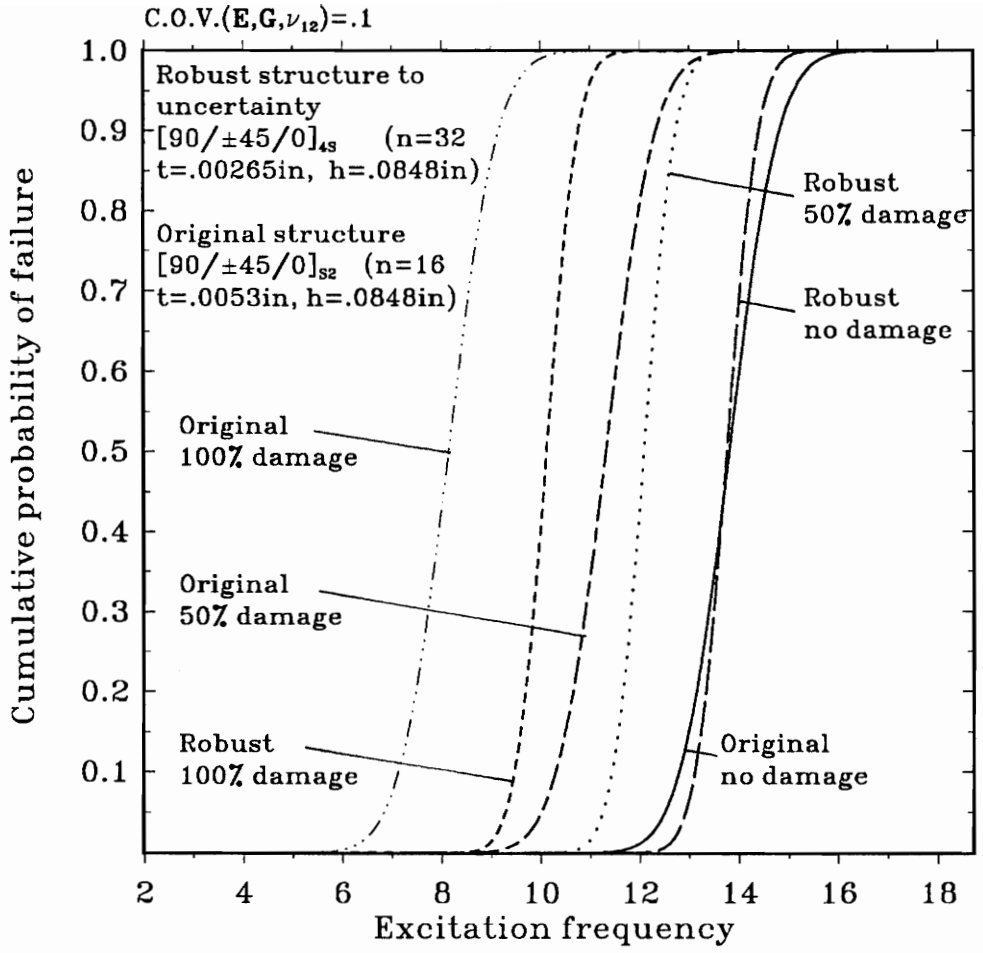

Figure 9.3 Probabilistic failure of original and robust structures (l = 9 in, c = 3 in) to uncertainties with damaged composite layers (whole span of 1st, 16th layers for original laminate $[90/\pm45/0]_{S2}$ and 1st, 2nd, 31st, 32nd layers for its robust counterpart $[90/\pm45/0]_{4S}$ are damaged, respectively, up to 100 %).

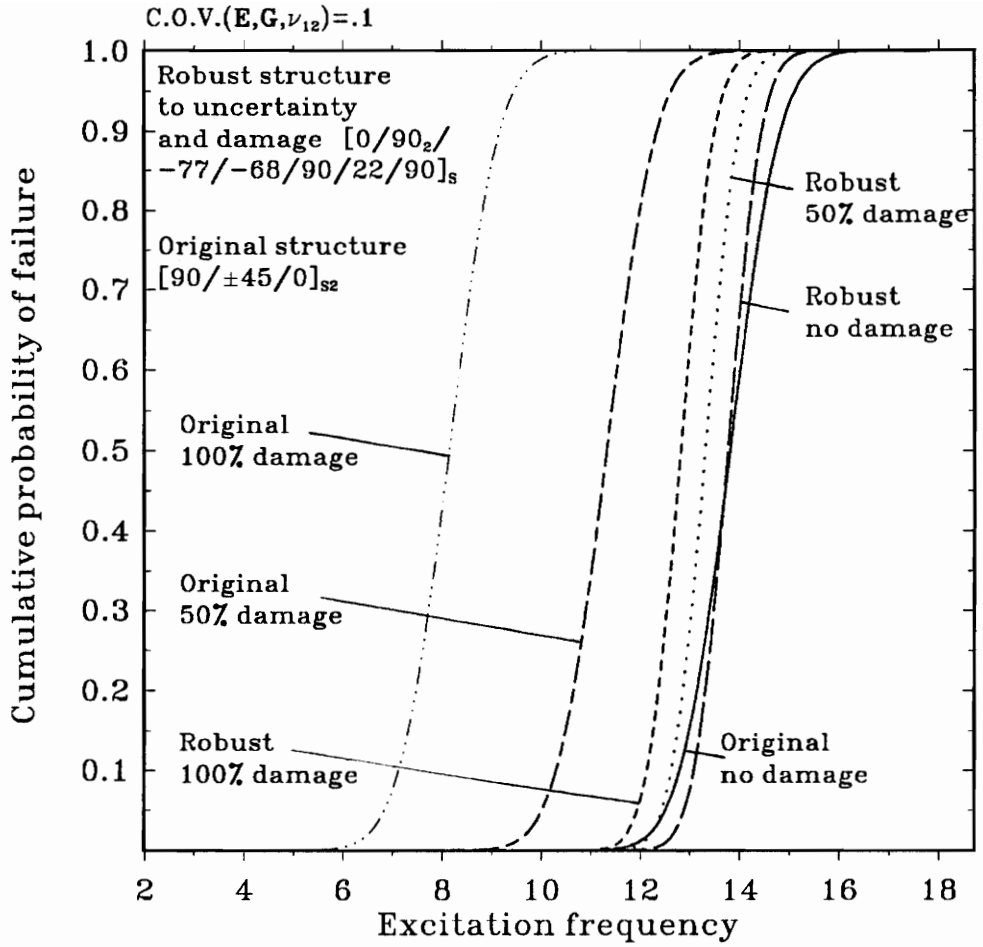

Figure 9.4 Probabilistic failure of original and robust structures (l = 9 in, $c = 3$ in) to uncertainties (C.O.V.($\mathbf{E}, \mathbf{G}, \nu_{12}$) = .1) and damage (whole span of 1st and 16th layers damaged up to 100 %) according to the newly designed material properties.

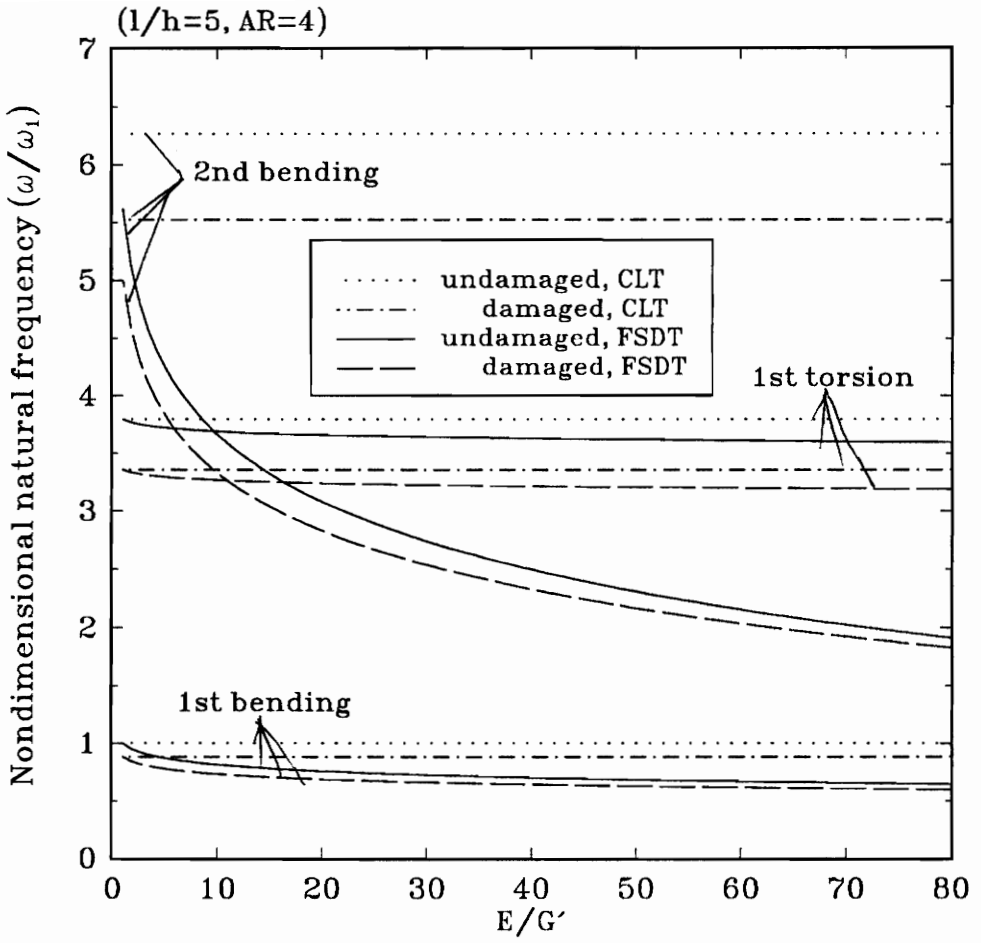

Figure 9.6 Natural frequencies of transversely isotropic structure ($l/h = 5$, $AR = 4$) before and after damage (whole span of the each top and bottom 5% thickness experiences 100% reduction of elastic moduli).

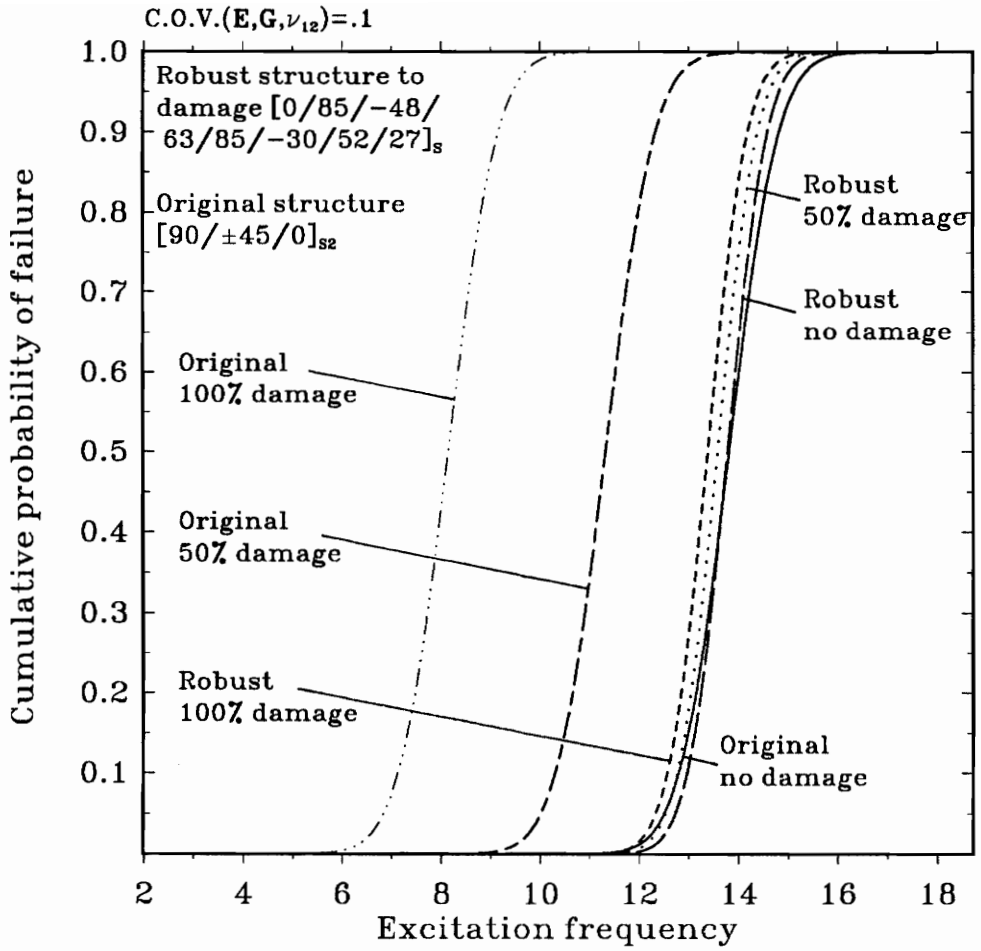

Figure 9.5 Probabilistic failure of original and robust structures (l = 9 in, $c = 3$ in) to damage (whole span of 1st and 16th layers damaged up to 100 %) with uncertain material properties.

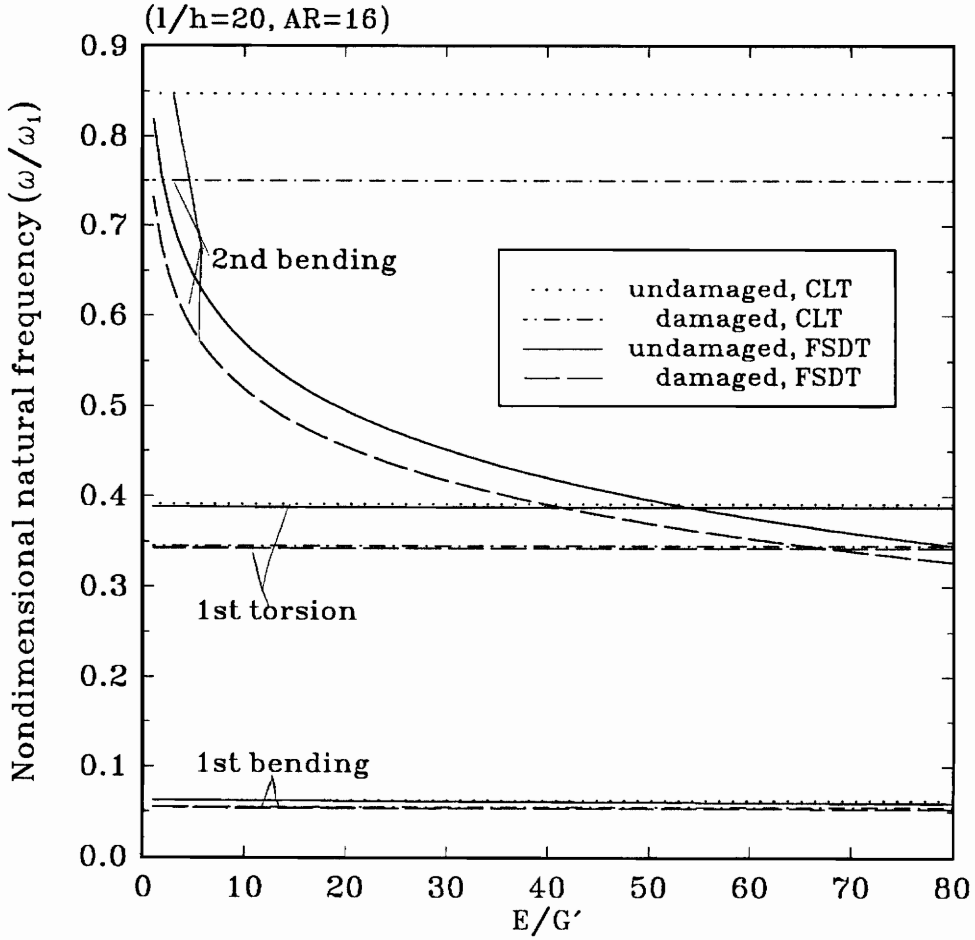

Figure 9.7 Natural frequencies of transversely isotropic structure ($l/h = 20$, $AR = 16$) before and after damage (whole span of the each top and bottom 5% thickness experiences 100% reduction of elastic moduli).

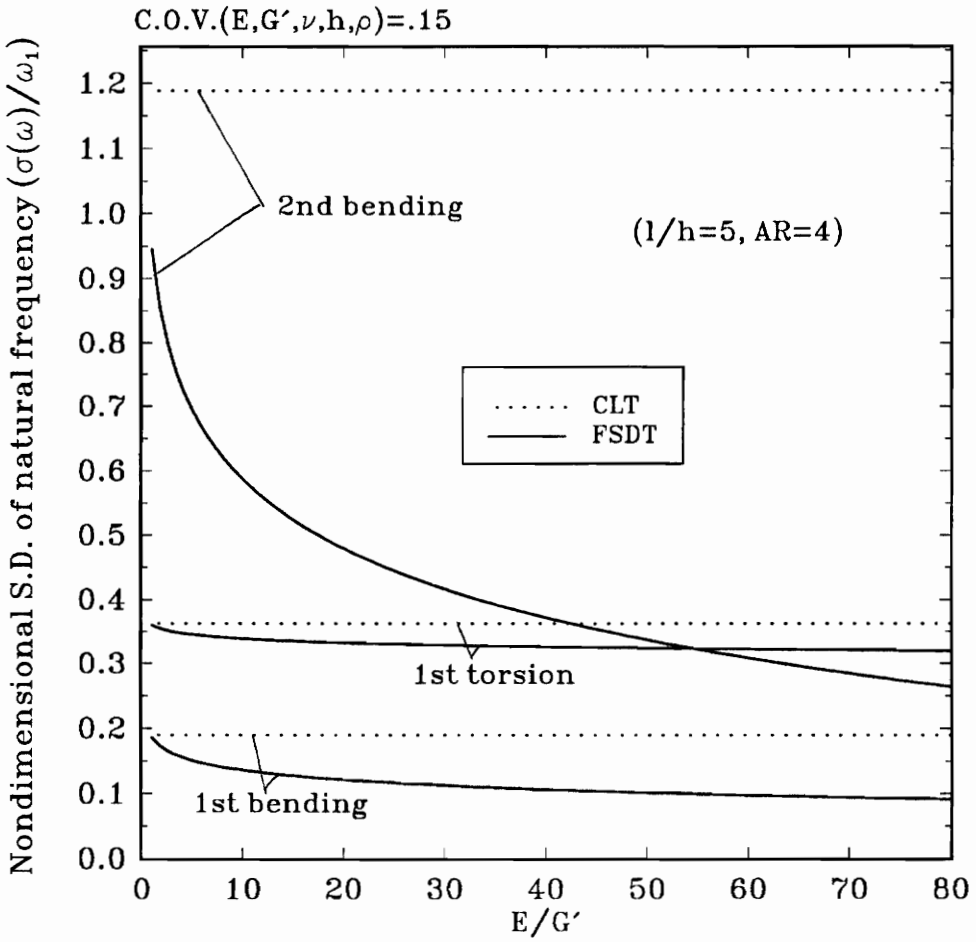

Figure 9.8 Standard deviations of natural frequencies of a transversely isotropic structure ($l/h = 5,\ \mathcal{AR} = 4$).

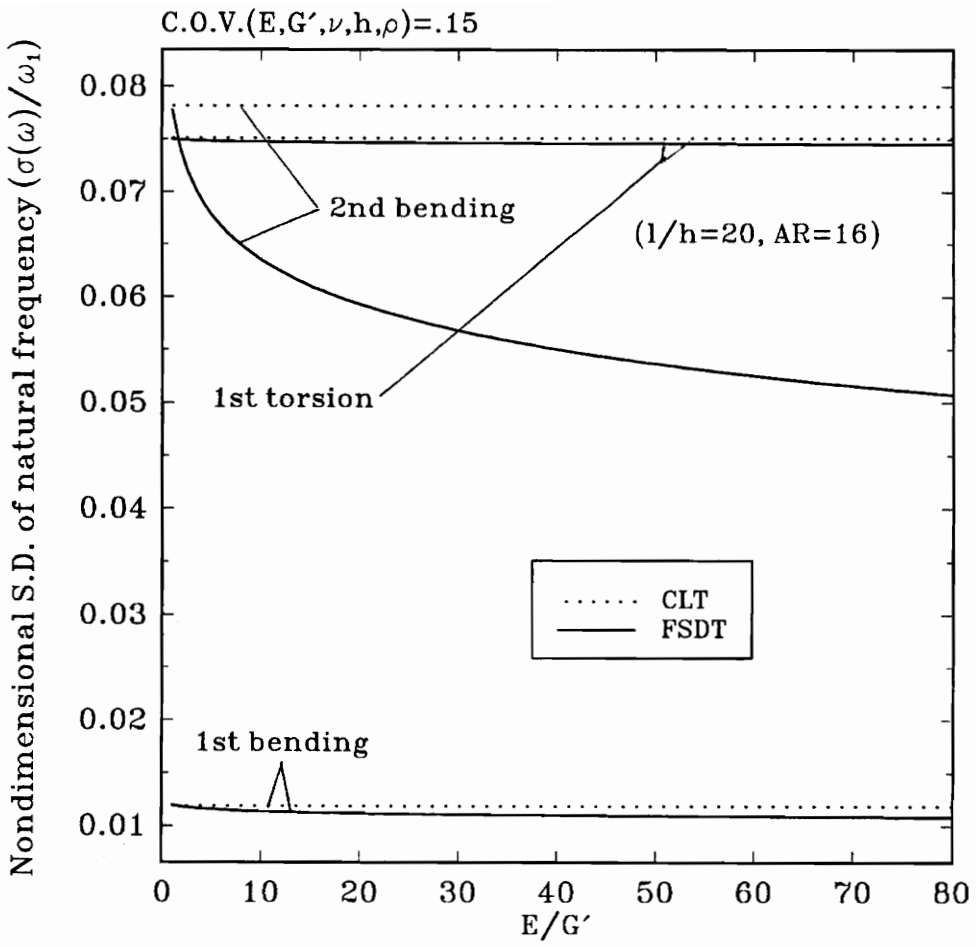

Figure 9.9 Standard deviations of natural frequencies of a transversely isotropic structure ($l/h = 20,\ AR = 16$).

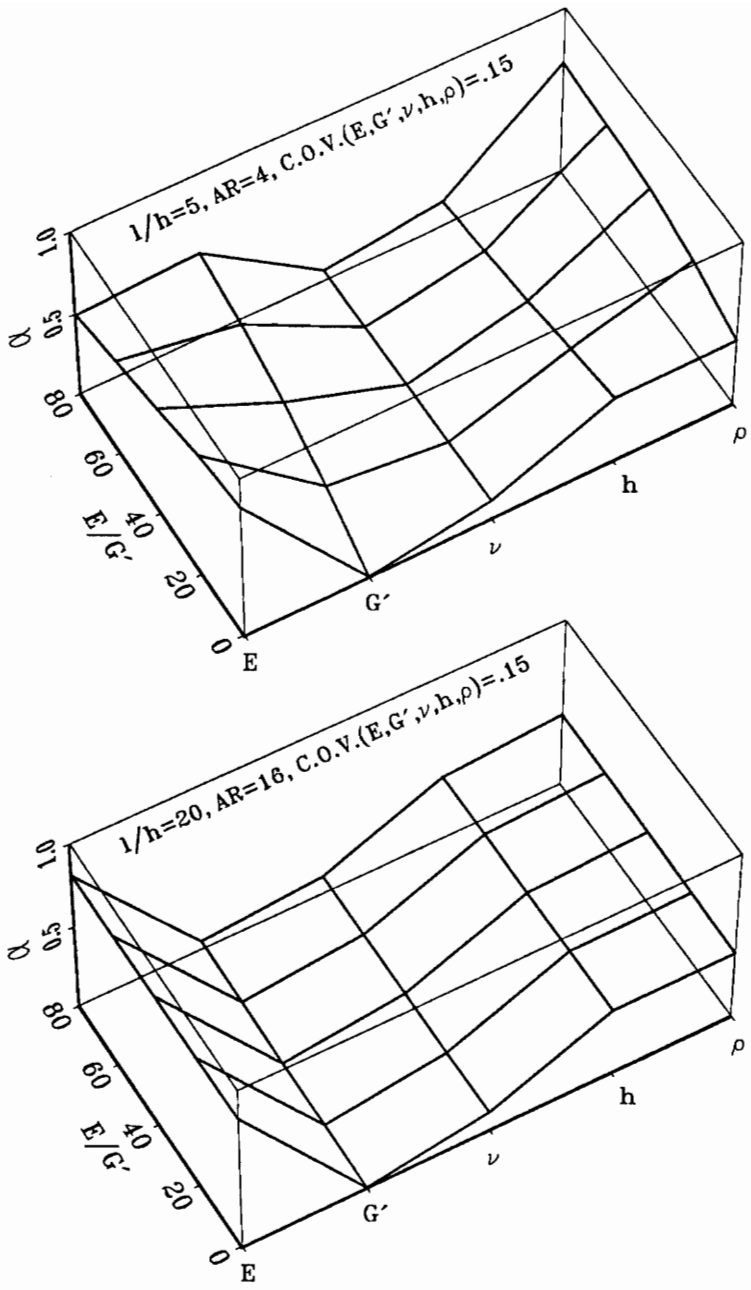

Figure 9.10 Alpha-value of random variables for a transversely isotropic structure.

10 ACTIVE VIBRATION CONTROL

10.1 Overview

It is well known that flight structures such as aircraft wings and helicopter blades exhibit undesirable vibrations which can result either in the fatigue of the structure or in its failure. To avoid such undesirable phenomena, vibration suppression of flight structures becomes extremely important. For the purpose of suppressing the vibrations, active control techniques have to be implemented.

Distributed-parameter systems have an infinite number of modes, thus treating the structures as discrete systems may be inadequate for control implementation. During the last two decades, precise control for distributed structures has been possible owing to new modal synthesis, so nowadays it is quite common to apply a modal approach to distributed structures. Hence this chapter focuses on the active vibration control of cantilevered structures by the modal approach.

Modal approaches break into two categories, independent modal space control (IMSC) and coupled control. In Ref. [76], independent modal space control is referred to as natural control due to the fact that natural coordinates for the open-loop system remain unchanged after the closed-loop system is designed. Coupled control is different from independent modal-space control in that controlled systems are recoupled again by a non-diagonal control gain matrix. To the best of the author's knowledge it should be remarked that in the case of composite structures, in contrast to their metallic counterpart, very few works have been devoted to their vibration control.

10.2 Active Vibration Control

The continuous structures without consideration of damping are described by partial differential equations representing distributed-parameter systems as

$$\mathcal{L}u(y,t) + m\ddot{u}(y,t) = f(y,t) \tag{10.1}$$

where $\mathcal{L}$ is a linear homogeneous differential operator. If the case of discrete actuators is considered, the control force will be in the form of

$$f(y,t) = \sum_{i=1}^{m} F_i(t)\delta(y - y_i), \qquad 0 < y < l \tag{10.2}$$

where F_i is force magnitude and $\delta(y - y_i)$ is the spatial Dirac delta function. In the previous section, discretization for free vibration analysis has resulted in

$$M\ddot{\mathbf{q}} + K\mathbf{q} = \mathbf{0} \tag{10.3}$$

wherefrom the eigenvalue problem results in

$$K\mathbf{u} = \omega^2 M\mathbf{u} \tag{10.4}$$

In Eq. (10.3), $\mathbf{q(t)}$ is the configuration column vector and $\mathbf{u}$ is the eigenvector. The desired modal equations are obtained, using the orthonormality condition of eigenvectors in Ref. [22]

$$\int_0^l mu_r u_s dy = \delta_{rs}, \quad \int_0^l \omega^2 u_r u_s dy = \omega^2 \delta_{rs},$$

where δ_{rs} is the Kronecker delta. Then the system is expressed in the modal coordinates η_r with compacted index notation as

$$\ddot{\eta}_r(t) + \omega_r^2 \eta_r(t) = \sum_{i=1}^{m} U_r(y_i) P_i(t), \qquad r = 1, 2, \ldots, n$$

or, in matrix form

$$\ddot{\eta}(t) + \mathbf{\Omega}^2 \eta(t) = \mathbf{B}' \mathbf{P}(t) \tag{10.5}$$

where

$$\mathbf{\Omega} = diag(w_r), \qquad r = 1, 2, \ldots, n$$

$$\mathbf{B}' = [b'_{ri}] = [U_r(y_i)] \tag{10.6}$$

The system can be expressed in modal state-variable form

$$\dot{\mathbf{z}}(t) = A\mathbf{z}(t) + B\mathbf{F}(t) \tag{10.7}$$

where

$$A = \begin{bmatrix} \mathbf{0} & \mathbf{I} \\ -\mathbf{\Omega}^2 & \mathbf{0} \end{bmatrix}, \qquad B = \begin{bmatrix} \mathbf{0} \\ \mathbf{B}' \end{bmatrix} \tag{10.8}$$

The continuous-time linear-quadratic regulator is designed associated with Riccati equations. The optimal feedback control gain matrix G is calculated such that the feedback law:

$$\mathbf{F}(t) = -G\mathbf{z}(t) \tag{10.9}$$

minimizes the performance index:

$$\mathbf{J} = \frac{1}{2} \int_0^\infty \left(\mathbf{z}^T Q \mathbf{z} + \mathbf{F}^T R \mathbf{F} \right) dt \tag{10.10}$$

subject to the constraint Eq. (10.7) where Q and R are weighting functions chosen according to the designer's experience. For a unique positive definite solution to the linear quadratic regulator problem, matrices Q and R are assumed to be symmetric and positive-semi-definite. In this problem, the control gain matrix G is

$$G = R^{-1}B^{T}K \tag{10.11}$$

and the associated matrix Riccati equation:

$$KA + A^{T}K - KBR^{-1}B^{T}K + Q = 0 \tag{10.12}$$

10.3 Numerical Simulation

Typical graphite/epoxy materials are chosen for the composite structure:

$$E_1 = 18.5 \times 10^6\ psi, \quad E_2 = 1.6 \times 10^6\ psi, \quad \nu_{12} = .35$$

$$G_{12} = .832 \times 10^6\ psi, \quad G_{23} = .332 \times 10^6\ psi, \quad G_{13} = .332 \times 10^6\ psi$$

Mass density and ply thickness are taken to be $\rho = .056\ lb/in^3$ and $t = .0053\ in$, respectively, and the stacking sequence is $[90_3/0]_{S2}$. The geometric dimensions are:

$$l = 15\ in, \quad c = 3\ in, \quad h = 0.0848\ in$$

For the numerical example considered in this section, six bending and six torsional modes are used. It is assumed that the contribution of the remaining

modes to the motion is negligible. The system is assumed to be deterministic, and no actuator or sensor dynamics are included. Coupled modal space control is employed, where weighting matrices are chosen

$$Q = \begin{bmatrix} \mathbf{\Omega}^2 & \mathbf{0} \\ \mathbf{0} & \mathbf{I}_{(12\times12)} \end{bmatrix}, \qquad R = \mathbf{I}_{(3\times3)} \tag{10.13}$$

where $\mathbf{I}_{(12\times12)}$ is 12×12 and $\mathbf{I}_{(3\times3)}$ is 3×3 identity matrices. A sinusoidal input is applied at (0.6, 0.6) with the magnitude 100 *psi* and frequency 2π *rad/sec* during time $t = 0$ to .3 *s*. Three point force actuators are placed at the following locations of the structure: (0, 0.5), (0, 0.75) and (0, 1). The quantities inside the parentheses represent the nondimensional coordinates, $\tilde{x}$ and $\tilde{y}$, respectively (see Figure 3.1 to refer to the geometry of the structure).

The dynamic responses of the composite cantilever determined using FSDT and CLT are compared in Figures 10.1-2. It is seen that the responses are underestimated by the CLT. Furthermore, the warping restraint is found to have a non-negligible effect on the responses. The responses of the uncontrolled and controlled first bending modes is shown in Figure 10.1. The results in Figure 10.1 reveal that the effects of transverse shear deformation and warping restraint are more prominent in the case of the controlled responses than in the case of their uncontrolled counterparts. In Figures 10.3-5, the effects of transverse shear deformation and warping restraint on the forces of the actuators placed on three locations are illustrated. The amplitude of the actuating forces increases with the increase of the transverse shear flexibility of the structures and when the warping

inhibition effect is discarded.

For an accurate control implementation, the influence of the transverse shear deformation and warping restraint should be accounted for in the modeling of the composite cantilever. It is also illustrated here that under control action, the vibration amplitude could be reduced significantly.

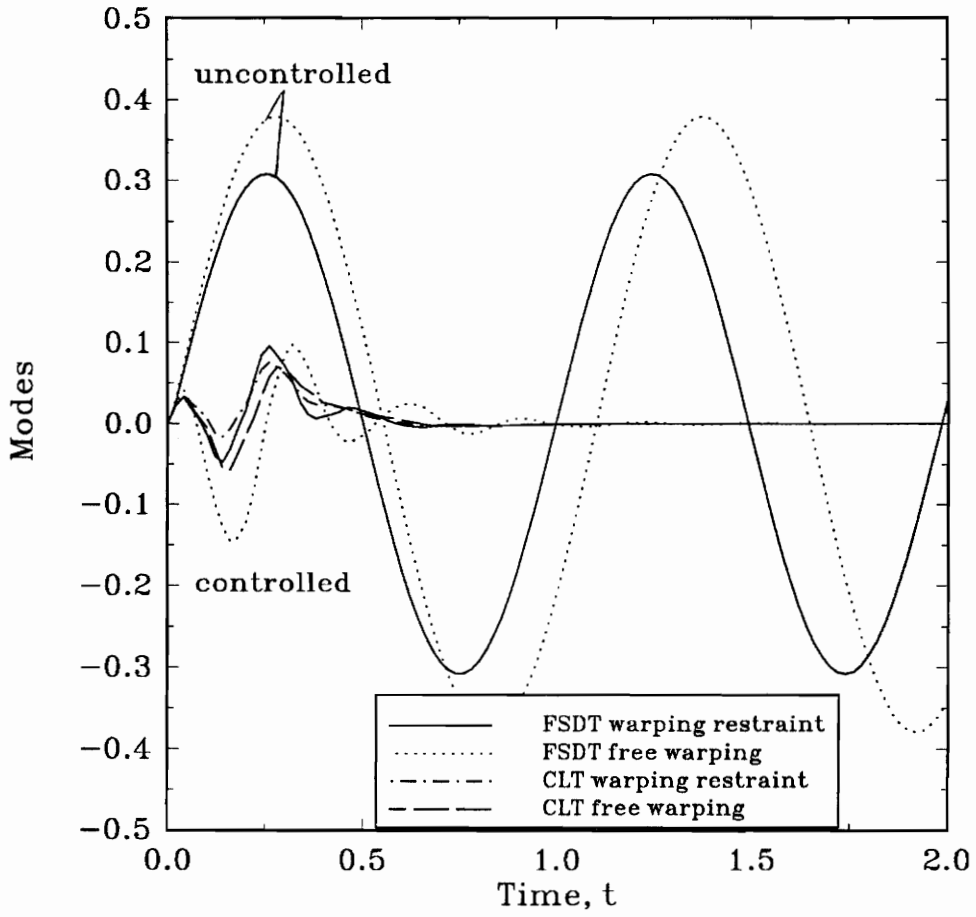

Figure 10.1 Controlled and uncontrolled responses of the first bending vibration mode for the cantilevered composite beam.

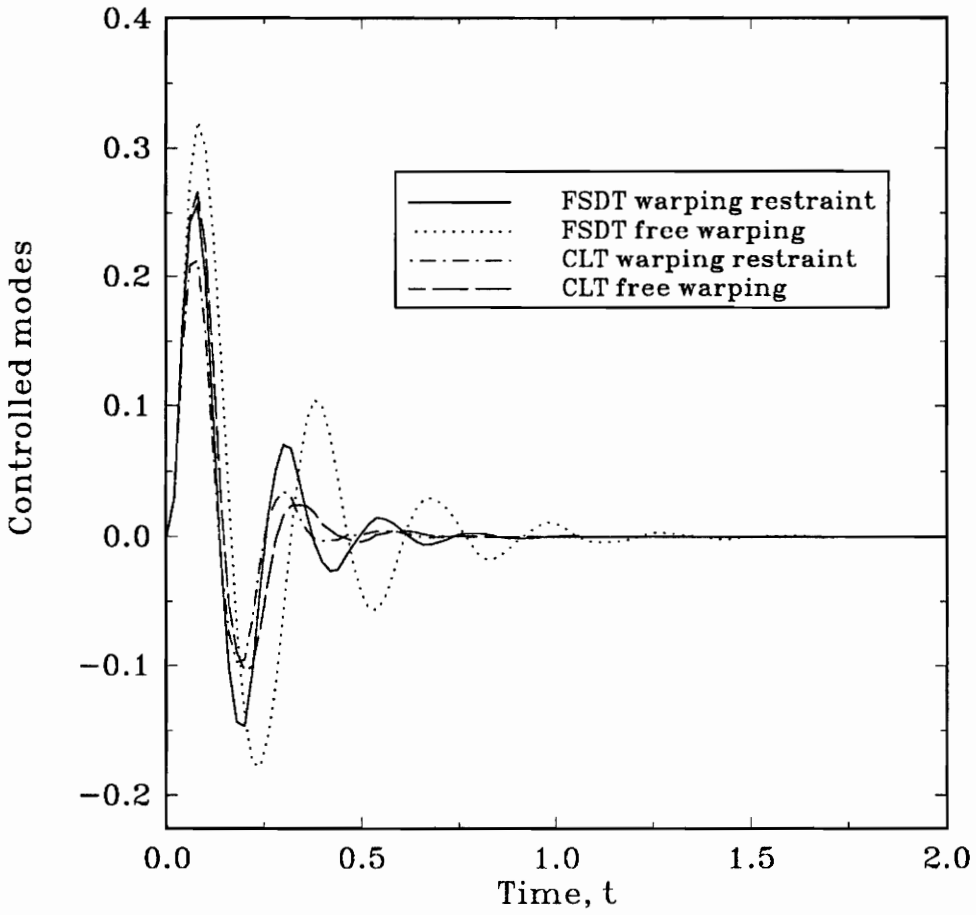

Figure 10.2 Controlled responses of the first torsional vibration mode for the cantilevered composite beam.

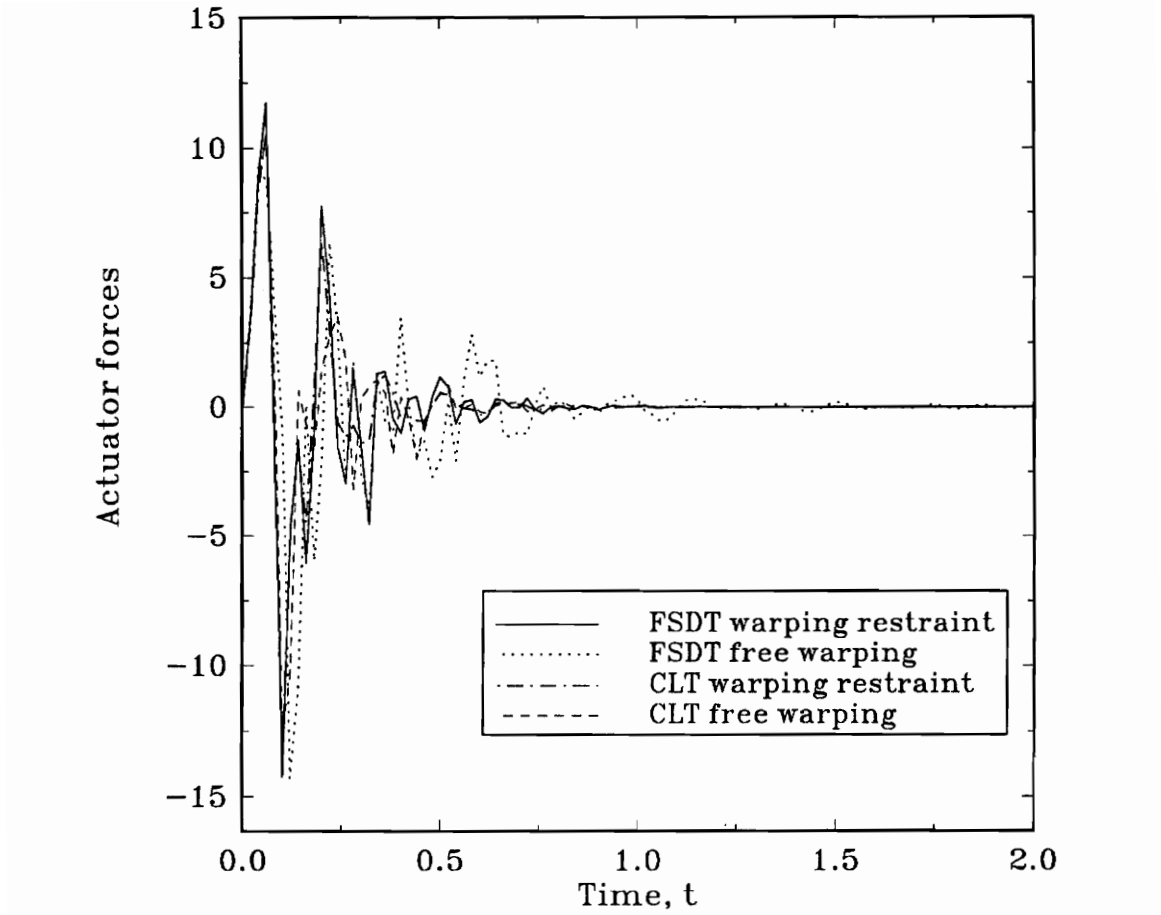

Figure 10.3 Magnitude of first actuator force.

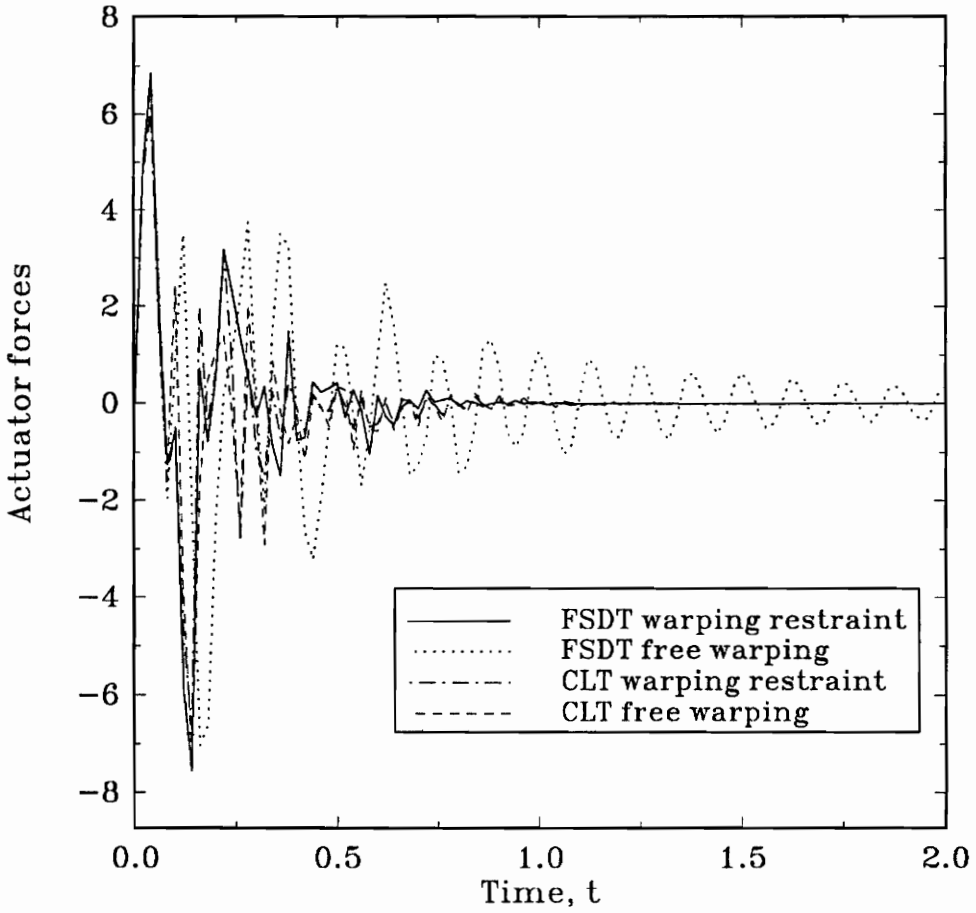

Figure 10.4 Magnitude of second actuator force.

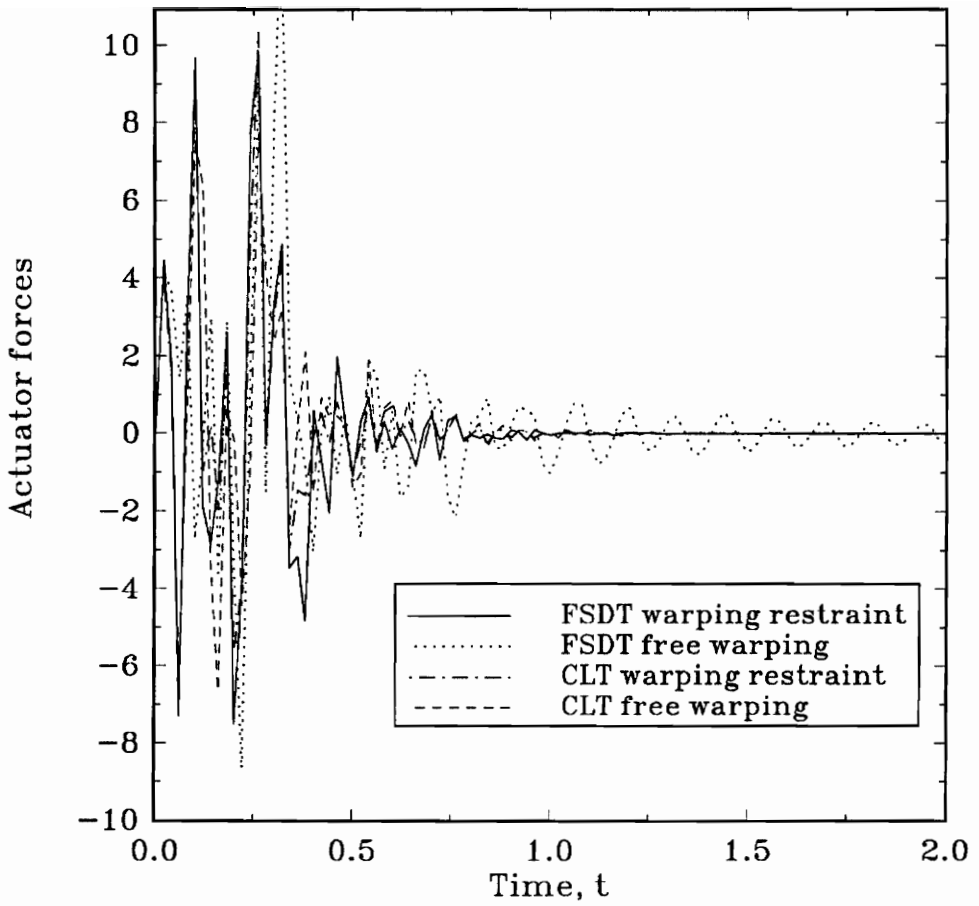

Figure 10.5 Magnitude of third actuator force.

11 CONCLUSIONS AND RECOMMENDATIONS

11.1 Summary and Conclusions

In this study, design methodologies aimed at improving the dynamic characteristics of cantilevered composite structures have been developed. Structural tailoring and optimization techniques are presented as a mean of passive vibration control. Structural damage and uncertainties are considered in the free vibration analysis. To minimize the effects of damage and uncertainties, robust structures have to be designed. Active vibration control is applied to quickly suppress vibration response.

The governing equations are developed using Hamilton's principle for displacement fields defined according to first-order transverse shear deformation theory and its classical lamination counterpart. To seek approximate solutions of the eigenvalue problem, spatial discretization using Rayleigh-Ritz, Extended-Galerkin and Finite Element methods are implemented. The free vibration problems of cantilevered composite structures with various stacking sequences and geometric configurations are examined. The effects of bending-twist coupling, warping restraint, and transverse shear flexibility on vibration frequencies and mode shapes are revealed. Structural tailoring and optimization techniques are applied to improve the dynamic performance of the structure.

The stochastic Rayleigh-Ritz method has been developed to deal with structural uncertainties due to parameter variations. Uncertain parameters include material properties (elastic constants, Poisson's ratio, mass density), geometry

(layer thicknesses) and design variables (ply orientations). Sensitivity and reliability analyses were accomplished for a structure under an external oscillatory load. The effects of locations, sizes and intensity of damage on free vibration characteristics of composite cantilevers were investigated. The structural tailoring technique was reapplied to alleviate the damage effect. Robust structures to damage and uncertainties were constructed by adopting an optimization technique with structural tailoring. Active vibration was proposed to suppress vibration in an effective way. A feedback control based on the linear quadratic regulator was implemented. A comparison was made between the controlled and uncontrolled modes predicted by two theories (FSDT, CLT) with the emphasis on the influence of the nonclassical effects.

Based on the results of numerical examples, the following concluding remarks are drawn:

1. *Free vibration analysis*

   The Rayleigh-Ritz method using polynomial functions results in a fast convergence. Approximate solution by the Rayleigh-Ritz method is accurate and efficient. Natural vibration frequencies and mode shapes are influenced by the elastic coupling between bending and torsion. The discrepancies in estimating the natural frequencies by the two theories (FSDT, CLT) are generally due to the neglect of a number of effects which in many important instances play a major role on the dynamic response of the structures. These effects are due to the transverse shear, bending-twist coupling induced by the anisotropicity of the material, and the warping restraint effect which becomes of extreme importance in the case of cantilevered-type beams. In connection with the selection of a shear correction factor, there is little change the global response quantities like frequencies for thin structure.

2. *Passive vibration control*

Passive vibration control has been accomplished by a structural tailoring technique, where remarkable improvement of the dynamic characteristics of the structure was noticed. The increase of the thickness of the structure, yielding an increase of the natural frequencies, has to be considered, for an enhanced design, in conjunction with the tailoring technique. Bending-twist coupling, which was induced by ply orientations, plays a significant role on changes of vibration characteristics. The warping restraint effect is reduced when bending and torsion are coupled. It is noted that enhancement of response characteristics via the tailoring technique is achieved without weight penalties. These high capabilities accomplished by structural tailoring are important in the practical application of active vibration control to save excessive amounts of control force.

3. *Structural optimization*

A nonlinear real programming technique was found to be its efficient in accomplishing an optimum design. Bending-stretching coupling is not beneficial to increase torsional frequencies, enabling the use of a symmetric laminate with simple analysis. Optimum torsional frequencies are strongly influenced by geometrical parameters, in general, and by the aspect ratio, in particular. Again, the nonclassical effects were examined and found to be important, so that their effects must be considered in optimum design.

4. *Analysis of structures with parameter uncertainties*

Stochastic Rayleigh-Ritz method based on a mean-centered second-order moment and first-order perturbation technique has been developed. By comparing results with the Monte- Carlo simulation, it is concluded that the method

is quite accurate and efficient. The uncertainties of bending vibration frequencies are dominated by variation of the elasticity modulus E_1. Unlike bending, the uncertainties of torsional frequencies can be influenced by variation of local geometric parameters, layer thicknesses. Correlation of uncertain parameters increases greatly the overall uncertainties of the structure. The effects of uncertainties are underestimated by CLT. In addition to fiber orientation, the number of layers and total thickness of the laminated structure can be tailored to reduce the uncertainty effects.

5. *Analysis of damaged structures*

   Structural safety is significantly jeopardized by damage, especially by damage neat the root. The damage location is most critical. A structural designer must be aware not only on the location of the damage, but also of the intensity and size of the damage. Probabilistic failure analysis provides safety measures for damaged structures with parameter uncertainties. Structural tailoring plays an important role in reducing the damage effect by orienting fibers along the chordwise direction.

6. *Design of robust structures*

   In reliability-based design, structures have been constructed to be robust to uncertainties. Material properties are changed to reduce the uncertainty effects, which implies cost-effective construction. Moreover, the robust structure to uncertainties can be made tolerant to damage by applying the structural tailoring technique. The effect of damage on the structure is much greater than that of uncertainties. The damage effect is reduced significantly using the structural tailoring technique; however, the effect of uncertainties decreases in a small amount. The design of a robust structure to damage

without changing material properties, while applying the structural tailoring technique, has been shown to be the best for alleviating the damage effect. In view of the influence of the ratio E'/G in transversely isotropic structures (E_1/G_{13} in anisotropic structures), one should include the effect of transverse shear flexibility in the design. Such a consideration could lead to a reliable design of robust structures.

7. *Active vibration control*

Under control action, vibration is significantly reduced in a short time. It was shown that the controlled modes are more influenced by the transverse shear deformation and warping restraint than the uncontrolled one. Warping restraint was shown to have a beneficial effect on the performance of the controlled structure, and the uncontrolled one as well. It was shown that the controlled response and actuator output were underestimated in the closed-loop system based on the classical structural model. Hence, if a controller is based on the CLT model, the vibration of the structure may exceed the certain level that is predicted by CLT model. Moreover, the actual outputs of some actuators will be so large that actuators may become saturated, which, of course, will yield an unsatisfactory performance or even failure of the control system. From these results, one can conclude that, for effective vibration control of cantilevered composite structures that are not thin, the control system should be designed exclusively based on the refined structural model which includes the transverse shear deformation effect. Furthermore, the constraint parameters which have a stabilizing effect as, e.g., warping restraint must be included in the model that is used to design the controller.

11.2 Recommendations for Future Work

Herein, some suggestions for future extensions of this work are presented.

1. Energy dissipation during vibration can be included in the form of damping.
2. Progressive failure due to damage growth and degrading material properties can be considered in the reliability analysis.
3. A more realistic model for the aircraft wing, i.e. a thin-walled beam can be adopted.
4. The study has been limited to the one-dimensional damage problem. This approach can be extended to the two-dimensional one.
5. Other statistical distributions (Weibull, lognormal, etc.) can be used to approach the problem of uncertainties.
6. For the safe operation of the structure in the presence of structural uncertainties and damage, adaptive uncertainty-tolerant multi-variable feedback control algorithm is necessary.

REFERENCES

1. Timoshenko, S. P., "On the Transverse Vibrations of Bars of Uniform Cross Section," *Philosophical Magazine*, Series 6, Vol. 43, 1922, pp. 125–131.

2. Kruszewski, E.T., "Effect of Transverse Shear and Rotary Inertia on the Natural Frequency of a Uniform Beam," *NACA TN-1909*, July 1949.

3. Traill-Nash, R. W. and Collar, A. R., "The Effects of Shear Flexibility and Rotatory Inertia on the Bending Vibrations of Beams," *Quarterly Journal of Mechanics and Applied Mathematics*, Vol. 6, 1953, pp. 186–222.

4. Cowper, G. R., "The Shear Coefficient in Timoshenko's Beam Theory," *Journal of Applied Mechanics*, Vol. 33, June 1966, pp. 335–340.

5. Huang, T. C., "The Effect of Rotatory Inertia and of Shear Deformation on the Frequency and Normal Mode Equations of Uniform Beams with Simple End Conditions," *Journal of Applied Mechanics*, Vol. 28, 1961, pp. 579–584.

6. Reissner, E. and Stein, M., "Torsion and Transverse Bending of Cantilevered Plates," *NACA TN-2369*, June 1951.

7. Petre, A., Stanescu, C. and Librescu, L., "Aeroelastic Divergence of Multicell Wings (Taking their Fixing Restraints into Account)," *Revue de Mécanique Appliquée*, Vol. 19, No. 6, 1961, pp. 689–698.

8. Ambartsumian, S. A., *Theory of Anisotropic Plates*, English translation, Technomic Publishing Co., 1967.

9. Librescu, L., "On the Theory of Anisotropic Elastic Shells and Plates," *International Journal of Solids and Structures*, Vol. 3, 1967, pp. 53–68.

10. Whitney, J. M. and Leissa, A. W., "Analysis of Heterogeneous Anisotropic Plates," *Journal of Applied Mechanics*, Vol. 36, 1969, pp. 261–266.

11. Crawley, E. F. and Dugundji, J., "Frequency Determination and Nondimensionalization for Composite Cantilever Plates," *Journal of Sound and Vibration*, Vol. 72, No. 1, 1980, pp. 1–10.

12. Jensen, D. W., Crawley, E. F. and Dugundji, J., "Vibration of Cantilevered Graphite/Epoxy Plates with Bending-Torsion Coupling," *Journal of Reinforced Plastics and Composites*, Vol. 1, July 1982, pp. 254–269.

13. Jensen, D. W. and, Crawley, E. F., "Frequency Determination Techniques for Cantilevered Plates with Bending-Torsion Coupling," *AIAA Journal*, Vol. 22, No. 1, March 1984, pp. 415–420.

14. Kaza, K. R. V. and Kielb, R. E., "Effects of Warping and Pretwist on Torsional Vibration of Rotating Beams," *Journal of Applied Mechanics*, Vol. 51, Dec. 1984, pp. 913–920.

15. Song, O., "Modeling and Response Analysis of Thin–Walled Beam Structures Constructed of Advanced Composite Materials," *Ph.D. Dissertation*, Virginia Polytechnic Institute and State University, 1990.

16. Hodges, D. H., Atilgan, A. R., Fulton, M. V. and Rehfield, L. W., "Free-Vibration Analysis of Composite Beams," *Journal of the American Helicopter Society*, Vol. 36, No. 3, 1991, pp. 36–47.

17. Reddy, J. N., "A Simple Higher-Order Theory for Laminated Composite Plates," *Journal of Applied Mechanics*, Vol. 51, 1984, pp. 745–752.

18. Librescu, L., *Elastostatics and Kinetics of Anisotropic and Heterogeneous Shell – Type Structures*, Sijthoff & Noordhoff, The Netherlands, 1975.

19. Librescu, L. and Simovich, J., "A General Formulation for the Aeroelastic Divergence of Composite Swept Forward Wing Structures," *Journal of Aircraft*, Vol. 25, No. 4, 1988, pp. 364–371.

20. Thangjitham, S. and Librescu, L., "Vibration Characteristics of Anisotropic Composite Wing Structures," *Proc. of 32nd AIAA/ASME/ASCE/AHS/ASC Structures, Structural Dynamics and Materials Conference*, 1991, pp. 2115–2122.

21. Karpouzian, G. and Librescu, L., "Aeroelasticity of Anisotropic Composite Wing Structures Including the Transverse Shear Flexibility and Warping Restraint Effects," *Proc. of 32nd AIAA/ASME/ASCE/AHS/ASC Structures, Structural Dynamics and Materials Conference*, 1991, pp. 1683–1691 (to appear also in Journal of Aircraft).

22. Meirovitch, L., *Analytical Methods in Vibrations*, The Macmillan Co., New York, 1967.

23. Meirovitch, L., *Computational Methods in Structural Dynamics*, Sijthoff & Noordhoff, The Netherlands, 1980.

24. Reddy, J. N., *Energy and Variational Methods in Applied Mechanics*, John Wiley, New York, 1984.

25. Wang, J. T. S., Mahrenholtz, O. and Böhm, J., "Extended Galerkin's Method for Rotating Beam Vibrations Using Legendre Polynomials," *Solid Mechanics Archives*, Vol. 1, 1976, pp. 341-365.

26. Leipholz, H. H. E., "On the Convergence of Ritz and Galerkin's Method in the Case of Certain Nonconservative Systems and Using Admissible Coordinate Functions," *Acta Mechanica*, Vol. 19, 1974, pp. 57 –76.

27. Librescu, L. and Thangjitham, S., "The Static Aeroelastic Behavior of Swept Forward Composite Wing Structures Taking into Account Their Warping Restraint Effect," *Proceedings of the Fourth Japan-U. S. Conference on Composite Materials*, June 22-29, 1988, Washington, D.C., pp. 914–922.

28. Oyibo, G. A. and Bentson, J., " Exact Solution to the Oscillations of Composite Aircraft Wings with Warping Constraint and Elastic Coupling," *AIAA Journal*, Vol. 28, 1990, pp. 1075–1081.

29. Jones, R. M., *Mechanics of Composite Materials*, Hemisphere Publishing Co., New York, 1975.

30. Caprino, G. and Crivelli Visconti, I., "A Note on Specially Orthotropic Laminates," *Journal of Composite Materials*, Vol. 16, 1982, pp. 395–399.

31. Gunnink J. W., "Comment on "A Note on Specially Orthotropic Laminates," *Journal of Composite Materials*, Vol. 17, 1983, pp. 508–509.

32. Kandil, N. and Verchery, G., "New Methods of Design for Stacking Sequences of Laminates," *Proceedings of the International Conference on "Computer Aided Design in Composite Material Technology"*, Eds. Brebbia, C. A., de Wilde, W. P. and Blain, W. R., 1988, pp. 243–257.

33. Bert, C. W., "Optimal Design of a Composite-material Plate to Maximize its Fundamental Frequency," *Journal of Sound and Vibration*, Vol. 50, No. 2, 1977, pp .229-237.

34. Starnes, J. H. Jr. and Haftka, R. T., "Preliminary Design of Composite Wings for Buckling, Strength, and Displacement Constraint," *Journal of Aircraft*, Vol. 16, 1979, pp. 564–570.

35. Shin, Y. S., Haftka, R. T., Watson, L. T. and Plaut, R. H., "Design of Laminated Plates for Maximum Buckling Load," *Journal of Composite Materials*, Vol. 23, No. 4, 1989, pp. 348–369.

36. Rao, S. S. and Singh, K., "Optimum Design of Laminates with Natural Frequency Constraints," *Journal of Sound and Vibration*, Vol. 67, 1979, pp. 101-112.

37. Hirano, Y., "Optimum Design of Laminated Plates Under Axial Compression," *AIAA Journal*, Vol. 17, No. 9, 1979, pp. 1017–1019.

38. Powell, M. J. D., "A Fast Algorithm for Nonlinearly Constrained Optimization Calculations," *Numerical Analysis*, ed. G. A. Watson, Lecture Notes in Mathematics, Vol. 630, 1978.

39. Mesquita, L. and Kamat, M. P., "Structural Optimization for Control of Stiffened Laminated Composite Structures," *Journal of Sound and Vibration*, Vol. 116, No. 1, 1987, pp. 33-48.

40. Haftka, R. T. and Walsh, J. L., "Stacking-Sequence Optimization for Buckling of Laminated Plates by Integer Programming," *AIAA Journal*, Vol. 30, No. 3, 1992, pp. 564–570.

41. Shirk, M. H., Hertz, T. J. and Weisshaar, T. A., "Aeroelastic Tailoring–Theory, Practice, and Promise," *Journal of Aircraft*, Vol. 23, No. 1, 1986, pp. 6–18.

42. Weisshaar, T. A. and Foist, B. L., "Vibration Tailoring of Advanced Composite Lifting Surfaces," *Journal of Aircraft*, Vol 22, No. 2, 1985, pp. 141–147.

43. Librescu, L. and Khdeir, A. A., "Aeroelastic Divergence of Swept-Forward Composite Wings Including Warping Restraint Effect," *AIAA Journal*, Vol. 26, No. 11, 1988, pp. 1373–1378.

44. Seitz, T. J., "Formulation of a Structural Model for Flutter Analysis of Low Aspect Ratio Composite Aircraft Wings," *Ph.D. Dissertation*, Virginia Polytechnic Institute and State University, 1992.

45. Boyce, W. E., "Random Eigenvalue Problem," *Probabilistic Methods in Applied Mathematics Vol. I*, Academic, New York, 1968, pp. 1–73.

46. Collins, J. D., and Thomson, W. T., "The Eigenvalue Problem for Structural Systems with Statistical Properties," *AIAA Journal*, Vol. 7, No. 4, 1969, pp. 642–648.

47. Soong, T. T., *Random Differential Equations in Science and Engineering*, Academic, New York, 1973.

48. Lin, Y. K. and Yang, J. N., "Free Vibration of a Disordered Periodic Beam," *Journal of Applied Mechanics*, Vol. 41, 1974, pp. 383–391.

49. Ang, A. H. S. and Tang, W. K., *Probability Concepts in Engineering Planning and Design, Vol. I and II, Basic Principles*, John Wiley & Sons, Inc., 1984.

50. Romstad, K. M., Hutchinson, J. R. and Runge, K. H., "Design Parameter Variation and Structural Response," *International Journal for Numerical Methods in Engineering*, Vol. 5, 1973, pp. 337–349.

51. Chen, P. -C. and Soroka, W. W., "Multi-degree Dynamic Response on a System with Statistical Properties," *Journal of Sound and Vibration*, Vol. 37, No. 4, 1974, pp. 547–556.

52. Vanmarcke, E., *Random Field: Analysis and Synthesis*, MIT Press, Cambridge MA, 1984.

53. Nakagiri, S. and Hisada, T., "Stochastic Finite Element Method Applied to Eigenvalue Analysis of Uncertain Structural System," *Transactions of the Japan Society of Mechanical Engineers*, Series A, Vol. 49, No. 438, 1983, pp. 239–246.

54. Vanmarcke, E., Shinozuka, M., Nakagiri, S., Schuëller G. I. and Grigoriu, M., "Random Fields and Stochastic Finite Elements," *Structural Safety*, Vol. 3, 1986, pp. 143–166.

55. Ibrahim, R. A., "Structural Dynamics with Parameter Uncertainties," *Applied Mechanics Review*, Vol. 40, No. 3, 1987, pp. 309–328.

56. Nakagiri, S., Takabatake, H. and Tani, S., "Uncertain Eigenvalue Analysis of Composite Laminated Plates by the Stochastic Finite Element Method," *Journal of Engineering for Industry*, Vol. 109, No. 1, 1987, pp. 9–12.

57. Weiqiu, Z. and Weiqiang, W., "Applications of Stochastic FEM Based on the Local Average of Random Field in Random Eigenvalue Problems," *Chinese Journal of Aeronautics*, Vol. 3, No. 1, 1990, pp. 1–6.

58. Liaw, D. G. and Yang, T. Y., "Reliability of Initially Compressed Uncertain Laminated Plates in Supersonic Flow," *AIAA Journal*, Vol. 29, No. 6, 1990, pp. 952–960.

59. Engelstad, S. P. and Reddy, J. N., "Nonlinear Probabilistic Finite Element Models of Laminated Composite Shells," *CCMS Report, VPI & SU*, CCMS-91-02, 1991.

60. Thangjitham, S. and Rantis, T. D., "Probability-Based Buckling Instability Analysis of a Laminated Composite Plate," *Proc. of 33nd AIAA/ ASME/ ASCE/ AHS/ ASC Structures, Structural Dynamics and Materials Conference*, April, 1992, Dallas, Texas, pp. 454–462.

61. Chang, C. and Yang, T. Y., "Reliability of Uncertain Flexible Laminated Skewed Plates Under Random Compressions," *AIAA Journal*, Vol. 30, No. 2, 1992, pp. 464–472.

62. Heller, R. A., *Class Notes on the "Reliability Methods in Structures and Mechanics"*, Spring 1990, ESM Dept., VPI& SU, Blacksburg, VA.

63. Sato H., "Free Vibration of Beams with Abrupt Changes of Cross-Section," *Journal of Sound and Vibration*, Vol. 89, No. 1, 1983, pp. 59-64.

64. Cawley P. and Adams, R. D., "The Location of Defects in Structures from Measurements of Natural Frequencies," *Journal of Strain Analysis*, Vol. 14, No. 2, 1979, pp. 49-57.

65. Hemming, F. G., Venkayya, V. B. and Eastep, F. E., "Flutter Speed Degradation of Damaged, Optimized Flight Vehicles," *Journal of Aircraft*, Vol. 17, Dec., 1980, pp. 833–834.

66. Eastep, F. E., Venkayya, V. B. and Tishler, V. A., "Divergence Speed Degradation of Forward-Swept Wings with Damaged Composite Skin," *Journal of Aircraft*, Vol. 21, No. 11, 1984, pp. 921–923.

67. Castel, F. and Kapania, R. K., "A Beam Element for Aeroelastic Analysis of Damaged and Undamaged Laminated Wings," *CCMS Report, VPI & SU*, CCMS-88-13, 1988.

68. Joshi, A. and Madhusudhan, B. S., "Sensitivity of Vibration and Flutter Characteristics of Isotropic Rectangular Panels to Localized Damage," *Advances in Structural Testing Analysis and Design, ICSTAD Proceedings*, July 29 - August 3, 1990, Bangalore, India, pp. 362–367.

69. Kim, Y. I. and Stragnac, T. W., "Aeroelastic Stability of Damaged Composite Structures," *SDM Conference*, Dallas, Texas, 1992.

70. Porter, B. and Crossley, R., *Modal Control*, Taylor & Francis Ltd. 1972.

71. Gould, L. A. and Murray-Lasso, M. A., "On the Modal Control of Distributed Systems with Distributed Feedback," *IEEE Transactions on Automatic Control*, AC-11, No. 4, 1966, pp. 729–737.

72. Wykes, J. H. and Mori, A. S., "An Analysis of Flexible Aircraft Structural Mode Control," Part 1. *North American Aviation Technical Report AFFDL-TR-65-190*, June 1966.

73. Simon, J. D. and Mitter, S. K., "A Theory of Modal Control," *Information and Control*, Vol. 13, 1968, pp. 316–353.

74. Brogan, W. L., *Modern Control Theory*, 2nd Edition, Prentice-Hall, Inc., 1985.

75. Meirovitch, L., "A New Modal Method for the Response of Structures Rotating in Space," *25th International Astronautical Congress of the I.A.F.*, Sept. 30–Oct. 5, 1974, Amsterdam, The Netherlands.

76. Meirovitch, L. Baruh, H. and Öz, H., "A Comparison of Control Techniques for Large Flexible Systems," *Journal of Guidance, Control, and Dynamics*, Vol. 6, No. 4, 1983, pp. 302–310.

77. Meirovitch, L. and Silverberg, L. M., "Globally Optimal Control of Self-Adjoint Distributed Systems," *Optimal Control Applications & Methods*, Vol. 4, No. 1, 1983, pp. 365–386.

78. Meirovitch, L. and Silverberg, L. M., "Control of Non-Self-Adjoint Distributed-Parameter Systems," *Journal of Optimization Theory and Applications*, Vol. 47, No. 1, 1985, pp. 77–90.

79. Krabs, W., "On Boundary Controllability of One-Dimensional Vibrating Systems," *Mathematical Methods in the Applied Science*, Vol. 1, 1979, pp. 322-345.

80. Sadek, I., Sloss, J. M., Bruch, J. C., and Adali, S., "Optimal Control of a Timoshenko Beam by Distributed Forces," *SIAM Journal of Optimization Theory and Applications*, Vol. 50, No. 3, September 1986, pp. 451–461.

81. Kim, J. U. and Renardy, Y., "Boundary Control of the Timoshenko Beam," *SIAM Journal of Control and Optimization*, Vol. 25, No. 6, November 1987, pp. 1417–1429.

82. Meirovitch, L. and Silverberg, L. M., "Active Vibration Suppression of a Cantilever Wing," *Journal of Sound and Vibration*, Vol. 97, No. 3, 1984, pp. 489–498.

83. Horikawa, H., Dowell, E. H. and Moon, F. C., "Active Feedback Control of a Beam Subjected to a Nonconservative Force," *International Journal of Solids and Structures*, Vol. 14, 1978, pp. 821–839.

84. Schulz, G. and Heimbold, H., "Integrated Actuator/Sensor Positioning and Feedback Design for Large Flexible Structures," *AIAA Paper 82-1590*, Aug., 1982.

85. Williams, J. P. and Montgomery, R. C., "Simulation and Testing of Digital Control on a Flexible Beam," *AIAA Paper 82-1569*, Aug. 1982.

86. Weinmann, A., *Uncertain Models and Robust Control*, Springer-Verlag Wien, 1991.

87. Soong, T. T., *Active Structural Control: Theory and Practice*, Longman Scientific & Technical, 1990.

88. Schäfer, B. E. and Holzach, H., "Experimental Research on Flexible Beam Modal Control," *Journal of Guidance*, Vol. 8, No. 5, 1985, pp. 597–604.

89. Inman, D. J. and Garcia, E., "Smart Structures for Vibration Suppression," *Fourth International Conference on Recent Advances in Structural Dynamics*, 15–18 July, 1991, Institute of Sound and Vibration Research, University of Southampton.

90. Chang, M. Y., "Active Vibration Control of Composite Structures," *Ph.D. Dissertation*, Virginia Polytechnic Institute and State University, 1990.

91. Adali, S., Sadek, I. S., Sloss, J. M. and Bruch, J. C., "Distributed Control of Layered Orthotropic Plates with Damping," *Optimal Control Applications and Methods*, Vol. 9, 1988, pp. 1–17.

92. Sloss, J. M., Sadek, I. S., Bruch, J. C. and Adali, S., "Optimal Vibration Control of Laminated Cross-ply Cylindrical Panels," *Math. Eng Ind.*, Vol. 2, No. 3, 1989, pp. 169–188.

VITA

Donghoon Oh was born on July 24, 1961, in Daejeon, Korea. He entered the Aeronautical Engineering Program at Inha University at Incheon, Korea in March 1980. After two years, he served his country at an air base as a military obligation, rejoined the school in March 1983, and received the B.S. degree in Feb. 1985.

In order to pursue his graduate studies, he enrolled in the master's program in Mechanical Engineering at Oklahoma State University in the fall of 1985, and obtained the M.S. degree in July 1987. Upon graduation, he continued graduate study for the degree of Doctor of Philosophy in Mechanical Engineering at the Polytechnic University at Brooklyn, New York.

He transferred to the Ph.D. program in Engineering Mechanics at Virginia Polytechnic Institute and State University in Sept. 1989. The author is married to Seon-ki Lim.